UNIVERSITE BRETAGNE LOIRE

UNIVERSITÉ DE NANTES

Thèse de Doctorat

Corentin HUMEAU

Mémoire présenté en vue de l'obtention du
grade de Docteur de l'Université de Nantes
sous le sceau de l'Université Bretagne Loire

École doctorale : *SPI*

Discipline : *Mécanique des solides, des matériaux, des structures et des surfaces*
Spécialité : *Sciences pour l'ingénieur*
Unité de recherche : *GeM*

Soutenue le *14 Novembre 2017*
Thèse N° :

Contribution to the study of coupling between moisture diffusion and mechanical stress, in high performance marine materials

Contribution à l'étude du couplage entre diffusion d'eau et contraintes mécaniques dans les matériaux marins hautes performances

JURY

Président du jury	**Philippe OLIVIER**, Professeur, Université de Toulouse
Rapporteurs :	**Jean-Claude GRANDIDIER**, Professeur, ISAE-ENSMA **Vincent PLACET**, HDR, Université de Franche-Comté
Examinateurs :	**Bruno FAYOLLE,** Professeur, ENSAM
Directeur de Thèse :	**Frédéric JACQUEMIN**, Professeur, Université de Nantes
Co-directeur de Thèse :	**Peter DAVIES**, HDR, IFREMER - Centre Brest

A mes grands-parents.

Remerciements

Il parait que l'on réserve toujours le meilleur pour la fin… Trois années se sont passées depuis le commencement de cette thèse et, alors que je termine, il me reste simplement à remercier toutes les personnes ayant permis que ce travail voit le jour, évolue et aboutisse de cette façon.

Je tiens particulièrement à remercier Frédéric Jacquemin et Peter Davies sans qui cette thèse n'aurait tout simplement pas existé, mais aussi et surtout pour le plaisir que j'ai pu avoir à travailler avec vous. Merci pour votre présence, la confiance que vous m'avez accordée et les échanges enrichissants que nous avons pu avoir autour d'une table… ou d'une bière. Je suis convaincu que nous serons amenés à nous recroiser dans nos différentes vies professionnelles et j'en suis ravi.

Merci à Jean-Claude Grandidier, Vincent Placet, Philippe Olivier et Bruno Fayolle d'avoir accepté de faire partie du jury de cette thèse. J'ai particulièrement apprécié l'intérêt et le temps que vous avez accordé à l'examen de mon travail ainsi que la pertinence de vos questions ayant permis de très intéressantes discussions. Je tiens aussi à remercier personnellement Bruno qui a suivi mon parcours depuis ma dernière année d'école jusqu'à maintenant (cinq années déjà !), et qui a toujours eu un regard critique et attentionné sur mon travail.

Les personnes impliquées dans cette thèse ne s'arrêtent évidemment pas aux simples noms écrits sur la première page du document. Toutes les personnes que j'ai pu croiser au Laboratoire LCSM de l'IFREMER ont contribué de façon très diverse à ce que ce travail soit ce qu'il est aujourd'hui. Merci à tous : Maelenn, Pierre-Yves, Mael, Nico, Benoit pour vos conseils avisés lors de certaines prises de décisions ; Nico, Josselin, Bertrand, Patrick, Christophe, Mathieu, Mick pour m'avoir aidé à mettre en place beaucoup de manip' pas toujours très « académiques » ; Tatiana, Nico, Antoine, Alin, Antoine parce que seuls les thésards se comprennent entre eux ; et aussi Anne-Sophie et Marie Michèle…

Malgré, mes passages souvent éclairs à Saint-Nazaire j'ai pu rencontrer de nombreuses personnes du laboratoire du GeM avec qui j'ai apprécié échanger : Amandine, Sylvain, Alex, Pascal, Georgina, Hassan…

La thèse a aussi été pour moi l'occasion de travailler en collaboration avec des personnes extérieures aux laboratoires. Je tiens spécifiquement à remercier Florian Madec avec qui j'ai eu une collaboration et des échanges très intéressants. Je suis d'ailleurs heureux de savoir que notre travail de collaboration ne s'arrêtera surement pas à la suite de cette thèse.
J'ai aussi eu l'occasion de travailler trois mois chez DSM Dyneema aux Pays-Bas et je tenais à remercier Paul Smeets et Tom Engels sans qui cet échange n'aurait pu se faire et être aussi prolifique.

Mais finalement l'essentiel de ces trois années de thèse ne se résume pas au temps passé au travail. J'ai donc envie de remercier toutes les personnes m'ayant permis d'avoir une vie à côté du travail ! Une quelconque ressemblance avec les prénoms cités précédemment serait fortuite.
Aurélien, Mael mes ex-ancien coloc' et potes avec qui on a tout partagé ou presque (surf, escalade, maison, appart', galères…) ! Et tous les autres toujours prêts à profiter de la vie extraprofessionnelle à Brest : PY, « la chef », Antoine, Alin, « p'tit poulet », « Chouchou »… ; à Paris : Claire, Quentin et Guillaume ; en Mayenne : Aurélien, Gégé, Arthur, Alexia, Pauline, Péto et les autres.

Bien sûr, des remerciements ne sont rien sans un petit mot pour ses parents. Merci de m'avoir toujours soutenu dans mes choix et de m'avoir poussé à aller au bout de toutes les choses que j'entreprenais. C'est à mon avis ce qui fait que j'en suis là aujourd'hui. Bravo c'est malin !
Les personnes qui suivent après les parents sont forcément les sœurs : Marion et Clidane, merci, vous êtes sans doute les personnes qui ont le plus impacté l'avancé de ma thèse par votre soutien moral !
Et pour finir, un grand merci Floriane ! Tu as su transformer la période de rédaction de thèse en une période agréable, par le nombre de bons moments que j'ai pu passer avec toi en dehors de ma petite bulle de thésard en rédaction.

Les remerciements sont sans aucun doute la partie la plus personnelle d'une thèse et donc la plus agréable à lire. Cependant je vous invite vivement à ne pas vous arrêter en si bon chemin et poursuivre votre lecture, la suite pourrait vous intéresser !

Table of contents

General introduction

During the last decades the multiple crises (economic and environmental) have accelerated the reflexion on the way of producing energy. On one hand, the sources of fossil power have started to become scarce, therefore some other exploitation techniques have been developed. On the other hand, the recent environmental events (e.g. global warming) have initiated the consideration of new potential renewable source of energy. This global reflexion comes to the conclusion that on Earth the oceans represent an important potential in terms of energy. They represent more than 70% of the Earth's surface and contain various interesting sources of energy: both renewable (current, tide, wind) and fossil (oil, gas, ore). These observations have oriented the research in two directions: first, the exploration of new power sources and second, the exploitation of these energies.

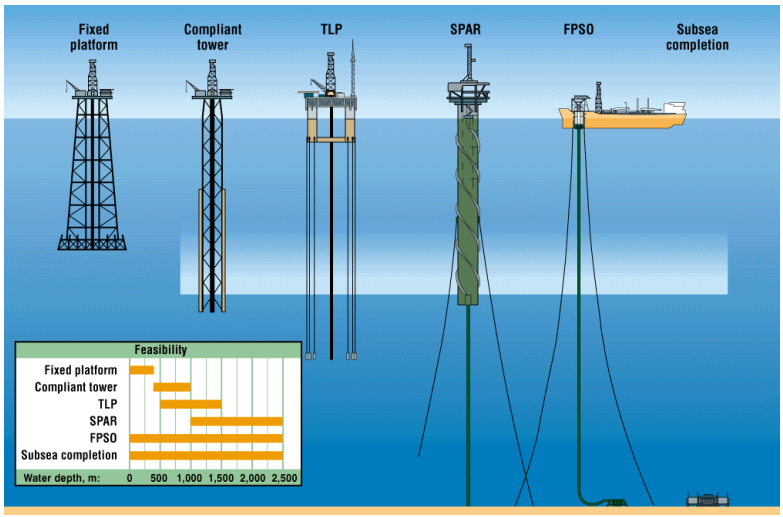

Figure I. Change in mooring techniques with the increase in depth [1].

Until recently, vessel and offshore installations were limited due to the lack of mooring techniques for deep water. As summarised in Figure I the rigid structures can only be used for shallow water down to 1,000 meters depth (for compliant tower) [2]. These types of metallic installations are mainly limited by their own weight and by structure displacements induced by current, waves and wind. To reach further seabed depth new mooring techniques have been developed since the early 80's with for example Tensioned Leg Platforms (TLP) [3] and Floating Production Storage and Offloading units (FPSO). These types of mooring use ropes to link the platform to the seabed while resisting environmental stresses from wind and waves [4]. The first offshore installations of this kind were constructed with steel wire rope mooring lines which induce important issues: first, steel material is subject to corrosion and second, for deepwater application the weight of the rope can become critical and even break the rope itself. While the corrosion problem can be avoided using a polymer cover, the weight issue for

wire ropes is an intrinsic property and cannot be avoided. Therefore, more recent projects started to investigate the possible replacement of the steel by polymers in the mooring lines. Some of these materials can indeed combine low sensitivity to water and very interesting strength/weight ratios.

The other key issue in marine application is the durability of offshore structures. Initially metallic materials were used to build marine vessels, offshore plants or submarine units. As in the case of ropes, metallic structures appear to have quite limiting properties when used in offshore applications. Most of them are highly subject to corrosion and result in high weight structures. Corrosion is critical in offshore applications due to the high conductivity of salt water, and can generate the ruin of the structure by reducing the thickness of healthy material [5]–[7]. Indeed, this phenomenon lowers the ultimate strength of the material and can even create leaks (critical for surface vessels and submarines). On the other hand the strength over weight ratio is not optimum in the case of metals, therefore metallic structures subjected to high mechanical stresses are necessarily heavy and hard to handle.

Figure II. Examples of composites used for marine application: *Nautile* submarine vessel (composite in yellow) [left] and Sabella tidal turbine (composites in blue) [right]

The development of polymer materials has resulted in a major change in the type of material used in offshore structures [8]. As for ropes, many polymers present good properties when immersed in sea water and attractive strength to weight ratios. Moreover, in order to get high mechanical properties polymers are often combined with fibre reinforcements to create composites. These show all the benefits from polymers and have good properties when stressed under either static or dynamic loads. Therefore, metals are progressively being replaced by composite materials in underwater applications such as submarines and immersed structures such as tidal turbines, Figure II.

These two high-performance materials (synthetic ropes and polymer based composites) are chosen as they are capable of resisting the aggressive marine environment.

This can be considered to have two main components: the effects due to water and the mechanical stresses applied on the material. In real marine applications materials are subjected to these two phenomena at the same time. Nevertheless, tests which combine both stresses are hard to perform. Therefore, this study aims to compare the tests performed under uncoupled, semi-coupled and coupled conditions (as shown schematically in Figure III); the aim is to highlight the additional effects caused by coupling, in order to conclude on whether there is a need for fully coupled tests or not. Moreover, the study is divided into two distinct parts, which are focused on the two types of high performance material critical to many new applications: polymer based composites and synthetic fibre ropes. Finally, the results obtained in both cases will be compared, to highlight differences and similarities between these materials when subjected to different cases of exposure (uncoupled, semi-coupled and coupled).

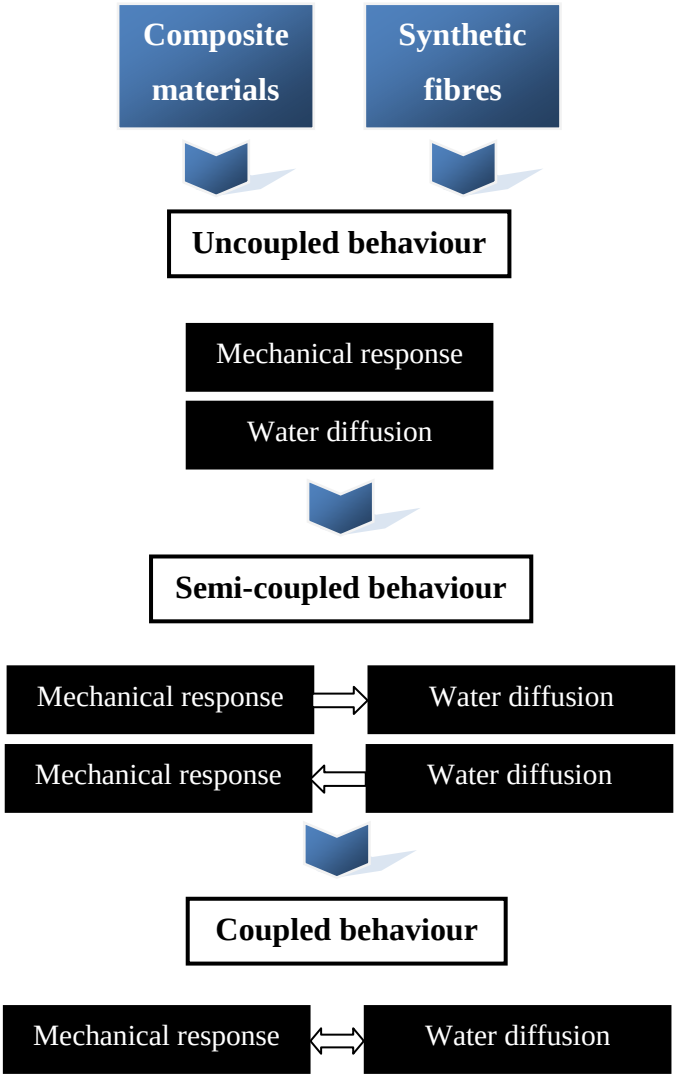

Figure III. Schematic diagram of the document structure.

Part A.
Composite materials

Chapter 1.

Bibliography on composites

1.1. Introduction

In offshore applications, the structures are subjected to extreme conditions in terms of mechanical loading and seawater immersion. In this harsh environment composites have shown important advantages over metallic materials, especially since they are not subjected to corrosion, have good properties under fatigue loading and attractive strength to weight ratios. For these reasons polymer reinforced materials are progressively replacing metal parts for marine uses.

Carbon fibres show particularly good characteristics when used as reinforcements, thanks to their excellent strength/weight ratio and good interface properties with thermoset resins. Therefore the material studied here is an epoxy resin reinforced with continuous carbon fibres.

Composites exposed to the marine environment are subjected to two main issues, water uptake and mechanical stress. These issues can be studied one by one, as separated variables, partly coupled behaviours by analysing the effects of one on the other, or as fully coupled phenomena.

The aim of this literature review is to summarize current knowledge on stress and water effects on composites, and provide guidance for future tests. The approach chosen for this bibliographic study follows the three main axes of the study. First, uncoupled effects are discussed, then previous studies related to partly coupled behaviour, and finally fully-coupled phenomena.

1.2. Uncoupled properties

To start the literature review mechanical behaviour and water diffusion will be considered independently. This will provide a baseline for further considerations on coupled phenomena.

1.2.1. Composites mechanical behaviour

Stresses applied to composites during their lifetime can be quite diverse (static or dynamic; tension, shear or compression). In order to establish a baseline for studies on coupling in composite materials we will exclusively focus on static behaviour, to minimise the number of parameters. Moreover, tension loads will be the main mechanical loading applied in this work, to simplify the testing devices required to study coupled effects.

Composites are materials made from two or more components combined together in order to adapt their properties to a specific application. In the case of polymer matrix

reinforced with fibres the aim is to get good mechanical properties from fibres and to ensure stress transfer between them by the resin properties. To better understand the mechanical behaviour of these composites we start by examining the properties of each component separately.

1.2.1.1. Mechanical properties of epoxy resin

Epoxy resins are the most common matrix polymers in high performance composite materials for marine applications, because of their high modulus and ultimate strain/stress values. These are generally polymers with an elastic mechanical behaviour (as shown in Figure 1.1) for temperatures up to their glass transition (between 60°C and 200°C for common epoxies).

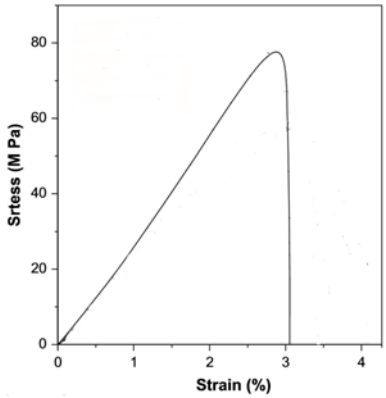

Figure 1.1. Stress strain curve for a tensile test on a pure epoxy resin specimen [9].

Nevertheless, it should be emphasized that properties of epoxies can still vary considerably, since they are crosslinked thermoset polymers, highly dependent on the chemistry and crosslink density. For some types of epoxy a non linear behaviour can be observed close to failure. This non-linearity does not necessarily correspond to a plastic behaviour. In such cases loading-unloading tests have to be performed to investigate possible permanent deformation and modulus change.

This mainly elastic behaviour nevertheless leads to failure strains sufficiently high to allow the resin to be combined with reinforcements which fail at small elongations, such as continuous fibres (carbon, glass…).

1.2.1.2. Mechanical properties of fibres

Carbon fibres are used as reinforcements in resins as they have high failure stress (typically around 5 GPa) and modulus (around 250 GPa). In our case we used the TR50S fibres from Pyrofil^{TM}, a classical carbon fibre with a purely brittle failure and mechanical

properties shown in Table 1.1.

Tow Tensile	Strength	4,900 MPa
	Strain	2.0 %
	Modulus	240 GPa
Typical Density		1.82 g/cm^3

Table 1.1. Mechanical properties of TR50S fibres [10].

The carbon fibres shown in Table 1.1 are unidirectional reinforcements with high properties in the fibre direction, but they are usually woven or stitched together to obtain a laminate with good properties in off-axis directions.

1.2.1.3. Mechanical properties of composites

Tensile Properties	0°	Strength	2,950 MPa	ASTM D3039 ; V_f=60.0%
		Modulus	142 GPa	ASTM D3039 ; V_f=60.0%
	90°	Strength	79 MPa	ASTM D3039 ; V_f=56.0%
		Modulus	9 GPa	ASTM D3039 ; V_f=56.0%
Compressive Properties	0°	Strength	1,600 MPa	SRM 1-88 ; V_f=60.0%
		Modulus	130 GPa	SRM 1-88 ; V_f=60.0%
Flexural Properties	0°	Strength	3,000 MPa	ASTM D790 ; L/d=40 ; V_f=60.0%
		Modulus	130 GPa	ASTM D790 ; L/d=40 ; V_f=60.0%
	90°	Strength	140 MPa	ASTM D790 ; L/d=16 ; V_f=56.0%
		Modulus	1.3 GPa	ASTM D790 ; L/d=16 ; V_f=56.0%
Short-Beam Shear	Strength		90 MPa	ASTM D2344 ; L/d=4 ; V_f=56.0%

Table 1.2. Mechanical properties for a prepreg composite: epoxy (Mitsubishi Rayon #340) reinforced with the carbon fibres used in the current study (TR50S) for different fibre orientations [10].

Despite good axial properties, carbon fibre is not a structural material. Fibres are usually combined with polymer materials to get cohesion and allow load transfer between

themselves. Carbon fibre is a brittle material which needs to be combined with a stiff matrix to minimise the strain difference between resin and reinforcements. Thermosets have these characteristics and have shown good properties when combined with carbon fibres. Among the thermoset resins, epoxies are the most frequently used in high performance marine applications.

The mechanical properties of composites depend on the angle of the stress direction to the fibres and on the properties of the fibres and resin in a proportional way. These fundamental aspects are highlighted by the values for a carbon epoxy composite provided by the fibre supplier, shown in Table 1.2 and in studies like [11], a review of the knowledge of polymer and composites mechanical behaviour.

1.2.1.4. Damage characterisation in composites and polymers

Studies on the effects of stress are essential to understand their impact on the material behaviour. Tensile loads induce damage in polymers and composites, among these we can distinguish two types: plasticity and cracking.

In neat rein, plasticity can appear during tensile loading above a certain yield stress, this results from slippage phenomena between polymer chains. This type of damage is characterised by a non linear behaviour coupled with a permanent deformation and a modulus change after unloading.

Crack appearance can also be noted in some neat resins stressed in tension. In this case, a crazing phenomenon appears inside the sample for high stress loading. This type of damage is characterised by whitening in transparent resin specimens (such as epoxy).

For composite materials the same damage mechanisms are observed. Some materials stressed in directions away from their reinforcement orientation present a modulus change and permanent deformation after a loading-unloading cycle. This behaviour can be the results of both damage types. As in the resin case, chain slippage generates plasticization and induces permanent strain. Moreover, in composites, matrix cracks can induce de-cohesion between matrix and fibres which can also create a permanent deformation. To get more information on the damage properties other tests have to be conducted in addition to loading/unloading cycles, such as crack analysis (developed in the following paragraph).

Carbon epoxy composites are not transparent and therefore do not whiten by when cracks initiate. Many techniques have been developed to quantify damage density in stressed composites. For example: acoustic emission signal analysis which has been investigated in [12], [13], X-ray analysis [14]–[16] or a physical damage characterisation using direct crack

density identification such as [13], [17], [18].

For this study we chose to characterise damage with the latter technique: crack density measurements, in order to have a simple method (compared to acoustic emission) which could characterise damage in quasi-isotropic composites (contrary to the modulus change criterion, D) in-situ. In addition, we performed loading-unloading cycle tests to get plasticization information on neat epoxy resin and ±45° woven composites from permanent deformation and modulus change measurements.

1.2.2. Water diffusion in composites

The specificity of marine applications is the interaction between sea water and the material. In carbon reinforced composites, the fibres do not take up water due to their hydrophobic behaviour, water diffusion is mainly located in the resin. In some cases it has also been shown that the interface between matrix and fibres can modify the diffusion results significantly [19], [20].

First, we will focus on water uptake in the epoxy matrix, the mechanisms involved and the type of theory used to represent water diffusion. A second section will highlight the most influent parameters on the water uptake in polymers and composites, such as temperature, water concentration in the surrounding and the fibre orientations.

1.2.2.1. Water uptake in the matrix

Water diffusion depends on many parameters, and therefore has to be understood first in the resin. The studies used for the review treat different diffusion mechanisms, in order to illustrate the different phenomena involved in water uptake.

Water in epoxy:

Epoxy matrix resins are hydrophilic thermoset polymers, which can take up large amounts of water (typically from 3% to 5% in weight). This behaviour is due to the epoxy resin structure which can accommodate two different types of water:

- *Free water molecules*. From a physical point of view, we consider that spaces between resin chains can be assimilated to “free volumes”, big enough for water molecules to migrate in them (Figure 1.2) [21].
- *Bonded water molecules*. Based on a chemical approach, we know that water is a polarized molecule which can create bonds with polarized sites of the epoxy chain (-OH,

NH-, O=C-OH…). Two types of bonded molecules can be distinguished [22]: water with simple hydrogen bond or multiple H-bonds (see Figure 1.3).

Diffusion mechanisms:

Polymers take up water through surfaces in contact with a wet environment by transient diffusion mechanisms until reaching an equilibrium water content. Two types of diffusion can take place, depending on the nature of the water uptake (free or bonded).

The first diffusion is induced by free water in the polymer. Epoxy chain structures have high and low density regions. Low density parts include voids within polymer resins, and depend on morphological properties such as chain length, cross-link density or crystalline ratio. These voids are located between molecular entanglements or at the interface between matrix and fibre.

In this case, water molecules are located in these cavities and diffuse from one to another free volume. This results in a water uptake mechanism depending on the free volume ratio, and the attraction forces with the polymer. The influence of these parameters on diffusion is represented by an activation energy (E) needed to transfer a molecule from one void to another.

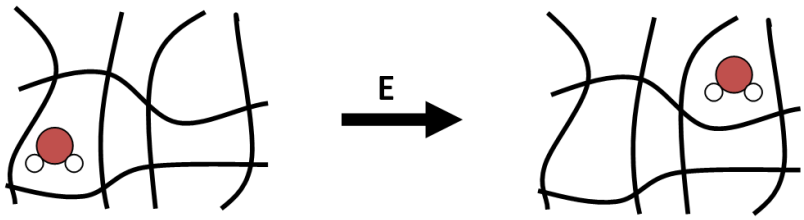

Figure 1.2. Mechanism of the free volume diffusion of water in a polymer network

The water can also diffuse in polymers as bonded molecules due to their polarization: negative pole: O, positive pole: H_2 (Figure 1.3 represents the diffusion in epoxy). This property induces an attraction with charged chemical groups of the polymer chain, and therefore designated as hydrophilic groups. The diffusion is created by water retention to these hydrophilic sites and their displacement takes place when a sufficient energy (>Ea) is applied. This energy depends on the bond type between polymer chains and water molecules.

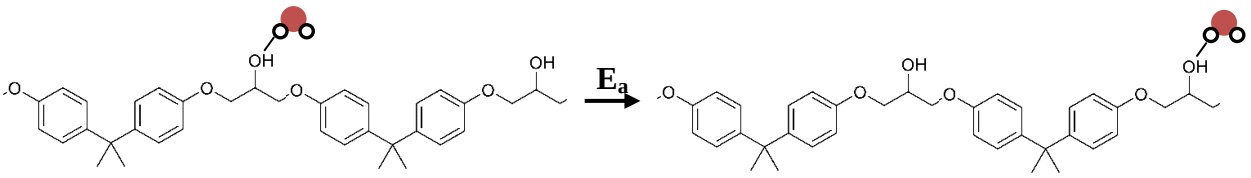

Figure 1.3. Diffusion mechanism with molecular approach, example for bond with -OH sites.

Analytical representation:

Historically, Fourier [23] established the first diffusion equation in 1822, for heat conduction. In 1855 Fick [24] proposed phenomenological laws for molecular diffusion inspired by Fourier's work. Fick's first theory can be summarized by defining the diffusive flux ($\vec{\varphi}$) as the opposite of the moisture concentration (c) gradient multiplied by the diffusion coefficient of the diffused molecule in the surrounding material (D) (Eq. 1.1).

$$\vec{\varphi} = -D\ \overrightarrow{grad}\ c \qquad \textbf{Eq. 1.1}$$

In a second law Fick has established the time derivative of moisture concentration as the divergence of the diffusion flux. By substitution of the flux with the expression from Eq. 1.1, we obtain Eq. 1.2.

$$\frac{\partial c}{\partial t} = div(D\ \overrightarrow{grad}\ c) \qquad \textbf{Eq. 1.2}$$

Eq. 1.2 cannot be solved for a generic case. Nevertheless in the following work diffusion is mainly studied in square plate specimens. Therefore the divergence and gradient operators can be expressed in Cartesian coordinates, which gives the expression in Eq. 1.3.

$$\frac{\partial c}{\partial t} = D_x \frac{\partial^2 c}{\partial x^2} + D_y \frac{\partial^2 c}{\partial y^2} + D_z \frac{\partial^2 c}{\partial z^2} \qquad \textbf{Eq. 1.3}$$

D_x, D_y, D_z are the diffusion coefficients along axes x, y, z respectively.

The global moisture content *C(t)* in the polymer cannot be established directly from Eq. 1.3. The boundary conditions have to be defined before integration. In the study [25], Crank has summarised numerous cases of water diffusion in materials. In the case of the present study every surface of square plate samples is exposed to water, which gives the moisture content defined in Eq. 1.4, from [25], by considering diffusion in the three directions.

C_∞ stands for moisture content in the saturated material, it is sometimes noted as M_s. L, l, e are the dimensions of the sample respectively along the x, y, z axes.

$$\frac{C_{3D}\ (t)}{C_\infty} = 1 - \left(\frac{8}{\pi^2}\right)^3 \sum_{i=0}^{\infty}\sum_{j=0}^{\infty}\sum_{k=0}^{\infty} \frac{exp\left(-\pi^2 t\left(D_x\left(\frac{2i+1}{L}\right)^2 + D_y\left(\frac{2j+1}{l}\right)^2 + D_z\left(\frac{2k+1}{e}\right)^2\right)\right)}{\left((2i+1)(2j+1)(2k+1)\right)^2} \qquad \textbf{Eq. 1.4}$$

For square plates samples with long length and width compared to their thickness (typically ten times more), the diffusion can be approximated as unidirectional in the depth. In

this case the Eq. 1.4 simplifies in Eq. 1.5.

$$\frac{C_{1D}\,(t)}{C_\infty} = 1 - \left(\frac{8}{\pi^2}\right)^3 \sum_{k=0}^{\infty} \frac{exp\left(-\pi^2 t D_z \left(\frac{2k+1}{e}\right)^2\right)}{(2k+1)^2} \qquad \textbf{Eq. 1.5}$$

These equations result in a curve represented in Figure 1.4 by the black line (0). Some deviations from the reference have been highlighted in the literature (coloured lines in Figure 1.4). Less common theories can represent some of these divergent behaviours, such as Dual Fick (curve 2) and Langmuir (curve 1). Other shapes of diffusion curves can appear in particular cases, for example: some curves show acceleration of the diffusion kinetics (curve 3) while others highlight a weight reduction (curve 4). For these last examples, specific theories have to be established, taking into account the additional reactions involved, such as damage for curve 3 and chemical degradation for curve 4.

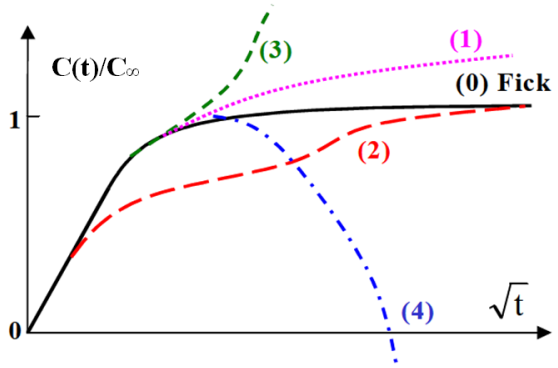

Figure 1.4. Four examples of non Fickian behaviour [26]

Identification method:

The aim of identification is to evaluate all the five parameters of the diffusion equation Eq. 1.4 (D_x, D_y, D_z, C_∞ and $C\ (t)$). In this problem, there is one equation for five unknowns, so to perform an identification some assumptions have to be made. We used the method from [27], by considering the following hypothesis:

- The first assumption is that $C_\infty = C_{max}$ *(**1** equation/**4** unknowns)*
- The second assumption consists in reducing the number of diffusion coefficients: by establishing equalities or by neglecting some of them (regarding the geometrical properties of the specimens). *(**1** equation/**2** unknowns)*
- Then the least squares method is used between experimental moisture content M_i and the corresponding value from the analytical solution $C(t_i)$:

$$S = \sum_i [C(t_i) - C_i]^2$$

*(**2** equation/**2** unknowns)*

Finally we have 2 equations and two unknowns and the identification can be performed. The details of the technique used will be developed later in the Materials and Method Chapter.

1.2.2.2. Influent parameters on water uptake

Water uptake is a diffusion mechanism which involves three main factors: the solvent that diffuses (water), the material that absorbs water (composite) and the surrounding environment (water or humid air). Each factor will influence the water uptake (kinetics, saturation level, etc). Among the parameters which influence these factors we can highlight three main ones: the temperature, the surrounding water concentration and, in the case of composites, the fibre orientations and fibre content.

Temperature:

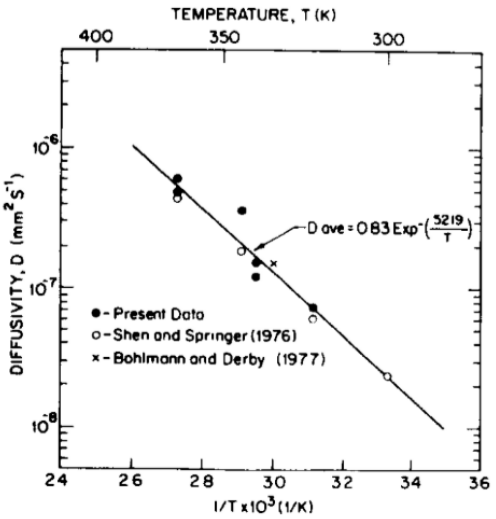

Figure 1.5. Diffusivity vs. inverse of the temperature [28].

In a polymer, the temperature modifies the chain mobility and therefore modifies the ability of water to diffuse. Previous studies have highlighted a strong influence of temperature on the diffusion kinetics in epoxy materials. They have showed that diffusion coefficients significantly increase when temperature increases and it is admitted that D often follows an Arrhenius law of the temperature (eg. [28]) described with Eq. 1.6. In this equation, Ea, stands for the activation energy and R is the ideal gas constant.

$$D = D_0 e^{-E_a/RT} \quad \textbf{Eq. 1.6}$$

On the other hand, the moisture concentration can slightly increase with temperature rise; nevertheless this variation is not as significant as that of the diffusion coefficient.

Water Concentration:

Water diffusion can be seen as a reaction which tends to reach an equilibrium between the thermodynamic potentials of water in the surrounding environment and in the composite or polymer material. The thermodynamic potential of a chemical species is directly dependent on its concentration. Therefore, water content in the surrounding environment influences the water diffusion through the saturation equilibrium and the diffusion kinetics. Loos and Springer have worked on this phenomenon by testing Graphite-Epoxy composites, and they predict an increase of maximum moisture content with water concentration (in [28]).

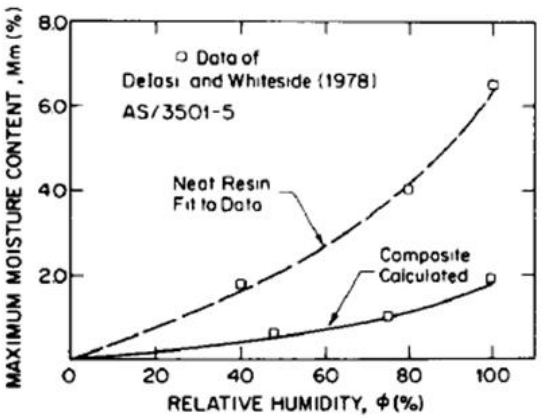

Figure 1.6. Moisture content vs. relative humidity from [28].

Example of sea water:

Seawater is the combination of multiple chemical components [29] therefore the water concentration (≈95%) is lower than in the case of deionised water. In the case of samples immersed in seawater, water content at saturation will decrease compared to immersion in deionised water.

Fibre orientation

The structure of a composite is by definition heterogeneous which induces heterogeneous moisture diffusions. If we consider a unidirectional composite with hydrophobic fibres perfectly aligned along one axis, diffusing molecules in the matrix in the fibre direction will not have any obstacle to their displacement. Therefore, diffusion in the

longitudinal direction is equivalent to the pure resin.

Transverse diffusion will be affected by the fibres which represent obstacles to water movement. In this case, diffusion is usually considered as equivalent in the y and z directions for unidirectional reinforcements as in Figure 1.7 ($D_z = D_y = D_T$) and different to that in the fibre direction, x ($D_x = D_L$). Eq. 1.4 can be replaced by Eq. 1.7 .

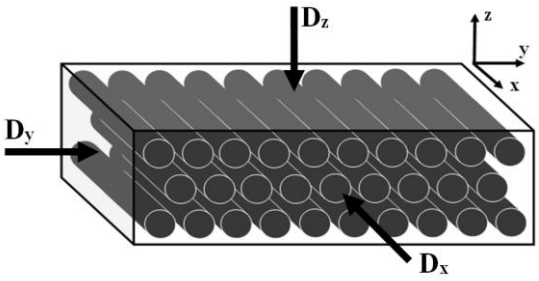

Figure 1.7. The main directions of diffusion in a UD composite material

Many studies have tried to quantify the transverse kinetics of diffusion considering an homogenous equivalent material. The main homogenization relations for transverse diffusion coefficient (D_T) are summarised in Table 1.3 from [30]. In all these theories the diffusion coefficient along the reinforcement (D_L) is considered as equal to that of the resin.

$$\frac{C_{3D}(t)}{C_\infty} = 1 - \left(\frac{8}{\pi^2}\right)^3 \sum_{i=0}^{\infty}\sum_{j=0}^{\infty}\sum_{k=0}^{\infty} \frac{exp\left(-\pi^2 t\left(D_T\left(\left(\frac{2i+1}{e}\right)^2 + \left(\frac{2j+1}{l}\right)^2\right) + D_L\left(\frac{2k+1}{L}\right)^2\right)\right)}{\left((2i+1)(2j+1)(2k+1)\right)^2} \qquad \textbf{Eq. 1.7}$$

Method	Effective diffusion coefficients	
Hahn-Tsai [31], [32]	$D_T = D_r(1 - 2.v_f)$	*For impermeable fibres*
Shen-Springer [33]	$D_T = D_r\left(1 - 2.\sqrt{\frac{v_f}{\pi}}\right)$	
Springer-Tsai [34]	$D_T = D_r\left(\frac{1 - 2.\sqrt{\frac{v_f}{\pi}}}{1 - v_f}\right)$	
Shirrel-Halpin [35]	$D_T = D_r\left(\frac{1}{1 + v_f}\right)$	
Rayleigh [36]	$D_T = D_r \frac{1 - v_f - 0.3058\, {v_f}^4}{(1 + v_f - 0.3058\, {v_f}^4)(1 - v_f)}$	

Table 1.3. Different homogenization methods taking into account the effect of fibres on the water diffusion in a composite (from [30])

The first method gives a simple relationship between the diffusion coefficient in the resin and

in composites. Moreover it has been shown that it can be demonstrated by a self consistent model, considering a resin material reinforced with cylindrical fibres in [32].

For the following study the transverse diffusion coefficient (D_T) will be determined with the expression from [31] and [32], and the longitudinal coefficient (D_L) will be considered as equal to the coefficient in the resin.

1.3. Partly-coupled behaviour

Before getting deeper in the literature review of coupled behaviour we will focus on semi-combined phenomena. Previous studies [37]–[53] have shown important impacts of the loading history of one type on the other. These can be divided in two sub-sections, corresponding to each case of pre-loading (humid or mechanical).

1.3.1. Water effects on the material properties

The action of water on polymers has been extensively studied by Verdu and colleagues [37], and they highlighted a correlation between the mechanical properties' change and water content in the material. They proposed two main degradation mechanisms induced by water uptake: one mechanical, and another chemical.

1.3.1.1. Water effects on mechanical properties

Studies on water effects on mechanical behaviour indicate two mechanical degradation types: plasticization of the material and differential swelling.

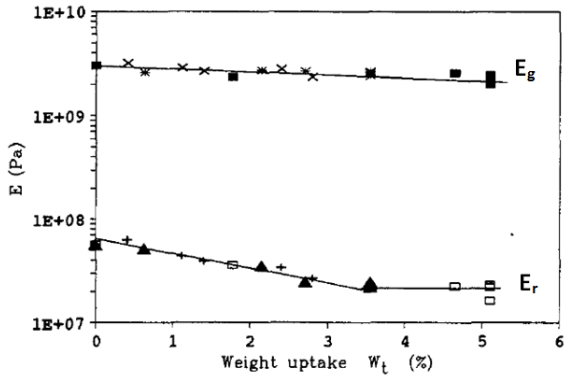

Figure 1.8. Young's modulus of epoxy resin vs. weight of water uptake in rubbery case (Er) and in glassy state (Eg) [38]

Plasticization is induced by water molecule uptake in the polymer which creates boundaries with polarized groups. This mechanism breaks secondary bonds between polarized groups from adjacent chains and partly destroys the mechanical cohesion of the network and

increases the molecular mobility.

This water uptake induces two phenomena: a mechanical property degradation (example in Figure 1.8) and glass transition temperature (Tg) decreases as showed by De'Nève et al. in [38].

Water included within the polymer network also creates swelling by chain stretching. The swelling intensity depends on the stretching potential of the polymer network and the higher the chain mobility, the more important will be the swelling. For example, in the glassy state molecular mobility is lower than in the rubbery state, so the swelling will also be lower (see Figure 1.8). This is a time and space dependant phenomenon linked to the water concentration which creates differential elongations from the edge to the centre and induces internal stresses.

In most cases, these phenomena do not change the polymer network in an irreversible way; the mechanical properties will be recovered after water desorption.

1.3.1.2. Chemical modification

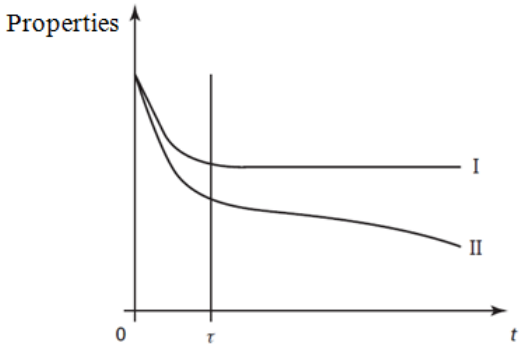

Figure 1.9. Mechanical properties as a function of exposure time for I – a material without hydrolysis and II – a material with hydrolysis (from [37]).

In some polymers there can also be degradation created by chemical reactions. Epoxy resins can be hydrolysed by water, by chain scission to form two shorter molecules: one linked to an OH^- group and the other to the H+ group of the water molecule. This reaction is quite slow at low temperature and can be activated by temperature rise. It is characterised by a loss in weight during diffusion or after saturation, identified on absorption curves by pseudo-saturation and weight decrease (e.g. curve 4 in Figure 1.4). Another way to highlight chemical degradation is by showing a difference between the dry material's weight before and after aging. This water action is translated in a loss of mechanical properties due to the reduction of chain linear density (Figure 1.9).

This type of degradation changes the material in an irreversible way (by bond

breakage) and therefore the mechanical properties will be changed even after water desorption.

1.3.2. Pre-stress effects on water diffusion

In terms of semi coupled behaviours some studies highlight an influence of pre stress on water diffusion in polymers and composites. Both experimental [26] and model studies [26], [39]–[43] are available on this subject, and among them we can distinguish two types of pre loading with or without damage introduction.

1.3.2.1. Pre-loading without damage

In the case of undamaged composites, two theories are used to quantify the effect of stress on water uptake:

- The first one is based on the free volume expression. Studies [42]–[45] have shown that diffusion depends directly on the free-volume variation. The link between maximum moisture content and free volume is proportional and is expressed as in Eq. 1.8. In this expression C_∞ stands for the moisture content at equilibrium in the polymer, v_f the free-volume fraction, ρ_w and ρ_m respectively used for the density of water and matrix resin.

$$C_\infty = v_f \frac{\rho_w}{\rho_m} \qquad \textbf{Eq. 1.8}$$

  The free volume theory also predicts the variation of the diffusion coefficient, which increases with the free-volume fraction, following Doolittle's equation, Eq. 1.9. In this equation, the index "0" stands for the unstressed state and σ is related to the stressed material, a is a proportional constant.

$$\ln\left(\frac{D_\sigma}{D_0}\right) = a\left(\frac{1}{v_{f0}} - \frac{1}{v_{f\sigma}}\right) \qquad \textbf{Eq. 1.9}$$

- The second theory is based on the expression of water chemical potentials, as in [40], [41]. As a chemical reaction, the water diffusion in pre-loaded materials is driven by the difference between the thermodynamic potentials of water in the polymer and in the surrounding environment. From this model, we can determine the water uptake at saturation and the diffusion kinetics.

Even if these theories predict the same effects of pre-loading on water diffusion, their main limitation is the lack of experimental studies to validate the models.

1.3.2.2. Pre-loading with damage

Theories on pre-stressing and damage effects on water diffusion have been developed either in a thermodynamic way in [46], [47], by considering diffusion inside cracks, by changing boundary conditions as Perreux et al. studied in [48]–[51]or seeing the diffusion as two interconnected diffusions in [52], [53].

Weitsman et al. [26], [39], [54] worked on the effect of damage on water diffusion in composites from 1987. Based on a thermodynamic approach, they developed a model for semi-coupled damage and water absorption in a transversly isotropic composite. In that case, they expressed the damage as a skew-symmetric tensor included in the model as an internal state variable.

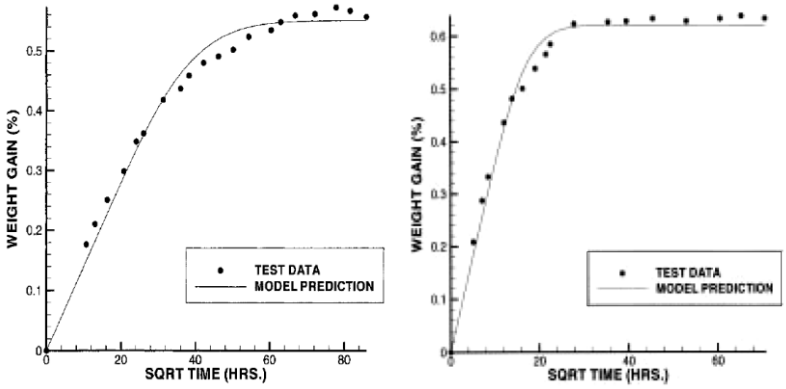

Figure 1.10. Predicted vs. measured weight gain in the composite for δ_1 = 0 crack per ply per cm [left] and δ_1 = 11.142 cracks per ply per cm [right] (from [47]).

The theory predicts an absorption enhanced by the presence of micro-cracks (damage). This phenomenon is also observed experimentally (in Figure 1.10) and seems intuitive since cracked regions could contain more water than undamaged polymer or composite. The model was defined for the case of static stress loading and could be transposed to any kind of static stress condition, such as hydrostatic pressure. Nevertheless, it was mathematically complex and was not amenable to a simple closed-form solution.

Later, Roy et al. [47] worked on a modelling method derived from Weitsman's work in [26]. Their aim was to develop a model with a simple closed-form solution; they obtained such a solution by representing damage as a symmetric tensor and an independent state variable. This model allows the effect of cracks on the water diffusion in a given material to be predicted as shown in Figure 1.10.

All these theories predict increased water uptake after damage introduction. Limited experimental work shows the same trend, and some studies [46]–[48], [50] have related

theory and experimental data with good correlations.

1.4. Coupled phenomena

In the marine environment water diffusion and mechanical stresses are never acting as separate or partly-coupled phenomena. Therefore this study focuses mainly on two fully coupled behaviours: water uptake under static tensile stress and diffusion under hydrostatic pressure. These phenomena correspond to real loading cases: hydrostatic pressure is involved for every underwater application, such as oceanographic instrument housings or submarine vessels, and immersed static tension tests represent one of the cases simulating the impact of external loads such as current, waves or wind on floating and immersed structures. Nevertheless experimental data on fully-coupled behaviours are very rare in the literature.

1.4.1. Immersed tensile loading

For the influence of static tensile stress on immersed samples reference [55] is one of the main experimental studies which focuses on fully coupled behaviour. In their work Weitsman et al. studied the stress assisted diffusion in a unidirectional carbon epoxy composites with reinforcement oriented at 90° to the stress direction. The tests were performed in an environmental chamber to impose a relative humidity of 97% and a temperature of 40°C. Water diffusion coefficient shows a proportional increase to pre-loading level (Figure 1.11).

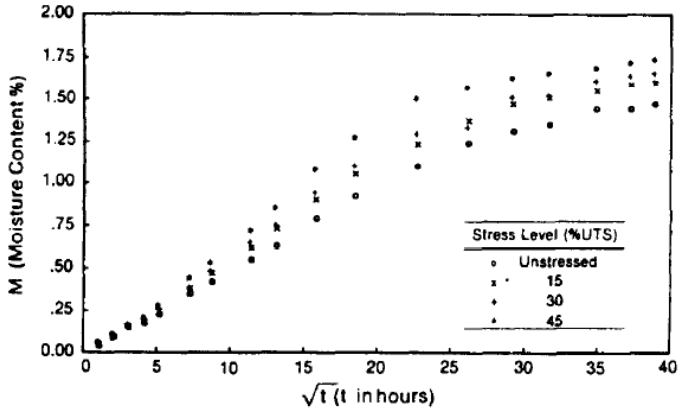

Figure 1.11. Moisture content vs. root of time under different stress levels (from [55]).

Weitsman worked on the theory to understand the phenomena involved in stress assisted diffusion in [39]. His model is based on a thermodynamic approach as in [26], [54] and shows interesting results compared to experimental data. Nevertheless it is still cumbersome to manage this method, especially due to the use of tensor expressions. Some other methods exist to couple both phenomena without damage, as [32], but none predict the impact of

damage and stress combined with water diffusion.

The experimental study [55]was performed under relative humidity conditions. In terms of coupled studies under immersion we only can find the study [56]. In this study samples were first saturated in seawater and maintained in this condition during the tests using a pocket filled with water, attached to the central region. Nevertheless this technique can only be used for short term testing otherwise there will be slippage issues of the pocket. Moreover, the tests were achieved in the saturated state whereas, in real conditions, many composite structures are immersed in seawater around 15°C or lower, and will therefore spend most or all of their lifetime in the transient stage of diffusion. However, those tests were performed under tension-tension fatigue loading on vinyl-ester composites, whereas the present study only treats the case of static loading on carbon/epoxy composites.

This brief literature overview highlights a lack of experimental data and theories for static tensile stress assisted diffusion. Therefore, the present study aims to investigate the water diffusion and mechanical stress from this coupled angle.

1.4.2. Hydrostatic pressure effects

The maximum service depth of composite use is constantly increasing in applications such as submarines, subsea oil industry structures or oceanographic profilers. Moisture diffusion in immersed composites is well known [57], [58] and its influence on mechanical properties has been studied [26], [59]–[63]. However, when we consider the moisture uptake coupled with hydrostatic pressure a general trend cannot be established. While the models we have presented in part 1.3.2 tend to predict lower moisture uptake at higher pressure, experimental results can show increases [64], no effect [65], or reductions [40], [65], [66]. The aim of the present work is to perform tests on different materials in order to understand this coupled phenomenon. Large differences in diffusion behaviour have been noted for different types of polymers. For example, Pollard et al. in [67] established a linear relationship between pressure and moisture content in saturated glass fibre reinforced polyester.

Other studies have focused on less common matrix resins: Whitaker et al. studied in [68] the combined influence of pressure and temperature on the diffusion parameters in a polyester containing styrene monomer. In this case, pressure reduces the diffusion coefficient in the specimens only for temperatures over 25°C, and has no influence on moisture saturation level.

Nevertheless, even for identical materials differences still exist, mainly induced by processing differences. For example, Avena and Bunsell in [65] studied the effect of

hydrostatic pressure on water diffusion in two types of glass fibre-reinforced composite based on the same epoxy resin reinforced either with un-sized fibres or with fibres treated with an organosilane size. Specimens were in the form of rectangular plates (150 x 25mm), 0.73mm thick and with a fibre volume fraction of 60%. Tests were performed in distilled water at 23°C under hydrostatic pressures of 1, 50, 100 and 200 bar.

Under these conditions the two materials reacted in a different way to pressure: for un-sized fibres samples, the diffusion coefficient and saturation level decreased with pressure rise whereas, for treated fibres, both diffusion parameters remained unchanged with respect to pressure variations. This clearly showed that the fibre/matrix interface can play a role in moisture ingress under pressure.

Davies et al. in [64] tested a filament wound carbon fibre-reinforced epoxy under a hydrostatic pressure of 100 bar at 60°C for 3.5 years. Specimens were square plates (50 x 50mm) with a thickness of 3mm. Their study showed a significant rise in saturation level with pressure rise for specimens either dry or previously saturated without pressure (Figure 1).

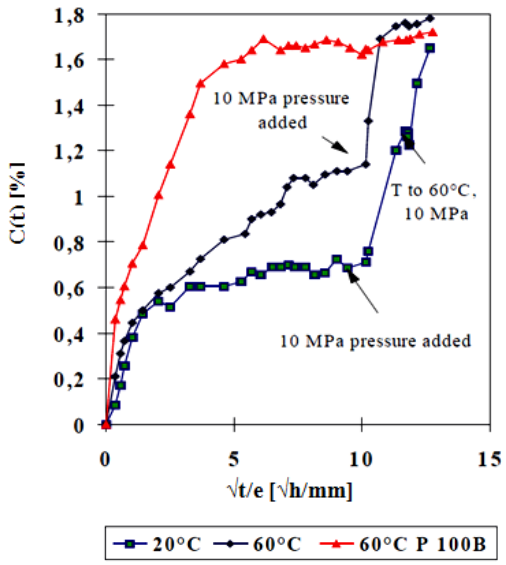

Figure 1.12. Pressure influence on water diffusion in dried carbon/epoxy specimens (red) and in previously saturated specimens (blue) from [64].

These studies illustrate the difficulty in establishing a clear, unique influence of the hydrostatic pressure on the water diffusion even for one type of material. Considering this background, in the following work three aspects will be considered. First, the experimental procedure is described: materials used, testing conditions, measurements, and first weight gain results are presented. Then the second part is devoted to the identification of the water diffusion laws and constants for each condition. Finally parameters which influence the water

diffusion under pressure are discussed.

1.5. Conclusion

The bibliographical study shows that a large body of knowledge is available on the mechanical behaviour of polymer composites, damage mechanisms and on water diffusion, treated as independent phenomena. The effect of loading on aged composites is also a well understood subject, as is the influence of ageing on global mechanical behaviour (Young's modulus, ultimate strength), local state of stress (swelling effects) and intrinsic properties (Tg). The influence of damage on water diffusion has also been well studied. Nevertheless, the influence of pre-loading without damage is still a subject with a lack of experimental data.

In real applications, composites are subjected to coupled effects of stress, damage and water diffusion. On this specific issue, there is a lack of information in the literature. Indeed even if some work has been conducted to predict the coupled behaviour (eg. [26], [40], [47], [66]), very few experimental data are available and they indicate some contradictions (e.g. hydrostatic pressure effects).

Therefore the aim of the present study is to develop experimental studies to highlight coupling effects of water uptake and stress, in order to establish a model to predict the coupled phenomena.

The approach will start with an overview of all the experimental techniques used in the study. Then, as in the literature review, the uncoupled behaviour will be examined first, followed by partly-coupled effects of one loading on the other. The final section will be focused on fully coupled phenomena: the hydrostatic pressure effects on diffusion and the water uptake in composites immersed and loaded under static tensile stress.

Chapter 2.

Materials and methods

This chapter describes all the composite and resin materials and test methods which were used in the study. First, the different materials tested are presented in two sections, one focused on the resin materials and the other on the composites. The manufacturing processes are introduced, followed by the description of the materials' intrinsic properties (density, fibre volume fraction, etc). Second, we list the standard methods used to get the physicochemical properties, followed by the test techniques employed to obtain the mechanical behaviours. Third, the different coupled and uncoupled ageing devices are explained. Finally, the different imaging techniques, useful for this work, are presented. All the tests performed and the numbers of specimens tested are reported in Appendix 1.

2.1. Materials

The biphasic property of composite materials has been discussed in the literature review. It highlighted the influence of both fibre and resin on the composite properties. Therefore, we choose to study both resin and composite in each case (mechanical behaviour, uncoupled and coupled ageing) in order to get all the properties useful for the modelling. The fibre was not studied since it is assumed to be hydrophobic and therefore does not significantly change the ageing behaviour (from uncoupled to fully coupled).

2.1.1. Neat epoxy resins

As noted in the literature review, all the materials studied are based on epoxy resins. This choice of this polymer was based on its good properties and widespread use. The main difference between epoxy resins is the nature of the hardener used and the chemical reaction involved in the curing. In this study, the matrices used are the results of the reaction between epoxy chains and polyamine hardeners.

Throughout the work one reference epoxy resin is studied but some additional polymer types are also investigated. The reference material is a commercial epoxy, from Huntsman (LY556), combined with the polyamine hardener XB3403 from the same supplier. The polymer is mixed with the hardener and placed in a heated vacuum chamber. The curing cycle is based on the supplier's datasheet (120°C during 2 hours). Once cured, the density of the system reaches 1.12 g/cm^3 and the plates obtained were 2.6 mm thick.

The additional materials were introduced in the study of coupling under hydrostatic pressure. The idea was to understand the influence of the process on the coupled water diffusion. The other resin type is also an epoxy (SR1500 – Sicomin) with a polyamine hardener (SD2505 – Sicomin). This resin is used for hand lay-up processing and is highly fluid, so it does not

require a vacuum chamber. These epoxy resins are cured in an oven at 60°C during six hours (as prescribed by the supplier) which gave materials with 1.10 g/cm^3 of density and a thickness of 2.7mm.

2.1.2. Composites

All the composite materials are based on one of the two epoxies previously introduced. The long carbon fibres have been chosen as reinforcements for their good mechanical properties for the loadings involved in marine applications. For the study, the carbon fibres are a common grade (TR50S, from Pyrofil^{TM}), and their properties have been described in the literature review in Chapter 1.

The main resin used is the LY556 (2.1.1) reinforced with woven carbon fibres. These composites are manufactured by a first pre-impregnation of the fibres followed by weaving. The pre-impregnated plies are then superposed on an aluminium plate in three different manners: $[\pm 45°]_6$, $[0°/90°]_6$, and a quasi-isotropic sequence [±45°; 0°/90°; ±45°; 0°/90°|0°/90°; ±45°; 0°/90; ±45°]. The composite plates are then cured in an autoclave with the same curing cycle as for the neat resin (120°C, 2h), a vacuum is used to minimise defects and a pressure is applied on a counter plate to homogenize the fibre concentration. The thickness of the samples obtained from this manufacturing process is 3.2mm for the quasi-isotropic sequence and 2.3mm in the other cases.

The study dedicated to the coupling effects between hydrostatic pressure and water diffusion introduced hand lay-up glass fibre composites. In this case, the material is based on the SR1500 (2.1.1) resin and unidirectional glass fibres stitched together by other fibres (glass). The same curing cycle as for SR1500 neat resin was applied (60°C, 6h), in oven without vacuum, we obtain plates with a thickness of 4mm.

2.2. Physicochemical properties

Physicochemical properties provide important information on the polymer structure, composition and degradation during ageing. For these reasons, several techniques were used to investigate these properties.

2.2.1. ThermoGravimetric Analysis (TGA)

The fibre fraction (in volume or mass) in a composite has a direct impact on many of its properties. In order to determine the mass fraction of fibres, TGA analyses were conducted on SDT Q600 equipment from TA instruments. This technique compares the initial composite

weight with the weight of fibres after heating to remove the matrix. To do so, the samples are heated at 600°C (burn-off of all epoxy resins) at 20°C/min under a nitrogen environment. This temperature is then held for 120 minutes to make sure that all of the matrix is removed.

2.2.2. Differential Scanning Calorimetry (DSC)

The glass transition temperature (Tg) is a key property providing information on the polymer degradation during ageing. There are different ways to define this temperature; among them we can quote the differential scanning calorimetry (DSC) method. This technique is based on the analysis of the heat capacity variation with the temperature. Tg is then defined as the inflexion point of the curve, this technique gives a purely thermal value of Tg. In the present study, the Tg was measured on Q200 DSC equipment from TA Instruments at a heating rate of 10°C/min from the ambient temperature to 300°C. For the dried polymers, we typically find a Tg of 60°C for SR1500 resins and 120°C for LY556 systems.

2.2.3. Dynamic Mechanical Analysis (DMA)

Another way to define the glass transition temperature is by a thermo-mechanical method such as DMA. This technique translates better the mechanical property degradation of the polymer during ageing. In this case, Tg can be measured with different methods: the storage modulus, onset point, the peak of loss modulus and the peak of tangent delta curve. In the study, all the Tg values from DMA analysis are determined with the storage modulus to get a value which represents the beginning of the mechanical property degradation.

Dynamic mechanical analyses were performed on DMA^{+} 150N equipment from Metravib. Measurements were made in tensile mode on neat LY556 resin samples of dimensions (30 x 10 x 2.6) mm^3 for different ageing times. These specimens were tested at 2°C/min over the temperature range from 20°C to 150°C, and stressed under a frequency of 1Hz and a dynamic strain amplitude of 5.10^{-3} The water desorption during DMA tests can be neglected here due to the short testing time (4 hours) compared to the desorption time.

The Tg study was not performed during hydrostatic pressure investigations and therefore the SR1500 epoxy was not studied.

2.3. Mechanical characterization

The first uncoupled behaviour studied is the mechanical response of materials under stress. Different types of loadings are studied, according to the predominant stresses involved in marine applications.

2.3.1. Sample preparation

After processing, the neat resin and composite samples were prepared in order to perform mechanical tests.

Neat resin plates were cut with a diamond miller on a CNC machine to obtain complex samples needed for the tensile tests.

Composite samples were obtained by cutting with a cooled diamond disc to the chosen dimension (with precision of ±0.5mm). For tensile testing, the specimens were end-tabbed with $[\pm 45°]_3$ glass/epoxy laminates made by hand lay-up. The tabs measure 50mm in length and 2mm in thickness, the edge near the specimen centre is tapered with a thin angle (around 15°) to reduce the stress concentration [69]. Finally, they were bonded to the samples with Araldite™ 420 A/B adhesive, in order to resist ageing effects.

For each test five specimens were tested, the results shown are the average and standard deviation is indicated on the property values (modulus, ultimate stress and strain). All mechanical tests were performed in a relative humidity and temperature controlled laboratory, according to the standards ($50^{\pm 5}$% RH and $21^{\pm 2}$°C). Moduli are determined in the strain range from 0.1 to 0.3%.

2.3.2. Quasi-static tensile tests

The tensile tests on the neat resin samples were performed according to the standard (ASTM D638 [70, p. 638]) on an electro-mechanical Instron testing machine. The specimens have a dumbbell shape, with the following measurements: 120mm in length, 10mm wide and 2.6mm thick. The strain is determined by image analysis, following the relative displacement between two marks on the specimen. The cross head speed was 5mm/min for tensile tests.

For quasi-static tensile tests on composites the loading rate and strain measurement method were the same as in the resin case, for the other parameters we followed the ASTM D3039 standard [71]. The measurements of the samples are 250 mm in length, 25 mm in width and with a thickness depending on the composite nature (see part 2.1.2).

2.3.3. Four point bending tests

Four point bending tests were performed on composite materials with Zwick hydraulic testing machines. The standard followed for this type of tests is the ASTM D6272 [72]. Specimens were rectangular plates of 120mm length and 15mm width, placed between a lower span of 100mm and an upper span of 50 mm. The cross head speed was 5 mm/min and

the centre deflexion was defined with the formulae from the standard.

2.3.4. Inter-Laminar Shear Stress (ILSS)

In the case of composite materials the interfacial properties between fibres and resin are key properties which can be affected by ageing. To estimate the interfacial behaviour of composites, ILSS tests were performed on both types of composite specimens following the standard method ASTM D2344 [73]. Samples tested have the following dimensions: 10mm span, 15mm x15mm square surface, and a thickness depending on the composite's types. Both series of tests were performed on an electro-mechanical Instron test machine with a loading speed of 5mm/min.

2.4. Ageing conditions

The second uncoupled behaviour of the study is the water diffusion in polymer based materials. In this section, the ageing protocol is described as well as the devices used for coupled studies.

2.4.1. Sea water ageing

The water absorption was determined from the weight measurements of square plates of (50x50) mm^2 in surface and with the thickness depending on the material. Weighing was performed periodically on a Sartorius LA310S device with a precision of 0.1mg. The diffusions were studied at different temperatures: 25, 40, 60 and 80°C, to verify the Arrhenius law of the diffusion coefficient. The specimens were immersed in natural sea water which is continuously renewed. For each temperature and type of samples, 3 specimens were used to measure the variability.

For the water uptake investigation the quantities are noted as follows throughout the study. *C(t)* represents the global water content in all the material, *W(t)* stands for the measured weight of the material (W_0 is the initial weight), *Vt* is the volume of the sample and *c(t,x,y,z)* corresponds to the local water content at a specific point in space. These quantities are linked together by the Eq. 1.5.

$$C(t) = \frac{W(t) - W_0}{W_0} = \frac{1}{V_t} \iiint c(t,x,y,z)\, dV \qquad \textbf{Eq. 2.1}$$

Another quantity is also used: C_∞ representing the specific designation for the maximal water content.

2.4.2. Ageing under static tensile stress

In this study, one of the coupled phenomena investigated is the effect of static tensile stress on water diffusion. For this type of tests, there is no standardised method and few previous studies. Therefore, we developed a specific testing device capable of loading immersed specimens. The specimens used are rectangular plates of 20 mm in width and 200 mm in length. They are clamped, maintained in position by clamping, and the loading is applied by a weight amplified by sheaves and a lever arm (the load on the sample is equal to 73 times the weight, Figure 2.1). Loads up to 50 kN can be applied on each one of the five specimens at the same time.

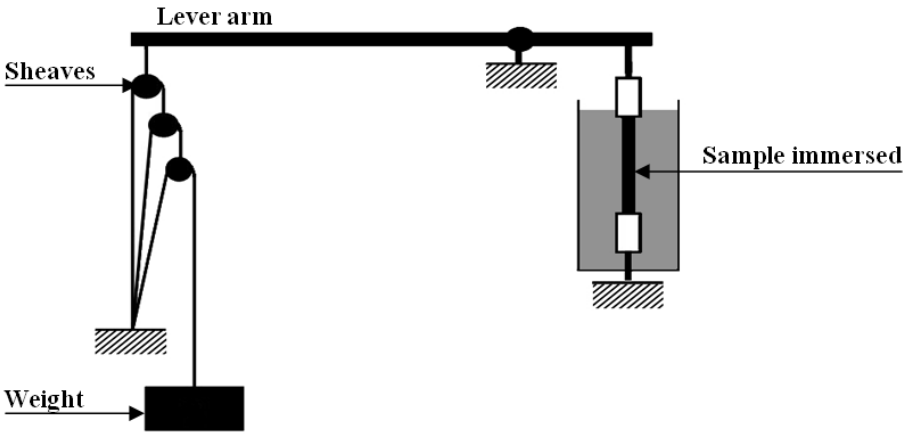

Figure 2.1. Scheme of the testing device principle

The immersion is ensured by a stainless steel tank placed around the samples, and filled with tap water renewed and heated at 60°C. The choice of tap water immersion was made in order to simplify the testing devices since this is a relatively new type of machine. Moreover, the diffusion differences between tap and sea water are well known.

Figure 2.2 Testing device to study static tensile loading effects of water diffusion

The samples were periodically removed and weighed on a Sartorius LA310S device after unloading. This procedure was applied on one specimen at each time to avoid long drying and unloading times.

2.4.3. Ageing under hydrostatic pressure

The other coupled study on neat resin and composite material focused on the effect of hydrostatic pressure on water uptake. The testing device for this study has also been specifically developed. It consists of pressure chambers made in stainless steel in which the samples are immersed, designed to support pressures up to 1000 bar (Figure 2.3). A special closure system has been designed to support such pressures and ease the opening, and reduce the handling time (Figure 2.4). The chamber is placed in an oven, in order to maintain the water temperature 60°C. A hand pump enables a specific pressure to be applied (Figure 2.3), controlled by a pressure sensor with sensitivity of 1 bar.

Figure 2.3. Pressure vessel in the oven [left] and the hand pump device to apply pressure [right]

The specimens were classical ageing samples (50 mm x 50 mm square plates), and they were placed in racks (Figure 2.4) in order to avoid contact between them, which could affect the diffusion behaviour. They were weighed periodically on a Sartorius LA310S device after depressurisation.

Figure 2.4. Specimens' rack used in the pressure chamber [left] and the specific lid employed [right]

2.5. Imaging techniques

Water diffusion is known to be dependent on the presence of defects in the polymer. Therefore, imaging techniques are used to characterise damage, voids and inclusions in the materials. Different methods have been used, depending on the type of defects and their localisation in the materials.

2.5.1. Optical microscopy

Void ratio in composites was determined by optical microscopy analysis of polished sections. The microscope used was a LEICA DM ILM and the images obtained were analysed using the software *ImageJ*. The volume ratio of voids is obtained by following the AFNOR NF T57-109 [74], and is a mean value of at least 10 images for each sample.
Examples of both composites' polished sections (carbon/LY556 and glass/SR1500) are shown in Figure 2.5.

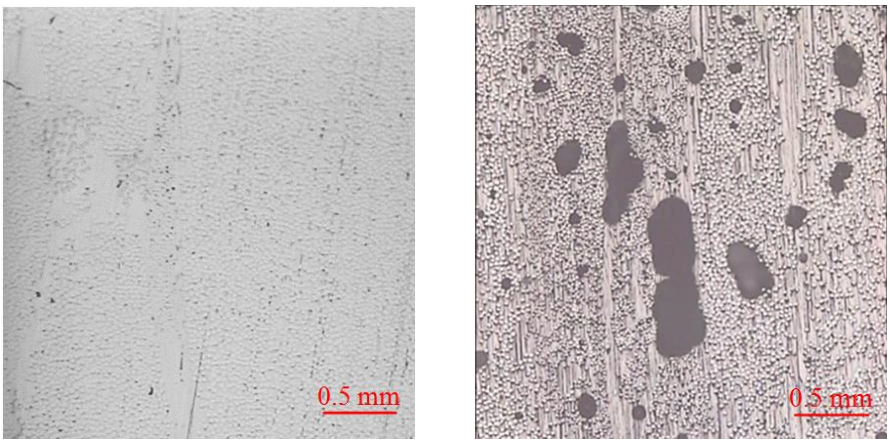

Figure 2.5. Polished section of Carbon/Epoxy (LY556) [left] and Glass/Epoxy (SR1500) composites [right]

The main drawback of this method is the fact that it is destructive and therefore the surface fraction of voids is only known after testing.

2.5.2. UltraSonic C-scan (US)

Ultrasonic C-scan analysis is a non-destructive method which highlights the presence of voids through changes in attenuation. Moreover, this technique can be useful in the case of investigation of water uptake in voids. Indeed, ultrasound propagates in water and not in air which will highlight differences between results for wet and dry samples.
However, the results obtained are only qualitative and not quantitative, unlike optical microscopy analysis. A Sofratest™ ultrasonic inspection system was used to measure through the thickness attenuation using 2MHz focused transducers by placing the plates in a water

tank and scanning their surface.

2.5.3. X-Ray tomography

X-ray tomography is also a non destructive method to get information on the defects in the structure. This technique allows a 3D reconstruction of the sample morphology, with a contrast based on the difference of densities between regions. The device used in the study was a GE Phoenix V-TOM-X240 which can analyse 50x50mm specimens with a resolution of 28 mm^3/voxcel (for beam characteristics of 100 kV and 280 mA).
Unlike US analysis, X-Ray tomography does not reveal the presence of water inside the voids.

2.5.4. Crack density analysis

The previous methods detect voids and defects in unstressed samples. Nevertheless, in the study, we have to establish the crack density during tensile tests. We used a technique already studied by Tual et al. in [17], the sample edge is painted to highlight the appearance of material cracks (black regions in Figure 2.6). The specimen edge is first polished in order to get a perfectly planar surface on which to apply the paint. During the tensile test, images are saved every second with a Basler™ camera of 2040x1080 pixels resolution.

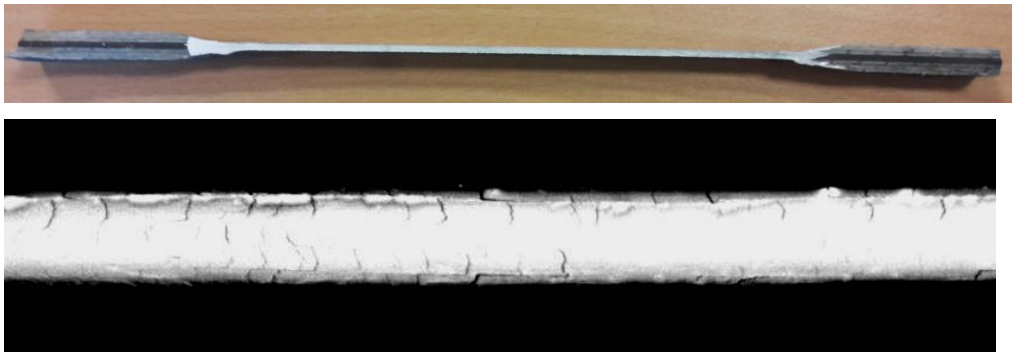

Figure 2.6. Specimen with the edge painted [top] and an image taken during the tensile test of a ±45° composite [bottom]

The second step is different from the method applied in the previous study [17], it involves the calculation of the surface ratio of damage. This cracked area is analysed by image subtraction compared with a reference (the image of the sample before loading) using a Matlab™ routine. A threshold is applied on this subtraction defined by the operator in order to highlight the crack and erase the parasitic defects. The threshold adjustments are applied based on the image of the first crack appearance which represents the worst case in terms of crack density calculation. An area analysis is then performed, to obtain the proportion of

black regions (cracks).

2.6. Modelling

COMSOL™ Multi-physics software was used to model the water diffusion inside the neat resin and polymer in the study.

First, it provided the theoretical water uptake in the composite based on the diffusion in the resin and on the theory of fibre influence on the diffusion. These results were then compared to experimental results and discussed.

Second, two coupled models were developed using COMSOL™ Multi-physics to take into account the effect of porosity on diffusion under hydrostatic pressure. One model is homogenised and the other represents porosity with its interaction with the composite.

Both models are managed in two dimensions: the diffusion in the samples is invariable by translation along the axis orthogonal to the fibres.

Chapter 3.

Uncoupled behaviour

In order to get background knowledge on the coupled behaviour, we first study the responses as uncoupled phenomena.

The water uptake is investigated in the first section for each material, from the neat resin to the quasi-isotropic composite. The presentation is divided in two parts. First, we present the experimental results and the identification of the diffusion law. Then, we discuss identifications using the resin diffusion coefficient, based on multiscale analytical relationships.

In the second section, mechanical responses are studied for all the materials. The main part of this section is dedicated to tensile tests, in order to have the unaged properties for further consideration of the coupling. The remaining part is focused on some additional composites' mechanical tests to get information on interfacial and compression properties. These properties can also have an impact on the global behaviour of immersed composites.

3.1. Water diffusion

Epoxy matrix is known to be a hydrophilic polymer, as highlighted by the literature review (Chapter 1, [21], [22], [38]). To understand the diffusion behaviour of materials based on this type of resin, we study the diffusion of water into both the neat polymer and the composites.

First, experimental results and identification of water diffusion behaviour are presented; then, predictive models are tested and discussed.

3.1.1. Experimental results and identification

To begin with the uncoupled water uptake study, we first present the experimental data obtained by weighing the samples during diffusion. Then, these results are used to identify an existing diffusion law (introduced in the literature review), in order to predict the water uptake in the different samples.

3.1.1.1. Experimental results

In composite materials, the fibres present a hydrophobic phase while the resin can take up a significant water content. For these reasons, all the moisture uptake values are calculated with the initial resin weight (taken as reference weight); in the case of composites the fibre weight is subtracted from the total. In this case, we can summarise the water uptake quantity by the expression Eq. 3.1; with Xm_r the weight ratio of resin (equal to 1 for neat resin), and W_0 the initial sample weight and $W(t)$ its weight at time t.

$$C(t) = \frac{W(t) - W_0}{W_0 . Xm_r} \qquad \textbf{Eq. 3.1}$$

The experiments have been performed in water at 60°C for the neat resin materials and at different temperatures in the case of composites. These experimental results will give information on the impact of the heating at 60°C on the water diffusion (diffusion speed and maximal water uptake). To get a clearer view of the results, Figure 3.1 presents average moisture uptake in composites with an error bar corresponding to the standard deviation of the values of the five samples tested for the same conditions.

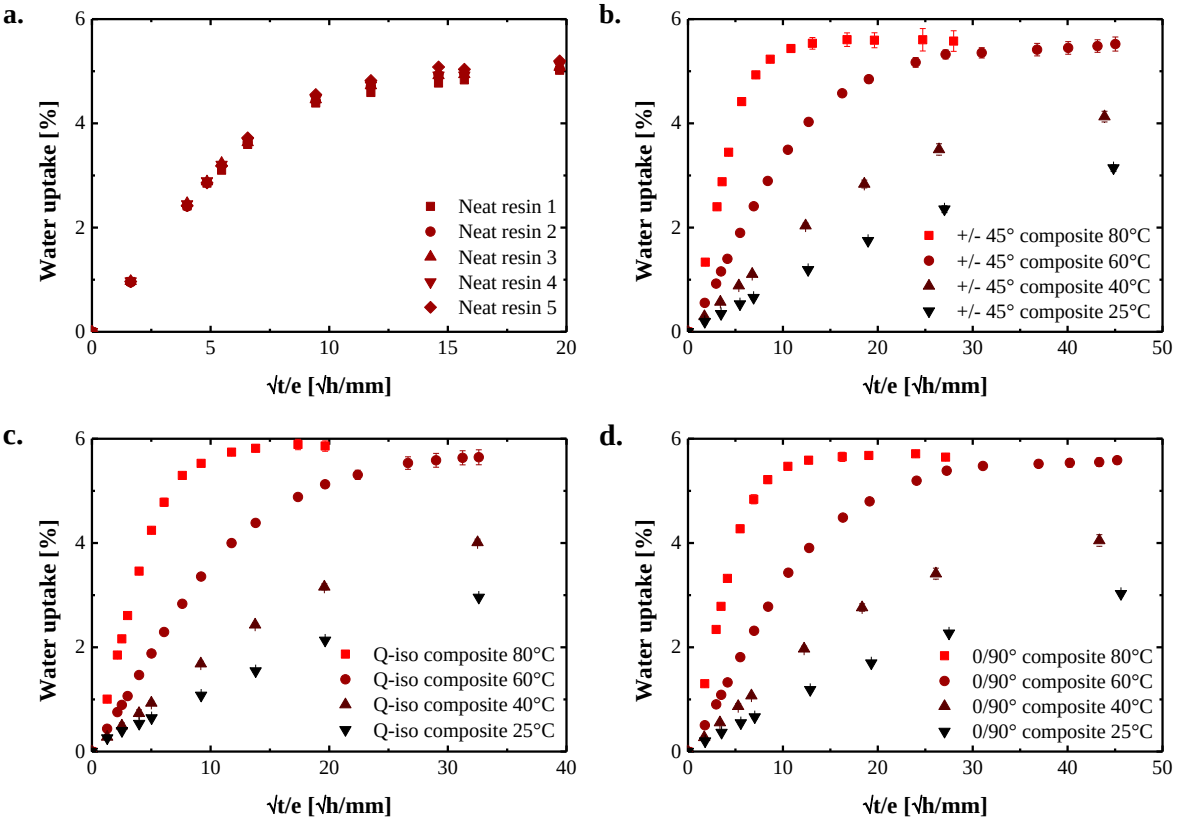

Figure 3.1. Water uptake in neat resin at 60°C [a.] and +/-45° [b.], Q-iso [c.] and 0/90° composites [d.] at different temperatures.

Water uptake in all the materials follows the same trend with square root of time. The initial moisture increases linearly up to half of the maximal water uptake. The second section is characterised by a transient non linear behaviour, for normalized water uptake values from 0.5 to 1. Finally, the last stage highlights a water uptake which stabilises to reach a maximum value.

Two qualitative observations can be made from these results. First, the maximal water uptake in neat resin is of the same order of magnitude as in the matrix of the composites. Second, at raised temperatures the water uptake speed increases significantly, as previously shown in the

literature review.

This type of behaviour has already been highlighted in the case of water diffusion in epoxy resins, and presents all the characteristics of a Fickian diffusion. Therefore, the identification was made using the parameters of Fick's diffusion law.

3.1.1.2. Identification

The aim of identification is to get the best representation of the experimental values with a model curve. In the present study, we use a least squares method to optimise the curve shape based on experimental data. This technique consists of minimizing the difference between water uptake values from theory ($C(t_i)$) and experiments (C_i) at every time (t_i) of weight measurements. These differences are minimised by searching for the diffusion parameters (D and C_∞) which minimise the sum of the square differences (S).

$$S = \sum_{i=0}^{i_{max}} (C(t_i) - C_i)^2 \qquad \textbf{Eq. 3.2}$$

The samples used are square plates with low thicknesses (e) compared to the other dimensions (at least sixteen times lower), therefore the diffusion can be simplified as a one directional diffusion. Moreover, as previously noted, epoxy based materials often show a water diffusion which follows Fick's law (Figure 3.1), which leads to a water uptake defined by the expression Eq. 3.3.

$$C(t_i) = C_\infty \left(1 - \left(\frac{8}{\pi^2}\right)^3 \sum_{k=0}^{\infty} \frac{exp\left(-\pi^2 t_i D \left(\frac{2k+1}{e}\right)^2\right)}{(2k+1)^2} \right) \qquad \textbf{Eq. 3.3}$$

The identification process begins using arbitrary diffusion parameters chosen to be of the order of magnitude of the real ones, and the maximum moisture content is taken to be equal to the maximal experimental value. For the initial value of the resin's diffusion coefficient we use a value of $10^{-13} m^2/s$ which is of a similar order of magnitude to values in the literature.

Then, we randomly generate a large number of parameters in an interval centred on the chosen parameters.

The next step consists of the identification of the association of parameters with lower S value in order to replace the previous ones for the next iteration.

Finally, this routine is run until either it reaches a maximum number of iterations, defined by the user (5 in our case), or until the S value becomes lower than a minimum defined as equal to 10^{-15} in the study.

		25°C		40°C		60°C		80°C	
		M_∞ [%]	D [m²/s]	M_∞ [%]	D [m²/s]	M_∞ [%]	D [m²/s]	M_∞ [%]	D [m²/s]
Neat resin	*Average*					4.84	7.5E-13		
	Standard deviation					*0.10*	*2.791E-14*		
±45° composite	*Average*	3.25	4.35E-14	4.16	7.12E-14	5.36	2.08E-13	5.56	1.13E-12
	Standard deviation	*0.06*	*1.961E-15*	*0.11*	*8.64E-16*	*0.06*	*2.24E-15*	*0.14*	*8.09E-14*
0/90° composite	*Average*	3.23	4.38E-14	4.17	7.06E-14	5.50	1.85E-13	5.63	1.11E-12
	Standard deviation	*0.03*	*4.041E-16*	*0.11*	*2.12E-15*	*0.12*	*1.36E-14*	*0.05*	*8.01E-14*
Q-Iso composite	*Average*	3.22	6.54E-14	4.32	7.94E-14	5.50	2.24E-13	5.79	1.16E-12
	Standard deviation	*0.03*	*3.70E-15*	*0.06*	*4.596E-15*	*0.12*	*1.12E-14*	*0.07*	*7.31E-14*

Table 3.1. Identified diffusion coefficients [m²/s] and maximal water uptakes in the materials [%] at different temperatures.

The identification of diffusion parameters is performed on water uptake values from each sample. The average value and standard deviation are stored in Table 3.1 by material type and water temperature.

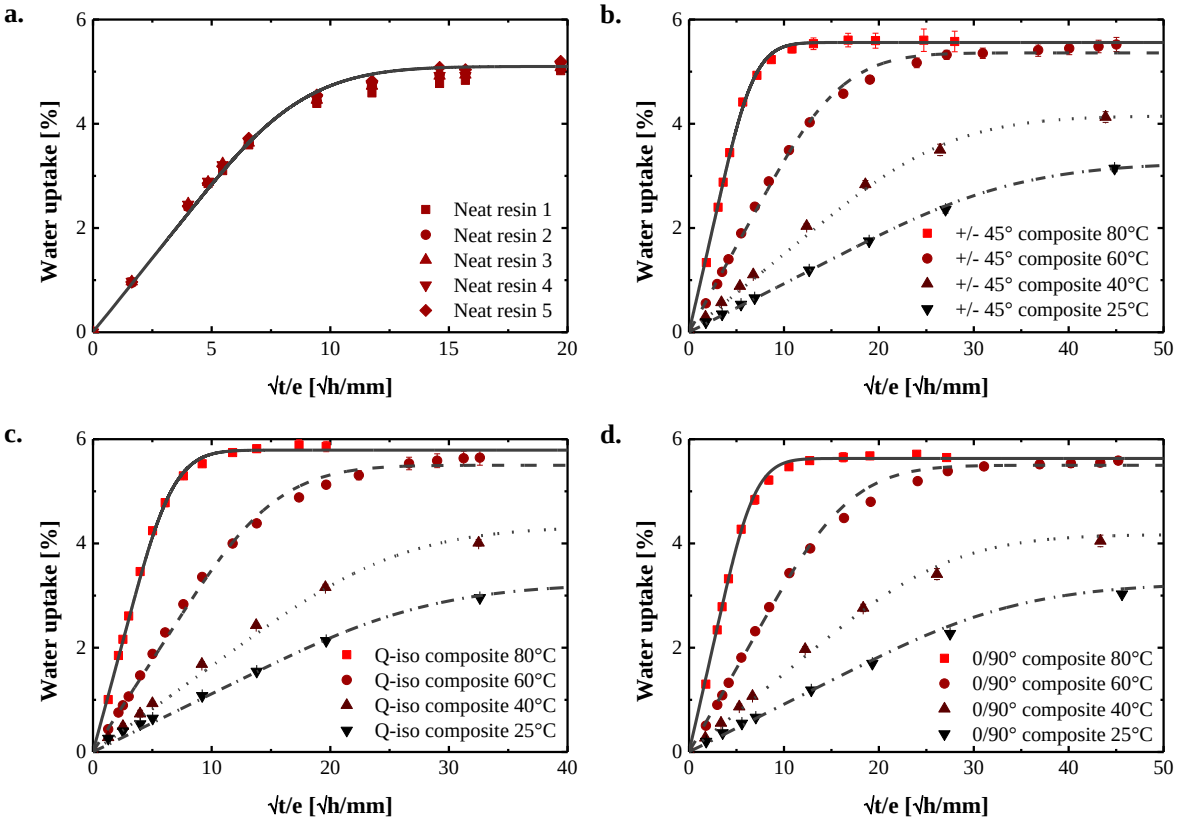

Figure 3.2. Identified diffusion laws in neat resin at 60°C [a.] and +/-45° [b.], Q-iso [c.] and 0/90° composites [d.] at different temperatures.

The literature review highlights a water entry speed reduced by fibre inclusion and the values from Table 3.1 confirm this tendency.

The maximal moisture content obtained with identification appears to increase with heating (Table 3.1). This trend was also noted in previous work on the influence of temperature on

water diffusion as in [75]. Nevertheless, it has to be taken with caution since the identification is made on non-saturated curves in the case of 40 and 25 °C. This fact can exaggerate the differences between saturation values. Finally, these results also highlight the similarities between the diffusion behaviour in all the composites. This can be explained by the transverse orientation to the diffusion of fibres for each type of composite studied.

3.1.2. Prediction and discussion

Identification results provide a good understanding of the water diffusion in epoxy based materials. Nevertheless, this technique needs experimental water uptake data for each material type.

There is another way to get diffusion behaviour of the composites with fewer experiments. To do so, we can use a prediction based on the identification made on the neat resin samples. This method is based on the theory quantifying the impact of fibres on the diffusion coefficient.

3.1.2.1. Prediction of diffusion coefficient in composites

Method	Effective diffusion coefficients
Hahn-Tsai	$D_t = D_r(1 - v_f) \quad = 3.00 \times 10^{-13}\ m^2/s$
Shen-Springer	$D_t = D_r\left(1 - 2.\sqrt{\frac{v_f}{\pi}}\right) \quad = 9.45 \times 10^{-14}\ m^2/s$
Springer-Tsai	$D_t = D_r\left(\frac{1 - 2.\sqrt{\frac{v_f}{\pi}}}{1 - v_f}\right) \quad = 2.36 \times 10^{-13}\ m^2/s$
Shirrel-Halpin	$D_t = D_r\left(\frac{1}{1 + v_f}\right) \quad = 1.88 \times 10^{-12}\ m^2/s$

Table 3.2. Methods used to predict the diffusion coefficient in composites

Several previous studies [31], [33]–[35] established expressions to link diffusion coefficients in neat resin and in composites (Chapter 1). In the present study, we consider the diffusion in only one direction: through the thickness of samples, which is orthogonal to fibres in all the composites. This section aims to compare the main theories (summarised in Table 3.2) predicting the water diffusion coefficient orthogonal to fibres direction. For these predictions, the diffusion coefficient in the neat resin (D_r) is taken from the identification results (Table 3.1) and the fibre volume ratio (V_f) is evaluated by ATG analysis for each type of composite (Table 3.3).

Moreover, the composite materials do not show any voids (Figure 3.4) and therefore the maximum moisture content in the matrix should be the same as in neat resin. Nevertheless Table 3.1 highlights a slight difference between composites and resin maximum water uptake. This difference could be induced by interfacial effects, heterogeneous resin weight ratio, void inclusion in the matrix and also increased by the identification method. For these reasons, the maximum water uptake is defined from the average value identified on the composite materials.

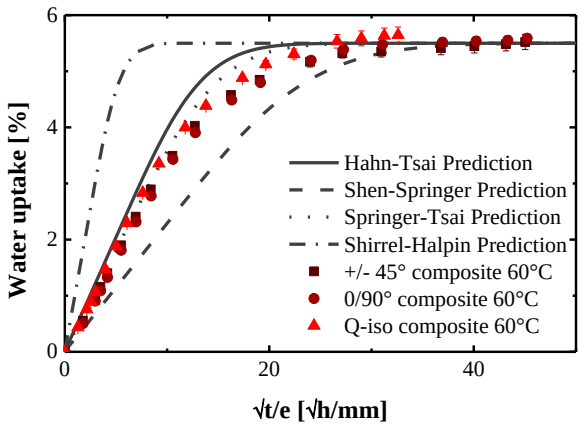

Figure 3.3. Water diffusion curves in composites with diffusion coefficients from prediction [lines] compared to experimental values [points]

Each curve of Figure 3.3 represents the water uptake predicted by the models reported in Table 3.2. The most relevant predictions are based on the Hahn-Tsai and Springer-Tsai models (cf. Figure 3.3). For further consideration, we chose to use the Hahn-Tsai model which gives a simple relationship between the diffusion coefficients in the resin and in composites. Moreover, it has been shown that this expression can be demonstrated by a self consistent model, considering a resin material reinforced with cylindrical fibres (cf. Chapter 1 [32]).

3.1.2.2. Discussion

	Resin content by weight [%m]
+/-45° composites	$30^{\pm 0.5}$
Q-iso composites	$33^{\pm 0.7}$

Table 3.3. Resin weight ratio and their variation intervals for three different measurement locations.

First, prediction curves have been established using the maximum water uptake, due to its deviation from the neat resin values.

The resin weight fraction has been determined in each plate in 3 different locations (sides, centre and corner) in order to evaluate its variability. The results shown in Table 3.3 highlight very low differences between these values, therefore the resin weight ratio variations cannot be the reason for the additional water uptake in the composites.

The presence of voids can induce a water uptake increase due to water molecule inclusion in the defects. To evaluate this property for ±45° and quasi-isotropic composite, we analysed images from optical microscopy and X-ray tomography of samples before ageing and without loading history. Neither investigation detected any void presence in either composite (Figure 3.4).

Nevertheless, the void detection is limited by the resolution of the techniques used, and could miss some defects significant enough to modify the theoretical water uptake in composites.

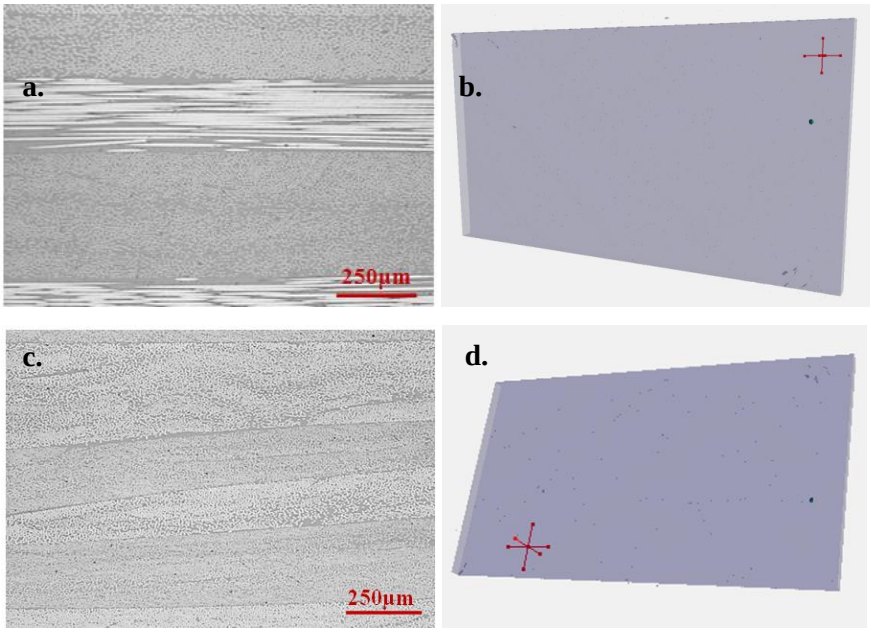

Figure 3.4. Defects and voids analysis in Q-iso materials, by optical microscopy [a.] and X-ray tomography [b.] and ±45° composites, by optical microscopy [c.] and X-ray tomography [d.]

3.2. Mechanical properties

In offshore applications, in addition to water diffusion, materials are also subjected to significant mechanical loadings. Depending on the type of structure and environmental conditions, the stresses can be highly variable (tension/bending/compression, static/dynamic or combined). The present study aims to understand the static tensile behaviour in uncoupled, semi and fully coupled configurations.

The following section is dedicated to the mechanical behaviour of neat resin and composites based on LY556 epoxy. First, we describe their damage and mechanical response during

quasi-static tensile tests. Second, four point bending and inter-laminar shear stress tests are studied to get complementary information on interfaces and in compression.

3.2.1. Tensile mechanical behaviour

Although stresses can be diverse, the present study only focuses on tensile loading, which is the most frequently encountered loading, the best understood behaviour and with the most extensively developed testing techniques. The next subsection is dedicated to tensile behaviour and the damage created by this type of stress.

3.2.1.1. Tensile tests

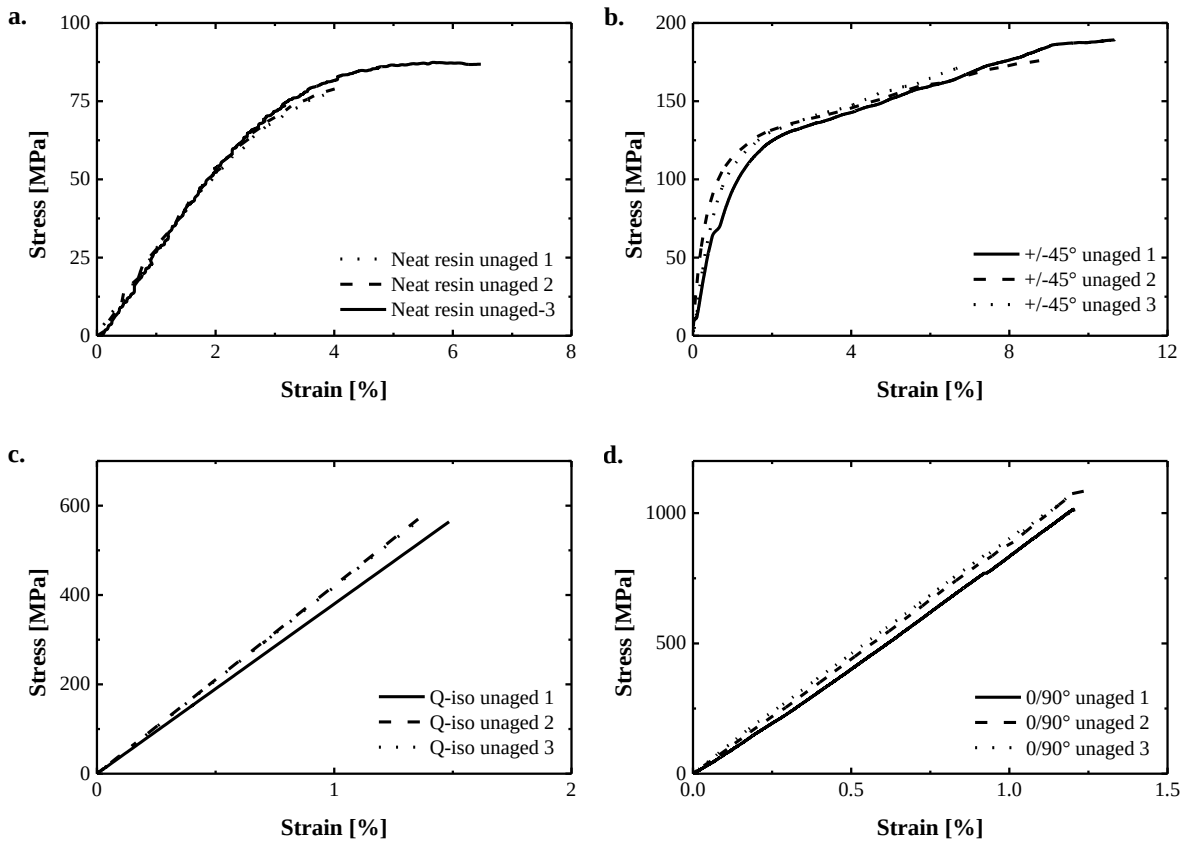

Figure 3.5. Stress-strain curves from tensile tests performed on neat resin [a.], ±45° [b.], Q-iso [c.] and 0/90° composite [d.]

Tensile tests were performed on each type of material, from neat resin to quasi-isotropic composites, all unaged and stored for one week in a 0%RH and 60°C environment. These results will be used as the reference for future tensile test results partially or totally coupled. The identified average values and standard deviations of ultimate stress and strain, yield stress and strain, and modulus are reported in Table 3.4.

Among the mechanical responses of tested materials, we can distinguish two cases: on one

hand, the neat resin and ±45° composites show a non-linear behaviour, and on the other hand, 0/90° and quasi-isotropic composite which show a linear behaviour (Figure 3.5).

Neat resin shows a linear elastic behaviour during a first phase until the stress reaches a yield limit (around 75MPa). This first stage of the mechanical response corresponds to a purely elastic behaviour of the polymer. Moreover, to get information on the type of behaviour involved in the non linear part of the curve, we use cyclic load-unload testing. Samples are cycled up to four different stresses (20, 50, 70 and 80 MPa) and after each unloading, the permanent strain is recorded. These tests (Figure 3.6) reveal no permanent deformation and therefore no plastic behaviour during quasi static loading.

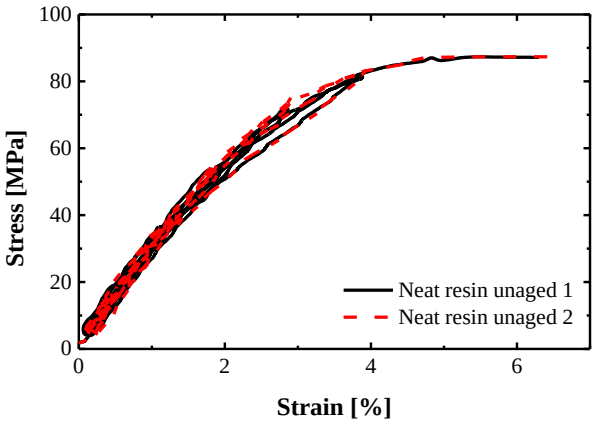

Figure 3.6. Stress strain curve for cyclic tensile tests on neat resin samples.

Materials reinforced with ±45° woven fibres also present an initial linear elastic behaviour, up to 70 MPa, which coincides with the matrix yield (75MPa). The second linear part of the stress/strain curve translates the fibre reorientation, possibly also including de-cohesion with the matrix, and characterised by large strain variations and a decrease in specimen width.

In contrast to these behaviours, quasi-isotropic and 0/90° composites present stress/strain responses which are purely linear and elastic. We can deduce that the classic stress/strain representation (Figure 3.5) does not give any information on the damage in the specimens after applying a certain stress.

3.2.1.2. Damage

We know that damage and voids modify the water uptake in polymers and composites. For future semi and fully coupled studies, it is crucial to quantify the damage creation inside the resin during tensile tests (in neat polymer or composite samples).

For neat resin specimens, the exact crack density cannot be easily quantified. Nevertheless, damage can be detected in the form of whitening of the specimen during the

tensile test. To enhance this phenomenon, the epoxy samples were polished to obtain a good transparency (Figure 3.7) and images were taken during the tensile tests. In the case of LY556 epoxy resin, no whitening has been detected during tests (Figure 3.7), and therefore no macroscopic damage is created by quasi static tension.

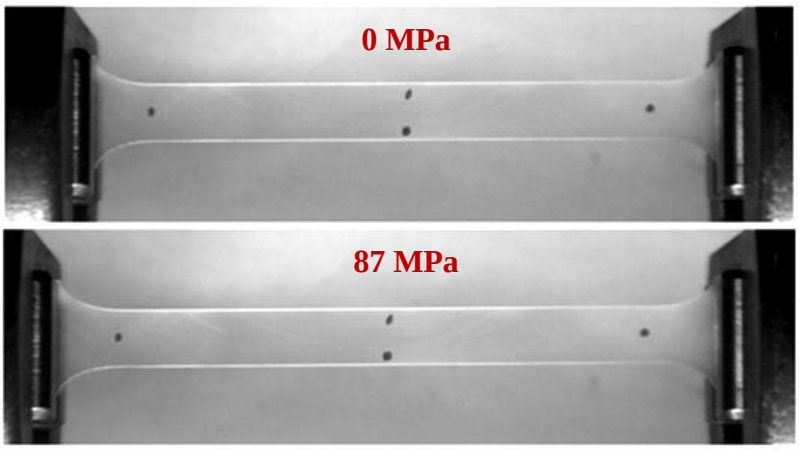

Figure 3.7. Image of specimen transparency during a tensile test on neat resin: at the beginning [upper] and just before failure [lower]

In the case of composites, the damage can be quantified with a 2D optical technique, detailed in Chapter 2. This damage identification technique has been chosen to be able to identify damage in ±45°, 0/90° and quasi-isotropic composites. In the case of ±45°composites, we compared this technique to the modulus variation criterion (not usable in the case of the other composites with 0° fibres).

For the 2D optical damage identification, the damage ratio is typically a function of stress and strain and it is characterised by three stages. Under a certain threshold limit (characterised by σ_d and ε_d), composites do not show any cracks, and above this threshold, damage D increases with a constant speed of the stress ($\dot{D}_\sigma$) and strain ($\dot{D}_\varepsilon$). We can also distinguish another stage between these two phases characterised by a non-linear transient behaviour of the damage function. All the parameters of the damage law used in the following paragraphs are reported in the Table 3.4.

During tensile tests in ±45° composites (Figure 3.8) the neat resin is highly loaded, due to the orientation of fibres away from the loading direction. In such cases, the first damage appears for low stresses (around 150MPa) and strain (4%) compared to the ultimate value (180MPa stress and 9% strain).

The ultimate crack density is very high (30%), since fibres allow maintaining the composite cohesion at stresses much higher than the ultimate stress of the resin (90MPa stress and 5% strain).

The damage/strain speed in ±45° materials is quite low compared to other composites (5.5%/$\%_{strain}$). The non-alignment of the fibres with the loading direction introduces considerable damage in the resin allowing reinforcements to realign and therefore inducing large strain which lowers the damage speed. For its part, the damage/stress speed reaches high values compared to other composites (0.75%/MPa). The damage mechanisms involved during ±45° composite testing, do not allow high loads whereas crack density is greatly increased.

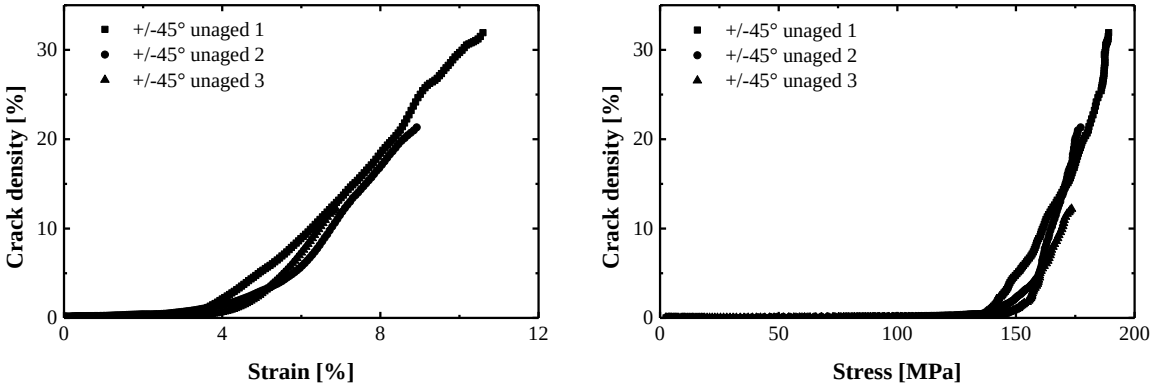

Figure 3.8. Surface crack density for tensile tests on ±45° composites as a function of strain [left] and stress [right]

The non-linear behaviour of ±45° composites also allows damage to be quantified by axial modulus variations. This technique is based on quasi-static cycling tests during which the modulus is recorded at the beginning of each loading cycle. The damage value *D* (Table 3.4) is assessed by calculating the loss of modulus compared to the reference value (during the first loading).

The results shown in Figure 3.9 highlight an important loss of stiffness for loadings up to 120MPa, the modulus seems to stabilise above this stress. This behaviour is entirely different from the crack density changes, shows large variability between the different specimens (Figure 3.9 [right]) and can only be used for ±45° composites (no modulus variation for quasi-iso and 0/90° materials). For these reasons, this damage value will only studied for the former, and will be referred to as an additional way to evaluate damage.

To conclude, the resin of ±45° composites is the most highly damaged matrix, and its damage/stress speed reaches the highest values.

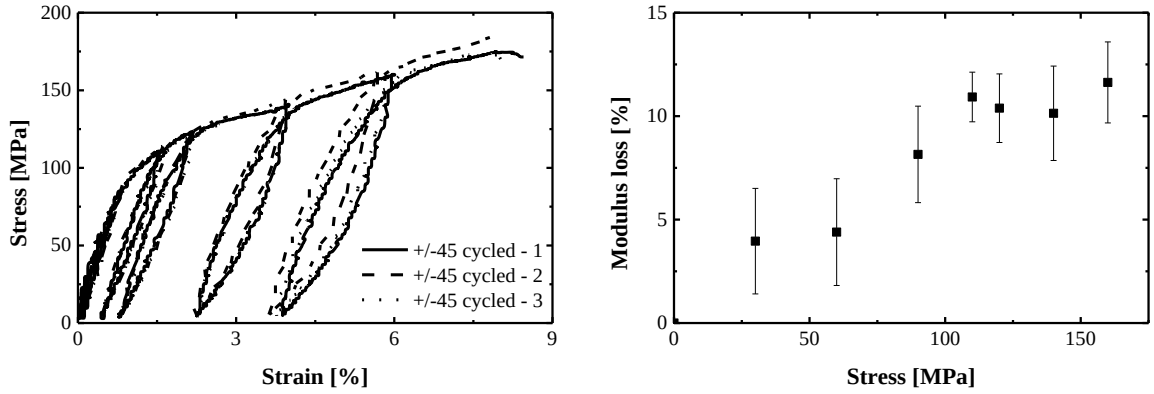

Figure 3.9. Stress/strain curves for cyclic quasi-static tensile tests [left] and modulus loss during these tests [right] on ±45° composites

The 0/90° material is the composite with the highest density of fibres aligned with the loading direction. In this case, the stress is mainly supported by reinforcements and the composite behaviour has a tensile response highly dependent on the fibres. In contrast, the matrix is only weakly stressed and damage density remains very low during tensile loadings (0.2% for the maximal damage).

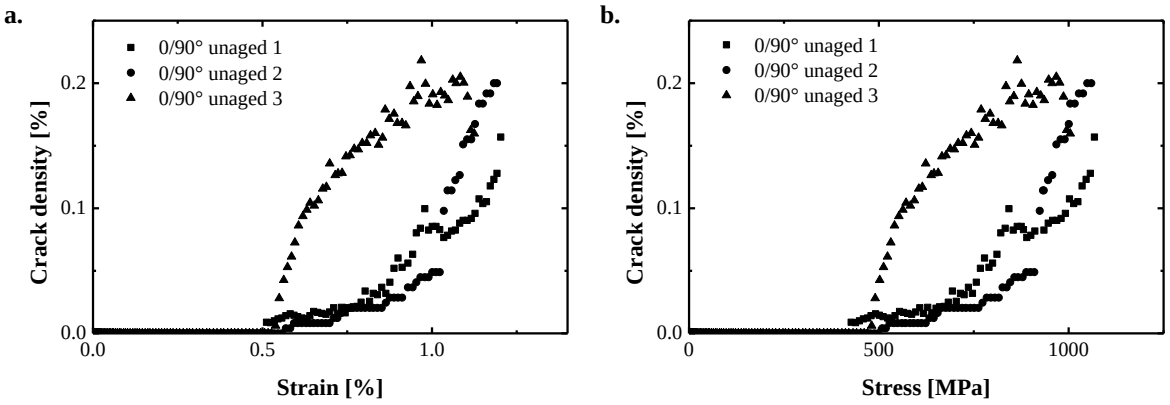

Figure 3.10. Surface crack density for tensile tests on 0/90° composites represented as a function of strain [a.] and stress [b.]

The damage threshold appears for higher stresses than in other composites. Nevertheless, the damage remains very low and therefore the threshold cannot be considered as significant.

For this type of material no damage development speed can be established, due to the large variation from one specimen to another (Figure 3.10). This scatter is due to the woven structure: this construction concentrates stresses in the fibre crossing points, and the damage variation will be highly dependent on the distance of these crossing points from the surface on which the damage is studied.

For future investigation on semi and fully coupled behaviour, we will keep in mind that the 0/90° composites' matrix is very weakly damaged during a tensile test compared to other

composites.

Finally, the quasi-isotropic composite construction is a combination of both the previously described materials' sequences (±45° and 0/90°) and their volume proportions are equal.

In this case, the density of fibres aligned with the loading direction is lower than for 0/90° samples, therefore the resin is more highly stressed which induces more damage (maximum damage is equal to 20%). We can also emphasize that the maximum damage level is higher than the sum of the ultimate damage in both sequences considered separately. Indeed, if we consider one half of the material damaged up to 30% (as +/-45° specimens) and the other half with a maximal crack density of 0.2% (0/90°composites), the entire damage ratio should reach 15.1%. The measured ultimate damage reaches higher values because of the 0/90° plies which allow the quasi-isotropic specimens to be loaded above the breaking state of ±45°composites plies, which will reach damage values higher than 30%.

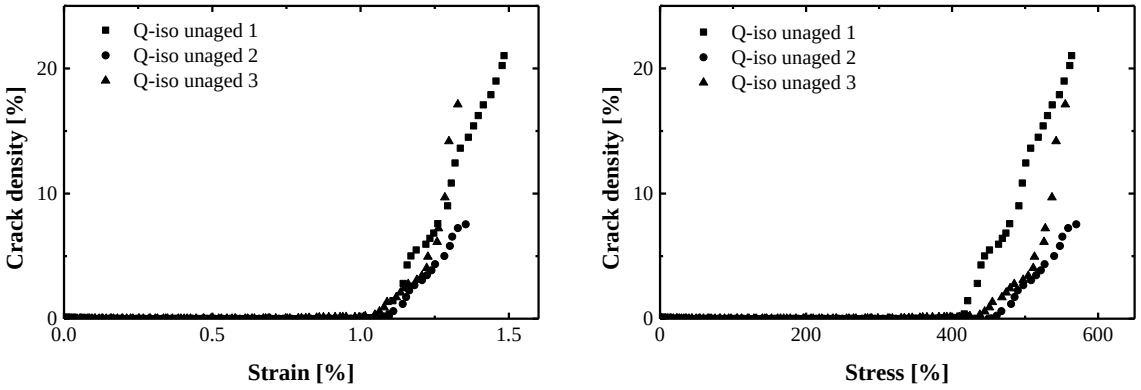

Figure 3.11. Surface crack density for tensile tests on Q-iso composites as a function of strain [left] and stress [right]

			Break stress [MPa]	Break strain [%]	Modulus [GPa]	Yield stress Stress [MPa]	Yield stress Strain [%]	Damage threshold Stress [MPa]	Damage threshold Strain [%]	Damage speed Stress [%/MPa]	Damage speed Strain [%/%]	Ultimate crack density [%]
Unaged	Resin	Average	81.4	4.8	2.8	75.3	3.6					
		Standard deviation	*5.3*	*1.4*	*0.0*	*2.2*	*0.2*					
	+/-45	Average	179.7	9.0	18.5	120.3	1.5	147.7	4.3	0.75	5.5	27.4
		Standard deviation	*8.7*	*1.7*	*6.5*	*2.5*	*0.3*	*6.0*	*0.4*	*0.18*	*0.2*	*10.8*
	0/90°	Average	1036.9	1.2	85.3			472.3	0.5			0.2
		Standard deviation	*42.6*	*0.0*	*6.1*			*41.6*	*0.0*			*0.0*
	Q-iso	Average	566.7	1.4	40.7			448.3	1.4	0.13	51.3	15.2
		Standard deviation	*3.2*	*0.1*	*2.3*			*28.7*	*0.5*	*0.05*	*21.0*	*6.9*

Table 3.4. Tensile properties of neat reins and composites samples unaged

Quasi-isotropic composites have a damage threshold limit close to their failure point, and their ultimate crack density is comparable to the case of 0/90° composites. Indeed, as long as

the fibre material remains undamaged, 0/90° plies support the load. Nevertheless, when fibres start to damage the stress is transferred to +/-45° sequences which crack instantaneously, resulting in the failure of the sample. This phenomenon induces high damage/stress and strain speeds.

To summarise on quasi-isotropic materials, we can note that the damage initiation is controlled by the 0/90° composites plies, while the ultimate damage ratio translates behaviour closer to that of ±45° samples.

3.2.1.3. Damage characterisation

The previous section established the damage behaviours of each composite type from results of 2D crack density measurements. Nevertheless, this technique does not give information on the crack nature and localisation. This section focuses on the characterisation of damage from images of the cracks used previously, and combined with X-ray tomography and 3D reconstruction.

2D analysis

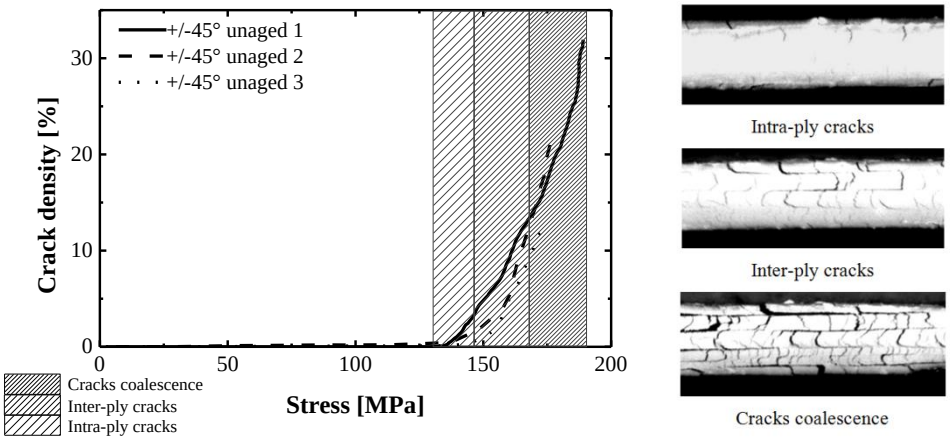

Figure 3.12. Type of cracks in +/-45° composites during tensile tests.

Images from crack analysis can provide information on the type of damage involved during a tensile test. The typical stages we can identify with a 2D study on ±45° samples are: intra-ply cracking, inter-ply cracking, and crack coalescence. For each test, images were manually analysed in order to identify these different stages of damage (Figure 3.12); the limit values are reported in Table 3.5. The damage occurs in three steps, first the resin starts to fail inside the plies creating transversal cracks. Second, the resin failures inside the cracks induce larger deformation of the specimens and the plies start to slip with respect to each other and longitudinal inter-ply cracks appear. Finally, the cracks propagate and start to merge, which

decreases the number of cracks and increases significantly their area.

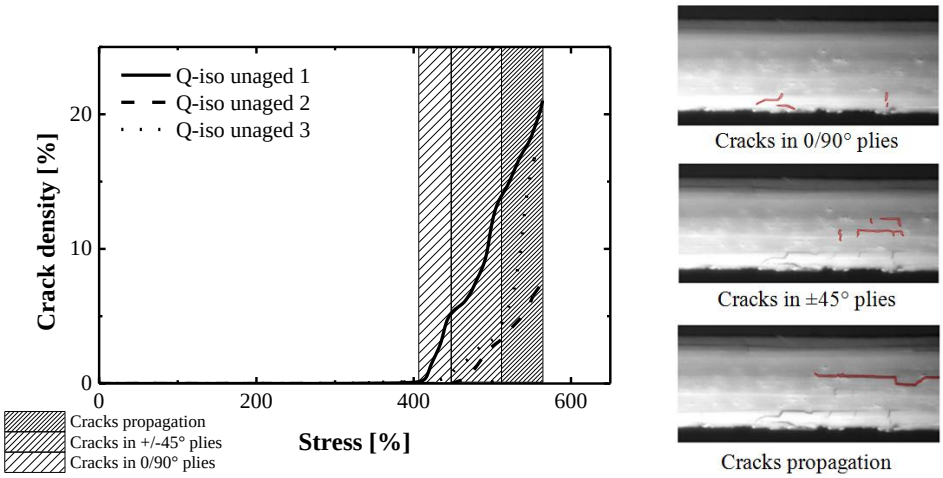

Figure 3.13. Type of cracks in quasi-iso composites during tensile tests.

		Stress limit ±45° [MPa]
Intra-ply cracks	Average	128.0
	Standard deviation	*9.6*
Inter-ply cracks	Average	148.5
	Standard deviation	*6.9*
Cracks coalescence	Average	172.5
	Standard deviation	*9.6*

		Stress limit Q-iso [MPa]
Cracks in 0/90° plies	Average	413.5
	Standard deviation	*24.8*
Cracks in ±45° plies	Average	458.6
	Standard deviation	*20.8*
Cracks propagation	Average	516.4
	Standard deviation	*22.0*

Table 3.5. Stress limits for each type of cracks in ±45° [left] and Q-iso [right] composites

For tests on quasi isotropic composites, the limits between the different stages of damage are less distinct. The different woven constructions represent a barrier to the intra-ply crack propagation, whereas the inter-ply propagation does not have any obstacle. For this reason, when a crack appears, the preferential type of propagation is delamination. Nevertheless, we still can identify the location of the cracks to determine at which stress each type of ply starts to damage. The quasi-isotropic composite of the study has the 0/90° plies on its external face and the ±45° plies are located in the centre. The crack characterisation highlights a first damage appearing inside the 0/90° plies, rapidly followed by a crack initiation in the centre of the sample, and finally these cracks propagate rapidly. The strain is lower than the ±45° damage threshold, therefore the cracks appear first in the 0/90° composites above its damage threshold in terms of strain (0.5 to 1%). Later, the damaged 0/90° plies no longesupport the loading and cracks appear in the ±45°construction which are stressed above their threshold stress value .

This analysis gives important information on the crack types and their location in the

composite during a tensile test. Nevertheless, we have to emphasis the fact that it does not represent the damage density within the sample volume.

3D analysis

As the 2D study does not provide information on the crack shape inside the sample, the cracks are considered to extend across the specimen width. To get more information on the damage inside the specimen volume, we use X-ray tomography analysis and 3D reconstruction of samples pre-loaded to different levels. The pre-stresses were chosen to correspond to each stage of damage propagation identified in the previous sub-section.

In the case of ±45° composites high crack density can be identified after unloading (Figure 3.14), even for a pre-stress of 60MPa. For materials stressed below 60MPa, the crack density estimated by 2D analysis does not reveal everything. Indeed, crack density by surface analysis reports no damage, whereas volume investigation shows some voids. Moreover, cracks introduced by pre-stressing are not entirely closed after unloading (Figure 3.14) and therefore they can affect the water diffusion.

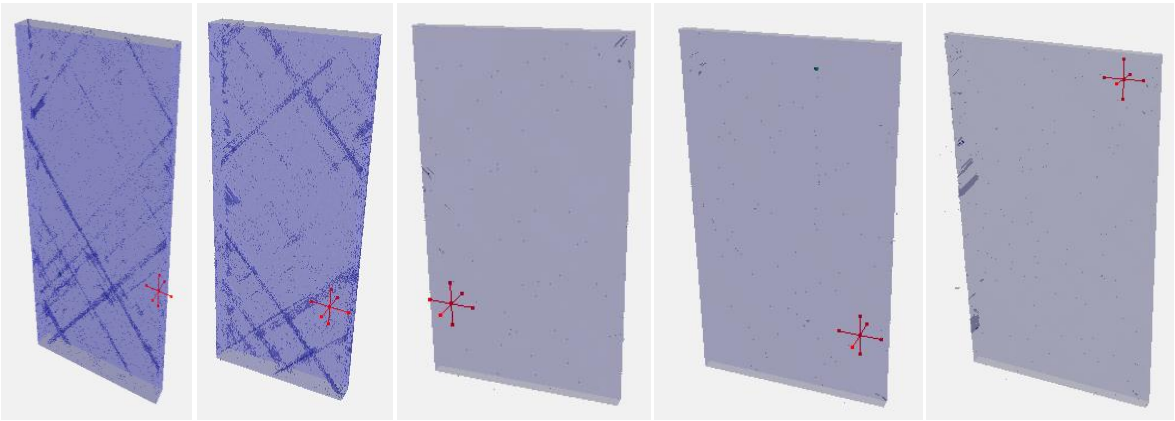

Figure 3.14. X-Ray tomography analysis of (from left to right): ±45° composites pre-stressed at 60 and 130 MPa, and quasi-isotropic composites pre-stressed at 0, 280 and 450 MPa.

In the case of quasi-isotropic samples, there is no sign of cracks (Figure 3.14), which is surprising as at this stress level cracks could be detected visually on the specimen edges during loading. It thus appears that cracks in this composite close up completely when the load is removed. This phenomenon has to be taken into account for future analysis of water diffusion after and during loading. Indeed, it could create significant differences in water uptake between the two cases.

3.2.2. Other mechanical behaviours

The mechanical behaviour studied in this work is mainly the tensile response, but in addition we studied the interfacial and compression/flexure properties of the composites before and after ageing in order to determine the degradation of other properties and understand possible side effects of these degradations.

3.2.2.1. Inter-Laminar Shear Stress (ILSS)

The inter-laminar properties of composites depend directly on the resin behaviour and therefore can be highly affected by water ageing. Moreover, these properties are essential in most marine applications, since they are involved as soon as there is a strain difference between plies. ILSS tests do not investigate in-plane properties of the plies and therefore we can use any type of composite if it has the same inter ply properties. In the study, we tested quasi-isotropic materials.

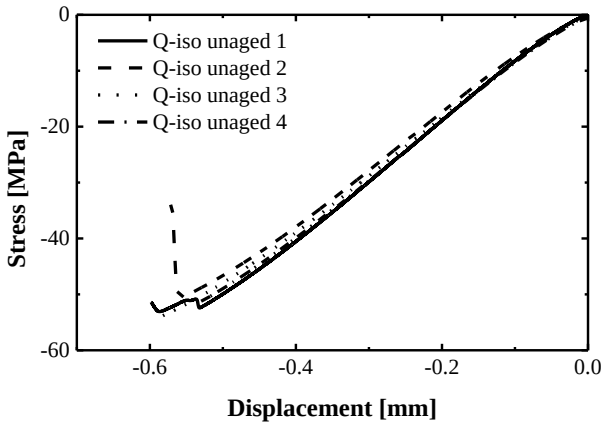

Figure 3.15. Stress/strain curves from ILSS tests on Quasi-iso composites

The tests are based on the standard ASTM D2344 [73], previously mentioned in Chapter 2, which establishes the expression of the inter-laminar shear stress as a function of the loading and sample dimensions. The results obtained in Figure 3.15 will be used as a reference for tests on aged samples, in order to evaluate the degradation of the mechanical inter-laminar properties of the composites after water ageing.

3.2.2.2. Four points bending

Compressive stresses are commonly encountered in the case of offshore applications. For example, in the case of deep water immersion, the hydrostatic pressure induces important compressive stresses as well as other more common loadings involving flexure (e.g. current on turbine blades). The aim here is to understand the compressive behaviour in the optimum

configuration, therefore, we studied the mechanical response of 0/90° composite samples using a four point flexure test.

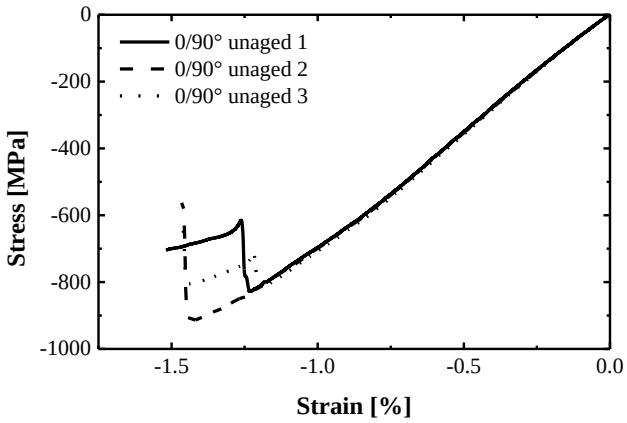

Figure 3.16. Stress/strain curve of four points bending tests on 0/90°composites

The compressive stress in the upper plies is determined by the expression Eq. 3.4 as a function of the applied load at failure *F*, the width of the samples l_w and its depth l_d. In order to determine whether the ply in compression is the first to break, we analyse the location of the failure on the samples visually.

$$\sigma = \frac{3.F}{4.l_d.{l_w}^2} \qquad \textbf{Eq. 3.4}$$

It appears (in Figure 3.17) that the failed plies are the ones subjected to compression stress, only one of the samples showed broken plies stressed in tension and compression. Therefore, the ultimate values obtained in Figure 3.16 are compression failures of 0/90°woven plies. We also can notice some delamination near the failure zone which can lower the ultimate values, especially for future tests after water ageing.

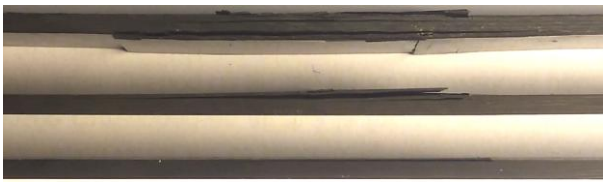

Figure 3.17. Type of failure involved during four point bending tests the upper face of the samples are stressed in compression while the lower are in tension.

3.3. Conclusion

The present chapter aimed to establish the bases of mechanical and diffusion behaviour in the composites. Both subjects were studied separately in order to get the intrinsic uncoupled properties.

The water diffusion was studied first. It appears in the study that for epoxy based

composites, we can model the water diffusion with a Fickian law prediction. This technique has been verified for temperatures from 25 to 80°C and for neat resin, ±45°, 0/90° and quasi-isotropic composites. The temperature rise induces an increase of the diffusion kinetics and the inclusion of reinforcements in the resin reduces the diffusion kinetics and the latter appears to be well represented by Hahn-Tsai prediction.

Second, mechanical behaviour of the studied materials was investigated under quasi-static tension, flexure and shear stress. Tensile tests show stress strain curves with non-linear elastic behaviour for neat epoxy, linear elastic trend for quasi-isotropic and 0/90° composites. On the contrary, ±45° samples show a more complex behaviour; with a first linear part, followed by a non-linearity and permanent deformation in a second phase. Tension is the mechanical behaviour mainly studied in this work; therefore it has been coupled with a damage investigation. This showed that neat resin does not present macroscopic damage, in contrast to the composite samples. The latter appear to have comparable damage propagation behaviour composed of two stages: initially the specimens appear to be unaffected by tensile stress, then the damage ratio start to increase until failure. In the last stage, the damage increases linearly with strain and stress in the case of ±45° and quasi-isotropic composites while we cannot distinguish a clear trend for 0/90° composite. Finally, by studying the type of crack introduced during a tensile test, we show that the ±45° plies are the most damaged, this introduces important crack density in quasi-isotropic and ±45° composites compared to 0/90° samples.

The study of inter laminar shear stress and four point bending were respectively performed on quasi-isotropic and 0/90° composites. These tests were performed in order to compare them to tests on aged samples, and conclude on the effect of water diffusion on these behaviours.

In this chapter we have established the uncoupled reference behaviours, which will be used for the following studies on semi-coupled and coupled behaviours.

Chapter 4.

Semi-coupled behaviour

In the previous section it was assumed that water diffusion and mechanical behaviour were independent phenomena. In practice, these may be combined; therefore, the following section is devoted to semi-coupled behaviour to get closer to the real applications and limit the number of complex phenomena introduced. The idea is to understand the influence of one phenomenon on the other. In this study two semi-coupled sequences are treated: pre-loading impact on the water uptake, and ageing influence on the mechanical behaviour.

The influence of mechanical stress on moisture content is studied as follows; first experimental results are reported and diffusion laws are identified on these data. Second, the results obtained for maximum water uptake and diffusion coefficient are discussed for each type of material. Finally, we conclude on the influence of pre-stress for each orientation of fibres in the plies.

4.1. Water diffusion in pre-stressed materials

Results in Chapter 3 showed high crack density in composites after loading. Previous studies presented in Chapter 1 [48], [52], [76], [77] have shown a variation of the water uptake with voids, defects or crack inclusions in composites. The two phenomena combined can result in water diffusion in the composites being highly affected by tensile pre-stress. The following section aims to understand the link between the two behaviours.

4.1.1. Experimental results and identification

The experimental and identification methods used are similar to those used in Chapter 3. The samples were first pre-stressed at 2 or 3 different pre-loading levels (see Figure 4.1). They were then unloaded and immersed to study their water diffusion behaviours, and finally identification was performed on each type of specimen and for each pre-stress level.

4.1.1.1. Experimental results

First, neat resin samples were investigated. In this case, pre-loading does not induce cracks, therefore semi-coupled results will only give us information on the pre-loading impact on water uptake (with no crack introduction).

The pre-loading levels were chosen to be equal to 30 MPa, 70 MPa and 80 MPa which respectively correspond to 37, 87 and 98% of the ultimate stress. These stresses were chosen in order to have one loading in the linear part of the tensile behaviour, another just above the yield stress and the last one close to failure.

Water uptake results in Figure 4.1 show no significant variation for any loading level.

Therefore the water uptake behaviour in neat resin epoxy is assumed not to be affected by tensile pre-stress, and can be predicted with the same law as unloaded specimens.

The ±45° composites are the most damaged materials when they are stressed in tension (cf. Chapter 3). Moreover this composite does not have reinforcement in the loading direction; there is a significant permanent strain for pre-loading levels above its yield limit. Therefore, the cracks created by tensile stress will stay "open" after unloading (as X-ray images show in Chapter 3).

The pre-stress levels were chosen to get one value clearly below the damage threshold (60 MPa: 33% of ultimate stress), another corresponding to the first crack appearance (130 MPa: 72% of ultimate stress) and the last one between the damage threshold and failure (160 MPa: 88% of ultimate stress).

Results in Figure 4.1 show maximum moisture content increased by pre-stress and an acceleration of the diffusion kinetics, even for samples stressed below the damage threshold (60MPa).

In the case of 0/90° composites crack density analysis indicated very low damage when specimens were stressed in tension (cf. chapter 3). In addition, the high density of fibres oriented in the tension direction gives samples a complete recovery after unloading. The study of these samples gives information on water diffusion in slightly damaged materials with cracks closed after unloading (cf. Figure 3.14 in Chapter 3).

Pre-stress levels correspond to samples loaded up to the first crack appearance (520 MPa: 50% of ultimate stress), between damage threshold and failure (780 MPa: 75% of ultimate stress), and just before failure (830 MPa: 80% of ultimate stress).

Low crack density combined with no permanent strain after unloading indicates no significant difference between pre-stressed and undamaged samples (see identified parameters in next section 4.1.1.2).

Quasi-isotropic samples showed significant damage introduction during tensile tests: up to 20% of the edge surface for unaged materials. Nevertheless, the fibres oriented in the tension direction enable the composite to recover completely after unloading. These two phenomena combined give information on water diffusion in damaged materials with cracks closed after unloading (cf. Figure 3.14 in Chapter 3).

The pre-loading levels are defined to correspond to samples pre-stressed and undamaged (280 MPa: 50% of ultimate stress) or pre-stressed and damaged (450 MPa: 80% of ultimate stress).

The water diffusion kinetics increase (Figure 4.1) in pre-loaded quasi-isotropic materials as pre-loading level increases. The second stage of diffusion data highlights a maximum

moisture content which can be considered as unchanged by pre loading

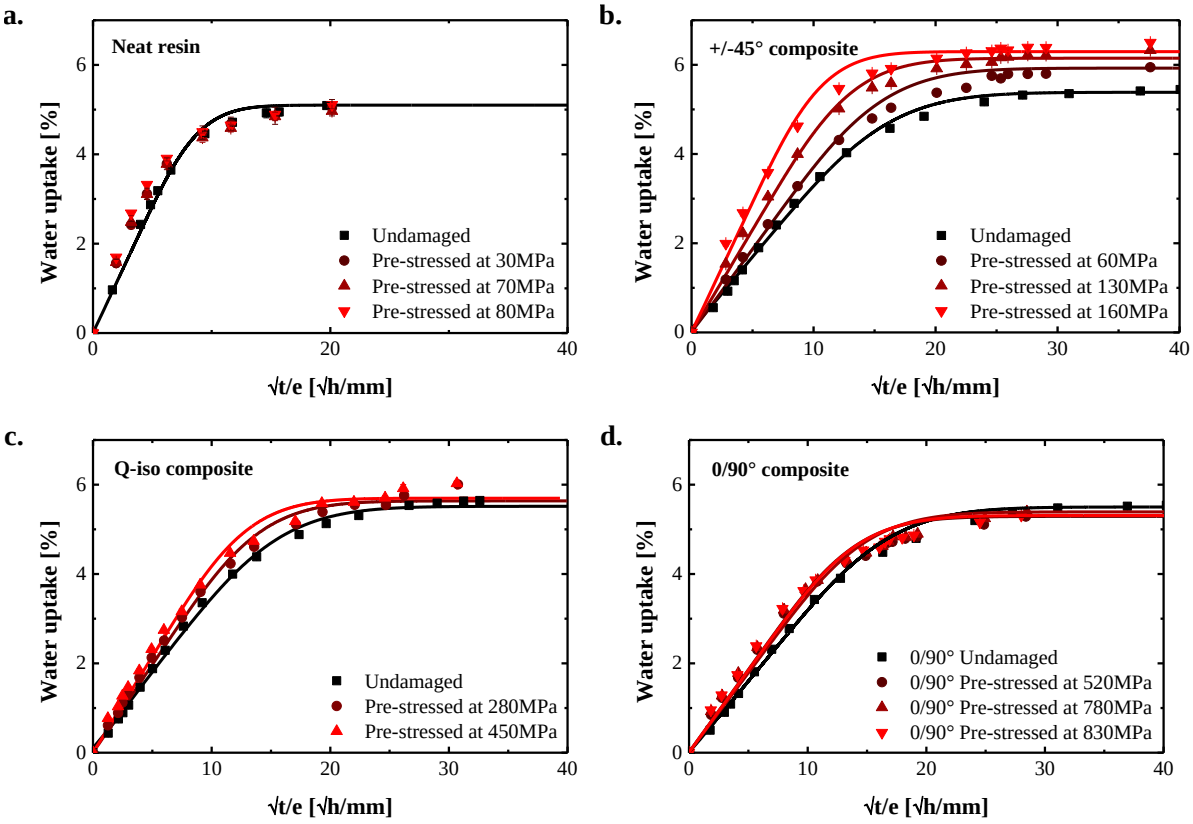

Figure 4.1. Water uptake experimental data [dots] and identification [lines] in pre-stressed materials: neat resin [a.], ±45° [b.], Q-iso [c.] and 0/90° [d.] composites.

4.1.1.2. Identification

For each material and loading level, we identify a Fickian law on experimental data. The identified curves are shown in Figure 4.1 and show good correlation with experimental values. The same identification method as in Chapter 3, is used in this section, and the diffusion coefficient *D* and maximum water uptake *Ms* are reported in Table 4.1. These parameters confirm and quantify the trends qualitatively highlighted in the previous section.

To summarise, the water diffusion remains unchanged in materials not damaged by tensile stresses, with neither cracks nor permanent strain (neat resin).

In samples damaged by tension and with strain recovery after unloading (0/90° and quasi-isotropic composites), the water uptake is slightly accelerated while maximum moisture content remain constant.

Finally water diffusion is highly modified in specimens with important damage and permanent strain (±45° composites). The diffusion coefficient and the moisture content at saturation are increased as pre-stress level is increased.

From these first observations, we can conclude that the presence of cracks modifies the

diffusion behaviour. Moreover, when the cracks are closed by strain recovery, only the diffusion coefficient is increased, whereas if the defects remain open after unloading, the maximum moisture content is also enhanced.

			Identified diffusion parameters	
			Diffusion coefficient [m²/s]	Maximal water uptake [%]
±45° composites	0MPa	Average	2.08E-13	5.36
		Standard deviation	*2.24E-15*	*0.06*
	60MPa	Average	2.17E-13	5.80
		Standard deviation	*4.67E-15*	*0.04*
	130MPa	Average	3.06E-13	6.15
		Standard deviation	*1.66E-14*	*0.05*
	160MPa	Average	4.68E-13	6.29
		Standard deviation	*6.22E-14*	*0.05*
Q-iso composites	0MPa	Average	2.24E-13	5.50
		Standard deviation	*1.12E-14*	*0.12*
	280MPa	Average	2.68E-13	5.64
		Standard deviation	*9.01E-15*	*0.07*
	450MPa	Average	3.12E-13	5.71
		Standard deviation	*4.07E-14*	*0.14*
0/90° composites	0MPa	Average	1.85E-13	5.50
		Standard deviation	*1.36E-14*	*0.12*
	520MPa	Average	2.46E-13	5.29
		Standard deviation	*9.98E-15*	*0.09*
	780MPa	Average	2.39E-13	5.39
		Standard deviation	*1.29E-14*	*0.03*
	830MPa	Average	2.64E-13	5.31
		Standard deviation	*3.28E-14*	*0.10*

Table 4.1. Identified diffusion parameters on pre-stressed composite materials (immersed at 60°C)

4.1.2. Discussion

The identification results point out different influences of damage on the diffusion kinetics and maximum water content, depending mainly on the state of the cracks. The aim of the next sub-section is to understand the factors which influence these two water uptake parameters.

4.1.2.1. Maximum water uptake

The diffusion identification highlights the link between maximum moisture uptake and pre-stress in the case of the presence of open cracks. In this paragraph, we focus on this subject in order to identify all the possible influent parameters and understand their impacts on the moisture content at saturation.

This diffusion parameter appears to be linearly dependent on the pre-stress level in the case of ±45° materials (Figure 4.2). For the other type of composites, the variation is not significant: the slope changes are similar to the standard deviation (Figure 4.2 [right]).

Thus maximum water uptake values are only modified when the material presents open cracks. Under such conditions, the diffusion parameter increases linearly with the stress level (Figure 4.2).

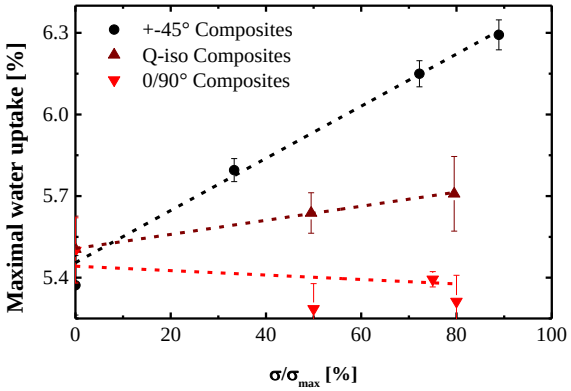

		Linear fit parameters	
		Initial value [%]	Slope [-]
45° composites	Average	5.46	9.59E-03
	Standard deviation	*0.06*	*1.01E-03*
Q-iso composites	Average	5.51	2.59E-03
	Standard deviation	*0.11*	*2.21E-03*
0/90° composites	Average	5.44	-0.82E-03
	Standard deviation	*0.11*	*1.53E-03*

Figure 4.2. Maximum water uptake as a function of the normalized pre-stress level [left] and identified parameters with a linear dependence [right].

4.1.2.2. Diffusion coefficient

Diffusion coefficient dependence on pre-stress is much more complex than maximum moisture content. Identification of the diffusion law reveals faster kinetics for damaged samples. Nevertheless, the influence of pre-loading is different from one specimen to another. Figure 4.3 [left] shows linear dependence of the diffusion coefficient with the pre-loading level for 0/90° and quasi-isotropic composites while ±45° materials show kinetics with a non linear dependence on pre-stress. Part 3.2.1.2 indicated a linear dependence of the modulus on the stress level; therefore this cannot explain the acceleration of the diffusion.

Since diffusion coefficient is affected only when cracks are present (the neat resin diffusion coefficient is unaffected by pre-loading) and that damage presents a threshold in stress (as the diffusion coefficient), we study the dependence of the kinetics on crack density (Figure 4.3 [right]). This representation reveals an impact of the crack density for high pre-stressing levels. Nevertheless for lower loading values the diffusion coefficient increases without important surface damage.

The first hypothesis could be that the diffusion coefficient is dependent on both pre-stressing level and crack density. In this case, more tests should be performed in order to investigate the impact of both parameters and especially near the appearance of the first crack, in order to identify the transition between the two phenomena.

Another possibility is that the surface crack density analysis is under estimating the real volume damage as shown by the X-ray tomography analysis in Figure 3.14 (Chapter 3). In

this case, the real crack density could be higher for lower stress levels.

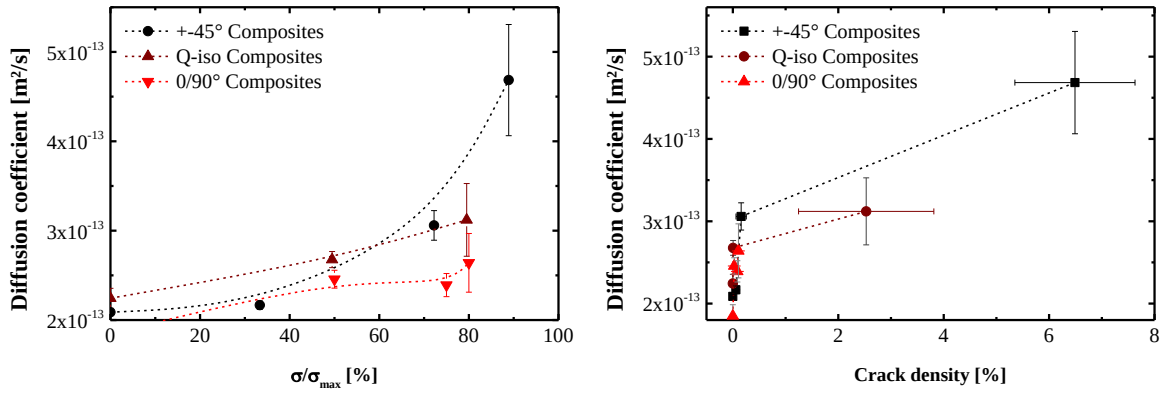

Figure 4.3. Diffusion coefficient as a function of normalised pre-stress level [left] and as a function of crack density [right].

Here, we consider the latter hypothesis and explain the additional moisture content by a diffusion in the damage. Moreover, Figure 3.14 shows cracks created by tensile tests are voids with an elongated shape (important length compared to their other dimensions). Under such conditions, the only water diffusion possible in the defects is by a capillary phenomenon. Some authors have focused their studies on this phenomenon, notably Carlsson and al. [76], who have highlighted a flow rate in interfacial voids, controlled by the expression Eq. 3.3 as a function of void shape (length l and diameter d), pressure drop along the defect Δp and water viscosity μ.

$$Q = \frac{\pi . d^4 . \Delta p}{128 . \mu . l} \qquad \textbf{Eq. 4.1}$$

We will examine this hypothesis which considers water diffusion in voids for our material. To do so, we predict the total water uptake considering an instantaneous capillary diffusion in addition to the Fickian water uptake behviour. Moreover, the additional maximum water content ($C_{\infty,add} = C_{\infty,stressed} - C_{\infty,ref}$) is considered to be entirely located in the defects. Capillary effects and water diffusion are considered to be uncoupled phenomena. Therefore, the total moisture uptake in the composite can be expressed as the superposition of a Fickian diffusion and a constant additional water uptake located in the cracks (Eq. 4.2).

$$C_{stressed}(t) = C_{ref}(t) + C_{\infty,add} \qquad \textbf{Eq. 4.2}$$

The water uptake obtained with this method is represented in Figure 4.4, and compared with the experimental results for materials with significant water diffusion variation (quasi isotropic and ±45° composites).

The proposed hypothesis on capillary moisture transport in cracks gives good prediction of the experimental water uptake for ±45° and q-iso composites. The prediction deviates from

experiments only in the case of ±45° composites pre-loaded at 90% of the ultimate stress. For such an extreme loading, the cracks cannot be considered as capillary voids anymore due to damage coalescence (see chapter 3). This can therefore explain the deviation from the model.

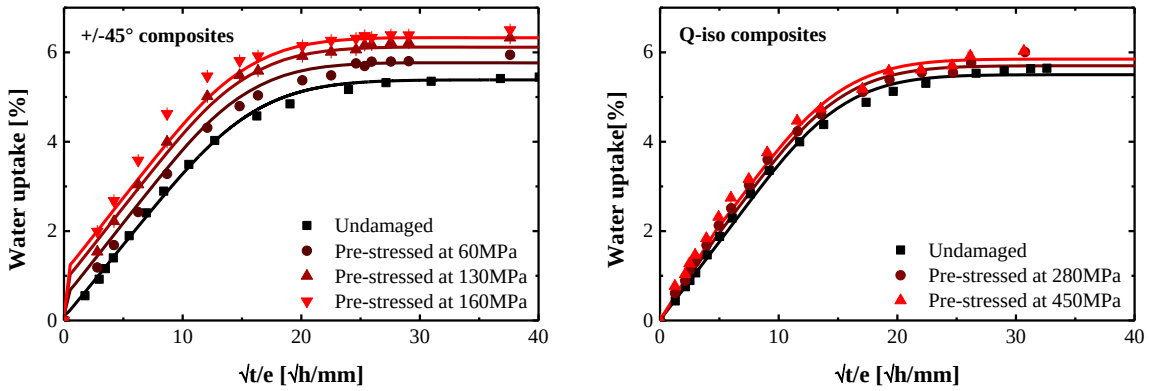

Figure 4.4. Water uptake prediction considering instantaneous capillary phenomena in ±45° [left] and q-iso composites [right].

To conclude, water diffusion can be reasonably well predicted by considering capillary diffusion inside the damage, up to pre-loading of 80% of ultimate stress. In future work, it would be interesting to study the influence of crack shape and density by tomography, in order to use the full capillary model of Eq. 3.3 and predict the water uptake in these materials.

4.2. Mechanical behaviour after ageing

Previous studies presented in chapter 1 show that mechanical behaviour can be highly affected by water ageing. Marine applications all involve water diffusion, therefore the current section focuses on how ageing affects the mechanical behaviour previously studied in chapter 3. The first part of this section is devoted to tensile behaviour, the main mechanical aspect of the study. This subject is studied in two axes, first, the ageing impact on stress/strain relationships for each material, second, the damage relationship with water uptake.

The second part of the study presents other critical mechanical behaviour after ageing. The sub-section investigates inter-laminar properties and mechanical response in flexure of specimens saturated with water.

4.2.1. Tensile mechanical behaviour

The impact of ageing on tensile behaviour is quantified for each material, together with the damage induced by such stresses. For each case, the results are compared to those for unaged materials and then we discuss the impact of water on the mechanical behaviours.

4.2.1.1. Tensile tests

For the study of tensile behaviour of aged specimens, we chose to dissociate the neat resin from the composite, since their mechanical behaviours are quite different (cf. chapter 3).

Neat resin

First, we investigated the resin tensile behaviour during ageing in order to get information on the composite's matrix. The tests were performed at different ageing times in order to have the mechanical property variations with the water content in the polymer. Three exposure times were chosen to correspond to each characteristic stages of the diffusion curve: the first linear part for t=218 h, the transition phase for t=1008 h and the saturation stage for t=1800 h.

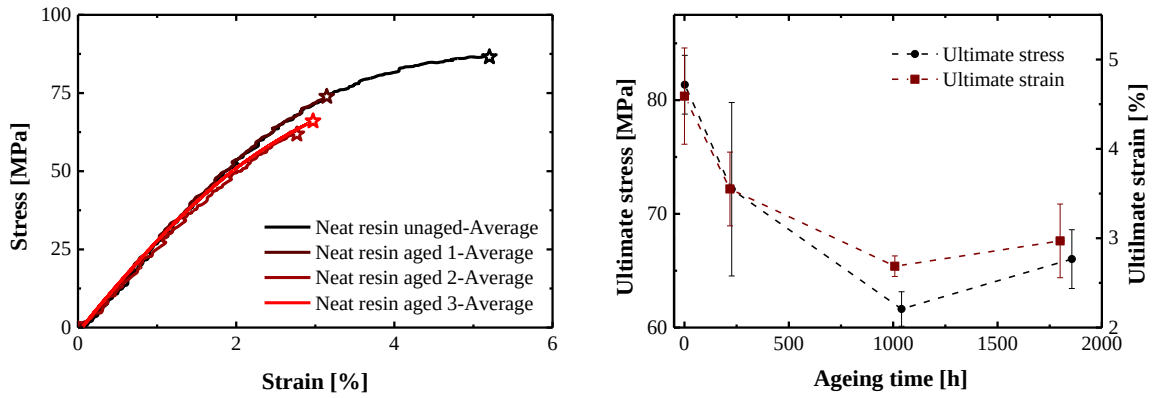

Figure 4.5. Ageing effects on neat resin tensile behaviour [left] and on the ultimate values [right].

Tensile tests performed after these different exposure times show the same effect of water ageing on mechanical behaviour. The initial modulus of the resin remains unchanged for all the samples tested. Moreover, failure occurs earlier for aged specimens and stabilises for high water content (Figure 4.5). This phenomenon has already been studied by Verdu et al. in [37], it translates a physical degradation of the resin without any chemical reaction.

This physical degradation induces an increase of the chains' mobility which decreases the glass transition temperature. This variation can be critical if the glass transition temperature decreases below the temperature of testing. In this case, the polymer would be tested in its rubbery state and would have a very different mechanical behaviour. In order to avoid this phenomenon, we quantify this variation with DMA tests performed at the same ageing times as the tensile tests. We consider Tg as the temperature corresponding to the modulus loss decrease (Figure 4.6 [left]).

The glass transition appears to be highly affected by water diffusion, and drops from 120°C to

70°C (Figure 4.6 [left]). Previous studies have highlighted a similar phenomenon and established laws to predict it [78]. Among these predictions, the Simha-Boyer equation (Eq. 4.3) allows the glass transition temperature of the aged polymer (Tg) to be linked with the Tg of the unaged resin (Tg_p), the glass transition temperature of the water (Tg_w), the water uptake ($C(t)$) and the density of the water and the polymer (ρ_w and ρ_p).

$$\frac{1}{T_g} = \frac{1}{T_{gp}} + \left[\frac{1}{T_{gw}} - \frac{1}{T_{gp}}\right].\frac{\rho_p}{\rho_w}.C(t) \qquad \textbf{Eq. 4.3}$$

The prediction results in a Tg vs. water uptake curve in good agreement with the experimental data. It confirms the reliability of the tests on coupled phenomenon which will be performed at 60°C as this remains below the glass transition temperature after ageing.

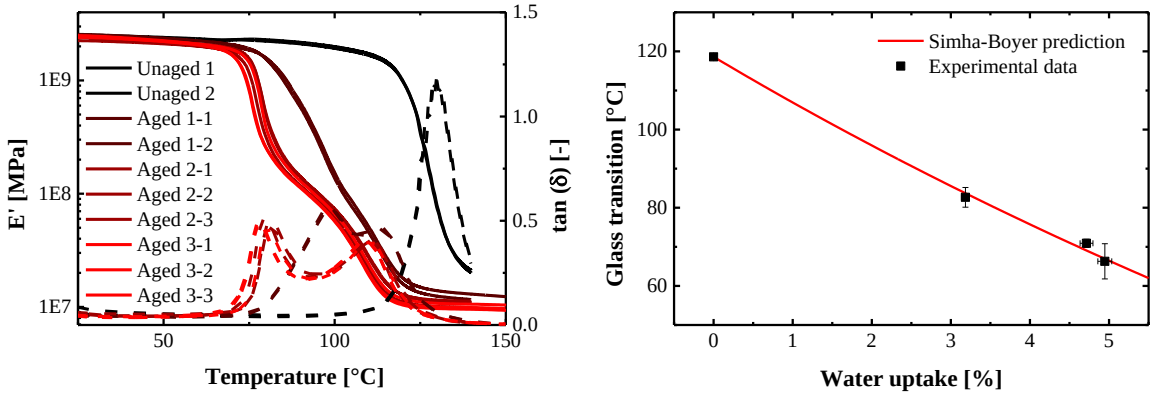

Figure 4.6. Glass transition temperature determined by DMA testing for different exposure times [left]. Simha-Boyer prediction and experimental data of Tg presented as a function of water uptake [right].

Composite materials

The previous paragraph describes a significant influence of water in the neat resin on its mechanical behaviour. This phenomenon will necessarily induce a modification in the mechanical behaviour of the composites. Therefore, each composite type was tested after saturation, to evaluate the impact of the resin degradation on the reinforced materials.

The ±45° material is the composite the most affected by resin behaviour variations due to the absence of reinforcement in the tension direction. Indeed, the results show a degradation of all the tensile mechanical parameters after ageing (Table 4.2).

First, the initial modulus decreases with water uptake rise from 18 to 12 GPa. Second, the yield limit is one of the most degraded tensile properties: the yield stress is almost divided by two (Table 4.2), and the failure stress shows a similar drop. This loss of properties is due to the degradation of the failure properties (in stress and strain) of the matrix resin, which starts to degrade earlier (yield limit reduced) and therefore supports lower stress, resulting in earlier

failure of ±45° composites.

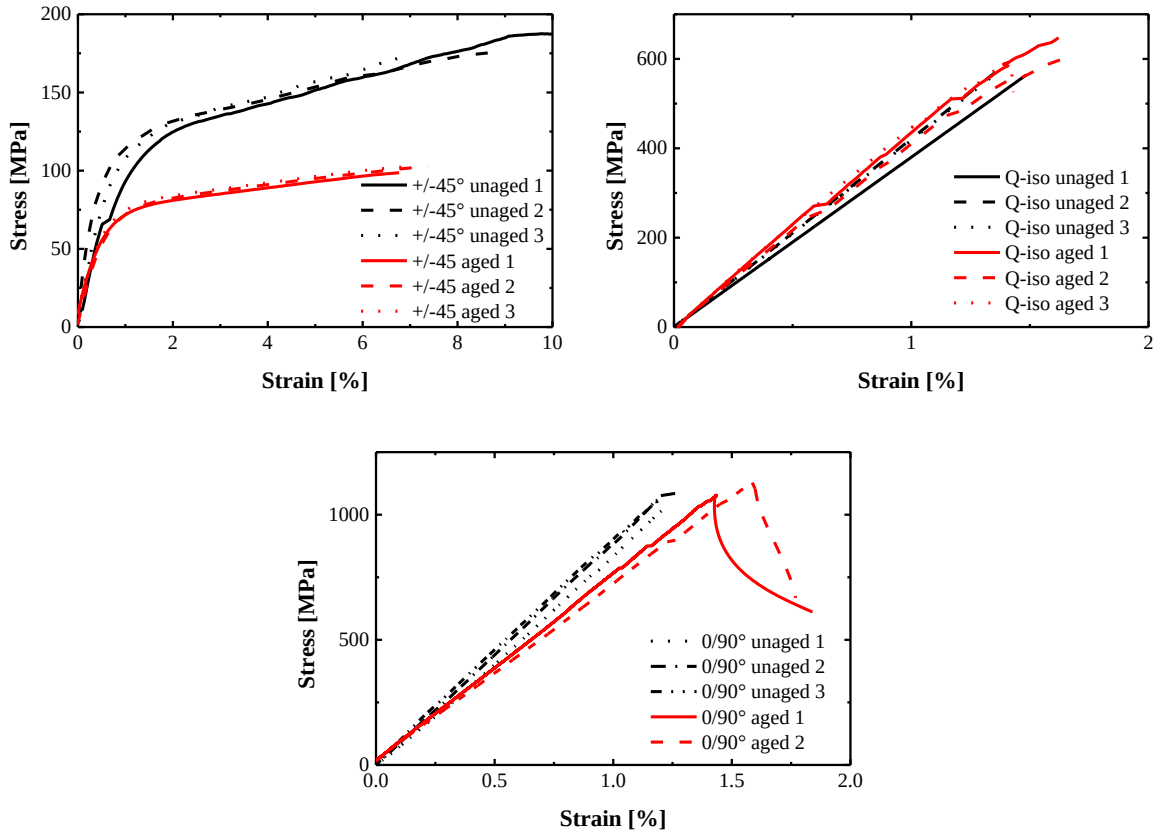

Figure 4.7. Ageing impact on tensile behaviour of ±45° [upper], Q-iso [lower left] and 0/90° composites [lower right].

When we look at the tensile behaviour of quasi-isotropic and 0/90° composites, we see that the influence of ageing is much less significant. Contrary to ±45° materials, the presence of fibres in the stress direction reduces the impact of resin's property variations. Nevertheless, the matrix still has an impact on their behaviour especially due to interfacial cohesion.

For quasi-isotropic materials the ultimate failure is slightly delayed in the case of aged specimens. Nevertheless, this variation (50 MPa and 0.2%$_{def}$) is not significant compared to the standard deviation of the results (26 MPa and 0.1%$_{def}$).

0/90° composites show more degradation due to ageing, as the initial modulus decreases after ageing from 85 to 75 GPa. At the same time, failure occurs for the same stress, resulting in an increase in ultimate strain from 1.2 to 1.5%$_{def}$. This difference compared with quasi-isotropic composites may be due to the high density of fibres oriented in the transverse direction to tension, combined with the woven construction. Indeed, this can create stress concentrations at the weave crossover points which can induce inter-laminar cracks, which are highly dependent on the resin properties (cf. section 4.2.2.1).

4.2.1.2. Damage

The damage identification on unaged materials highlights a high crack density in these composites. This damage is exclusively located in the polymer resin and therefore it is highly dependent on the resin properties. As a consequence, the ageing effects will have an important impact on the crack density in composites especially when the resin is subjected to high stresses. All the identified parameters concerning damage behaviour are reported in Table 4.2 for the aged and unaged cases.

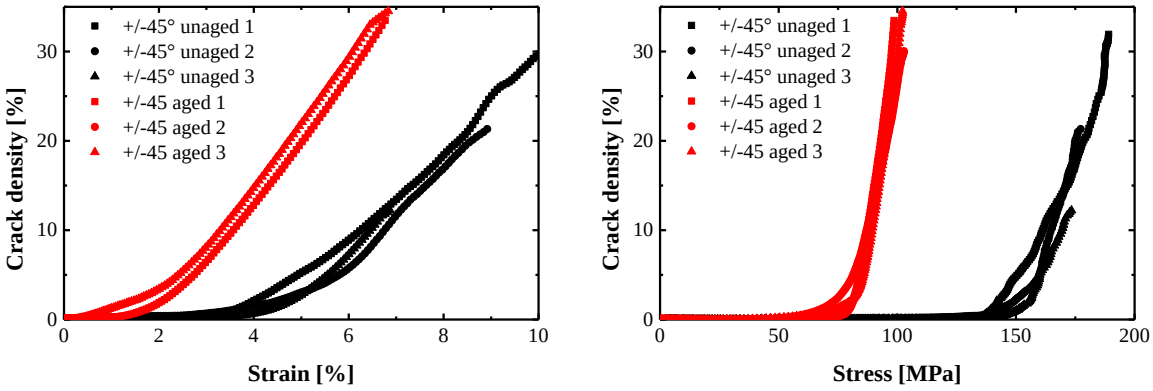

Figure 4.8. Surface crack density for tensile tests unaged and aged ±45° composites as a function of strain [left] and stress [right].

As for the mechanical behaviour, the ±45° composite presents the damage value the most affected by water ageing. The crack density behaviour still shows the same three phases as in the unaged case. Nevertheless, the characteristic values of each stage are highly affected by ageing.

The first crack appears for much lower strain and stress values from 147 MPa and 4.3%$_{def}$ in the reference case to 77 MPa and 1.4%$_{def}$ for saturated materials. This phenomenon is a direct consequence of the degradation of the resin's ultimate values inducing a premature damage in the matrix.

The damage propagation speed is also affected by water uptake: after ageing crack density increases faster than the reference (from 0.75%/MPa and 5.5%/%$_{def}$ to 1.74%/MPa and 6.4%/%$_{def}$).

Ultimate crack density is slightly increased after ageing: 32% of the surface compared to 27% in the unaged case. This is due to the mechanical behaviour of the fibres which remains unchanged after ageing, while the resin cracks for lower loads. Therefore, samples reach the same crack density as the unaged ultimate crack limit for a lower stress. This load is still supported by fibres which can be loaded to higher levels and induce higher ultimate crack

density.

In terms of tensile damage, 0/90° composites are the least affected material, therefore the ageing does not have a significant impact on this behaviour.

All the parameters used to characterise the damage behaviour remain in the same range as the reference from the threshold values to the ultimate crack density (cf. Table 4.2).

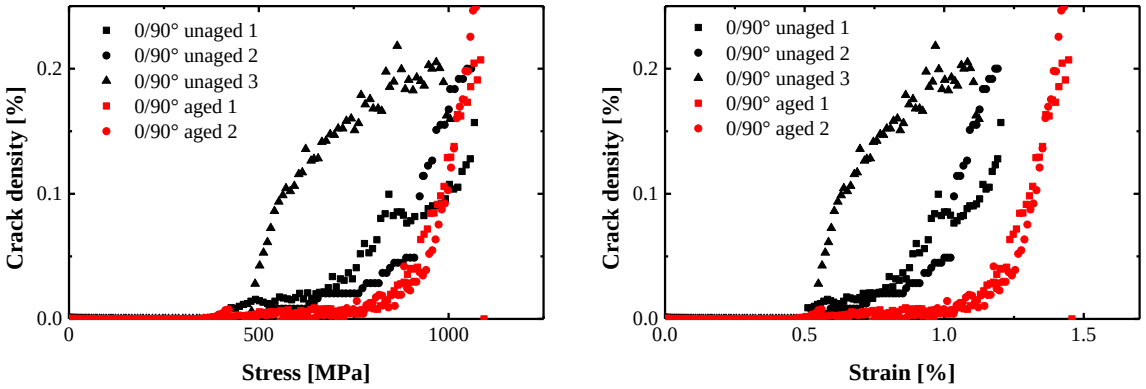

Figure 4.9. Surface crack density for tensile tests unaged and aged on 0/90° composites as a function of strain [left] and stress [right].

As noticed in the previous chapter the high density of fibres oriented along the tension axes gives to this composite a behaviour mainly dependent on the fibre response. The fibres are not degraded by ageing so the impact of the water uptake on this type of material is slight. Nevertheless, we can still notice a variation in terms of damage variation with strain in Figure 4.9. The transition between first crack appearance and the linear damage propagation present some differences compared with the reference. But if we compare this variation with the standard deviation of the reference, the behaviour change appears to be included within the standard deviation interval, therefore it can be considered as unchanged.

In the case of quasi-isotropic materials the damage is only slightly affected by water uptake. As a combination of both previous composites, quasi isotropic samples are affected by both types of behaviour.

Both threshold values and damage speed can be considered as equal in both aged and unaged cases (cf. Figure 4.10), the variations of these parameters are of similar orders of magnitude to their standard deviations.

The main difference between aged and unaged specimens appears for ultimate crack density value. Indeed, samples saturated with water present a damage ratio representing more than 41% of the surface while the reference only reaches an average value of 15%. As for composites with the same construction, the matrix in ±45° plies cracks for lower stress values. At the same time, the fibres, in 0/90° plies, remain unchanged in terms of mechanical

behaviour. The combination of these two phenomena results in a damage behaviour comparable in the case of aged and unaged specimens with only a more important ultimate crack density.

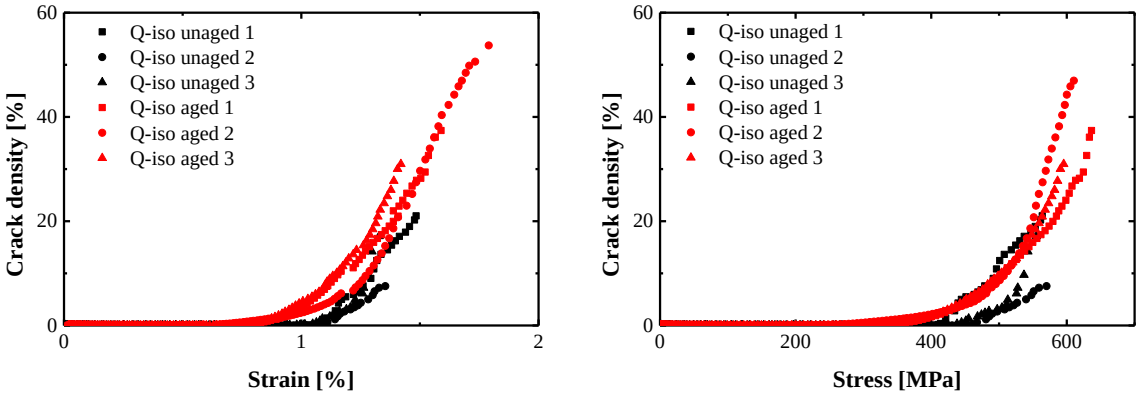

Figure 4.10. Surface crack density for tensile tests on unaged and aged quasi-isotropic composites as a function of strain [left] and stress [right].

			Break stress [MPa]	Break strain [%]	Modulus [GPa]	Yield stress Stress [MPa]	Yield stress Strain [%]	Damage threshold Stress [MPa]	Damage threshold Strain [%]	Damage speed Stress [%/MPa]	Damage speed Strain [%/%]	Ultimate crack density [%]
Unaged	Resin	Average	81.4	4.8	2.8	75.3	3.6					
		Standard deviation	*5.3*	*1.4*	*0.0*	*2.2*	*0.2*					
	+/-45	Average	179.7	9.0	18.5	120.3	1.5	147.7	4.3	0.75	5.5	27.4
		Standard deviation	*8.7*	*1.7*	*6.5*	*2.5*	*0.3*	*6.0*	*0.4*	*0.18*	*0.2*	*10.8*
	0/90°	Average	1036.9	1.2	85.3			472.3	0.5			0.2
		Standard deviation	*42.6*	*0.0*	*6.1*			*41.6*	*0.0*			*0.0*
	Q-iso	Average	566.7	1.4	40.7			448.3	1.4	0.13	51.3	15.2
		Standard deviation	*3.2*	*0.1*	*2.3*			*28.7*	*0.5*	*0.05*	*21.0*	*6.9*

			Break stress [MPa]	Break strain [%]	Modulus [GPa]	Yield stress Stress [MPa]	Yield stress Strain [%]	Damage threshold Stress [MPa]	Damage threshold Strain [%]	Damage speed Stress [%/MPa]	Damage speed Strain [%/%]	Ultimate crack density [%]
Aged	Resin	Average	61.6	2.7	2.6							
		Standard deviation	*3.0*	*0.2*	*0.0*							
	+/-45	Average	101.2	7.0	12.4	74.1	1.1	77.1	1.4	1.74	6.4	32.7
		Standard deviation	*2.3*	*0.3*	*0.5*	*0.9*	*0.1*	*4.4*	*0.5*	*0.38*	*1.4*	*2.3*
	0/90°	Average	1102.1	1.5	75.9			361.4	0.5			0.3
		Standard deviation	*24.9*	*0.0*	*1.2*			*1.9*	*0.0*			*0.1*
	Q-iso	Average	617.8	1.6	46.4			416.7	1.0	0.28	78.8	41.3
		Standard deviation	*26.8*	*0.1*	*1.7*			*2.9*	*0.0*	*0.12*	*14.8*	*12.7*

Table 4.2. Tensile mechanical parameters for all the materials, before [upper] and after ageing [lower]

To conclude, the damage behaviour translates quite well the construction of the composite. A composite with high loadings of the matrix (±45° samples) has a tensile behaviour highly dependent on the resin mechanical response and therefore will be

significantly affected by ageing. On the contrary, composites subjected to low stress in their matrix (quasi-isotropic and 0/90° specimens) have a tensile mechanical response dependent on the fibre behaviour and will be only slightly or not affected by water uptake.

4.2.2. Other mechanical behaviours

As for tensile behaviour, the other mechanical responses studied were also investigated after ageing to saturation, in order to understand the influence of water diffusion inside the matrix. The same plan is used as in Chapter 3: the first part of the study focuses on inter-laminar shear stress tests, the second section is dedicated to four point bending test results.

4.2.2.1. Inter-Laminar Shear Strength

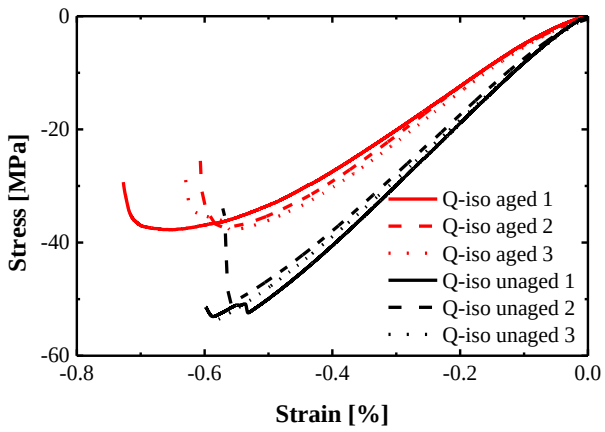

Figure 4.11. Stress-strain curves from inter-laminar shear stress tests on quasi-isotropic composites unaged and aged.

The inter-laminar shear strength indicates the quality of the interface properties between fibres and matrix. This type of property can become critical after ageing even in the case of tensile tests for woven composites. Indeed, the woven construction induces local stresses out of the plane of the sample which can generate shear stresses inside the composite.

The results reported in Figure 4.11 show a large influence of ageing on the ultimate inter-laminar shear stress which decreases from 55 MPa to 40 MPa.

This drop in out-of-plane strength is the result of the influence of water on the matrix resin.

4.2.2.2. Four point bending

The aim of the four point bending tests is to get information on the compressive

properties of the materials. The tests on unaged composites highlighted compression failures as expected.

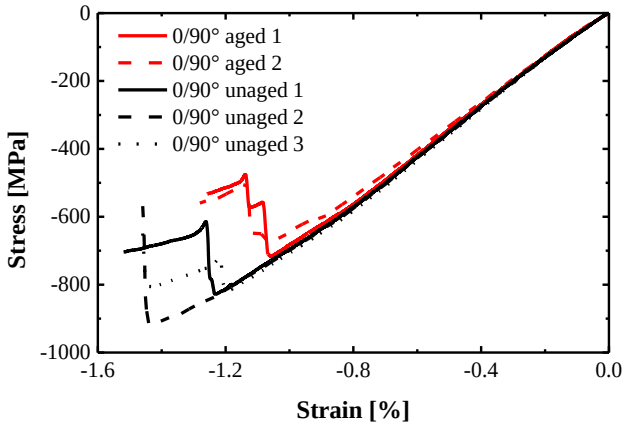

Figure 4.12. Stress strain curves from four point bending tests on 0/90° samples unaged and aged.

The specimens tested after water uptake do not show any change in terms of initial modulus and stress-strain trends. Nevertheless, the failure occurs earlier than in the unaged case. This phenomenon necessarily translates other types of failure than only fibre compression, which should be almost unaffected by water diffusion since 0° fibres remains unaffected by ageing.The load transfer through matrix shear is affected however, as noted above.

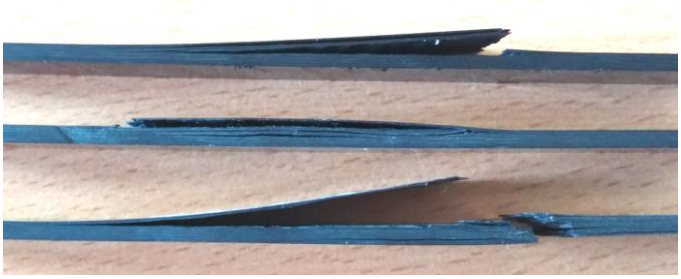

Figure 4.13. Sample failures after four point bending tests on aged 0/90° composites.

To better understand the failure mode, we study the shape of the aged specimens' failure from Figure 4.13. The upper plies of the samples still present fibres failed in compression. Nevertheless, Figure 4.13 also highlights more delamination in the composites' depth than in the unaged case (Figure 3.17). Therefore, the early failure for aged specimens is not only due to compression phenomenon but also to degradation of the inter ply properties which generates significant delamination in the samples.

4.3. Conclusion

This chapter aimed to understand the interaction between mechanical behaviour and

water diffusion when a sample was successively exposed to these stresses. Two cases can be encountered: water diffusion in a pre-stressed material and mechanical stress applied after water diffusion.

First we studied the influence of pre-tension stress on the water diffusion in resin, ±45°, 0/90° and quasi-isotropic composites. The different levels of pre-stress were chosen to correspond to a specific damage introduction apart for the resin samples which does not highlight damage during a tensile test.

This section enhances the link between water uptake increase and damage introduction. Indeed, resin samples do not highlight significant modification of water diffusion in specimens while it is affected for all type composites. Moreover, the more composites are damaged the more water uptake is increased.

Finally we identified some capillary effects which could the reason of the increase of water quantity inside the damaged samples. This phenomenon cannot directly affect the property of the material. Nevertheless, it could increase the weight of a structure, which can be critical in some cases. Moreover, the inclusion of water inside damage could accelerate the crack propagation especially when the materials are stressed in fatigue if the water stays partially in the defects during unloading.

The second section is dedicated to the comparison of the mechanical properties before ageing and after water saturation of the samples.

The tensile tests highlight no significant changes for 0/90° and quasi-isotropic composites while resin and ±45° samples shows significant behaviour changes after ageing. The resin specimens have the same mechanical response after any exposure time. The water content only induces a premature failure which stabilises after saturation of water in the sample. ±45° composites for their part have an initial behaviour unchanged while their threshold stresses are significantly decreased and their failure occurs prematurely after ageing. When we look to the damage of composite samples, we can identify the same behaviours: the ±45° specimens show a damage threshold which occurs for lower stress and strain and a damage speed increased in the aged samples. For quasi-isotropic and 0/90° composites we cannot notice significant differences between aged and unaged materials.

This section highlight important influence of ageing on material’s mechanical only when the resin is highly stressed.

In this chapter the properties obtained will be a reference for the further coupled tests in order to understand the impact of coupling on mechanical and diffusive behaviour.

Chapter 5.

Coupled behaviour

5.1. Introduction

Chapter 3 and 4 were intended to provide information on how tensile stress and water diffusion affect the different materials as semi and uncoupled phenomena. Now that this has been established, the following section can focus on the fully coupled effects of both types of external loading.

The first coupled study is dedicated to immersed static tension of composites. Only the case of ±45° and quasi-isotropic samples are discussed, to provide results for composites loaded in and away from the reinforcement direction.This section is divided into three main parts.

First, the experimental results of water diffusion and mechanical response are presented and commented, and compared to results for the undamaged reference.

Second, the effects of the coupling are highlighted by introducing new representations and by comparing them with the results from the semi-coupled case.

Finally, the impact of the coupling on water uptake is quantified, and the most critical phenomena are highlighted.

Water diffusion combined with hydrostatic pressure represents another critical coupling phenomenon which can be frequently encountered in underwater applications (submarines, profilers …). For this reason, this subject is studied in an additional section.

In that section, we start with the presentation of the experimental water uptake data obtained by coupling with different levels of hydrostatic pressures and we compare them to the reference unstressed values. These water diffusion behaviours are also identified with Fick's law to quantify the impact of pressure.

The second sub-section is devoted to the discussion of the results following three axes. First, the impact of the pressure on unstressed saturated samples is studied. Second, we investigate the influence of fibre orientation on the water uptake behaviour. Finally, the impact of porosity on the water weight in the all composites is highlighted.

In the last part of the section, we propose two models for the water diffusion. The first one is based on the representation of one void corresponding to the porosity ratio in the materials. The second one is an homogenised model, developed to reduce the calculation time for complex structures.

5.2. Immersed tension

Here, tensile stress combined with water diffusion is studied as a fully coupled phenomenon, starting from the experimental data and the identification of the impact of coupling on the water uptake.

5.2.1. Experimental results

In this sub-section, we present results from tests on composites under combined tensile stress and water exposure (at 60°C). For each material, one set of specimens was immersed without mechanical stress in the same water tank as stressed specimens, in order to identify the reference diffusion. The diffusion laws identified from these reference samples are represented by continuous lines on Figure 5.1 and Figure 5.2.

5.2.1.1. +/-45° woven composites

For +/-45° composites, four different stresses have been studied: 30, 60, 110 and 130MPa, representing respectively 16, 33, 60 and 71% of the ultimate break stress (for unaged samples tested at 25°C).

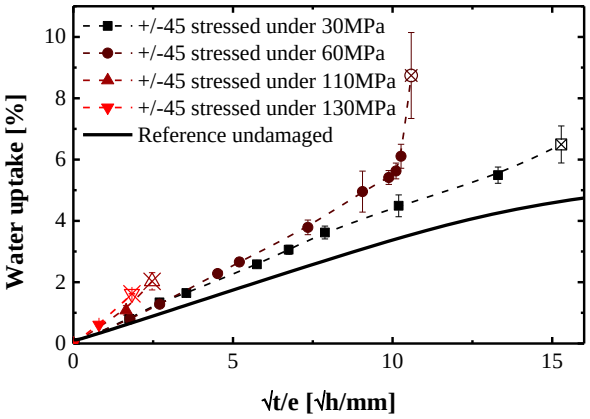

Figure 5.1. Water uptake in +/-45° composites under four different stress levels vs √t/e compared to the reference diffusion in undamaged samples. Crossed symbols represent failed samples.

From this experiment, three different water uptake behaviours can be highlighted. The time to failure (represented by crossed points in Figure 5.1) is highly dependent on the loading. To get a clearer representation of the diffusion variation with the applied stress, Figure 5.1 shows the difference between water uptake in stressed samples and water uptake in the unstressed reference specimens.

The water uptake of composites stressed above 110MPa is modified from the start of immersion, while lower stress levels do not affect the diffusion behaviour initially. This

difference depends on how close the stress levels are to the damage threshold (shown in Chapter 4, Figure 4.8), the damage induces an additional water uptake which accelerates the damage and failure occurs after short immersion times.

A second diffusion behaviour can be identified for specimens stressed above the aged threshold value but below the unaged threshold value. In the first case, water diffusion stays relatively close to the reference during a first stage and starts to deviate after a certain time as Figure 5.1 shows for samples stressed below 60MPa. These samples are stressed below the damage threshold of aged composites (60MPa); therefore if loading and water diffusion were acting separately, there would be no water diffusion acceleration. Nevertheless, the presence of the acceleration and failure highlights a coupling between both phenomena: creep behaviour and water influence on the mechanical response.

We propose in part 5.2.3.2 a technique to identify the predominant phenomenon involved during immersed tension.

5.2.1.2. Quasi-isotropic woven composites

Unlike for +/-45° composites, cracking in quasi-isotropic materials is not affected by ageing. Samples were tested at two stress levels: 300 and 430MPa (50 and 80% of the unaged breaking stress), corresponding respectively to a stress above and below the threshold value. The diffusion curves are shown in Figure 5.2.

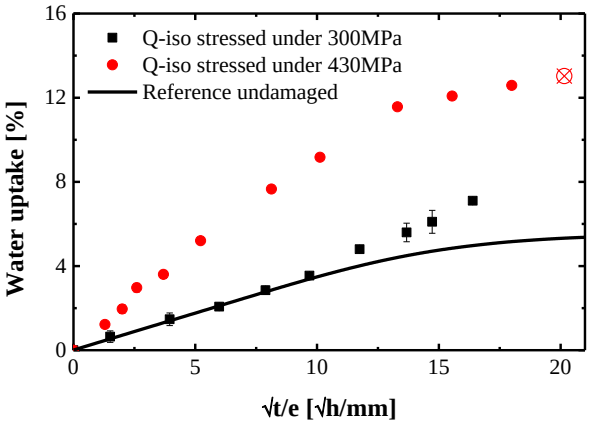

Figure 5.2. Water uptake in Q-iso composites under two different stresses.

For specimens stressed above the first crack appearance, water uptake increases significantly, compared to the reference. The failure occurs before the stabilisation of the water uptake and therefore we cannot clearly identify a diffusion coefficient. The high maximum moisture content highlights the importance of additional water in the composite.

Samples stressed below the damage limit follow the reference diffusion during a first part and

start to deviate before the saturation level. Since semi-coupled behaviour does not follow this kind of behaviour, this phenomenon is the result of combined effects of stress and water diffusion. A possible reason for this deviation could be the modification of the resin mechanical properties by ageing which induces earlier damage at the interface between fibres and matrix and modifies the water uptake.

5.2.2. Coupling effects

We previously identified the characteristics of the coupled phenomenon. To better understand the impact of coupling, the following section makes comparisons between uncoupled, semi and fully-coupled water diffusion in ±45° and quasi-isotropic composites.

5.2.2.1. Water diffusion

Results from the coupled study highlight a dependence of water diffusion on the applied stress. To show this coupling between mechanical behaviour and ageing more clearly, we have introduced a new representation.

A convenient way to translate the coupled effects of water diffusion and mechanical behaviour is by evaluating the water uptake difference between stressed and unstressed materials. Then, this parameter is represented as a function of √t/e in the case of diffusion after and during static loading in order to enhance the impact of the simultaneous effects of water and stress. This representation is shown in Figure 5.3 for ±45° (left) and quasi-isotropic (right) composites.

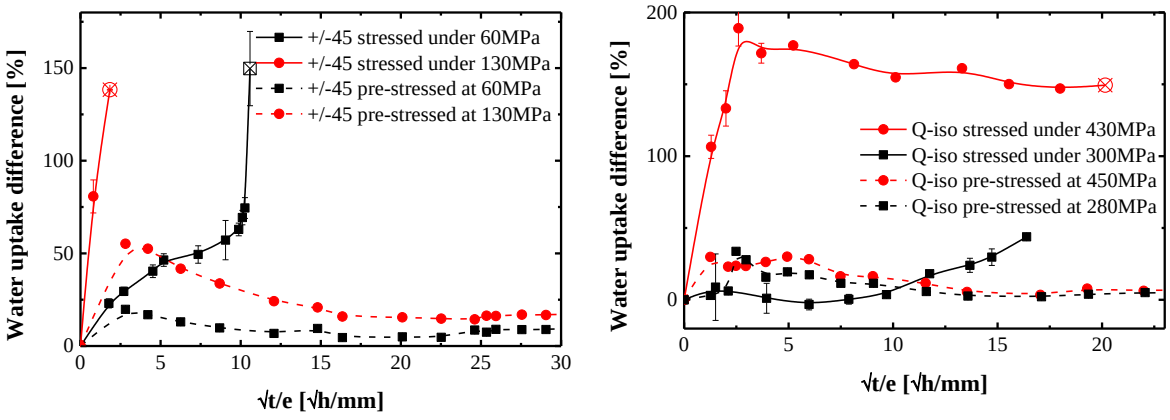

Figure 5.3. Water uptake difference of stressed/pre-stressed samples with the reference vs. √t/e for ±45° [left] and Q-iso [right] composites. Crossed symbols represent failed samples.

In the case of ±45° reinforcements, stressed and pre-stressed samples share the same first stage characterised by an increased water uptake; the duration of this phase depends on the pre-stress level. It translates the presence of water included in cracks created by tensile

stress, which could be modelled by capillary diffusion inside the damage, presented in pre-stressed and stressed materials.

The second phase is characterised by a decrease of the water uptake difference in pre-stressed samples while water diffusion starts to accelerate in specimens stressed above the damage threshold stress (60MPa). This acceleration is generated by coupled effects of water and static loadings. On one hand, the cracks reduce the loaded surface which results in a stress increase and therefore in an acceleration of the damage propagation. On the other hand, the water included in the defects can propagate the damage (especially in the case of loading/unloading cycles). These two phenomena combine into a self-accelerated degradation mechanism, as shown in Figure 5.3 [left].

In the case of quasi-isotropic composites, the initial and second stages are present for both pre-stressed and stressed materials.

Nevertheless, the failure does not occur at the end of the second phase, but the water uptake difference stabilises at a given value (150% in the case of samples stressed under 430MPa). The additional water uptake is created by cracks, and then its stabilisation translates a constant damage density. In quasi-isotropic samples, fibres oriented in the loading direction can support the stress applied on the sample and therefore stop the crack propagation. In this case, the water uptake should be constant from the beginning to the end (constant crack density). Nevertheless, damage investigation on resin aged samples (Chapter 4) shows mechanical properties degraded by water uptake. Therefore in the case of static loading on quasi-isotropic composites samples, above a given moisture content (depending on the stress level) the mechanical properties of the aged matrix will no longer support the loading and the resin will start cracking. This phenomenon will result in an increase of water uptake difference (Figure 5.3).

Finally the diffusion behaviour of quasi-isotropic and ±45° composites pre-stressed and stressed specimens highlights a strong influence of the coupling on the additional water uptake: 25% of the reference in the case of pre-stressed materials and 150% for samples stressed in water.

5.2.2.2. Mechanical behaviour

Another way to represent the behaviour of materials under coupled stresses is by investigating the characteristic parameters of the mechanical response. In this case, the samples are stressed under tensile creep loading. Therefore, the parameters which characterise this behaviour are the permanent elongation and the time to failure. Permanent strain was

recorded at the same time as weight gain during the diffusion and the time to failure was recorded for each sample tested.

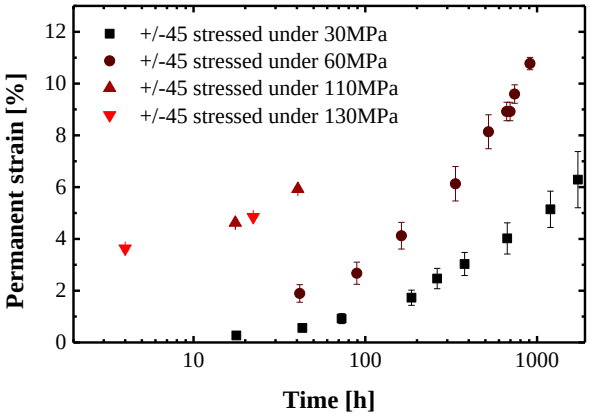

Figure 5.4. Permanent elongation as a function of time for ±45° composites immersed and stressed.

In the case of ±45° composites, the absence of reinforcement in the tension direction results in large permanent strains, due to the creep response of the epoxy polymer. The results for each loading level are reported in Figure 5.4 as a function of time in hours. We can distinguish the two sample groups as previously: the samples stressed above and those stressed below the damage threshold.

When stressed above their damage limit, the ±45° materials show an initial permanent strain followed by a logarithmic behaviour. This phenomenon can be compared to the permanent deformation observed after unloading in the case of the uncoupled specimens (Chapter 3, Figure 3.9). For unaged specimens, the permanent strain reaches 0.5% for 110MPa and 0.8% for 130MPa while the initial values obtained by logarithmic interpolation of the curve in Figure 5.4, reach more than 3% for 110 and 130MPa. Nevertheless, we have to note that the coupled tests were performed at 60°C and we know that temperature has a significant effect on the creep behaviour (as for ageing). Therefore, the increase of permanent strain value is the result of temperature, since the first measurement is made after three hours which corresponds to a water uptake below 1%. In order to get more information on the coupled effect on this variable, it would be necessary to perform coupled tests in air at 60°C to compare both variables uncoupled and coupled.

When stressed below their damage threshold, the samples present initial values which tend to zero. In a second time, the strain follows a logarithmic law of the time until the failure. The slope of each curve depends on the stress applied and we can also notice that the ultimate permanent strain depends on the loading level. Nevertheless, the ultimate strain is recorded during the last weight measurement, which corresponds to failure. Therefore, it would be

interesting to perform tests with more permanent strain measurements close to failure.

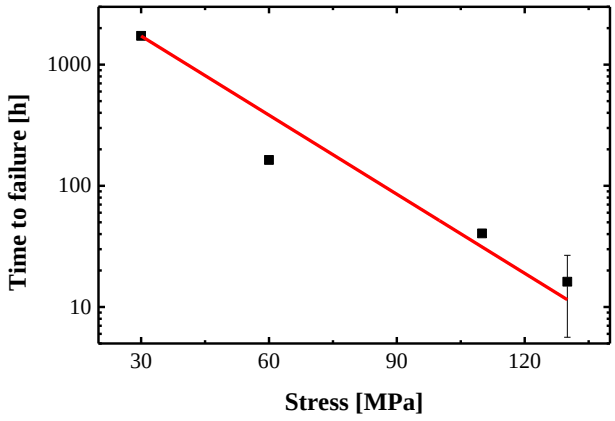

Figure 5.5. Time to failure for ±45° samples immersed stressed to different stress levels.

The second characteristic parameter studied is the time to failure for ±45° composites immersed and stressed under static tension. In this case, the failure occurs after times (t_{tf}) which follow an exponential trend with the normalised stress. This type of behaviour has already been encountered for creep on polymers as in [79]. In our case, we identified the two parameters of the exponential law (A and B) from the equation $t_{tf} = A.e^{B.\sigma}$, we obtain $A=7748.5\ h$ and $B=0.05MPa^{-1}$. To get information on the impact of the coupling with water, further creep tests in air at 60°C would be necessary, in order to compare both results.

To conclude, the creep behaviour of ±45° composites immersed at 60°C has been characterized. Nevertheless, to go further it would be necessary to perform additional reference tests at 60°C in ambient air, to be able to identify the water effect on creep behaviour. In this section, we did not consider the quasi-isotropic case for two reasons: first, the results show a constant permanent strain equal to zero for all the strains tested (300 and 430MPa), creep is not significant when there are fibres in the loading direction. Second, none of the samples failed, therefore we cannot identify the time to failure.

5.2.3. Discussion

The previous section was devoted to the presentation of the coupled effects on the water diffusion and mechanical behaviour. We highlight an important impact of the coupling on the water uptake, compared to the semi and uncoupled behaviours. Therefore, from these observations, we intend to identify tendencies on water diffusion behaviour in samples subjected to coupled stresses. First, we study the water uptake parameters as a function of the applied stress. Second, we investigate the predominant phenomena involved during coupling, by testing samples with two different thicknesses.

5.2.3.1. Influence of stress level on water diffusion

For coupled tests, we characterise the water diffusion with two parameters: one translating the water diffusion rate and another which is the maximum water uptake in all composites (voids and resin).

The diffusion kinetics are characterised by a virtual diffusion coefficient *D(σ)* determined using the same equation as for Fickian diffusion (Eq. 5.1) by considering the maximum water uptake of the undamaged reference $C_{ref,\infty}$ and the initial slope of the curve in Figure 5.1 ($\frac{C(\sigma,t)}{\sqrt{t}/_e}$). We have to keep in mind that this value does not correspond to a diffusion coefficient; it is only used to compare the initial rate of diffusion in the uncoupled and coupled cases.

$$D(\sigma) = \frac{\pi}{16.{C_{ref,\infty}}^2}\left[\frac{C(\sigma,t)}{\sqrt{t}/_e}\right]^2 \qquad \textbf{Eq. 5.1}$$

On the other hand, the maximal water uptake $C_\infty(\sigma)$ has been determined as the weight of water in the composites either at saturation or at failure.

For ±45° composites the diffusion parameter appears to be linearly dependant on the pre-stress level as shown in Figure 5.6 [left]. The linear fit shows a good correlation when modelled with the parameters reported on Figure 5.6 [left]. As in the semi-coupled case (Chapter 4, Figure 4.3), the diffusion coefficient increases with stress due to the capillary diffusion inside the defects. Nevertheless, while semi-coupled tests show an acceleration, in the coupled case, the diffusion coefficient is linear. This phenomenon can be explained by small cracks which are closed when unstressed and opened when we apply load to the sample.
If we look at the maximal water uptake in ±45° samples two aspects can be noted: an important gap between the values of undamaged and damaged specimens and an exponential trend of the damage growth values. The undamaged maximum water uptake necessarily diverges from that of damaged specimens which contain cracks after a certain time of exposure (different for each stress). Moreover, the maximum water uptake in the unstressed case is a value from a saturation stage while in the stressed case, this parameter represents the final quantity.
Now if we separate both cases, we can distinguish an exponential change of the maximal water uptake with the applied stress. The law identified is reported in Figure 5.6 [right] and shows a good correlation with the experimental data recorded. In this case, the experimental

data are quite different in the semi and fully coupled cases: when studied after loading, the maximum moisture uptake is increasing with the stress while it is decreasing when stressed during diffusion. This phenomenon can be explained by no saturation of the samples at failure, and moreover the highly stressed samples fail after a short exposure time, which results in lower water uptake at failure.

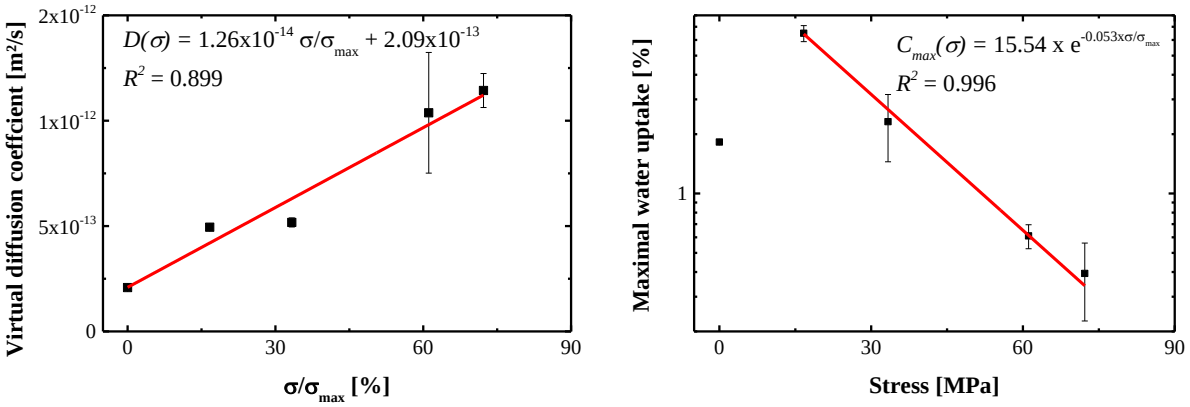

Figure 5.6. Virtual diffusion coefficient [left] and maximal water uptake [right] as functions of normalised stress in the case of coupled tests on ±45°composites.

Quasi-isotropic samples show quite different behaviour: even highly stressed, the samples appear to tend to a saturation stage, and their diffusion coefficient is highly modified only when the specimens are stressed above their damage threshold limit (Figure 5.2).

To conclude, the water uptake parameters show significant variations between the semi and fully coupled cases. Therefore, this shows the necessity to study the stress and water diffusion as coupled effects and not only as semi or uncoupled phenomena.

5.2.3.2. Size effects

It is interesting to examine what happens when thinner samples with the same ±45° stacking sequence are tested under coupled conditions. From the results of coupled tests presented above, two hypotheses can be made: either the water uptake modification is induced by damage created by the effect of water aging, in which case testing a thinner specimen to the same stress level would cause a weight increase at the same value of $\sqrt{t}/_{e}$, or it is due to a creep mechanism in which case weight will increase at the same time under load (i.e. a longer value of $\sqrt{t}/_{e}$) for a thinner specimen. To investigate this, 1mm thick samples were tested under a loading of 60MPa and compared with results from standard 2.2mm thick specimens (Figure 5.7). The fibre weight content was slightly higher in the thinner specimens (73%

compared to 70%), the glass transition temperature was identical.

In fact, results in Figure 5.7 show that water uptake is modified after a shorter time and $\sqrt{t}/_{e}$ in the case of the thin samples. This suggests that the coupling is affected by the scale of the tested samples.

This is an important result, which requires additional study, as it suggests that coupling effects cannot be simply treated in terms of families of stacking sequences but that even for simple tensile loading geometric effects must also be considered.

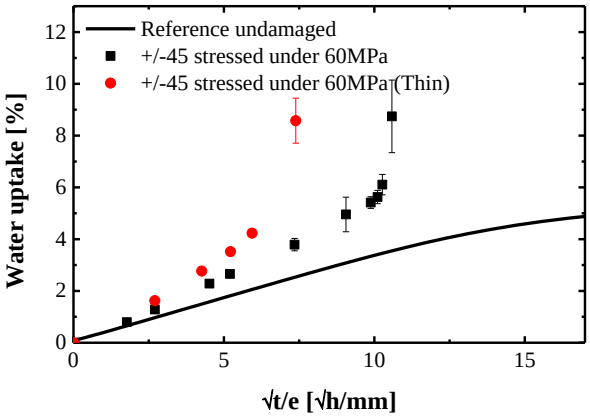

Figure 5.7. Influence of thickness on the water uptake in +/-45° composites stressed under 60MPa in water at 60°C.

The aim of this study was to provide experimental data on how coupling effects between water and mechanical loading affect water uptake and damage development in a carbon/epoxy composite. These effects have been shown to be quite small for partially coupled tests, in which water and stress are applied sequentially. However, when they are applied simultaneously large effects are observed, which lead to premature failure. These effects must be understood and modelled if lifetimes are to be predicted. Further work is underway to examine size effects, revealed to be present by preliminary tests, to quantify creep contributions at 60°C, and to examine how cyclic loads affect coupling.

5.3. Hydrostatic pressure

There are many marine applications which involve hydrostatic pressure loading, and in these cases the materials used are necessarily subjected to water diffusion at the same time. For this reason, we also chose to study the water diffusion in polymer based materials when they are stressed under hydrostatic pressure.

Material	Thickness [mm]	Vf	Tg	Porosity ratio
Epoxy resin	4.20 (+/0.20)	-	84°C	≈ 0%
Hand lay-up composite	2.20 (+/- 0.10)	30%	80°C	From 4% to 8%
Infused	2.25 (+/-0.05)	58%	75°C	1%
Prepreg	2.20 (+/-0.02)	60%	110°C	0.5%

Table 5.1. Characteristic parameters of specimens from each type of materials.

This study has been driven by previous work performed at IFREMER [64] which has shown an important influence of pressure on hand lay-up glass/epoxy composite with unidirectional reinforcements. Therefore, the materials studied in this section were different from those in the rest of the study. The main material used is the hand lay-up glass/epoxy composite presented in Chapter 2 (SR1500). In addition, we chose to compare these results to the diffusion in neat resin samples of the same epoxy material, and with infused and pre-impregnated glass/epoxy composites. Tests on infused and prepreg materials came from a specific study in which specimens were immersed at 40°C and 500 bars for 12 months. This second study was intended to extend the investigation to cover a wider range glass-epoxy composite manufacturing condition. Nevertheless, these results cannot be directly compared to others performed at 60°C. The thickness, fibre volume fraction, glass transition temperature and porosity ratio are reported in

Table 5.1, and show significant differences between each specimen type. These differences are mainly due to the type of processing (see Figure 5.8 for porosities).

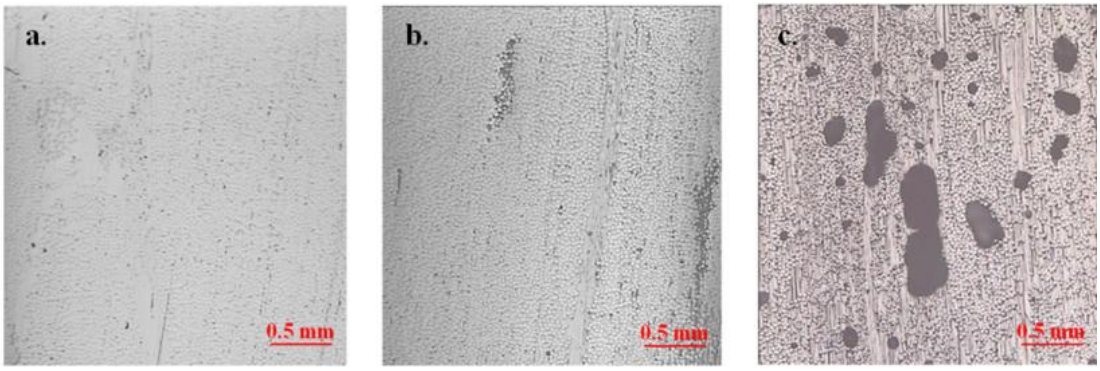

Figure 5.8. Optical microscopy view of polished sections of unidirectional pre-impregnated [a.], infused [b.]; and hand lay-up [c.], glass/epoxy composites.

5.3.1. Experimental results

In this section experimental data are presented, commented and then we perform a first identification based on Fick's law of diffusion.

5.3.1.1. Water uptake behaviour

Water uptake behaviours are studied for neat resin, hand lay up, infused and pre-impregnated composite samples. Neat polymer specimens were tested under pressures of 1, 50 and 500 bar, for hand lay up samples additional tests were also performed at 5 bar, to get a better understanding of the influence of pressure on the water uptake in the samples. Pre-impregnated and infused samples were only studied under pressures of 1 and 500 bar, in order to compare their behaviour with that of hand lay up composites.

Among the results obtained (Figure 5.9), we can identify three different water uptake trends. First, neat resin and infused composite show diffusion kinetics slightly modified by pressure rise and a maximal water quantity unaffected. Second, pre-impregnated samples have a moisture diffusion which remains unaffected by pressure. Finally, hand lay up samples show a large increase in water uptake when hydrostatic pressure is applied.

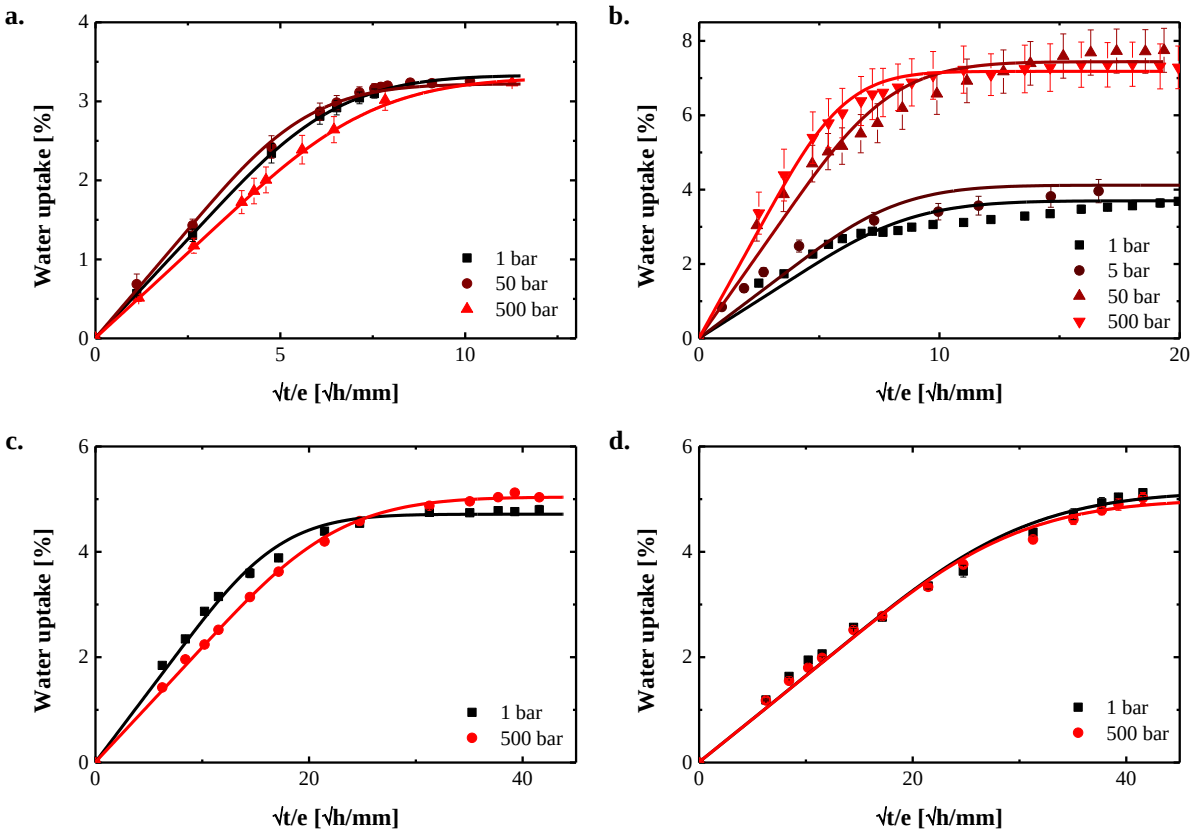

Figure 5.9. Experimental data and Fick identification of water uptake in neat resin [a.], hand lay up [b.], infused [c.] and pre-impregnated [d.] glass/epoxy composites under different pressure levels.

The main difference between these specimens is the processing method used, which can explain the different effects of pressure on water uptake.

5.3.1.2. First identification

In order to quantify the effect of pressure on water uptake kinetics and maximal moisture content, we performed a first identification with a Fickian diffusion law.

For each type of sample, the Fickian representation provides a satisfactory model of the experimental data. The hand lay composites are the only materials which show a significant difference between experiments and model.

		D [m²/s]		C_∞ [%]	
		Average	*Standard dev*	Average	*Standard dev*
Prepreg	**1 bar**	5.62E-14	*9.64E-16*	5.1	*0.2*
	500 bar	5.93E-14	*4.64E-15*	5.0	*0.2*
Infused	**1 bar**	1.79E-13	*1.18E-14*	4.7	*0.1*
	500 bar	1.03E-13	*3.41E-15*	5.0	*0.1*
Neat resin	**1 bar**	1.24E-12	*8.21E-14*	3.3	*0.0*
	50 bar	1.59E-12	*9.74E-14*	3.2	*0.0*
	500 bar	9.39E-13	*3.47E-14*	3.3	*0.0*
Hand lay up	**1 bar**	6.82E-13	*9.46E-14*	3.3	*0.1*
	5 bar	7.71E-13	*1.04E-13*	3.7	*0.3*
	50 bar	8.37E-13	*8.00E-14*	6.7	*0.5*
	500 bar	1.46E-12	*1.21E-13*	6.5	*0.5*

Table 5.2. Identified coefficients by optimisation of a Fickian law on the experimental data.

The diffusion parameters are reported in Table 5.2. Moreover, to get a better representation of all the parameters of the different types of materials, their variation compared to the reference (values at 1bar) are presented as a function of hydrostatic pressure on Figure 5.10.

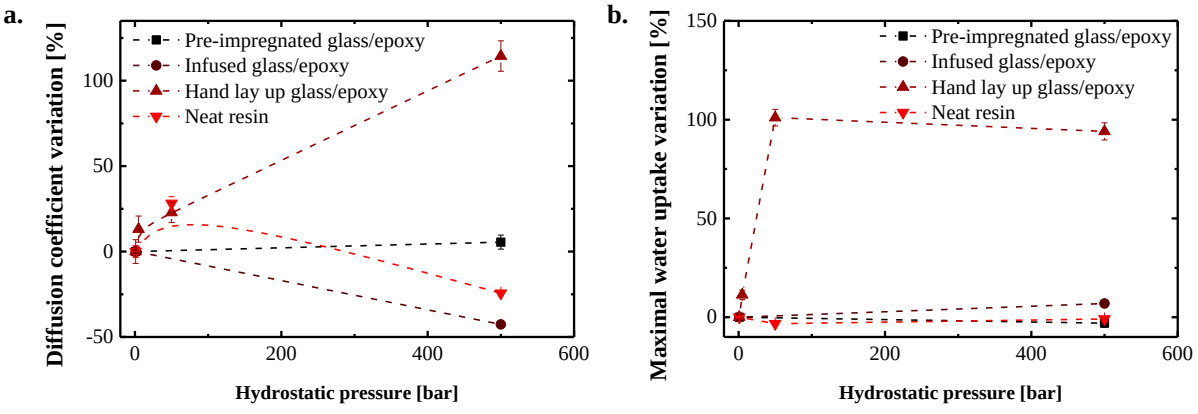

Figure 5.10. Variation of the diffusion coefficient [a.] and maximal moisture uptake [b.] with the hydrostatic pressure applied.

The same trends as those observed qualitatively previously can be noted. First, the maximal moisture uptake in neat resin, pre-impregnated and infused composites is unaffected by

hydrostatic pressure. Second, the diffusion coefficient of pre-impregnated samples remains the same under pressure while for neat resin and infused specimens the value is slightly reduced by a large pressure rise. Finally, hand lay up composites show an important increase in maximal water weight gain with pressure rise up to 50 bar and then it stabilises. In this case, the diffusion coefficient also shows an important increase with the pressure rise, with no stabilisation, at least up to 500 bar.

To conclude, previous studies [40], [67], [80] have predicted the pressure effects observed here on infused and neat resin samples. However, hand lay up composites show a significant and unexpected effect of pressure on water uptake. Moreover, the main difference between neat resin, infused and hand lay up samples is the processing method used. Therefore the impact of pressure should be influenced by the process itself or by one of its side effects (e.g. microstructure).

5.3.2. Discussion

This section aims to understand the reason for the additional moisture uptake in the hand lay up composites. As suggested above, it seems reasonable to suggest that the difference is related by the process or the microstructure it induces.

To examine this effect, we studied the water uptake in these samples in three ways: the influence of fibre orientations, the effect of porosity ratio and the diffusion under pressure in saturated materials.

5.3.2.1. Effect of fibre orientation

To get a better understanding of the water diffusion behaviour in the hand lay up composite, we will first identify the transverse and longitudinal diffusion coefficients. A study has been performed on rectangular plates immersed at 500 bars and 60°Cfor two types of hand lay-up composite specimens (Figure 5.11).

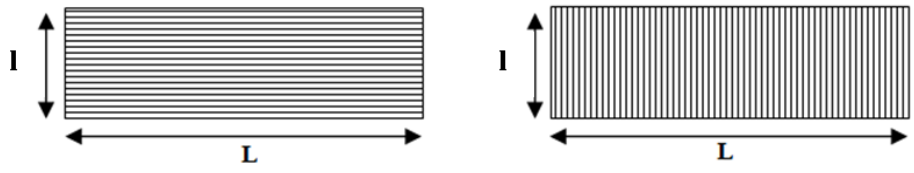

Figure 5.11. Specimens used to examine longitudinal [left] and transverse [right] diffusion. With the following dimension: L=50mm, l=15mm, d=2.2mm.

Transverse specimens will be noted T_i and longitudinal ones L_i (with i the number of the specimen). Longitudinal specimens will have a diffusion coefficient highly dependent on

the transverse diffusion coefficient, while the longitudinal coefficient will dominate diffusion in transverse plates. Three samples of each specimen type were immersed.

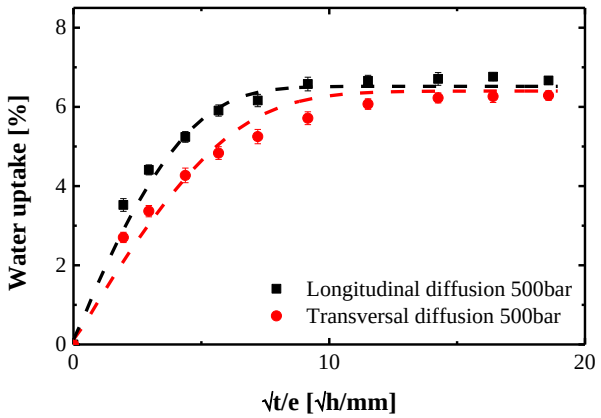

Figure 5.12. Water uptake in transverse and longitudinal plates at 500 bar, 60°C.

Figure 5.12 shows results obtained from this study, and it is clear that the diffusion kinetics are different for L and T specimen types. The transverse specimens show faster diffusion kinetics than the other specimens. In order to quantify the diffusion coefficient variations due to aligned porosity, an identification has been performed on these specimens, based on an iterative method as shown in Figure 5.13:

- Diffusion in longitudinal plates is used to identify D_T by setting a constant D_L
- Diffusion in transverse plates is used to identify D_L by setting a constant D_T

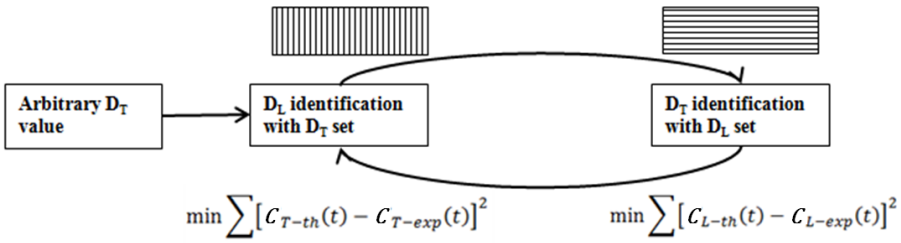

Figure 5.13. Identification method of D_T and D_L from diffusion in rectangular plates.

The diffusion curves obtained from identification are consistent with experimental values (Figure 5.12). The identified coefficients from the rectangular specimens are compared in Table 5.3 to theoretical values. There are various micro-mechanics models to predict diffusion coefficients [30]. Here an expression based on the work of Shirrell and Halpin [35] was applied, $D_L = D_{resin}$ and $D_T = D_{resin} / (1+v_f)$.

Table 5.3 shows that the transverse coefficient based on resin weight gain and fibre content is in good accordance with theory, whereas longitudinal diffusion is much higher than would be

expected in unstressed composites ($D_{L(identification)} > 40 \times D_{L(theory)}$).

Such an important deviation with the theory necessarily translates the influence of other parameters than only fibre orientations.

	D_{RESIN}	D_L	D_T
Identification results	1.24×10^{-12}	4.91×10^{-11}	7.71×10^{-13}
Theoretical values		1.24×10^{-12}	7.77×10^{-13}

Table 5.3. Diffusion coefficients (in m²/s) obtained by identification compared with theoretical ones from [35].

To identify the phenomenon responsible from this abnormal diffusion phenomenon, we performed an X-ray tomography analysis of the hand lay up specimens. The aim was to highlight morphological defects or an abnormal microstructure (Figure 5.14).

This study revealed high porosity which was oriented along the fibres. These defects can entirely explain the additional water uptake in the composites. First, the large void ratio increases the maximal moisture content in the samples. Second, the porosity orientation along the reinforcements induces water diffusion with a preferential diffusion along the axes (longitudinal diffusion coefficient increased).

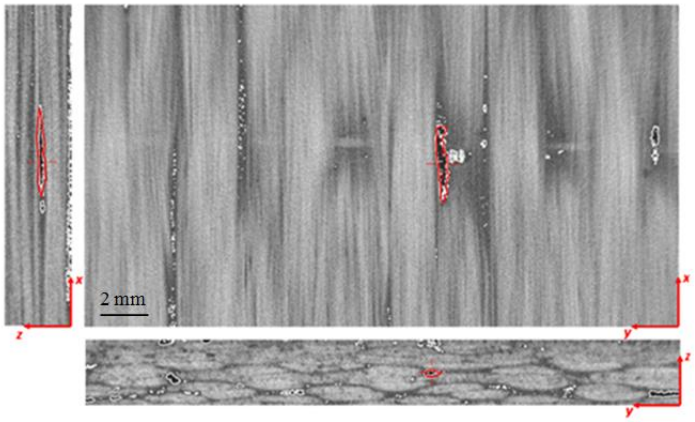

Figure 5.14. Typical shape of the void inclusions in the hand lay up composites.

Based on these observations, further analysis was performed, in order to confirm the hypothesis that additional water uptake is located inside the pores within the polymer.

5.3.2.1. Effect of porosity

First, the porosity identification in each type of material (Table 5.1) has shown a significant void content only in the case of the hand lay up composites. This observation is in good agreement with the additional water uptake which is only identified for that material.

A more accurate study has been performed on hand lay up samples, in order to

determine the exact porosity ratio of each samples tested. This technique consists of evaluating the void ratio from optical microscope images analysed with *ImageJ* software from ten different locations for each specimen. The results obtained (Table 5.4) show large porosity variations from one specimen to another.

First, the important scatter in the values can be compared to the significant standard deviations of the maximal water uptake in hand lay up composites under hydrostatic pressure (Table 5.2 and Figure 5.9).

Second, the large void contents and scatter do not seem to affect water diffusion at atmospheric pressure.

Pressure	Specimen	Void content
1 bar	1	**6.0%**
	2	**4.7%**
	3	**5.3%**
	4	**4.8%**
	5	**5.0%**

Pressure	Specimen	Void content
50 bar	2	**5.0%**
	3	**4.7%**
	4	**8.1%**
	5	**6.4%**

Pressure	Specimen	Void content
500 bar	1	**4.5%**
	2	**4.6%**
	3	**4.9%**
	4	**5.5%**
	5	**4.4%**
	6	**4.2%**

Table 5.4. Void content for each specimen.

The diffusion parameter the most affected by pressure is the maximal moisture content (Figure 5.10). Therefore, to verify the impact of porosity ratio on this value, we introduce a new parameter ($C_{add\infty}$) which can be related to the void content (Eq. 5.2). This value represents the difference between maximal water uptake in the neat resin ($C_{NR\infty}$) and in hand lay up composites under hydrostatic pressure ($C_{HL\infty}$).

$$C_{add\infty} = C_{HL\infty} - C_{NR\infty} \qquad \textbf{Eq. 5.2}$$

When we represent this new parameter as a function of the porosity ratio in each specimen for the different pressures, we obtain a clear dependence of the additional water uptake on porosity as soon as the pressure increases.

Moreover, the maximum water uptake stabilises for high void content (above 6%). This phenomenon can be induced by the variable size of porosities, which influences their fill ratio. This latter quantity is independent of the porosity ratio and can only depend on pressure levels, shape and size of the defects. If we make the assumption that water is in the liquid state, the pore fill ratio can be expressed as a function of the additional volume of water uptake $V_{add,water}$ and the volume of initial voids $V_{0,voids}$ (Eq. 5.3). The additional volume of water uptake is a function of the water density ρ_{water} and the additional weight gain ΔW_{add} (the difference between the maximal weight of composite sample from experimental data: W_∞ and

its theoretical value if the water would only diffuse in the resine: $W_{th,\infty}$).

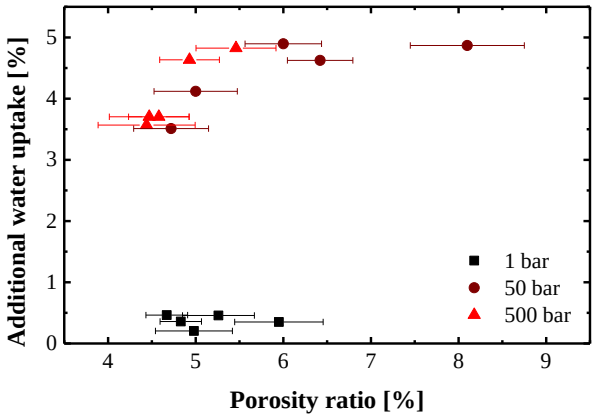

Figure 5.15. Maximal water uptake in defects as functions of void content at different pressure levels.

Figure 5.16 indicates that the rise in pressure between 1 and 50 bar has the same effect on this parameter as on the weight of water in porosities (Figure 5.15). Therefore, the voids are filled differently depending on the level of hydrostatic pressure.

$$\text{Pore fill ratio } (\%) = \frac{\Delta V_{add,water}}{V_{0,voids}} = \frac{\Delta W_{add} \cdot \rho_{water}}{V_{0,voids}} \qquad \textbf{Eq. 5.3}$$

Finally this section gives clear evidence for the influence of porosity on the water uptake behaviour when a sample is subjected to hydrostatic pressure. Moreover, the pressure level has an important impact on the water uptake inside the voids as shown in Figure 5.16. In order to have additional evidence, the next section focuses on the detection of water inside the voids.

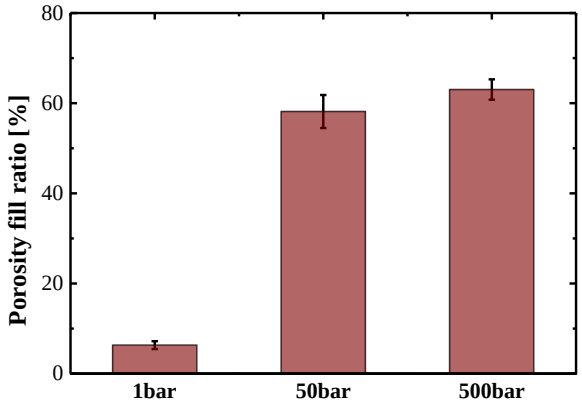

Figure 5.16. Porosity fill ratio for the different pressures applied.

5.3.2.2. Effect of pressure on saturated samples

The aim of the next section is to examine the presence of water inside the voids. To

get a good comparison between unaged samples and those aged under atmospheric and 500 bar pressure, we used five samples and studied them before ageing, after saturation at 1 bar and after a second diffusion at 500 bar. The diffusion curves obtained during these experiments are reported in Figure 5.17. To identify the presence of water in the voids, we chose to use ultrasonic signal (US) analysis. This technique can follow water ingress by comparison with a reference without water (unaged specimens). It is based on the property of ultrasound, which diffuses without loss in water but cannot propagate in the air. Therefore, a sample with unfilled voids will show a large loss of signal while a sample with water inside its voids will have lower signal attenuation.

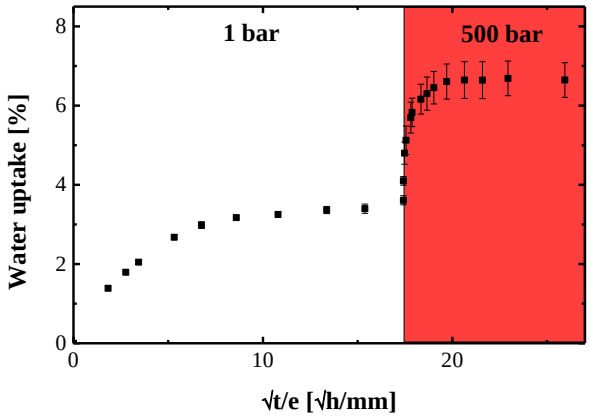

Figure 5.17. Water uptake in samples aged first at atmospheric pressure and then under 500 bar.

Samples subjected to successive levels of pressure highlight two diffusive behaviours. The first one is the reference diffusion at 1 bar which can be modelled by a Fickian law. The second one is only induced by pressure rise and therefore should entirely translate the water uptake inside the voids. The maximum water uptakes are equivalent to the ones shown in Figure 5.9 for diffusion at 1 and 500 bar.

The results from US analysis on the samples before ageing and after saturation at atmospheric and 500 bar pressure are reported in Figure 5.18 and show two main characteristics. First, analysis on unaged samples and after exposure at 1 bar reveal a large attenuation, which corresponds to the presence of defects. In contrast, the ultrasonic signal shows much lower attenuation when the same samples have been immersed under 500 bar pressure. This difference can only be induced by the presence of water inside voids, which allows ultrasonic signal propagation in contrast to the case of unfilled voids.

Finally, this section highlights the presence of water inside the defects of hand lay up composites. Moreover, as the samples aged at atmospheric pressure present some differences compared with the unaged specimens (Figure 5.18), we might expect that there is some water

in the voids in the case of immersed samples (as predicted in Figure 5.15). Nevertheless, the US analysis cannot quantify the amount of water inside voids, to get this type of information we can use an indirect method as in 5.3.2.1.

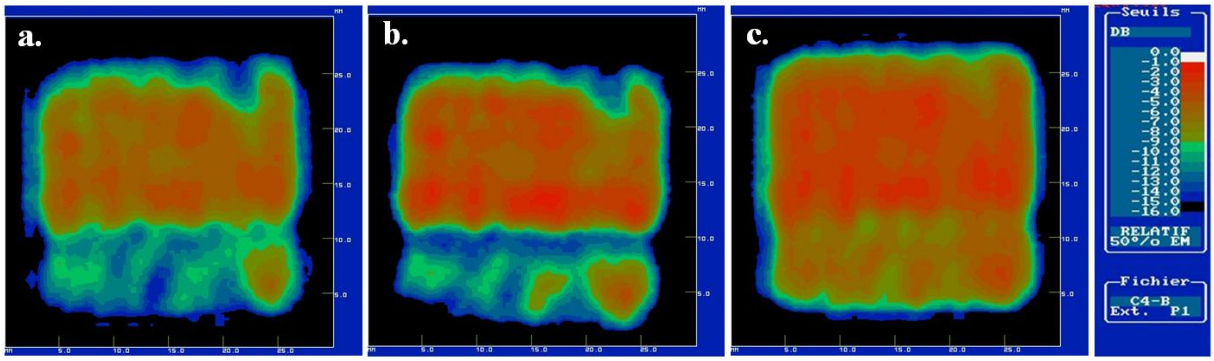

Figure 5.18. US analysis of unaged samples [a.], specimens saturated at atmospheric pressure [b.] and materials aged under 500 bar of hydrostatic pressure [c.].

5.3.3. Modelling

The previous section confirms that additional water uptake in hand lay up composites is induced by water diffusion inside voids. The next aim is to establish a theory which can model this type of diffusion by taking into account physical quantities such as void content, diffusion coefficient and maximal water uptake of the neat resin.

For this theory we established a water uptake quantity in voids M_{void} which can be expressed with the additional water weight in voids w_{add} and weight of the resin in the initial composite $w_{0,resin}$ (Eq. 5.4). From this quantity, we can also define a water concentration in the void (c_{void}), also defined in Eq. 5.4. In the next sections, we will present different techniques to link this quantity with the water uptake in the resin and predict the global value in the composite.

$$C_{voids}(t) = \frac{\Delta W_{add}(t)}{W_{0,resin}} = \frac{1}{V_{voids}} \iiint_{voids} c_{voids}(x,y,z,t)\, dV \qquad \textbf{Eq. 5.4}$$

$$C_{total}(t) = C_{resin}(t) + C_{voids}(t) \qquad \textbf{Eq. 5.5}$$

5.3.3.1. Model with porosity representation

The first way to model the impact of porosity on the water diffusion in the sample, is to represent the voids. Nevertheless, the voids shape and dimension are variable and can diverge from one specimen to another; therefore we have to make some assumptions. First, only one void is considered, and its surface ratio is defined as equal to the porosity density.

Second, the shape is first considered to be cylindrical and then with a rectangular shape. In both cases, the model considered is the same, as presented in the next sub-section.

Model presentation

Water diffusion inside the resin has been shown to follow a Fickian law here, and the fibres have only an effect on the diffusion coefficient value. Therefore, we consider a Fickian diffusion in the composite with a diffusion coefficient predicted by the relationship established in [35] (*D*).

We consider the effect of the porosity inclusion, by comparison with heat diffusion, as equivalent to a source term (as Lopez et al. did in [77]). This quantity is defined as the opposite of the water filling rate of the void ($\frac{\partial c_{void}(t,x,y,z)}{\partial t}$). Moreover, the water quantity in the void is considered as homogenous.

Considering these assumptions, the diffusion phenomenon can be summarised as a set of two equations: one for the diffusion in the material itself and the other which defines the fill rate in the voids (Eq. 5.6).

$$\begin{cases} \dfrac{\partial c_{resin}(x,y,z,t)}{\partial t} - D\ div\big(\nabla c_{resin}(x,y,z,t)\big) = 0 & in\ the\ material \\ \dfrac{\partial c_{resin}(x_f,y_f,z_f,t)}{\partial t} - D\ div\left(\nabla c_{resin,f}(x_f,y_f,z_f,t)\right) = \dfrac{\partial c_{voids}(x,y,z,t)}{\partial t} & on\ void\ limit \end{cases} \quad \textbf{Eq. 5.6}$$

The first equation in Eq. 5.6 can already be solved using results from previous studies ([24], [25]). However, the second equation has not been solved for such a case, and its implementation in a finite element model cannot be made in this form. To simplify this expression we define the void's filling rate by discretising the derivative operator (Eq. 5.7). In this case, we consider a fill rate with characteristic time τ, considered to be high compared to the diffusion kinetics in the material. Therefore, the water concentration in the void at the time ($t_+\tau$) is equal to the concentration on the frontier at the time *t*.

$$\frac{\partial c_{void}(t)}{\partial t} = \frac{c_{void}(t+\tau) - c_{void}(t)}{\tau} = \frac{c_{resin,f}(t) - c_{voids}(t)}{\tau} \quad \textbf{Eq. 5.7}$$

$$\frac{\partial c_{resin,f}(t)}{\partial t} = D\ div\big(\nabla c_{resin,f}(t)\big) - \frac{c_{resin,f}(t) - c_{voids}(t)}{\tau} \quad \textbf{Eq. 5.8}$$

Finally, by substitution of Eq. 5.7 in the second equation of Eq. 5.6, we obtain a relationship

between both concentrations on the void frontier (Eq. 5.8). This theory allows the global water uptake to be defined using the water diffusion coefficient in the composite without voids and adjusting the fill rate to fit the experimental results.

$$C_{voids}(t) = \frac{1}{V_{voids}} \iiint_{voids} c_{voids}(x,y,z,t)\, dV = \frac{1}{V_{voids}} \sum_{i} c_{void,i}(t).V_{void,i} \qquad \textbf{Eq. 5.9}$$

In addition, we define the diffusion of water into the defects as instantaneous and therefore water uptake in the voids $C_{voids}(t)$ is a constant for the volume of one porosity. This results in the expression of $C_{voids}(t)$ as the sum of water concentration in each void multiplied by its volume (Eq. 5.9) .

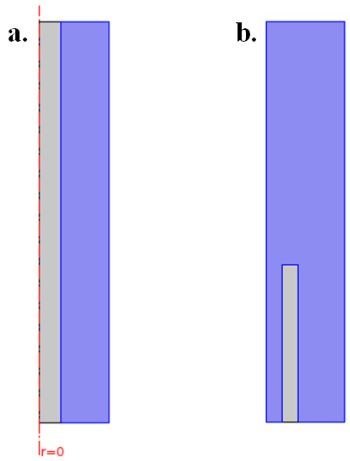

Figure 5.19. The two void representations used: a centred [a] and parametric porosity [b].

For the next sub-sections, we consider only one defect corresponding to the global volume of voids in the real sample ($V_{void} = Xv_{voids}.V_{composite}$). Two configurations are studied: porosity centred in the sample and a void located at a distance d from the specimen surface, Figure 5.19. In these cases, there is only one void represented and therefore the Eq. 5.9 can be simplified and becomes Eq. 5.10.

$$C_{voids}(t) = c_{void}(t) \qquad \textbf{Eq. 5.10}$$

To summarise, a standard Fickian diffusion is considered in the homogenised composite (blue part in Figure 5.19), with the diffusion coefficient based on neat resin identification and a theoretical equation (Figure 5.3). In the void, the diffusion is represented by an instantaneous diffusion with a characteristic time lower than the step time chosen. The boundary conditions on the porosity surface are controlled by the equation Eq. 5.8.

Concentric porosity

First, we investigate the case of concentric porosity in order to highlight if this model can represent the real diffusion correctly. And then, in the case of good correlation, we could investigate the possibility to establish an analytical solution to the problem.

The simulation takes into account some assumptions:

- First, on the dimensions: the void volume is considered as equal to the average value of porosity volume (identified in Table 5.4), the diameter of the cylinder is equal to the sample thickness and the void is considered to be all along the cylinder.
- Second, for the boundary conditions: we consider the diffusion as axis-symmetric and the diffusion at the extreme ends is neglected.

The results shown in Figure 5.20 show a good representation of diffusion for low pressure levels. Nevertheless, in the case of high hydrostatic pressure, the initial experimental diffusion shows significant deviation from the model. This can be explained by the localisation of the void in the centre: the defect will start to fill only when the water reaches its edges. Therefore, the diffusion delay in the case of the model is explained by the representation of the porosity.

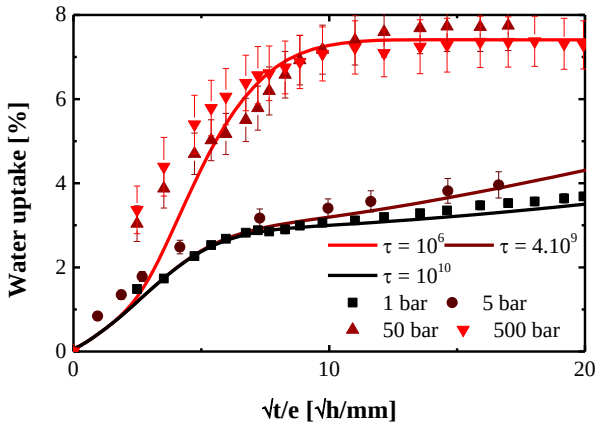

Figure 5.20. Diffusion curves from the concentric model compared to the experiments.

In order to avoid this problem, we used another representation of the void which is developed in the next sub-section.

Parametric porosity

The second representation considers a two dimensional diffusion and a porosity centred in the length but with a parametric distance to the thickness surface (*d*), as shown in

Figure 5.19 [b].

In this case we make the following assumptions:

- First, on the dimensions: the void volume is considered as equal to the average value of porosity volume (identified in Table 5.4) and the porosity has a shape factor *f* (length over width ratio).
- Second, for the boundary conditions: we consider the diffusion to be symmetric along the length.

We performed a study to understand the impact of each parameter on the diffusion behaviour of the model in Appendix 2. A good representation of the experimental diffusion behaviours was obtained with the following values of τ: 10^6, 10^7, 5.10^8 and 10^9 s for pressures respectively equal to 500, 50, 5 and 1 bar (obtained from the study presented in Appendix 2). In this case, the distance between porosity centre and the edge was equal to *0.12xd* (with d the sample thickness), shape factor *f* was fixed at 20 (corresponding to a shape factor comparable to the one observed in Figure 5.14)..

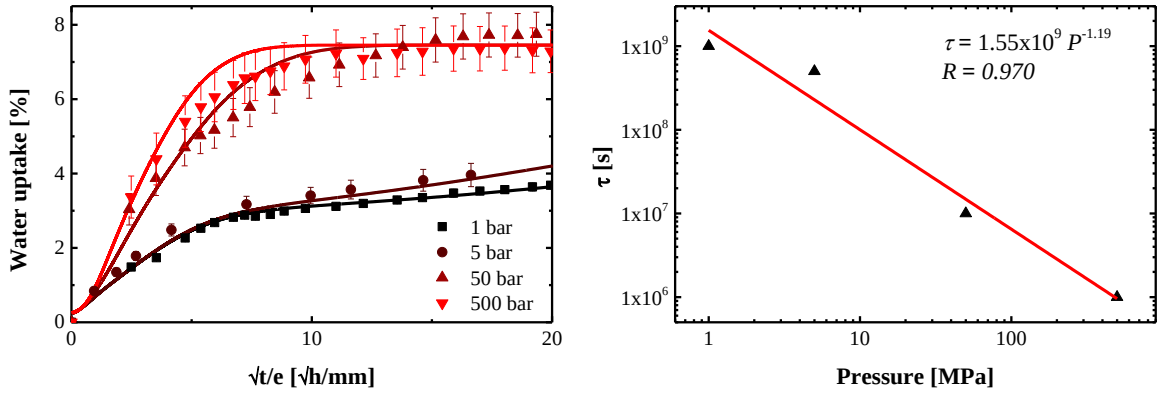

Figure 5.21. Diffusion curves from the parametric model compared to the experiments [left] and porosity fill rate as a function of pressure [right].

The results obtained with these parameters are reported in Figure 5.21 and show a reasonable correlation with the experimental data. Moreover, the porosity fill rate constant (τ) follows a power law function of the pressure (Figure 5.22 [right]).

The water content in the specimen depth is modified compared to classic Fickian diffusion: the porosity increases the kinetics and creates a decentred concentration shape (2).

To conclude, this type of model provides a reasonable representation of the diffusion behaviour. Nevertheless, we need to represent an artificial porosity and adjust its shape factor and its distance from the edge, therefore its usefulness is limited. The next sub-section introduces a more practical model.

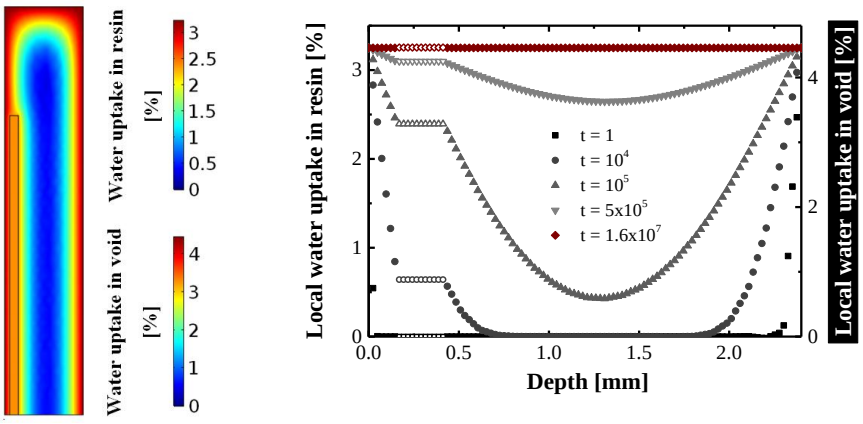

Figure 5.22. Profiles of water content from the parametric model, in the samples surface at t= 10^5s [left] and depth [right].

5.3.3.2. Homogenised model

In order to translate the effect of voids without the physical representation of porosity, we use an homogenised model, which takes into account the void density, fill ratio and fill rate.

In the homogenised case, we consider the influence of defects in each mesh element and therefore we have one equation to solve throughout the material Eq. 5.11.

$$\frac{\partial c_{resin}(x,y,z,t)}{\partial t} = D\ div\left(\nabla c_{resin}(x,y,z,t)\right) - \frac{c_{resin}(x,y,z,t) - c_{void}(x,y,z,t)}{\tau} \qquad \textbf{Eq. 5.11}$$

In the previous section we have presented the results obtained using a finite element calculation, nevertheless calculation with an homogenised model can also be made with finite differences using Matlab™ (Appendix 3).

The homogenised model shows a good correlation with experiments with $\tau=10^5$s for 500 bar and 50 bar, $\tau=3.10^7$s for 5 bar and $\tau=10^8$s for 1 bar. Compared to the previous model the values of τ are of the same order of magnitude, with only a slight decrease in the case of the homogenised model. In addition, we find a slight deviation for the initial values: the model kinetics are slightly slower than the real case. This phenomenon is explained by the void content which is considered as homogenous in the depth. In the real sample case, porosities are distributed in a more random way.

To develop this further, and to make the model more accurate, a porosity analysis should be performed in order to establish the void size distribution in the thickness. Once this parameter has been established, a porosity ratio could be associated which is dependent on the spatial

coordinates.

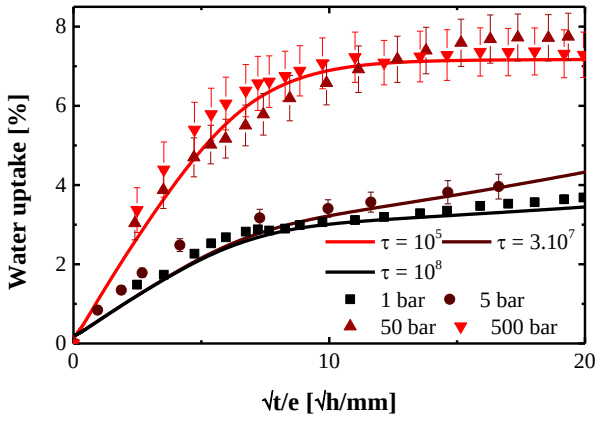

Figure 5.23. Diffusion curves from the homogenised model compared to the experiments.

5.4. Conclusion

Coupled behaviour in the case of immersed static tension shows significant differences compared to the semi-coupled case. This study has mainly focused on the comparison of water diffusion behaviour in the semi-coupled and coupled cases.

For composite samples stressed away from their reinforcement direction, water uptake follows the same increase in a first step and deviates in a second phase: the semi-coupled samples show a deviation which is decreasing compared to the reference while the specimens tested under fully coupled conditions show a deviation which increases until failure. For composites stressed along one of its reinforcement directions the semi-coupled behaviour shows no deviation from the reference, while specimens tested coupled show a diffusion behaviour which deviates: from the beginning of immersion for specimens stressed above their damage limit and after long times for other cases.

From these observations, it is clear that the damage introduced in samples modifies the diffusion behaviour of materials both stressed and pre-stressed away from their reinforcement direction and of samples stressed in the direction of one of their reinforcements. Moreover, in the case of ±45° composites, the acceleration of the diffusion translates the propagation of the cracks in the samples until failure.

Finally, for further studies the permanent or/and total deformation should be considered immersed and in air in order to quantify the effect of coupling on the composites' mechanical behaviour.

In the case of diffusion under hydrostatic pressure, glass/epoxy samples show different water uptake behaviour depending on the pressure level and the type of manufacturing process used.

All the samples with no significant macroscopic defects show a diffusion behaviour unaffected or slightly decreased by pressure rise. This phenomenon is predicted by models based on thermodynamic or free volume theories. Nevertheless, when a composite contains large void contents (between 5 and 8% in volume), the water uptake increases significantly with pressure rise. This increase depends on the void ratio and can be modelled using a Fickian diffusion coupled with a source term.

For further study, it would be interesting to investigate the localisation of porosities and introduce a quantity depending of their spatial coordinates. Moreover, we could complete the study by characterizing the purely mechanical effect of hydrostatic pressure on materials. This phenomenon will have a tendency to reduce void volume and therefore reduces the maximal water uptake (observed between 50 and 500 bar).

Part B.
Synthetic ropes

Chapter 1.

Bibliography on synthetic ropes

1.1. Introduction

The offshore oil and gas and marine renewable energy industries both require innovative mooring techniques in order to extend operational windows of floating structures. In this context, conventional wire rope and chain configurations are limited, both in terms of water depth and dynamic response, due to material and economic considerations. During the last decades, alternative mooring systems, involving synthetic ropes, have been studied and tested, in particular for station-keeping of floating platforms offshore as in studies [81]–[87]. While some of these systems are still at the test stage, others are currently in use and show important improvements compared to steel, in terms of break elongation, ultimate stress and modulus (Figure 1.1).

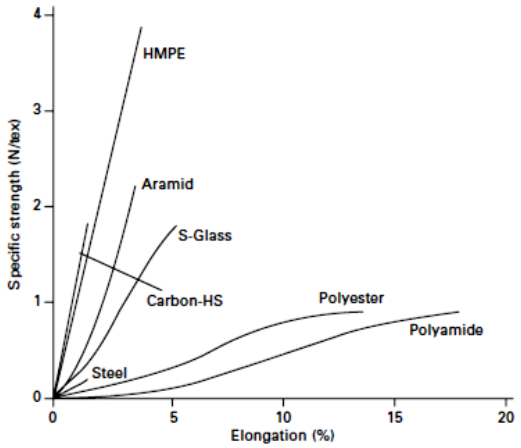

Figure 1.1. Tensile behaviour of different types of synthetic fibres compared to steel wire

Among the alternative systems, High Molecular weight PolyEthylene (HMPE) fibre ropes show great potential, thanks to their high mechanical properties and light weight. These fibres are not affected by water exposure. However, the remaining issue with most HMPE ropes is their poorer creep behaviour. For this reason, recent materials developments are focussed on alternative HMPE fibres with much lower creep deformation, such as the Dyneema DM20 grade, presented in [88].

At the other side of the synthetic fibre spectrum, we find Polyamide 6 fibres (low-cost synthetic). They represent a highly ductile fibre with low creep behaviour, compared to HMPE, and are much more highly hydrophilic.

These two materials have been chosen in order to understand the effect of the water on both scales of synthetic ropes: on the fibre material itself, in the case of polyamide and at the rope construction level in the case of HMPE.

Synthetic ropes can be constructed in different ways, among them three are mainly

used: laid, braided and plaited ropes (Figure 1.2). The laid ropes are the most efficient construction in terms of break stress compared to the others. Nevertheless, tension loadings on laid constructions have a tendency to generate rotation and therefore cannot be used for all applications. In dynamic loaded applications as in the offshore sector, plaited and braided ropes are preferred. Plaited ropes are mainly used for large scale applications. The study is focused on small scale ropes (5mm) and therefore will consider braided constructions.

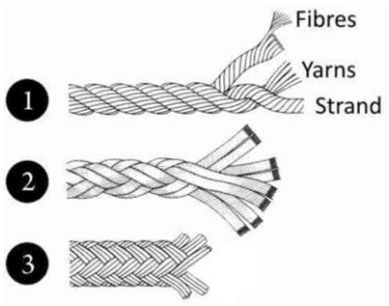

Figure 1.2. Different rope constructions: 1 – Laid rope; 2 – Plaited rope; 3 – Braided rope

Braided ropes are constructed at four scale levels: the fibre (or monofilament), the yarn, the strand and the rope. The fibre represents a single filament of a material composed of two phases, crystalline and amorphous, for both polyamide and HMPE. The yarn is the assembly of thousands of fibres to ease the handling during braiding. The strand is made up of yarns assembled together, as yarn can be twisted to increase its properties (part 1.2.1.2) and simplify rope making.

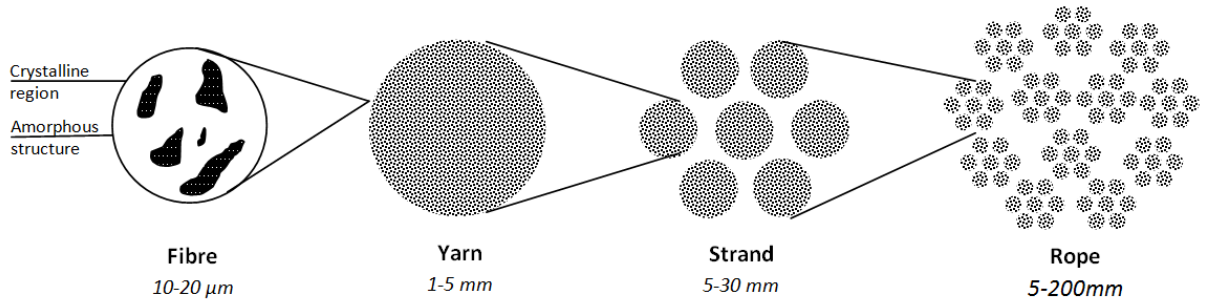

Figure 1.3. The different levels of sub-constructions in a braided rope

This literature review will be organised in a similar way to the section on composite materials. The first part will focus on the mechanical behaviour of the different fibres at the different scale levels. In a second step, the specificities of water diffusion inside these materials will be exposed. Finally, in the last section we will introduce the coupling effects previously studied in the literature: the mechanical response induced by water diffusion.

1.2. Mechanical behaviour

Synthetic ropes are used as mooring or handling lines in offshore applications, which involve important mechanical loadings. These stresses can be diverse, from static tensile loading (e.g. towing loading), to dynamic tensile stress (e.g. displacements created by waves). Moreover ropes are flexible materials which are mainly stressed in tension if we do not consider the end connexions and handling effects.

Therefore, the following section is focused on rope tensile behaviours under quasi-static, static creep, and dynamic tension loading.

1.2.1. Tensile behaviour

Ropes are multi-scale materials and tensile loading at the rope scale will induce other types of loadings at the yarn or fibre scale. The next sub-sections will focus on the different scales of the fibre construction, to understand the impact of the structure on the materials' static tensile behaviour.

1.2.1.1. Fibres tensile behaviours

The fibres studied here are both semi-crystalline materials and involve a biphasic structure with crystalline and amorphous regions. Therefore the starting point of the review is to list the different phases' mechanical behaviours before getting into the semi-crystalline material.

Amorphous fraction

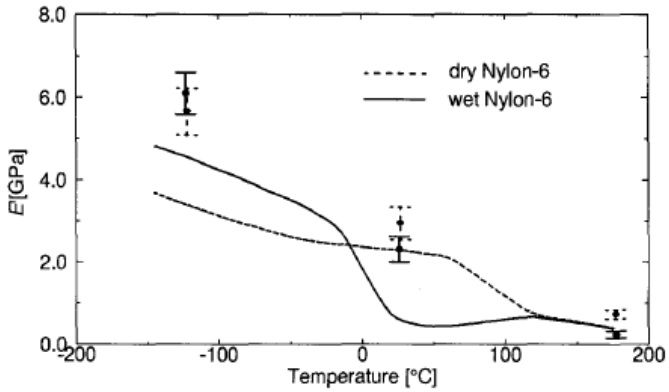

Figure 1.4. Experimental (lines) – 70% amorphous – and computed (circles and error bars) – 100% amorphous – storage moduli of dry and 'wet' (10 wt% water) PA-6 [89].

Amorphous regions are characterised by entangled chains with no specific organisation. This structure induces high variability in mechanical properties, highly

dependent on many parameters such as the entanglement density or chain length.
It is difficult to obtain purely amorphous fibre material and one solution to study the behaviour of 100% amorphous polymers is to use simulations. Zehnder et al. [89] studied the behaviour of Polyamide and Polyethylene amorphous structures with this technique. The simulation consists in building chains using the stepwise method of Theodorou and Suter [90]. Based on the simulation of chain bonds, the method recreates the polymer behaviour allowing the identification of mechanical parameters (see Figure 1.4).

Nevertheless, due to the unorganised structure of polymer chains in amorphous regions, the simulation is still hard to manage. The difficulty to represent this high variability in the structure can explain the difference between simulation and experiments.

Crystalline fraction

Fibre polymer cannot be fully crystalline and so the only way to investigate its mechanical properties is by modelling the chains structure. Nevertheless, unlike amorphous structures, chain arrangements of the crystalline phase are easy to compute thanks to their geometrical and cyclic structure (Figure 1.5).

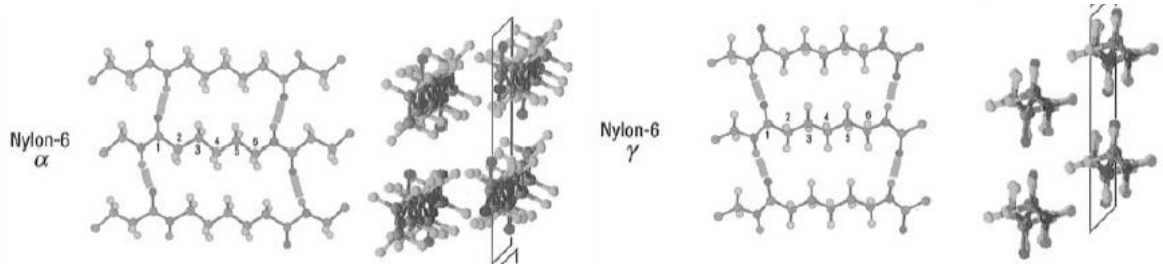

Figure 1.5. Structure α and γ of Nylon 6 (from [11])

Nylon 6 crystalline region is divided in two groups: α and γ structures (see Figure 1.5), the difference between these organisations resides in the location of bonds between chains.
Both of these structures have a specific mechanical response defined in [91] and [92]. These theories predict the behaviour by studying the bond energy and linking it to the full polymer behaviour.

In the case of polyethylene [93], there is only one form of crystalline structure studied: the orthorhombic crystal system.

Results from theoretical methods are compared in Table 1.1 to experimental values. These observations were made on Nylon by X-ray scanning method in [94] and [95], and for polyethylene by neutron scattering in [96].

Material		Young Modulus along the chain axis (GPa)		
		Observation	Calculated by Tashiro et al.	Calculated, from [92]
Nylon	α	100 [94]	311.5 [93]	235.29
	γ	27 [95]	53.7 [93]	131.97
PE		329 [96]	315.5 [97]	

Table 1.1. Comparison between different theories and observed data

Calculated and observed values of Nylon's Young's modulus are quite different. The calculation method gives modulus along the polymer chains axis in a perfect planar-zigzag conformation. The real molecular chains are slightly contracted from the fully extended conformation. Miyasaka et al. [94] have shown from a strain-stress curve (see Figure 1.6) that the Young's modulus increases with the chain stretching. Finally, stretched chains have a modulus which can be compared to the value from Tashiro's theory [92].

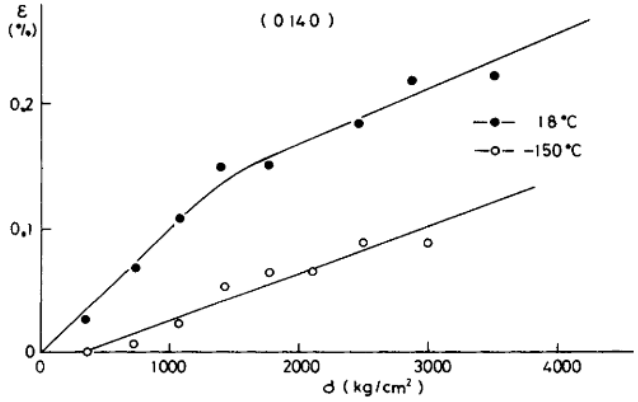

Figure 1.6. Strain-stress curve in the chain direction of α-phase crystal of Nylon 6 [94]

For polyethylene crystalline structure, an experimental value is obtained by the neutron scattering method in [96] in good agreement with the modulus calculated by Tashiro et al. [93] (see Table 1.1).

Filament scale

Once we have seen both phase behaviours separately, we can go further and study the behaviour of fibre materials.

In the case of polyamide fibres, the stress-strain curve follows a typical S-shaped profile. This behaviour is common for many melt-spun fibres (Figure 1.7.). These curves have been studied in [97] for Nylon 6-6 material characterised by a behaviour comparable to Polyamide 6 fibres. From this study, four different domains can be identified, corresponding each to a characteristic event (Figure 1.7).

- From 0 % to 3.5 % strain, the curve reflects an alignment of the amorphous regions, the crystalline domain remaining unloaded. As a consequence, amorphous regions are partly decreased, from 31 to 26 %, by the crystallisation induced by mechanical stress, the crystalline ratio increases significantly (from 46 to 51 %).
- From 3.5 to 10 % strain, he characteristic shape of the end of the amorphous domain orientation appears. In this part, the crystalline ratio increases slower than before (only 3.5 %).
- From 10 to 15 % strain, enthalpy mechanisms are activated: C-C bonds form crystals and oriented regions are elongated. The chains from crystalline regions start to be affected by the loading and then break.
- Above 15% strain, the visco-plastic mechanism is connected to macro-fibrils sliding.

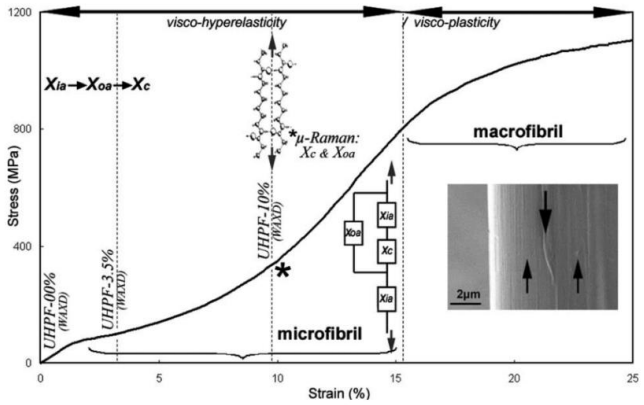

Figure 1.7. Schematic representation of the micro/macro-mechanisms involved in fibre deformation [97]

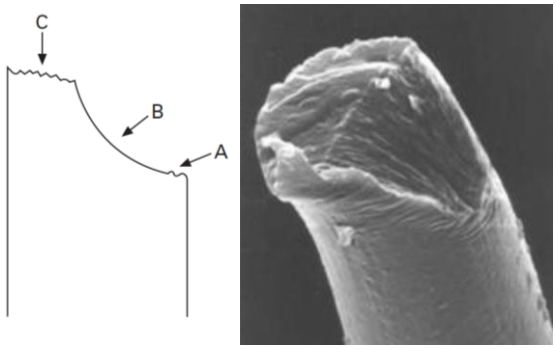

Figure 1.8. Tensile failure characterisation of a nylon 6 monofilament [98]

These micro and macro-damage mechanisms result in a ductile failure of the polyamide fibre. In this instance, fractography studies highlight three typical regions (Figure 1.8) corresponding to different fracture stages: A: initiation of the crack; B: stable propagation of damage; C: Failure. This phenomenon takes place in the last part of the curve Figure 1.7,

during macro-damage creation.

HMPE fibres are highly oriented and crystalline materials compared to Nylon fibres. Therefore, the first two stages of the nylon's mechanical behaviour, characterised by amorphous chain orientation and crystallisation, will not be present. Moreover, the visco-plasticity of HMPE only appears for long time loadings (Part 1.2.2) due to the highly oriented chains which represent obstacles to damage propagation. To conclude, HMPE's mechanical behaviour is considered as purely elastic under a quasi-static loading (Figure 1.9).

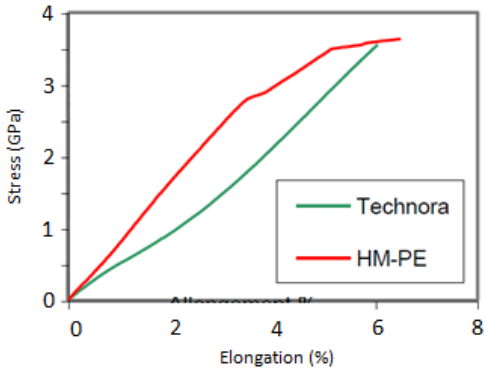

Figure 1.9. Stress-strain curve on monofilaments of Technora and HMPE [99].

Nevertheless, while testing HMPE mono-filament, there are slippage issues in the loading clamps. This phenomenon is for instance revealed in Figure 1.9 by the steps at the end of the curve. Therefore elongation values are hard to measure accurately, especially for high load levels. The materials and methods chapter will introduce a new method to get accurate strain measurement for monofilament testing.

1.2.1.2. Yarn and strand tensile behaviours

Fibres are usually combined together in yarns and strands to ease the handling during rope manufacturing. In the present study, only un-twisted yarns will be considered, the case of twist effect will be addressed in the following paragraph on strand. Then, we assume that all fibres are stressed in the direction of the yarn, and that mechanical loadings are the same for all the fibres in the yarn.

In this case, literature shows that the fracture stress for a yarn will be lower than that of the mono-filament. When the number of filaments in the structure increases, the fracture stress decreases, due to a phenomenon called "the bundle effect" directed by the inequality: $\sigma_{f,structure} < n.\sigma_{f,monofilament}$ [100] (with n the number of filaments in the structure).

Moreover, in the case of a linear behaviour for monofilaments, as HMPE, it has been shown [101] that a tensile test on yarn with a straight ramp to failure will induce a non linear stress-

strain curve (see Figure 1.10). This first nonlinear stage reflects the delay of tensioning between the different mono-filaments. This phenomenon can be reduced or suppressed, by tensile tests with initial bedding-in cycles (5 in the study in [102]) as shown by Figure 1.10, by careful handling before testing, and by introduction of a twist angle.

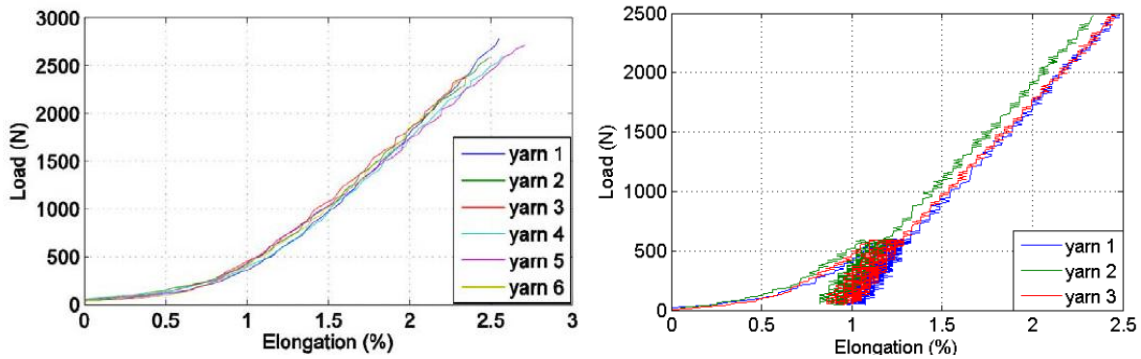

Figure 1.10. Stress strain curve for a tensile test straight to failure (left) and after 5 cycles at 600 MPa (right) (from [102])

As expected, the Nylon yarn and mono-filament follows the same mechanical behaviour (Figure 1.7 and Figure 1.11). The difference with HMPE is the absence of the first non-linear part which is explained by the ductile behaviour of Nylon, which hides the tensioning delay from one filament to another.

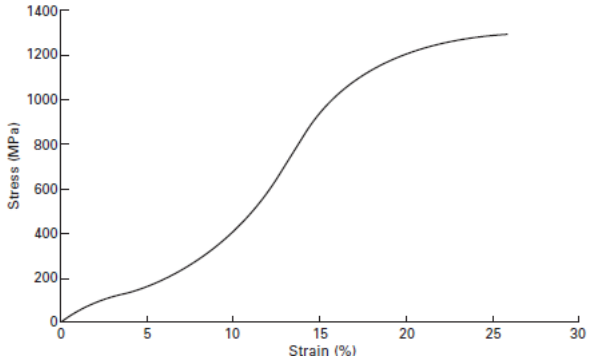

Figure 1.11. Stress-strain curve of Nylon 6-6 fibre [98]

The literature review already highlights the important influence of the mechanical behaviour's type (ductile or fragile) on the relationship between filament and yarn mechanical responses. Ductile fibres will have good correlation between filament and yarn behaviour while fragile materials will present a non-linear part only for yarns. This undesired phenomenon is usually avoided by pre-twist introduction in the yarn, before testing.

In the case of twisted strand (or yarn), the strength of strand is linked with the helix angle (α) introduced during manufacturing (see Figure 1.12). In the first part of the plot, the ultimate stress of strand increases with helix angle due to the homogenisation of the fibres

pre-tensioning. The tension will be distributed in the filaments in a more equal manner and therefore the break will appear later than in the untwisted case. In the second part of the plot, the strength is decreasing with further helix angle increase due to the misalignment of the stress with respect to the fibres direction. Hearle introduced in 1969 [103] a first mathematical expression describing this dependence: $\sigma \propto \sigma_0 - cos^2(\alpha)$ which gives a stress following the trend of Figure 1.12.

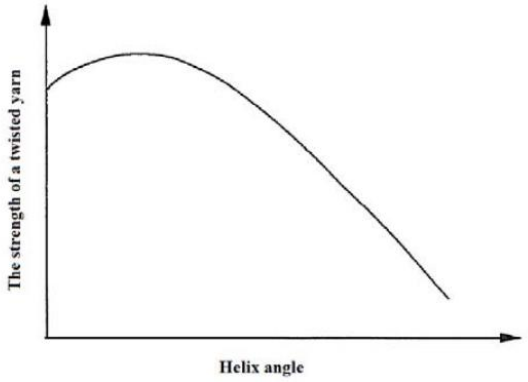

Figure 1.12. Tensile stress of a twisted yarn vs. its helix angle [104]

1.2.1.3. Ropes tensile behaviours

Since ropes are structures made of assembled fibres, their tensile behaviour highlights the same first nonlinear stage as yarn, as shown in [101] (Figure 1.13).

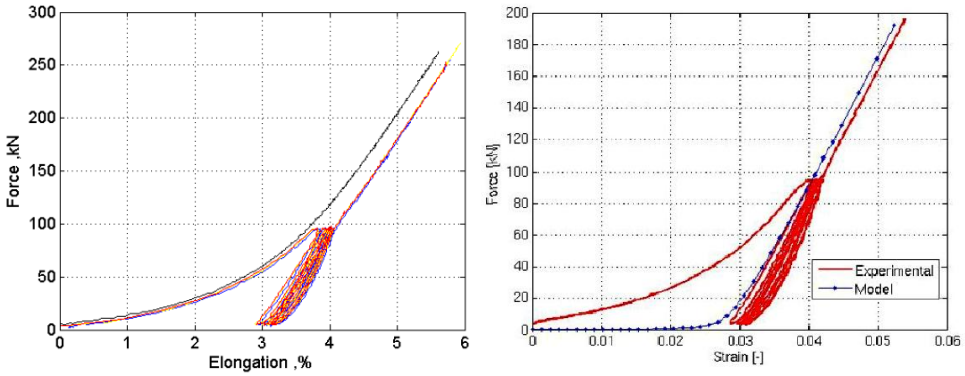

Figure 1.13. Tensile curve on HMPE braided ropes, straight to failure (black), with five bedding-in (coloured) [102] [left] – Stress strain curve of a tensile test on HMPE braided rope, experimental and simulation results [101] [right]

Unlike for yarn testing, we cannot introduce a twist angle before testing otherwise the rope structure will be modified and deviate from the real case application. Therefore, the non-linear response is usually removed following a standard pre-loading method, by applying five pre-loading cycles up to around fifty percent of the final break load (Figure 1.13) before testing to

failure.

This non-linear part can be easily modelled in the case of twisted ropes. These structures can be represented as parallel fibers with constant parameters, there is a broad literature based on this type of model, e.g. [105].

Nevertheless in the case of braided ropes, the orientation of the fibres is harder to evaluate and therefore less convenient to model. A few studies such as [106] have been made on trajectories of yarns in the braided rope during the processing by using Non-Uniform Rational B-splines: NURBS. Based on this method, finite element analyses can be performed and obtain linear elastic moduli of the structure. Nevertheless, classical finite element calculations are quite costly to use in the case of ropes since they are the assembly of multiple sub-structures.

Since this method is not optimised for mechanical simulation, other methods such as [107] have been developed without considering interactions and contact between rope elements. Yarn trajectories are estimated by simulating the rope-making process itself, applying at the end of yarns a motion equivalent to the one performed during processing, and taking into account the mechanical interactions between the yarns. This approach still requires considerable numerical capacity.

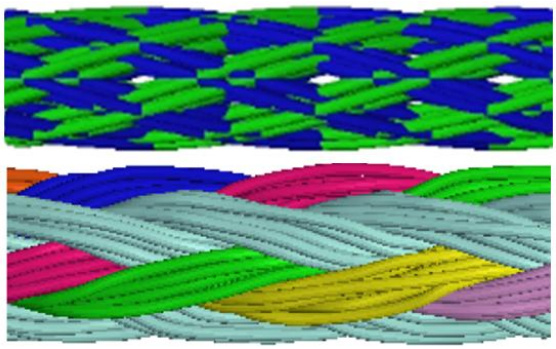

Figure 1.14. Initial arbitrary position (top) and position after simulation using Multifil code by Vu et al. (bottom) [101]

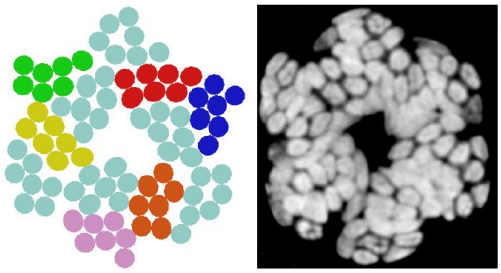

Figure 1.15. Comparison between structure obtained after simulation (left) and the measured one (right) [101]

To avoid simulating the whole braiding process, another method has been explored by Vu et al. [101] using the *Multifil* code. It starts from an arbitrary position (Figure 1.14 –top–), and searches for an equilibirum position for the yarns. This technique gives good structural simulations compared to the real case (Figure 1.15). Moreover, the mechanical behavour is modelled with yarns represented as a succession of 3D-beams, which take into account contact friction interactions between themselves. This method provides relevent stress-strain

curves (Figure 1.13 –right–) with a lighter model than usual finite element techniques.

1.2.2. Time-dependent behaviour

The previous section on quasi-static behaviour has shown the complexity induced by the rope structure. However, another specificity of polymer fibre materials is their important visco-elastic and visco-plastic responses. These characteristics induce necessarily time dependant behaviours.

1.2.3. HMPE fibres

For HMPE fibres, the first illustration of the visco-elastic behaviour is the important influence of the deformation rate and temperature on the mechanical properties (Figure 1.16). Modulus and maximum tenacity are the properties the most affected by deformation rate, while ultimate strain remains relatively constant. Moreover, the deformation rate has low effects on the properties for temperatures under 23°C.

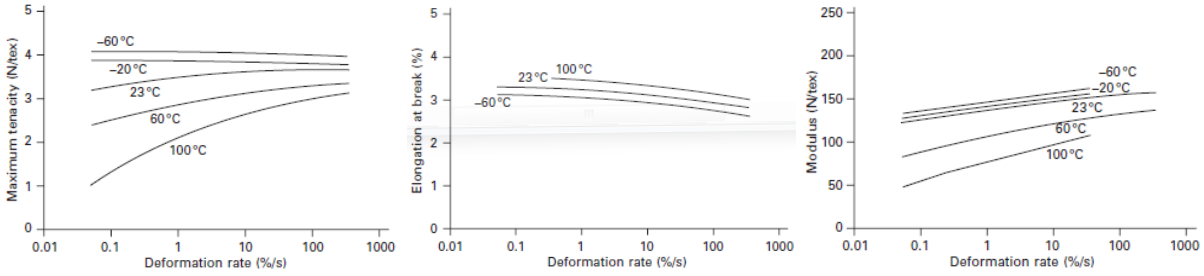

Figure 1.16. Deformation rate and temperature influence on HMPE SK76 mechanical properties [108]

The second illustration of viscous phenomena is the creep behaviour of the fibres. This constitutes a major issue since creep loadings are present in all real offshore applications: induced by towing tension, weight lifting or vessel drag. This behaviour has been identified in [81] for HMPE fibres, and characterised by a 3 stage behaviour, with: (I) an initiation phase where the material is hardening, this is characterised by a flow rate decrease; (II) a propagation phase in which the flow rate remains constant; (III) a breaking phase where the flow rate increases up to fracture (see Figure 1.16). These phenomena depend on the stress applied on the material. At high stress (near failure strength) the time to failure is low, while for lower stresses elongation and time to failure increase.

Smeets et al. [82] established relationships between elongation, load, temperature and time to failure for creep tests on HMPE fibres reported in Table 1.2. These expressions were developed in the work of Govaerts et al. [109] who developed a model based on a constant ultimate plastic strain and a plastic strain rate following a power law of the stress. Then,

Jacobs et al. [110] managed to link the plastic strain rate with stress and temperature by two thermally activated processes. Later Vlasblom et al. [111] considered a time dependent creep rate in regime II. They explained and modelled this phenomenon by recalculating the real stress at each time step using the cross section reduction. The model modification allows better representation of creep behaviour especially in the case of long term tests (i.e. for real applications).

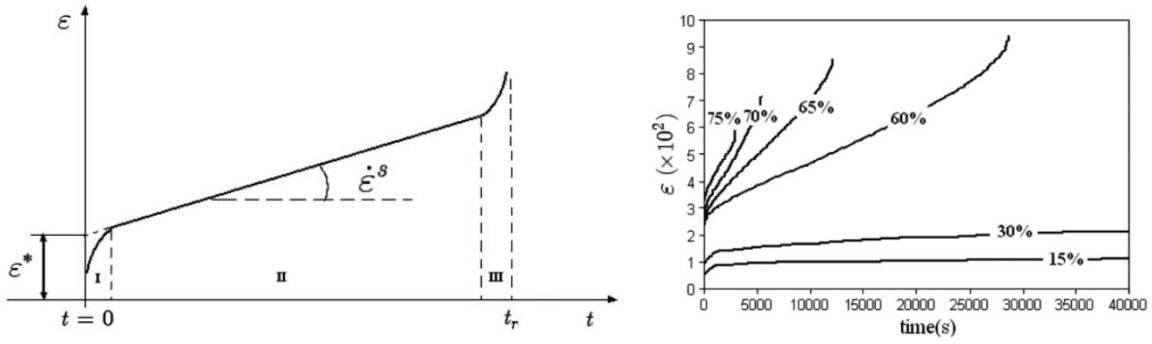

Figure 1.17. Creep test curve for Dyneema® SK75, (right) for different load levels [81]

	Regime I *Delayed elastic*	**Regime II** *Flow*	**Regime III** *Failure*
Time	Log(time)	Proportional	
Load	Proportional	Non-linear: $\sigma^{3.7}$	Not modelled
Temperature	Weak for 0->50°C: <30%	Exponential: x3.5-4/10°C	

Table 1.2. Elongation as a function of load, temperature and time for HMPE fibres

It should be noted that the constant flow rate domain can only be studied in HMPE fibres, and is one of the main drawbacks to using most HMPE fibres (apart from the most recent DM20 fibre grade). Other common polymer fibres show a logarithmic creep rate in the secondary domain, which is much easier to accommodate for long term applications under static load.

1.2.4. Polyamide 6 fibres

Polyamide 6 fibres have a visco-elatic, visco-plastic behaviour with a regime II characterised by a logarithmic creep rate. Hunt et al. [112]–[114] studied the creep of Nylon 6-6 and showed that it could be modelled using rheological [115] or thermodynamic techniques. In the present study we used a thermodynamic model already developed at IFREMER for other type of fibres such as polyester [116] and aramid [117], [118] based on

Schapery's theory [119]–[121].

1.2.4.1. Formalism

This approach is based on the division of total strain ε_{total} into a reversible part (non-linear viscoelacticity) ε_{ve} and an irreversible part (viscoplasticity) ε_{vp} [117], [122].

$$\varepsilon_{total} = \varepsilon_{ve} + \varepsilon_{vp} \quad \textbf{Eq. 1.1}$$

Schapery's model [119] has been used to describe the non-linear viscoelastic parts of this theory using thermodynamic assumptions. With these considerations, the simplified expression of viscoelastic strain is the Eq. 1.2.

$$\varepsilon_{ve} = g_0.S_0.\sigma + g_1 \int_0^t \Delta S\big(\phi(t) - \phi(\tau)\big).\frac{dg_2.\sigma}{d\tau}.d\tau \quad \textbf{Eq. 1.2}$$

S_0: instantaneous compliance; $\Delta S(\ldots)$: transient creep compliance; Φ (t): the reduced-time defined as: $\int_0^t \frac{ds}{a_\sigma}$; g_0, g_1, g_2 and a_σ are functions of stress.

The viscoplasticity can be expressed by different expressions depending on the material used. For example, bulk polyethylene has been studied by Lai and Bakker in [122] which shows a plastic strain defined by Eq. 1.3.

$$\varepsilon_{vp} = \int_0^t \frac{dP[\sigma(\tau).\hat{t}(\tau)]}{d\tau}.d\tau \quad \textbf{Eq. 1.3}$$

The plastic response is represented by the function P (σ,t), a non-linear function of time and stress. Then, we obtain the total strain of the material by substitution of viscoelastic and viscoplastic strain in Eq. 1.1 which results in Eq. 1.4.

$$\varepsilon_{total} = g_0.S_0.\sigma + g_1 \int_0^t \Delta S.\big(\phi(t) - \phi(\tau)\big).\frac{dg_2.\sigma}{d\tau}.d\tau + \int_0^t \frac{dP[\sigma(\tau).\hat{t}(\tau)]}{d\tau}.d\tau \quad \textbf{Eq. 1.4}$$

1.2.4.2. Model identification:

For the identification of the model's constants, we consider the creep and relaxation behaviour of fibres which gives more information on the real viscous behaviour of the material. Therefore, the identification will be divided in two steps of constant stress level, either equal to creep stress (σ_c) or null Eq. 1.5. This consideration simplifies the expression Eq. 1.4 into Eq. 1.6 for creep and Eq. 1.7 for relaxation.

$$\sigma(t) = \begin{cases} \sigma_c, & 0<t<t_1 \\ 0, & t_1<t<t_2 \end{cases} \qquad \textbf{Eq. 1.5}$$

For $0<t<t_1$, the Eq. 1.4 is reduced to:

$$\varepsilon_c = g_0.S_0.\sigma_c + g_1.g_2.\sigma_c.\Delta S\left(\frac{t}{a_{\sigma_c}}\right) + P(\sigma_c.t) \qquad \textbf{Eq. 1.6}$$

For $t_1<t<t_2$, the Eq. 1.4 becomes:

$$\varepsilon_r = g_2.\sigma_c.\left[\Delta S\left(\frac{t_1}{a_\sigma} + t - t_1\right) - \Delta S(t - t_1)\right] + P(\sigma_c.t) \qquad \textbf{Eq. 1.7}$$

The next step consists in the identification of the law's parameters. To do so, we have to define the creep compliance function named $\Delta S(t)$ in Eq. 1.6 and Eq. 1.7. This expression can be modelled by different functions, such as a power law [122], or a logarithmic function [117] depending on the material type. Then, the identification of these parameters can be made with the strain/time curve of a material subjected to a succession of creep-recovery tests at different stress levels. Chailleux and Davies [117] established an identification method of this type for aramid fibres [118] (shown in Figure 1.18).

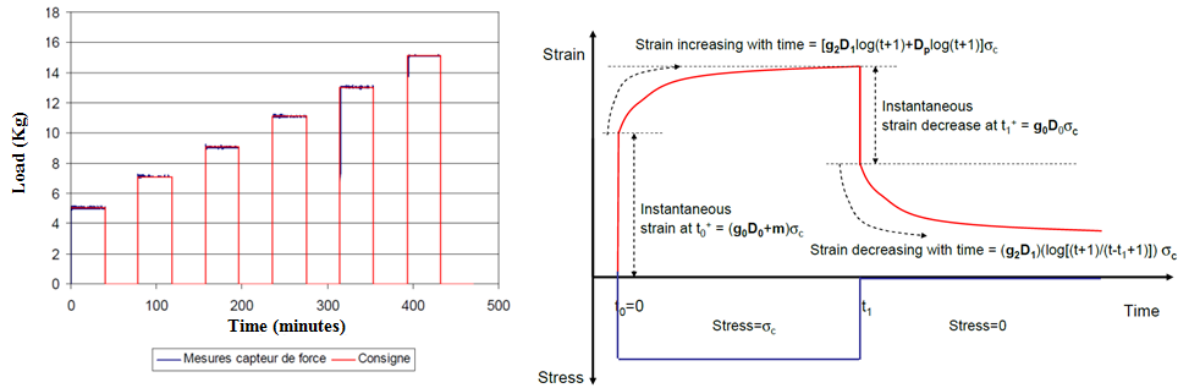

Figure 1.18. Identification method for aramid fibres [118].

They also established another modified approach, with an additional plasticity term, to model the polyester fibres behaviour in [116]. This identification technique has been well developed at IFREMER and has shown a good correlation with experimental data for each case studied to date.

1.2.5. Fatigue

Real marine applications do not only involve static loadings but also tend to have a non negligible dynamic component imposed by waves. Therefore, this section will focus on

fatigue tensile behaviour of inelastic fibres. For this kind of loading, there are three different experimental methods identified in [123].

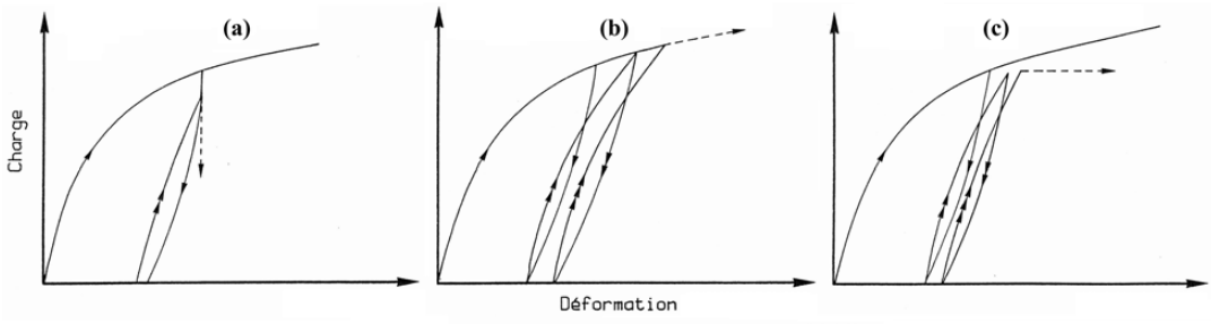

Figure 1.19. Fibre response under different types of fatigue tests (a) simple strain cycling (b) cumulative extension cycling (c) maximum load cycling. From [123].

The easiest test to perform is the cyclic strain with constant amplitude Figure 1.19 (a). Materials used in this study have a non-elastic response, which induces a residual elongation increasing with every cycle. This type of loading induces a stress which diminishes with time and therefore cannot generate failure.

To avoid this issue, the approach of cumulative extension cycling can be used Figure 1.19 (b). For this method, the plastic deformation produced during each strain cycle is removed by opening the bottom clamp. With this technique, the volume of the fibre is progressively decreasing and even if the displacement is constant, the fibre is taken up its stress-strain curve. In this case, the problem is the difficulty to identify the failure cause which can either be the fatigue loadings or the crossing of the quasi-static strain/stress limit.

The best way to study fatigue behaviour is to apply a cyclic loading with a constant maximum stress level (see Figure 1.19 (c)), as Hearle et al. established in 1967 [124].

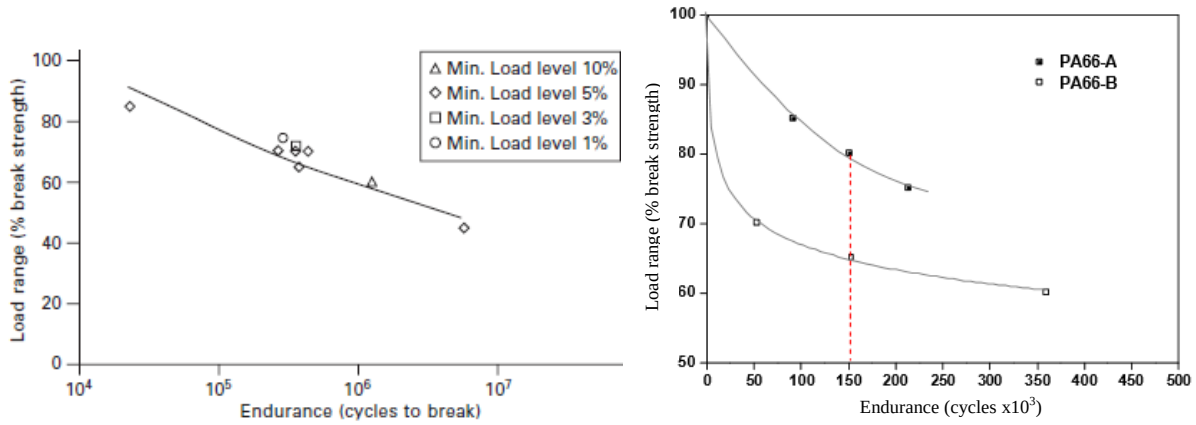

Figure 1.20. Tension-tension behaviour for Dyneema® SK75 yarns (left [108]) and Polyamide 66 (right [123])

Using this latter testing method, the tensile fatigue performances of both materials appear to be quite different, see Figure 1.20. First, we have to note that the break tenacity for Dyneema® and Nylon yarns are respectively equal to 2.7 and 0.7 N/tex. Moreover, when they are loaded in fatigue at 60% of their ultimate tensile strength Dyneema® fibres will break after 10^6 cycles while Nylon 6-6 will last $3.5x10^5$ cycles.

Fatigue testing on single filaments is not straightforward and requires special testing devices, as the loads are very low. Moreover, there are very few data available for fatigue on Dyneema® ropes.

1.3. Moisture diffusion in fibres

For marine applications, the other major issue is the effect of water on the materials. Synthetic fibres are based on polymer materials not subjected to corrosion, but could pick up water during their life time. Therefore, it is crucial to understand the diffusion behaviour in each material. First, we will investigate the impact of semi-crystalline structure and fibre shape on the diffusion, and the following sections will respectively focus on polyamide and HMPE water uptake.

1.3.1. General case of semi-crystalline fibres

For semi-crystalline polymers, the moisture diffusion only takes place in the amorphous phase. The moisture uptake is therefore a function of the crystallinity ratio as the studies [125] and [126] highlight. It is commonly admitted that the maximum moisture absorption capacity (C^{sat}) is linearly dependent on the polymer's crystalline ratio (Eq. 1.8). In this equation, X_a represents the ratio of amorphous fraction

$$C^{sat}{}_{X_a} = C^{sat}{}_{amorphous} \cdot X_a \qquad \textbf{Eq. 1.8}$$

Pant and Boyd [125] have shown that if we neglect the diffusion in the crystalline fraction, the diffusion coefficient in the amorphous ($D_{amorphous}$) region could be expressed as in Eq. 1.9, by analogy with dielectric constants. In this equation, D_{X_a} stands for the macroscopic diffusion coefficient in the polymer.

$$D_{amorphous} = \frac{3.D_{X_a}}{2.X_a} \qquad \textbf{Eq. 1.9}$$

In their study [125], experimental values have shown good agreements with the theory for five different materials, for temperatures from 20°C to more than 200°C.

To identify the diffusion inside the fibre, we can make the assumption that filaments have circular cross-sections and constant diameters. In this case, Fick established in–[24] a diffusion equation (Eq. 1.10) and Crank [25] proposed an analytical solution (Eq. 1.11), where *R* stands for the average fibre radius, and $\alpha_n$the roots of the Bessel function (see [25]).

$$\frac{\partial c(t,r,\theta,z)}{\partial t} = \frac{1}{r}\frac{\partial\left(rD\,\frac{\partial c(t,r,\theta,z)}{\partial r}\right)}{\partial r} \qquad \textbf{Eq. 1.10}$$

$$C(t) = \frac{1}{V_t}\iiint c(t,r,\theta,z).dV = {C^{sat}}_{X_a}\left[1 - \sum_{n=1}^{\infty}\frac{4}{R^2{\alpha_n}^2}\exp(-D{\alpha_n}^2 t)\right] \qquad \textbf{Eq. 1.11}$$

It is important to note that this solution (Eq. 1.11) for water diffusion inside a cylinder is only available in the case of a constant water concentration in the surrounding environment.

1.3.2. Diffusion in polyamide 6

Polyamide 6 is a polymer with a highly permeable amorphous phase in which the diffusion is well understood. For example, in the studies [127], [128] water absorption of immersed bulk polyamide was characterized for different temperatures, highlighting pseudo-Fickian behaviours (Figure 1.21). Arhant et al. [128] developed a model to predict this type of diffusion, based on the expression of local diffusion states depending on local glass transition temperature.

For polyamide materials in humid environment, Broudin et al. [129] show a maximum water content following a pseudo Henry's law (Figure 1.21). This law was previously modified by Park [130] and Guggenheim [131] models which take into account the effect of water clustering at high relative humidity and explain the water content increase.

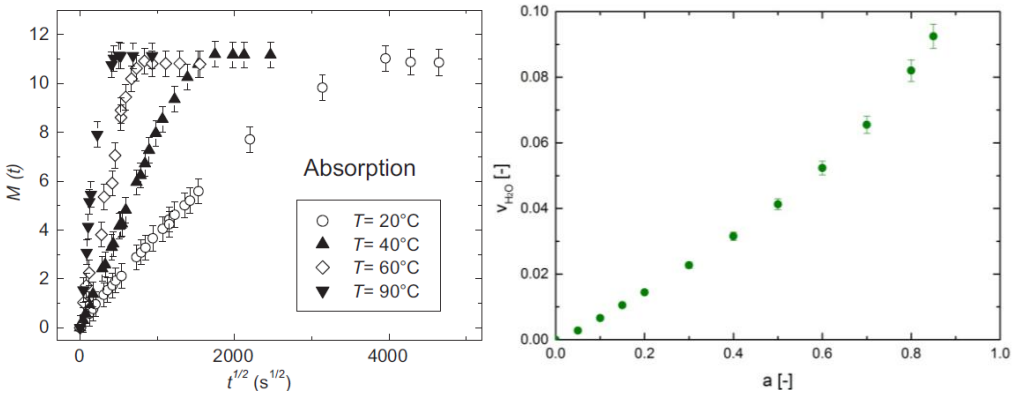

Figure 1.21. Moisture content vs. root of time for a polyamide 6 immersed at different temperatures (from [127]) –left– Evolution of volume water content in the amorphous part in PA66 with water activity at 40°C (from [129]) –right–

These studies demonstrate that if we know how the glass transition temperature changes with water content and the crystallinity ratio of the polyamide, we can predict the water uptake at saturation.

1.3.3. Water and HMPE

In polyethylene materials, the amorphous phase is hardly affected by water diffusion (Table 1.3): while most polymers take up water in the range of a few percent by weight, polyethylene only takes up 0,077% in its amorphous region [132].

Moreover in our case the crystallinity ratio of HMPE is higher than 80% which results in only a volume fraction of 0,077% in the amorphous phase (20% of all the material). The water uptake can therefore be considered as equal to zero, particularly given that this calculation is made on the amorphous phase of low density polyethylene, which has a higher free volume than HMPE).

Calculated Solubility of Water in Low Density Polyethylene

Solubility parameter for polyethylene δ_1, cal.$^{1/2}$/cm.$^{3/2}$	7.3[a]
Solubility parameter for water δ_2, cal.$^{1/2}$/cm.$^{3/2}$	24.0
Volume fraction water in amorphous phase ϕ_2	0.77×10^{-4}
Solubility of water in 40% amorphous polyethylene, mg./cm.^{3}	0.03

[a] If the empirical value, $\delta_1 = 7.9$ had been used, a solubility of 0.056 mg./cm.^{3} would have been obtained.

Table 1.3. Solubility of water in Low Density Polyethylene from [132]

This section has focussed on the diffusion in the material itself. However, in a rope structure water can be located either within or between the fibres, yarns and strands; this constructional aspect complicates the diffusion in the rope significantly. As a result, there is no published data for water diffusion in ropes or in their sub-structures.

1.4. Mechanical response induced by water diffusion

As in the case of composites, ropes used for marine applications are subjected to both mechanical loading and water diffusion. A review of the literature on synthetic rope materials reveals a lack of data on this subject, and the only studies we have found are focused on the effects of water on the mechanical behaviour. The action of water on the mechanical response can be divided into two physical phenomena: one microscopic, the plasticization, and the other macroscopic, the hygroscopic dilatation.

1.4.1. Plasticization of polymer

Water molecules interact with polymer molecules and degrade the material properties, especially mechanical properties. As discussed previously, there are two types of microscopic interactions: one is only a physical interaction, known as plasticization (see the Part A, sections 1.3.1.1 and 4.2.1.1 on diffusion in polymers) whereas the other is chemical (hydrolysis or oxidation of the polymer by the water). The work of Verdu et al. [37] highlights these two stages in the change in properties; first (for $t<\tau$) they are mainly degraded by the plasticization, then properties are stabilized or degraded by chemical effects.

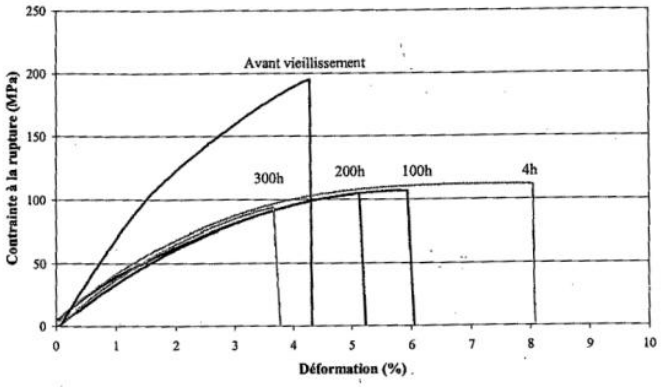

Figure 1.22. Water action on tensile behaviour of a Polyamide 6-6 resin for different times of exposure (dry, 4h, 100h, 200h, and 300h) (from [133])

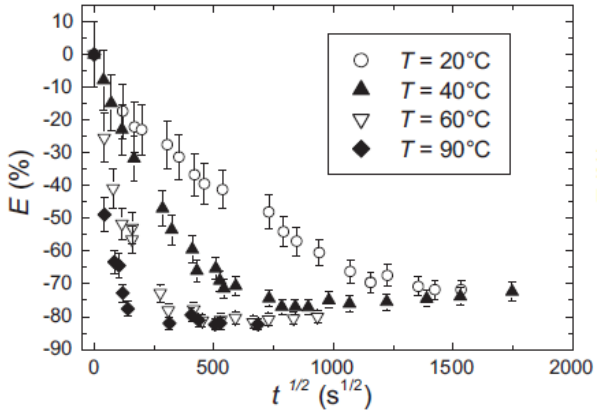

Figure 1.23. Variations in Young modulus (E) of a Polyamide 6 during the water absorption vs. √t for different temperatures (from [127]).

Polyamide can be hydrolysed by water; nevertheless this reaction is very slow at ambient temperature, in contact with acid or at higher temperatures the hydrolysis is faster. Figure 1.22 illustrates the hydrolysis effect: ultimate stress and strain decrease following the stress strain curve after 4h of exposure at 135°C. The hydrolysis has no further effect on the

Young's modulus which drops initially after a relatively short time of exposure then remains constant (see Figure 1.23).

Litvinov et al (2004) [134] have studied the plasticization mechanism by using proton Nuclear Molecular Resonance (NMR). This method reveals an important variation in the amplitude of the transverse magnetisation vs. time for different moisture contents (see Figure 1.24 right). Knowing that the amplitude is decreasing faster as a function of the time for rigid materials (see Figure 1.24 left), the study [134] reveals the plasticization of Nylon 6 with increasing moisture content.

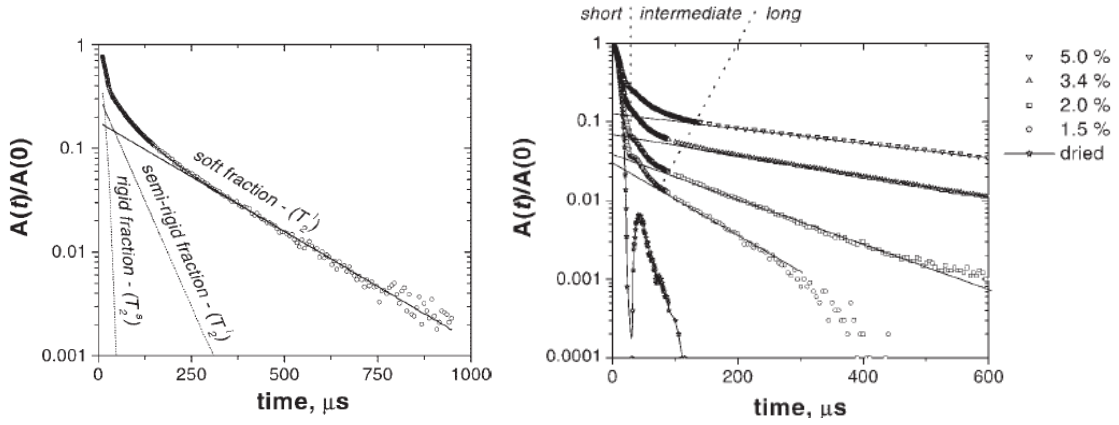

Figure 1.24. Amplitude of the transverse magnetisation after a 90° pulse excitation (left) for dry sampleat T=140°C (right) for dry and aged samples at 40°C [134].

1.4.2. The hygroscopic dilatation coefficient β

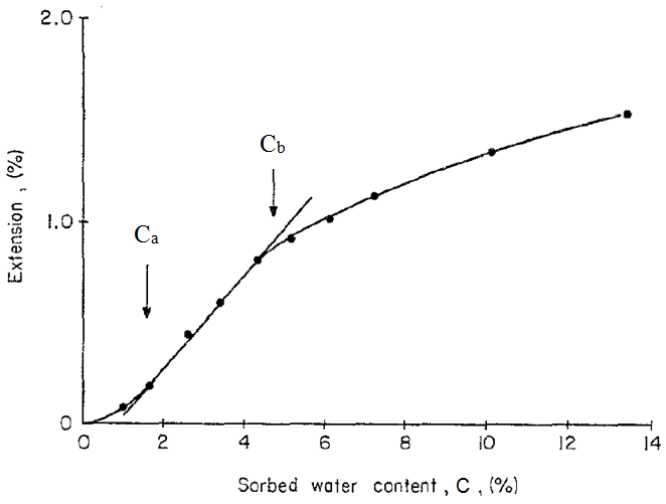

Figure 1.25. Longitudinal extension (%) of a Nylon 6 fibre vs. sorbed water content (%) [135]

The hygroscopic dilatation coefficient represents the macroscopic effects of water on materials. It has been studied for nylon fibres by Kawasaki et al. [135]. Their theory is based

on the dilatation effect of the water inclusion in the polymer, represented by a dilatation coefficient $\beta(C)$. This constant links the hygroscopic elongation to the water uptake in the material (Figure 1.25).

The results from [135] (Figure 1.25) have been obtained by hanging a mass of 1g at the end of a nylon fibre, and measuring the elongation with a cathetometer. The water sorption has been measured by following the elongation of a quartz spring, in an evacuated glass, on which the samples were suspended.

Figure 1.25 highlights three main types of hygroscopic elongation behaviours defined by the limits: $C=0$, $C=C_a$, $C=C_b$ and $C=C_\infty$.

For $C<C_a$:

The first-step sorption water vapour, M_a, is characterised by a very small extension of nylon fibres; the sorption only results from the interaction between water vapour and free amide groups (free sites). In this case [135] shows that the water content in the polymer (M) can be written as Eq. 1.12, with B_h a constant related to the heat of sorption and x the relative vapour pressure.

$$C = C_a.\frac{B_h.x}{(1-x).(1+(B_h-1).x)} \qquad \textbf{Eq. 1.12}$$

For $C_a<C<C_b$:

The second-step sorption water, $C = C_b - C_a$, is characterised by an extension of nylon fibres which increases linearly with the amount of water absorbed, the water molecules interact with amide groups bonded between chains. We consider n the number of amide groups in the polymer's amorphous region, αn represents the number of free amide groups, βn the number of amide groups between chains which interact with water, and γn the groups which cannot be bonded with water. We can write:

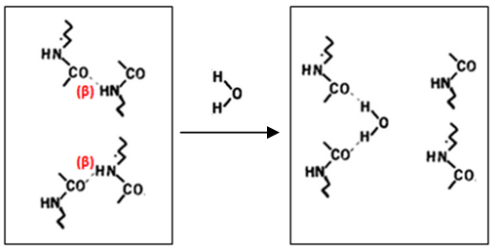

Figure 1.26. Water diffusion mechanism in second step sorption (two bonds between chains will attract one water molecule)

$$\alpha + \beta + \gamma = 1 \qquad \textbf{Eq. 1.13}$$

Knowing that the bonded groups interact less with water, we will have a number of active sites of *½βn* (see Figure 1.26), and it results in Eq. 1.14.

$$\frac{\alpha}{\frac{1}{2}.\beta} = \frac{C_a}{C_b - C_a} \qquad \textbf{Eq. 1.14}$$

If we consider the water absorbed for $C<C_a$ we can introduce Eq. 1.15, with n the number of water molecules absorbed in a structural unit with a free amide group, m_1 the molecular weight of water, m_2 the molecular weight of the structural unit and X the crystallinity in percent.

$$n = \frac{m_2}{m_1}.\frac{C_a}{100}.\frac{1}{\alpha(1-\frac{X}{100})} \qquad \textbf{Eq. 1.15}$$

Considering that all the free amide groups are bonded with water after sorption, we have *n=1*. C_a and C_b can be identified on Figure 1.27. Using these results and Eq. 1.13 and Eq. 1.15 α, β, γ can be known.

For $C_b<C$:

This stage represents a multilayer sorption, where water molecules in the upper strata are not affected by the polymer structure and are regrouped in clusters. The quantity of water molecules in a cluster depends on the geometry of the polyamide macromolecule.

1.4.3. Modelling perspectives

The main modelling method that we can use for stress coupled water diffusion is the hygromechanics approach. This theory involves three linked phenomena: water diffusion (Fick, Langmuir…) with $D(\varepsilon)$ (diffusion coefficient) and $C(\varepsilon)$ (moisture content), plasticization of polymers by water action on $L^m(C)$ (elastic stiffness tensor), hygroscopic dilatation (ε^{hygro}) of polymers.

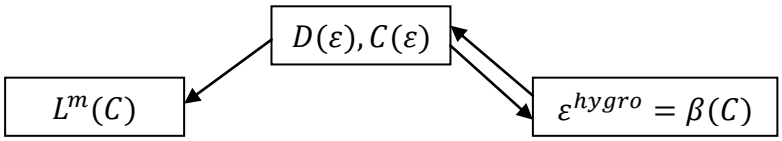

The theory of hygro-mechanical behaviour is based on the thermo dilatation theory in which the thermo dilatation coefficient is replaced by β the hygroscopic dilatation coefficient. Moreover ΔC (the moisture content variation) replaces ΔT (temperature variation). In this condition the deformation tensor used in [42] is defined by Eq. 1.16 with, L^f *the* elastic

stiffness tensor of the fibre which is a function of the moisture content *(C)*.

$$\varepsilon^f = \varepsilon^f_{el} + \varepsilon^f_{hygro} = L^{f^{-1}} : \sigma^f + \beta^f \Delta C^f \qquad \textbf{Eq. 1.16}$$

In practice, it is hard to identify this type of behaviour. The hygroscopic coefficient has already been identified with various methods in previous studies, such as that of Peret in [136]. Nevertheless, his study also shows the difficulties to get precise measurements. Moreover, the variations of the elastic stiffness tensor with the moisture uptake are even more complex to identify due to the number of parameters it includes.

Therefore for further study of coupled behaviour it is essential to dissociate the different response before getting to the fully coupled case.

1.5. Conclusion

The literature review shows that there is good knowledge available on uncoupled behaviours of polymer fibres. The mechanical response is well understood at the different scales of the structure and for different materials. Water uptake has been studied in HMPE and polyamide and there is an analytical solution to the diffusion equation in fibres. Nevertheless, while many authors have studied synthetic fibres and ropes, there are still missing data. Few reliable studies have been conducted on monofilament tensile behaviour in particular because of the small fibre diameter and slipping in loading clamps. Moisture diffusion in yarns and ropes is misunderstood especially because of the difficulty in quantifying the water located between fibres. The knowledge of this phenomenon is important, in order to be able to predict the water action on yarn and rope behaviour. And finally, few authors have investigated the interaction between water uptake and fibre mechanical behaviour.

Therefore, this study will focus on moisture uptake, mechanical behaviour and their combined effects, from the mono-filament scale to the rope. At the mono-filament level, the study will focus on mechanical behaviour, no water uptake will be considered mainly because of the small scale and low weight of specimens. For yarns and ropes, water diffusion, mechanical behaviour and their coupled effect will be studied. In this second part, there will be two main issues: the water effects on the material itself and its contribution to the behaviour of the rope. To better understand these phenomena two main types of fibre have been studied: one material highly affected by water, the polyamide 6, and another which is unaffected, the HMPE, the latter allowing us to examine only the effect of the water which is within the rope structure.

Chapter 2.

Materials and methods

This chapter describes all the types of fibre materials, constructions and methods which are used in the study. First the different materials and structures tested are presented in three sections, one for each material and the last one focused on the different structure scales. Second, we describe the standard methods used to obtain these physicochemical properties, followed by the test techniques employed and developed to characterize the mechanical behaviours. Finally, the different coupled and uncoupled ageing devices are presented. All the tests performed and the number of specimens tested are reported in Appendix 1.

2.1. Materials

In this study we investigate the coupled effects of water and mechanical stresses on the materials used for marine applications. This Part is dedicated to synthetic ropes. Rope structure induces two different types of water uptake: one inside the material and another inside the rope's construction. Based on this observation, we have chosen two materials which will allow the identification of each diffusion type.

First, we will focus on polyamide 6 fibres, which are highly hydrophilic but widely used in synthetic rope marine applications. Second, HMPE fibres have been examined, in order to represent a high performance material for deepwater handling applications.

Both materials are semi-crystalline polymers with very different crystallinity ratios: around 40% for Nylon and 90% for HMPE from Dyneema®. In order to describe these fibre materials a specific textile unit is used for the linear density: the titer, expressed in tex, equivalent to g/km.

2.1.1. Ultra-high molecular weight polyethylene

Ultra-high molecular weight polyethylene (HMPE) is a material produced from polyethylene $(-CH_2-)_n$. HMPE is a material with the same chemical properties as high density polyethylene (HDPE), with a higher molecular weight: $M > 10^6$ g.mol^{-1}.

To obtain such a high performance material, the molecular chains have to be straightened, oriented and crystallized in the direction of the fibre as much as possible Figure 2.1. To achieve this, the gel-spinning process has been developed, based on dissolution of molecular chains in the spinneret to disentangle them during and after processing [1].

Since the invention of this material, various improvements (degree of molecular chain orientation and level of crystallinity) have been made, especially since their industrial production (under the trademarks Dyneema® from DSM and Spectra™ from Honeywell). The

different grades (for example Dyneema® SK78 and DM20) illustrate those evolutions as shown in Table 2.1.

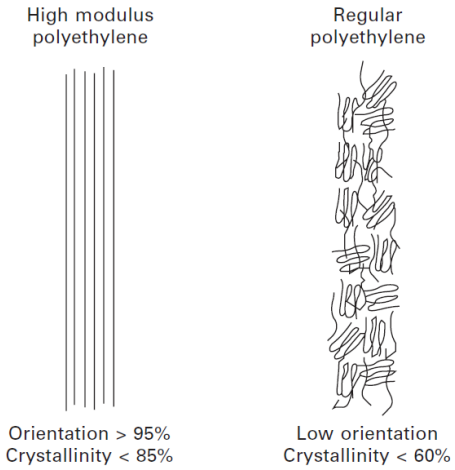

Figure 2.1. Orientation of polyethylene molecules [1]

For this study we chose to investigate the properties of the SK78 grade. This is a material developed specifically for the offshore oil and gas sector.

	Filament		Fiber linear density		Tensile strength			Tensile modulus			Elongation to break
	Diameter	Linear density									
	μm	den	den	dtex	g/den	N/tex	GPa	g/den	N/tex	GPa	%
DSM Dyneema (DSM, 2007)											
Dyneema® SK25	16	1.7	675	750	25	2.2	2.2	608	54	52	3.5
Dyneema® SK60	12	1.0	400–600	440–660	28–35	2.5–3.1	2.4–3.0	759–1080	67–95	65–93	3.5
Dyneema® SK62	17–21	2.0–3.0	400–2400	440–2640	33–35	2.9–3.1	2.8–3.0	974–1169	86–103	83–100	3.5
Dyneema® SK65	12	1.0	100–1200	110–1320	34–38	3.0–3.4	3.0–3.3	1082–1158	96–102	93–100	3.5
Dyneema® SK75	17–21	2.0–3.0	100–2400	110–2640	38–45	3.4–4.0	3.3–3.9	1267–1552	112–137	109–132	3.5
Dyneema® SK78	17–21	2.0–3.0	1600–2400	1760–2640	38–40	3.4–3.5	3.3–3.4	1267–1314	112–116	109–113	3.5
Dyneema Purity® SGX	17	2.0	50–400	55–440	36–37	3.2–3.3	3.1–3.2	1133–1246	100–110	97–107	3.5
Dyneema Purity® TG	12	0.9	23	25	43	3.8	3.7	1400	125	120	3.4
Dyneema Purity® UG	11	0.5	100–400	110–440	44–46	3.9–4.1	3.8–4.0	1473	130	126	3.3
Dyneema® NM22			400	440	17	1.5	1.5				
Dyneema® NM44			200	220	17	1.5	1.5				
Toyobo Co. (Toyobo, 2007)											
Dyneema® SK60 (Japan only)	12	1.0	50–1600	55–1760	29	2.6	2.6	895	79	79	3–5
Dyneema® SK71 (Japan only)	12	1.0	50–400	55–440	40	3.5	3.5	1246	110	110	3–5
Honeywell Specialty Materials (Honeywell, 2007)											
Spectra® fiber 900	38–40	10–10.8	650–4800	722–5333	26–31	2.3–2.7	2.2–2.6	850–920	75–81	73–79	3.6–3.9
Spectra® fiber 1000	23–28	3.6–5.4	215–2600	239–2888	34–38	3.0–3.4	2.9–3.3	1135–1320	100–117	97–113	2.9–3.5
Spectra® fiber 2000	19–23	2.5–3.6	100–180	111–200	38–39	3.4	3.3	1320–1450	117–128	113–124	2.5–3.6

Table 2.1. A non-exhaustive list of HMPE grades from different brands [108].

2.1.2. Nylon 6

Nylon fibres (polyamide) are produced from amide groups (-CONH-); there are several different types of nylon fibres: polyamide 6.6 / 6.12 / 4.6 / 6 / 12 (the number refers to the carbon atoms around the amide group in the monomer), which have found a wide range of applications. Polyamide 6 represents a low cost fibre material which is highly hydrophilic, in contrast to HMPE.

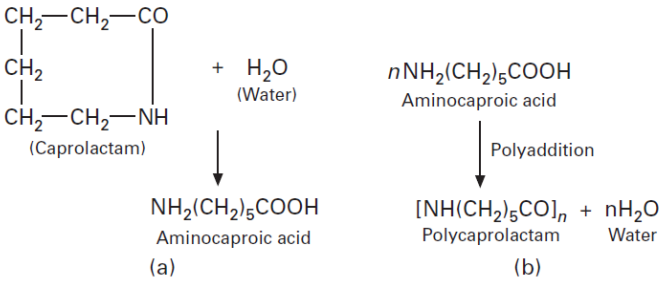

Figure 2.2. Synthesis of Nylon 6 [98]

Nylon 6 is produced from scission of caprolactam rings by water. First, water opens the rings and creates an aminocaproic acid, which then forms polycaprolactam by polyaddition, Figure 2.2.

Fibres are then produced by spinning from the melt. In the case of Nylon 6 the amorphous phase is more important than in HMPE (more than 50%). The micro-structure of one fibre can be schematically represented as the following:

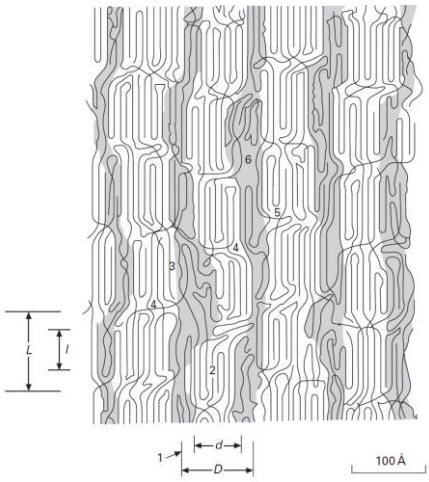

Figure 2.3. Nylon 6 structure with: (1) fibrils; (2) lamellae; (3) partially extended crystalline and interfibrillar amorphous regions; (4) tie molecules in the interlamellar region; (5) free chain ends; (6) amorphous segments with large free volume and which may gives rise to voids (7) fusion of adjacent microfibrils. Shaded areas represent the interfibrillar amorphous regions. From [98]

The Nylon used in the present study is manufactured by Nexis fibers and has the reference 1880 f 280 (with a titer of 190.5 tex)

2.1.3. Multi-scale issue

At a macromolecular level both fibres are semi crystalline polymers, and for the study they have to be considered as heterogeneous media. Mechanical and diffusive behaviour are

different for crystalline and amorphous structures (amorphous regions absorb water whereas crystalline sections do not), and various authors have indicated core/skin differences in polyamide fibres [97], [137] and fibrillar structure in HMPE [138].
For rope applications different structural levels can be classified as: fibre; yarn; strand; rope, as discussed in thee previous chapter (Figure 1.3).

These different structural levels are the guideline for the following discussions on fibres.The rope-making process also influences its global behaviour (braided, twisted, etc) and the machine parameters will affect the variations in construction geometry. To limit this influent factor, the structures in the present study are the same for each fibre material: yarn without twist, and rope braided with twisted strands.

2.2. Physicochemical properties

As for other polymer materials, we can determine the physicochemical properties of the fibres with standard methods. The following section presents the different techniques used in the study, together with their aims.

2.2.1. Differential Scanning Calorimetry (DSC)

Differential Scanning Calorimetry is used for two reasons in the work. First, section 2.1 highlights that polyamide and HMPE are semi-crystalline fibres. Their mechanical behaviours will strongly depend on the crystalline ratio, and therefore it is essential to identify this quantity. The degree of crystallinity (X_c) was determined by DSC on Q200 equipment from TA Instruments at a heating rate of 10°C/min from room temperature to 300°C for both materials. The crystalline ratio was then calculated from the enthalpy of fusion of the polymer – ΔH_f – which is compared with a theoretical 100% crystalline material value – $\Delta H_f{}^0$ – (Eq. 1.5).

$$X_c = \frac{\Delta H_f}{\Delta H_f{}^0} \qquad \textbf{Eq. 2.1}$$

The theoretical enthalpies of fusion of 100% crystalline polymer were taken as equal to 293.6 J/g for the SK78 HMPE and 188 J/g for the polyamide 6 (values from [6]).
The second reason to use the DSC device was to determine the water content in the fibres, an original test method has been developed and is described in section 3.2.1.2.

2.2.2. Dynamic Mechanical Analysis (DMA)

The glass transition temperatures (Tg) of the fibres were determined with the DMA

method. We have developed a special clamping method to test the fibres in the DMA device and avoid slippage issues. The yarn is clamped and wound twice around a pin as shown in Figure 2.4. Sample initial length is taken between the pins after a dynamic pre-stressing (with the parameters used for the subsequent test), its value was between 20 and 30 mm.

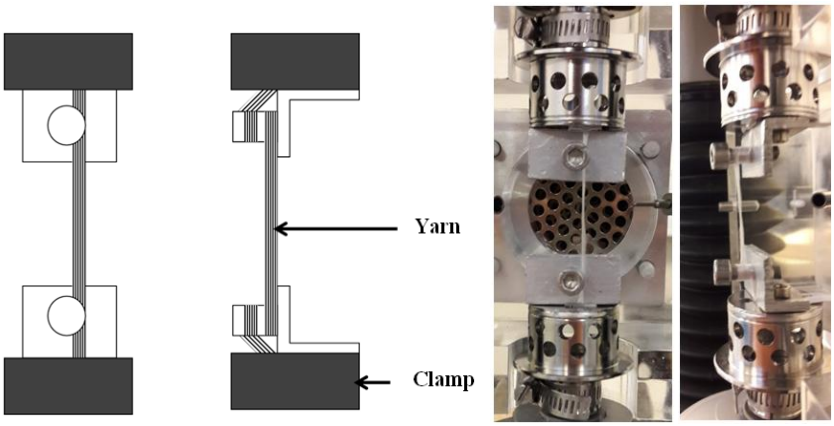

Figure 2.4. Clamp used for DMA testing of single fibres.

The tests were performed on a DMA^{+} 150N device from Metravib, in an oven filled with silica gel to get the properties at 0%RH and then in a humidity chamber to characterise the influence of water content on the properties. Specimens were tested at a frequency of 1Hz and a dynamic strain of 5.10^{-3}. The tests were conducted from 25°C to 150°C for polyamide 6 at 2°C/min in the oven. The humidity chamber can only regulate at a constant humidity and temperature, therefore, the modulus was determined at 5°C temperature steps from 25°C to 60°C and at 10% of relative humidity steps from 10%RH to 80%RH. These tests are not performed on HMPE fibres since their Tg is lower than the temperature limit of the DMA device (around 110°C).

2.3. Uncoupled behaviour

This section is focused on the uncoupled ageing and mechanical behaviours to understand how these materials respond with no interactions. First, we will see the techniques used and developed for quasi-static testing of each construction, then ageing conditions are presented.

2.3.1. Quasi-static tensile tests

Mechanical behaviour was studied first as an uncoupled phenomenon on both fibre types. For Nylon 6 only the filament and yarn scales were investigated whereas SK78 was studied at each scale from filament to rope.

Quasi-static tensile tests are quite different for each sub-structure level. There are standardised methods to test yarns and ropes. Nevertheless mono-filament loading is not standardised and is not easy to perform (Chapter 1). All these tests were performed in an environmentally controlled laboratory at $21^{\pm 2}$°C and $50^{\pm 5}$%RH, and samples were pre conditioned in this atmosphere for at least one week before testing. The results presented in the rest of the study are the average values from at least 5 specimens.

2.3.1.1. Tests on filaments

The filament testing issue is the slippage of the filament in the clamps. In this study we developed a technique to avoid this problem. The filament is placed between two cards glued together with Loctite 405, with a spacing of 35mm. The sample is placed in pneumatic clamps, and marked with black Loctite 480 (Figure 2.5). These markers are used in order to get the displacement during the test with image correlation analysis, using a Basler camera of 2040x1080 pixels resolution.

Quasi static tensile tests on mono-filaments were performed on a 10kN Instron 5566 testing machine at 1 mm/ min. With a N load cell.

2.3.1.2. Yarn testing

Yarn quasi static testing is a standardised test, in the study we followed the standard ASTM D885M [139, p. 885]. The initial gage length was 100mm, the tests were performed at a rate equal to 50 mm/min for HMPE (case of high modulus fibres) and 120 mm/min for Nylon 6. The yarns have initial lengths between markers (L_0) in the range between 35 and 40 mm. The strain evolution is again recorded by image correlation, but this time two cameras were used, one for each marker. This technique allows good resolution without an influence of the L_0 value.

2.3.1.3. Tests on rope

Rope quasi static behaviour presents some particularities compared to yarns and monofilaments. The braided construction induces a non-linear behaviour, due to the fibre reorientation [102] (phenomenon explained in Chapter 1). Some standards and studies give recommendation to limit this non linear part. In the present study we based the testing on the recommendations of ISO standard number 18692/2007 (for polyester ropes) and pre-cycled the samples five times up to 50% of the rope ultimate load. The tests were performed at a speed of 20 mm/min on a 200kN electro-mechanical Instron machine.

Figure 2.5. The different samples for quasi static testing on filament [left], yarn [middle] and rope [right]

2.3.2. Ageing conditions

Water conditionning in bulk polymers is a well studied subject, nevertheless when it comes to polymer fibres no standardised method has been developed. This section presents the techniques developed in order to characterise the water uptake in filaments and ropes.

2.3.2.1. Water uptake in the fibre

First, water uptake dependence on relative humidity was established with Dynamic Vapor Sorption (DVS). Measurements were performed on Q5000 SA equipment from TA Instruments. The weight change of a 5mm length of yarn was recorded by a microbalance of 0.1µg resolution at various temperatures (25, 40, 60 and 80°C) and for relative humidities from 0 to 90%RH. For these experiments, the results are the average of three samples. For both SK78 and Nylon 6, it represents a reference method highlighting whether or not there is condensation between fibres.

Water uptake in an immersed filament of polyamide 6 is hard to determine and dissociate from the water in between the fibres. This quantity was therefore determined with DSC analysis (part 2.2.1) on a filament group after immersion. The technique is based on the free/bonded water theory [140] the moisture inside the fibres is considered as bonded ($C_{b,\infty}$) while molecules in the structure are taken as free ($C_{f,\infty}$). The expressions Eq. 2.2 to Eq. 2.4 allow the different water quantities to be determined by analysis of fusion – ΔH_f – and

vaporisation – ΔH_v – enthalpies.

$$C_{f,\infty} = \frac{\Delta H_f}{X_c . \Delta H_f{}^0} \quad \textbf{Eq. 2.2}$$

$$C_{t,\infty} = \frac{\Delta H_v}{X_c . \Delta H_v{}^0} \quad \textbf{Eq. 2.3}$$

$$C_{b,\infty} = C_{t,\infty} - C_{f,\infty} \quad \textbf{Eq. 2.4}$$

2.3.2.2. Water uptake in the rope

In this section only HMPE is studied in order to exclusively identify the water sorption inside the structure ($C_{struc}(t)$) and not in the material. First the rope sample was weighed in air (W_0), and then to study water sorption in the rope the rope was suspended from a hook linked to precision balance (Sartorius ED124S) and immersed in water. . An additional weight was added, to avoid floating. The specimens were weighed periodically (ΔW) to get the water uptake in the rope structure as a function of the immersion time, Figure 2.7.

$$C_{struc}(t) = \frac{\Delta W}{W_0} \quad \textbf{Eq. 2.5}$$

Figure 2.6. Weighing scale for immersed materials with a suspended rope sample.

Each sample was dried initially for 1 week before immersion, to remove the water between fibres. To manufacture ropes, the fibres are lightly coated with a spin finish to avoid abrasion during the process. This additional compound is washed off by the water during the first immersion. Therefore each specimen was immersed twice, with a drying period between the two sorptions. The second immersion will reveal the real water uptake in the rope structure.

2.4. Coupled phenomena

Two types of coupled phenomena were studied in this work: the creep behaviour

immersed in water and the dynamic fatigue in water. The testing devices developed to identify these behaviours are described in the following sections. In each case, we also present the reference tests in air.

2.4.1. Static tensile creep tests

Static creep behaviour was studied on Nylon 6 yarns and SK78 ropes. In each case, the experiments were performed in environments from humid air exposure to complete immersion.

2.4.1.1. Humid environment

To identify the yarn creep behaviour the DMA method was used with the same device and clamps as described in section 2.2.2. Samples were loaded under successive loading levels from 10 to 70N with steps of 10N, held for 1500s. Between each creep loading the specimens were unloaded and allowed to recover for 2000s. The tests were performed under relative humidity from 15%RH to 80%RH with steps of 10%RH at 25°C. Tests under 0%RH were performed in an oven, from 25°C up to the Tg value.

This experimental protocol is based on the identification method developed by Schapery [119]–[121] (explained in Chapter 1), in order to define the creep and recovery parameters.

Experimental creep behaviour of ropes was also studied at 70°C in order to compare it to the life time prediction model used in the study. The testing device is equivalent to the one used for dynamic tests on ropes explained in part 2.4.2.

2.4.1.2. Immersed

The creep tests on immersed yarns were studied with a testing device specially designed for this application, Figure 2.8. The samples were immersed in a tank filled with tap water regulated at 23°C. One end of the specimen was fixed to the test bench and at the other end, a weight was suspended. Sheaves were used to transfer the load from the vertical to the horizontal direction. The strain variation was recorded during the test by filming markers bonded to the yarn, followed by image analysis.

These tests were performed on both Nylon 6 and SK78; in the case of HMPE the investigation aims to compare the results to the experimental literature values and to a lifetime prediction model.

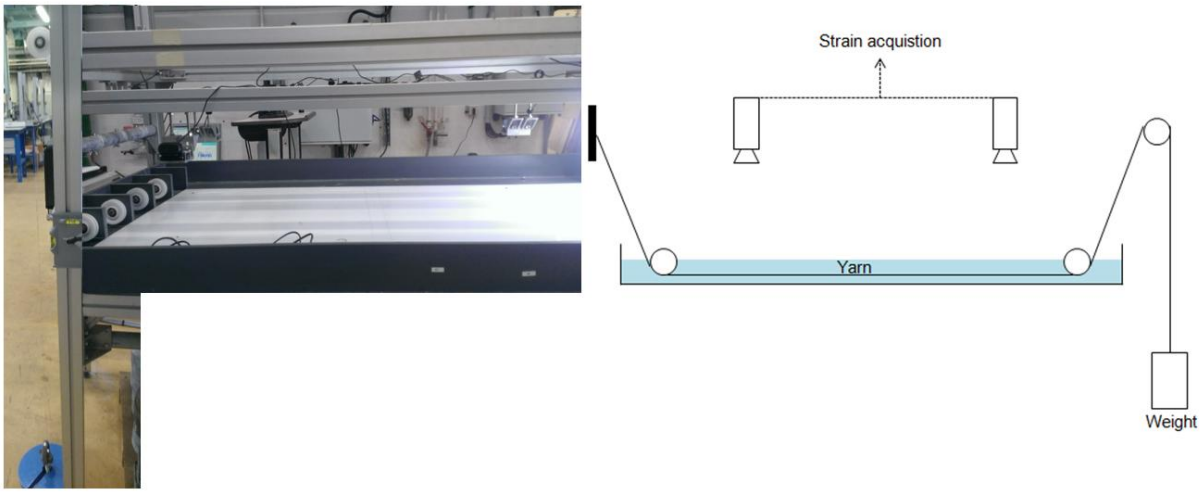

Figure 2.7. Testing device for immersed creep behaviour of yarns.

2.4.2. Dynamic tensile tests

Dynamic (cyclic) tensile behaviour is the second coupled behaviour studied here. These tests were exclusively performed on SK78 and ropes, since previous results [141] have shown that creep and fatigue in HMPE fibres are controlled by the same behaviour.

2.4.2.1. Humid environment

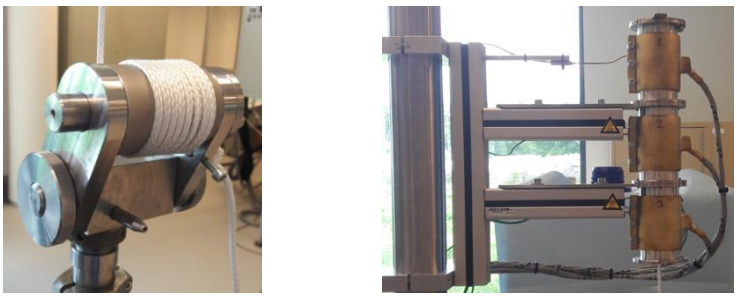

Figure 2.8. Experimental set-ups for dynamic test at high temperature: clamps [left] and oven [right]

Specific clamps have been developed for dynamic tensile tests in air in order to avoid slippage and abrasion issues. The rope is wound eight times on a cylinder and held in place by a screw at its end, Figure 2.9. The cylinder can rotate to have an offset from the actuator axes, which allows the rope to be perfectly centred (Figure 2.8). To accelerate the failure the tests are performed at temperatures from 70°C to 120°C. An oven has been developed to heat the central part of the rope up to 200°C (Figure 2.8).

The tests were performed on a Zwick hydro-mechanical device of 100kN capacity. Samples were loaded at frequencies from 0.1 to 1 Hz , R ratio from 0.1 to 1 ($R=\sigma_{min}/\sigma_{max}$) and maximum stress from 250 to 1200MPa. The room humidity was regulated at $50^{\pm5}$%RH

2.4.2.2. Immersed

To understand the water effect on the dynamic behaviour of ropes, a special fatigue testing device has been developed in order to perform tests on samples immersed in water. In this case the water is heated at 35°C by a heating device; therefore, the abrasion is more critical compared to the creep time to failure than in the case of 70°C testing. The clamps described in the previous section cannot be used, and were replaced by eye splicing, which appears to be the least critical type of end connection in terms of abrasion. To immerse the specimens the bottom axis was placed on a cylindrical base, which can be assembled with a transparent PMMA tube and with a sealing groove. Once these devices have been assembled the PMMA tube can be filled with water and the rope is tested immersed. The strain evolution was determined with the same techniques as in the previous sections (image analysis), after verifying that this was not distorted by taking images through the water-filled tube. The machine used in this case was a 250kN capacity hydraulic MTS device, Figure 2.10.

Figure 2.9. Testing device for dynamic tension-tension on immersed ropes: global view [left] and zoom on tube and end connexions [right]

During these dynamic tests, heating inside the rope was also recorded with a thermocouple (type K) introduced inside the rope. For each condition the temperature was recorded until its stabilisation.

2.5. Additional analyses

2.5.1. Scanning Electron Microscopy (SEM)

SEM imaging techniques were performed to get high resolution images of fibres pre-coated with platinum to ensure reflection of the electrons on the specimen. This method gives information on the surface aspects (kink bends, micro fibrils, etc) and the diameters of each type of filament (Figure 2.11).

SEM imaging techniques were also used after dynamic tensile tests to determine the type of failure involved. This provided information on the mechanisms involved (creep, abrasion, heating, etc) during dynamic loading. This analysis was based on the work of Hearle et al [142] who developed a reference atlas of fibre failure types and their causes.

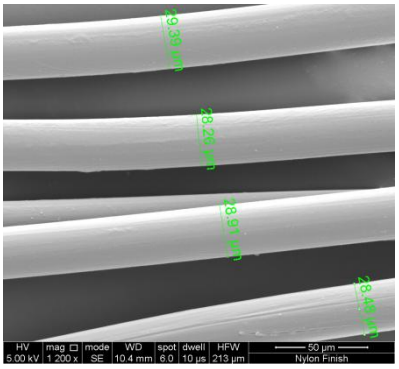

Figure 2.10. Example of SEM image with diameter calculation on a Nylon 6 yarn

2.5.2. Hygroscopic deformation

Water ageing also induces hygroscopic deformation of the polyamide 6 fibres. This property was investigated with the same DMA device as presented in part 2.2.2. The samples were exposed to different relative humidities (from 10 to 80%RH) at 25°C and stressed at a very low load (1N) to avoid creep behaviour. The strain variations between the different humidity exposures revealed the hygroscopic behaviour of the material. Moreover the tests by DVS (part 2.3.2.1) give a correspondence between the relative humidity and the moisture content in the fibres. Therefore the hygroscopic deformation can be linked to the water uptake in the Nylon 6.

Chapter 3.

Uncoupled and semi-coupled behaviours

3.1. Introduction

The two following chapters are focused on the understanding of uncoupled, semi coupled and coupled behaviour in the fibre material (yarn) and in its structure (rope). As previously said in general introduction, to study the effect of coupling on the yarn, we focus the study on an hydrophilic material, while an hydrophobic material is used to understand the coupling on rope structure. The tests presented in the chapters 3 and 4 can be summarised as in Figure 3.1.

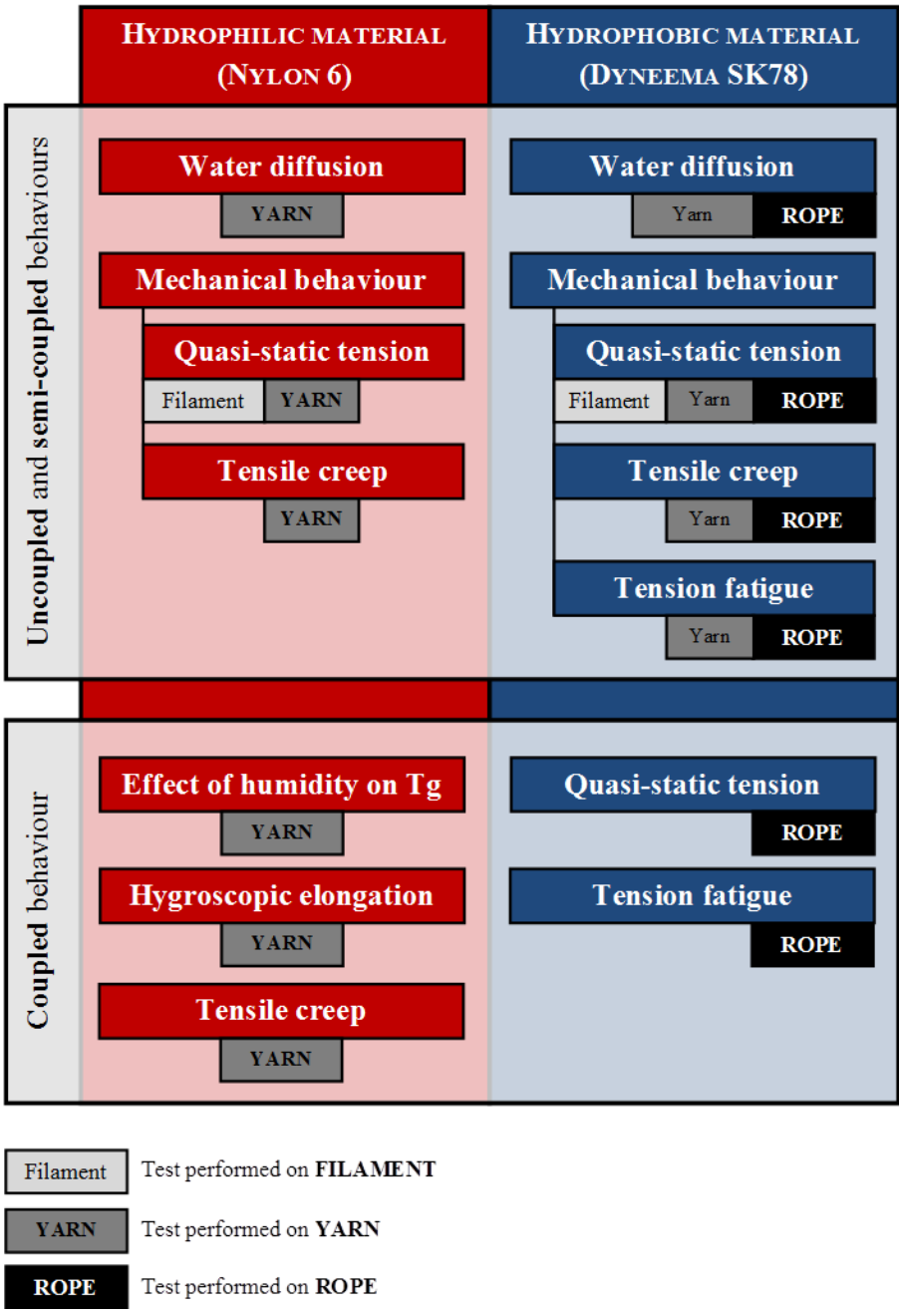

Figure 3.1. Schematic representation of the tests on fibre materials presented in Part B Chapter 3 and 4

This first part of the study aims to understand each uncoupled response (diffusive or

mechanical) and then to highlight their variations when they are semi-coupled.

First, water diffusion is studied on undamaged and pre-stressed samples. In this part, the study is divided into two sections: first, the study of water diffusion in filaments and yarns, and second, in ropes.

For the investigation on yarn and filament behaviour, we decided to group both scales since they are closely related. Moreover, some specific studies were performed to evaluate the water amount within and between fibres for relative humidity and immersion cases (with DVS and DSC).

Water inside a rope is only considered for SK78 ropes, to avoid any coupled effects between diffusion in the structure and in the material. At this scale some issues can be induced by coatings added during the rope processing (as processing finish for example). Therefore, we studied the diffusion in the rope both as received and after a first cycle of sorption/desorption, in order to examine the water amount in the structure and the quantity of finish removed by water.

Second, the tensile mechanical response of fibre constructions both unaged and aged was considered. First the quasi-static behaviour, then the static creep response and finally the influence of a dynamic fatigue stress are examined. For each step, we considered different scales of the rope construction. For the quasi static case the scale from filament to rope was studied, while creep and fatigue responses are only investigated on yarn and rope samples, due to the difficulty to perform such tests at the mono-filament level.

3.2. Water diffusion

Water diffusion inside fibres and ropes is not a well-known phenomenon. The diffusion into a fibre could be estimated by solving Fick's equation for the case of a cylinder [25]. However, the rope's construction introduces other types of phenomena, such as capillary effects or water diffusion into porous medium.

For these reasons and in order to characterize the diffusion in our material, we focus the diffusion study on the experimental aspect. To do so we developed some specific techniques to identify the location and quantity of water within the rope structure.

3.2.1. Water in filaments and yarns

The fibres are a much thinner material than bulk polymer and therefore their diffusion kinetics are much faster. This introduces two issues when it comes to quantifying water uptake in the material. First, the light weight of fibres makes the weight of water hard to

measure and second, the fast kinetics limit handling times.

3.2.1.1. Diffusion in humid environment

The first technique used to quantify the water uptake is DVS (Differential vapour Sorption), which gives information on the diffusive behaviour in a humid environment. In this case we studied the diffusion in both undamaged and pre-stressed material.

Diffusion in and between filaments

DVS techniques record the weight variation with a constant time step during tests where the relative humidity is controlled and progressively increased by steps (Figure 3.2). These tests were performed on short lengths of yarns (5mm) of Nylon 6 and SK78.

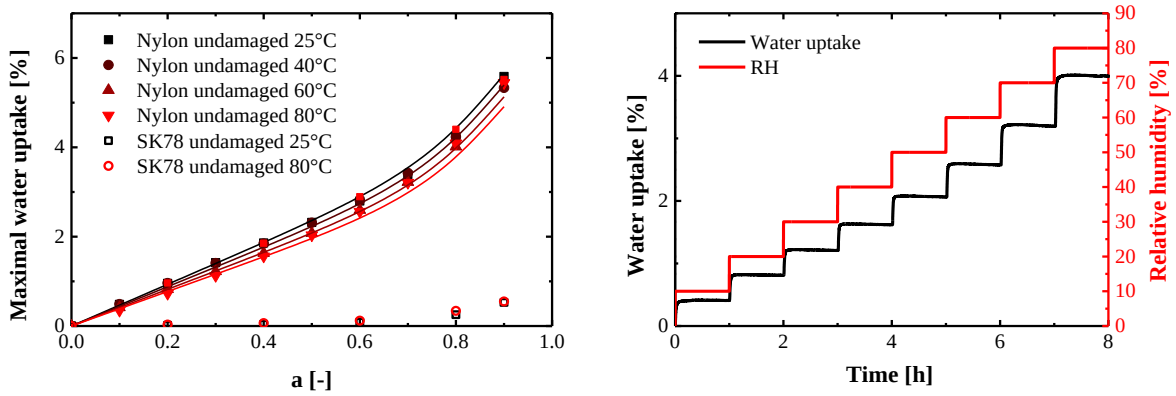

Figure 3.2. DVS results: maximal water uptake in Nylon6 and SK78 vs. the water activity [left] and a charcteristic curve of water uptake in fibres versus time (example from Nylon 6 at 25°C) [right]

The main problem we can encounter during such tests is condensation between fibres which can modify the water uptake values. In order to get the amount of this type of water, we also performed tests on SK78 samples. HMPE fibres take up very little water due to their chemical construction (as discussed in Chapter 1), therefore the DVS results for SK78 only indicate the water quantity between the fibres (Figure 3.2).

It appears that the amount of water included between the filaments can be neglected (less than 0.5%) compared to the amount recorded for the Nylon 6 fibres (up to 5.5%).
Second, water uptake in the Nylon 6 appears to follow Henry's law for low water activity (below a=0.5), for higher activity values the water quantity deviates from this law. Similar results was observed in previous studies of polyamide [128], [129]. This deviation is related to cluster creation inside the material and it appears to be controlled by the equation Eq. 5.1, with $C_\infty(a)$ and a the water activity. It as been shown that H can be represented by an Arrhenius law characterised by a pre-exponential factor H_0 and an activation energy E_a.

$$C_\infty(a) = H.a + b.a^m = H_0.\exp\left(-\frac{E_a}{R.T}\right).a + b.a^m \qquad \textbf{Eq. 3.1}$$

To establish the parameters of the law we use an identification in two steps. First, we consider that (*H.a)* is predominant compared to the power term and we identify H_0 and E_a from the curve of *ln(H)* vs. *1/T*. Second, we subtract the linear term from the initial maximal moisture content and identify *b* an *m* over the second part of the curve. These parameters appear to be independent of the temperature as previously shown in [128], [129]. In the case of Nylon 6 fibres we obtain the following parameters: $H_0 = 1.39$; $E_a = -7 kJ.mol^{-1}$; $b = 3$; $m = 7$. If we refer to the published values on bulk polyamide 6 materials in [128] we can note that the activation energy (E_a) and *b* are equal to the published parameters. Nevertheless, in the case of PA6 fibre materials the pre-exponential factor (H_0) and *m* are both diverging from the parameters of bulk specimens. The polymer chains in fibre materials are usually more oriented and their crystalline ratio are higher, this affects the maximal water uptake (*b* and H_0) significantly.

The model curves obtained (lines in Figure 3.2 [left]) show good correlation with experiments for temperatures up to 60°C. For 80°C tests the experimental data show deviations from the model for high water activities (above 0.7) which may be caused by water condensation on the fibres.

Influence of pre-stress on water diffusion

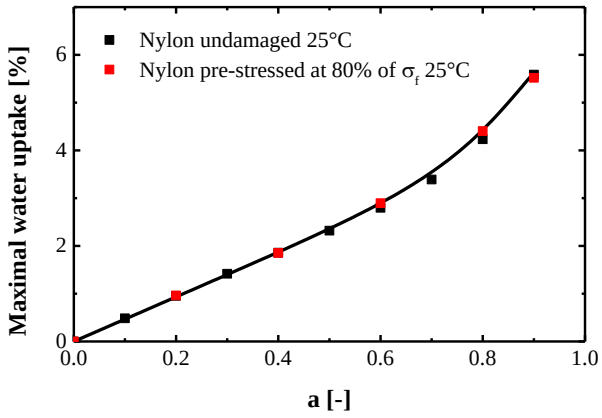

Figure 3.3. Maximum water content at 25°C in Nylon 6, undamaged and pre-stressed at 80% of σ_f

The previous section indicates virtually no water diffusion in SK78 compared to Nylon6 fibre samples. Therefore, in order to understand the influence of pre-stressing on water uptake in fibre materials we performed tests only on Nylon 6.

The pre-stress level chosen represents an extreme loading (80% of σ_f), which should indicate if the mechanical pre-stress has any influence on the diffusive behaviour.

The results obtained in Figure 3.3 show no significant variation compared with the reference values for the pre-loaded samples. Therefore, the model previously identified can still be used for pre-stressed materials.

3.2.1.2. Diffusion during immersion

Contrary to the case of water diffusion in a humid environment, when the samples are immersed there is no standard device which can record the weight variation with the same accuracy as DVS. Therefore, we developed a method to identify the different water quantities: inside filament, between fibres or in total, by DSC analysis (details in Chapter 2).

The samples were pre immersed in deionised water at 25°C for different times and then analyzed by DSC.

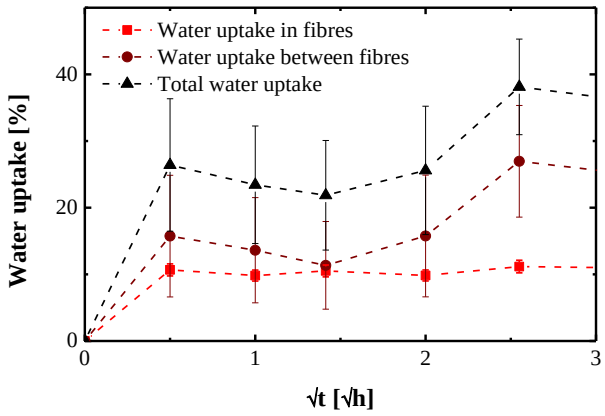

Figure 3.4. Water uptake in filaments after immersion, between fibres and in the yarn vs. square root of time

The results obtained with this technique are reported in Figure 3.4. First, the water uptakes, between fibres and in the entire sample, show a similar shape and large standard deviations (results from 3 tests for each point). The scatter in results is caused by the variation in handling between each specimen or drying. Nevertheless, the water content within the filament remains constant for all the measurements and shows only small variations for one time t. This can be explained by a handling time which remains low compared to the diffusion kinetics.

In the case of immersion we cannot describe the transient part of the diffusion curve since the exposure time would be too close to the diffusion characteristic time. Therefore, the handling time becomes critical, and has an impact on the water uptake values obtained within the

filaments.

Finally we compared the maximum moisture content in immersed filaments (10%) with the values from humid environment exposure and the model identified in 3.2.1.1 (Figure 3.5).

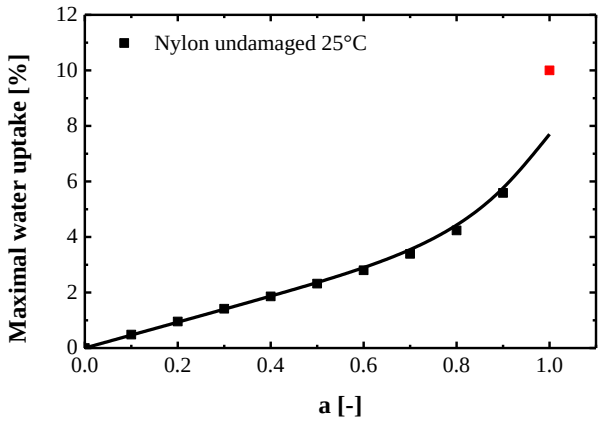

Figure 3.5. Maximal water uptake in humid environment [black points] and immersed [red point] compared to the identified model [black line].

This comparison highlights a clear difference between the diffusion behaviour immersed and in humid environment. The model established for relative humidity diffusion cannot therefore accurately predict the value in the case of immersion. For further study it would be interesting to perform additional tests in humid environments closer to 100%RH, in order to compare experimental values.

3.2.2. Water in rope

In the case of water diffusion in the rope construction, first we have to define which kind of water uptake we aim to quantify. The study target is to test the materials in the most representative way possible, therefore in the case of water diffusion inside the rope we chose to weigh the sample immersed.

As noted previously, rope-makers use various coatings (finishes), first in order to reduce friction and improve handling during the braiding process, and then to protect the fibres during marine use. Part or all of these chemical compounds can be removed during immersion, and affect the weight variation, which will then not only be induced by water uptake. We therefore performed a cycle of two sorptions and a desorption: the first sorption will correspond to the removal of unstable elements of the finish and water uptake, while the second will provide a better indication of water diffusion into the rope's construction.

3.2.2.1. First exposure

After a drying phase the rope samples were immersed for a first time in tap water, and the results obtained are shown in Figure 3.6 [left].

Three diffusion phases can be identified from these results. First, for short time exposure the finish is removed faster than the water entry: the rope is losing weight (black region). In a second part both phenomenon seem to act in parallel which induces a transient behaviour (white region). Finally, the weight gain stabilises for long time exposure: the water diffusion and finish removal stabilize or both phenomena compensate each other.

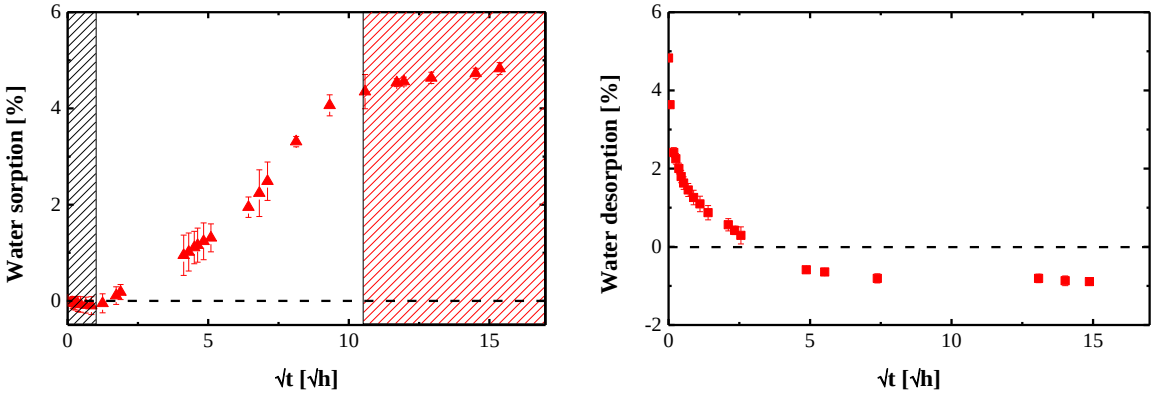

Figure 3.6. Sorption [left] and desorption [right] behaviour in a SK78 braided rope exposed to the water for the first time.

After the first cycle of sorption/de-sorption, the rope samples have lost 1.14% of their initial weight (Figure 3.6 [right]).

3.2.2.2. Second exposure

The weight variation results obtained during the second immersion are reported in Figure 3.7.

Water uptake in this case only shows two phases: a transient region characterised by a large rise in water content in the rope, and a stationary phase of the diffusion with a water content linearly increasing with the square root of time. Moreover, the rope appears to take up a large amount of water: up to 14% with no saturation.

The comparison between both diffusion plots (Figure 3.6 and Figure 3.7) shows a significant impact of finish leaching on sorption, which results in an additional weight gain during the second sorption (8% more). This difference appears important compared to the finish ratio by weight, which represents only around one percent (1.14% in our case, see part 3.2.2.1). Nevertheless, the finish leaching not only reduces the initial weight of the sample, it also

releases some volume in which water will diffuse during the second sorption. In addition, the presence of the coating may slow diffusion initially, and may act as a water repellent, but its role is difficult to evaluatehere.

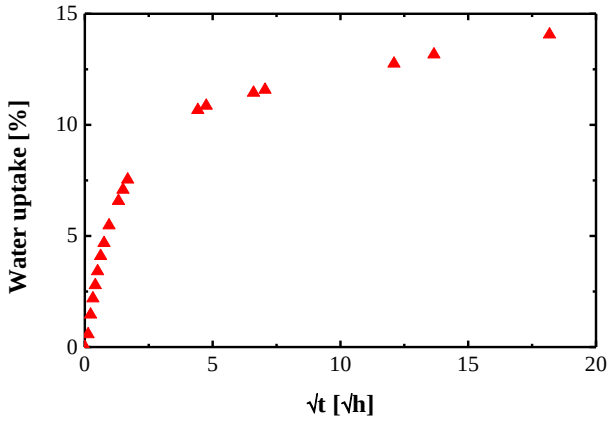

Figure 3.7. Diffusion behaviour in a SK78 braided rope exposed in to the water for the second time.

To conclude, the water uptake in ropes is hard to determine precisely due to the presence of coatings. It may be possible in future work to combine this gravimetric study with FTIR analysis, in order to identify the absence or presence of specific chemical species. However, clearly a significant quantity of water can enter into the rope construction during immersion.

3.3. Mechanical properties

During their lifetime, ropes are also subjected to important mechanical stresses in marine applications. These loadings are mainly induced by waves, currents, and pre-tensioning operations, and the result is mainly tension stresses in the rope. Only the end-connections and sections involved in handling operations (e.g. on sheaves and winches) see other types of loads. For this reason, the study is focused on rope tensile behaviour, under quasi-static, creep and dynamic loadings.

3.3.1. Quasi-static tensile behaviour

In this sub-section we focus on each scale level, from filament to rope for SK78 and from filament to yarn for Nylon 6. These are studied during quasi-static loading first unaged, and then after ageing in the case of ropes and yarns. Diffusion kinetics in monofilament materials are too rapid compared to the duration of the tensile test (around 10 minutes).

All the characteristic mechanical properties obtained from these experiments are reported in Table 3.1.

			SK78			Nylon 6		
			Modulus [Gpa]	Break Stress [Mpa]	Break Strain [%]	Modulus [Gpa]	Break Stress [Mpa]	Break Strain [%]
Monofilament	Unaged	Average	90.3	3103.7	3.6	3.0	825.7	18.8
		Standard deviation	*2.4*	*31.4*	*0.1*	*0.8*	*6.0*	*0.2*
Yarn	Unaged	Average	94.0	2517.6	2.6	3.5	821.4	18.4
		Standard deviation	*0.9*	*69.7*	*0.1*	*0.4*	*1.1*	*0.5*
	Aged	Average	96.9	2562.5	2.7	1.8	786.1	18.0
		Standard deviation	*2.1*	*53.2*	*0.1*	*0.2*	*7.0*	*0.7*
Rope	Unaged	Average	111.2	2579.8	2.7			
		Standard deviation	*3.2*	*91.9*	*0.3*			
	Aged	Average	93.9	2466.5	2.5			
		Standard deviation	*5.5*	*29.9*	*0.2*			

Table 3.1. Mechanical properties of SK78 and Nylon 6 fibre materials subjected to quasi-static tension.

3.3.1.1. Filament behaviour

Tests performed on filaments provide information on the optimum tensile behaviour of the material itself. The behaviour of all the higher level constructions made from the fibres will show premature failure in terms of stress, though the strain to failure may be higher.

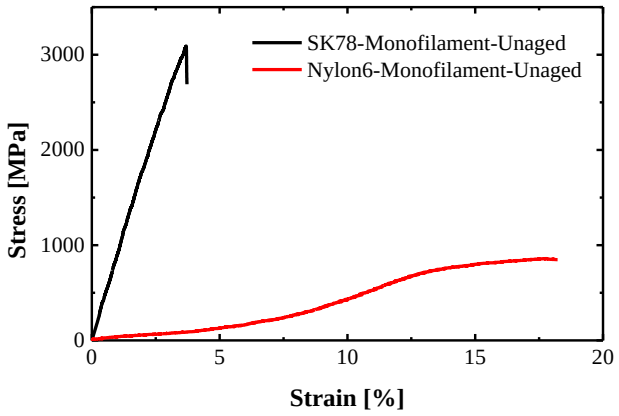

Figure 3.8. Quasi-static tensile behaviour of SK78 and Nylon 6 monofilaments

The results presented in Figure 3.8 highlight the important differences in tensile mechanical behaviour between the two materials.

HMPE SK78 monofilament has a purely elastic behaviour in the case of quasi-static testing, with a high modulus (90.3 GPa) and ultimate stress (3.1 GPa) and a low strain at failure (3.6 %), which makes HMPE one of the highest performance fibre materials.

Nylon 6 filaments show a very different behaviour. Their mechanical response follows an S-shaped curve with highly non-linear behaviour during tensile testing. This results in a low modulus value (3.0 GPa) and ultimate stress (825 MPa). However, Nylon 6 has a significantly higher ultimate strain (18.8%).

Quasi-static tensile tests on Nylon 6 and SK78 monofilament indicate the behaviour of the material itself. Once these baselines have been established we can consider other scale

levels of the rope and compare them to the reference (monofilament).

3.3.1.2. Yarns behaviour

Once the material properties are known the next step is to quantify how testing multiple monofilaments affects these quantities. In order to understand this size effect we perform tests on untwisted yarn samples. Moreover in this case the diffusion kinetics are slower than in the case of the monofilaments (due to the high number of filaments), therefore we also test them after ageing.

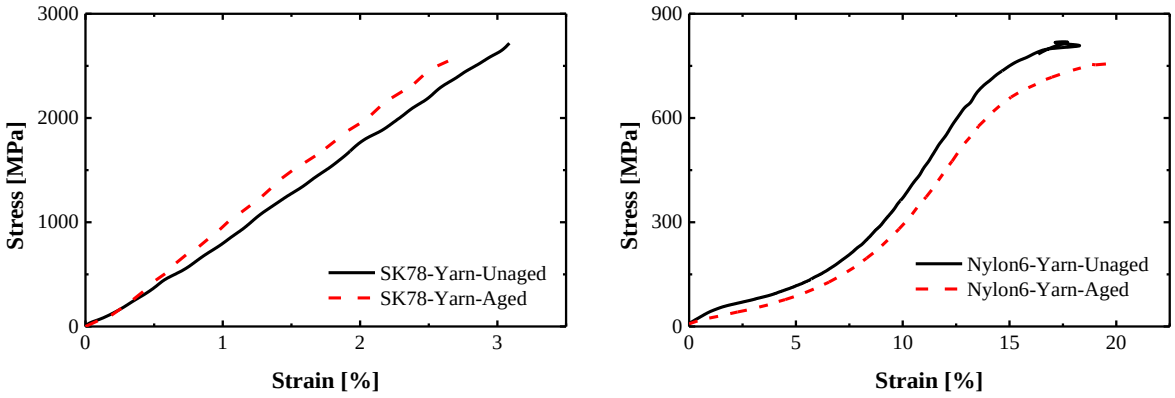

Figure 3.9. Quasi-static tensile behaviour of SK78 [left] and Nylon 6 yarns [right] unaged and aged

The HMPE and polyamide yarn tensile responses follow similar shaped curves to those of the monofilaments.

For SK78 yarns the modulus appears to be of the same order of magnitude as the monofilament (Table 3.1). This indicates a good alignment of the fibres at the beginning of the test, mainly induced by the parallel structure and a good bedding-in of all the filaments in the initial state. The failure occurs prematurely in the yarn compared to the filaments. This phenomenon is due to the early breakage of the most stressed or defective filaments. These breaks increase the stress in the other filaments and accelerate the failure mechanisms, resulting in a premature failure of the specimen.

Now, if we look to the behaviour after ageing there is no significant deviation from the reference. All the yarn's mechanical properties stay within the standard deviation interval (Table 3.1), therefore water has no significant impact on the SK78 yarn's properties when stressed in quasi-static tension.

The Nylon 6 yarns have an initial behaviour comparable to the monofilament reference. After ageing, the Nylon 6 yarn samples show a slight deviation from the unaged reference behaviour. All their mechanical properties are reduced by water diffusion, which can translate plasticization effects. Nevertheless, these changes are still low compared to

results for bulk polyamide in the literature [127], [143]–[145], for which large changes occur. The section 3.2.1.2 shows that short yarn samples are saturated in water after 15 minutes of exposure. Moreover, the time required for test preparation and execution of tensile tests on yarns is approximately 5 minutes, and therefore the fibres start to desorb significantly before testing. This suggests that the mechanical response obtained for the aged yarns here is not representative of the true wet behaviour.

To conclude, the transition from monofilament to parallel yarn is quite easy to make. The size effect only seems to affect the failure behaviour, which occurs earlier in the yarn case. However, the effect of water on the yarn is hard to identify, since the diffusion kinetics are fast compared to handling times. Therefore, the best way to test aged yarn specimens is to perform coupled tests immersed and in humid environment.

3.3.1.3. Rope behaviour

The last step of the quasi-static behaviour investigation is the study of the rope response. In this case we only consider SK78 materials Tests were performed before and after seven days' ageing (based on the results in 3.2.2).

The unaged rope behaviour is comparable to yarn response in terms of ultimate values: stress around 2.5 GPa and strain of 2.5%. Nevertheless, the modulus shows a deviation from the previous values by rising from 94.0 to 111.2 GPa. Various authors have shown that the stiffness of both HMPE fibres and ropes increases after a bedding-in operation [101], [146]–[148]. The increase observed here, which results in a final rope stiffness greater than that of the filaments, suggests that the rope manufacturing process includes significant load levels which reorient the molecular structure of the fibres in the load direction.

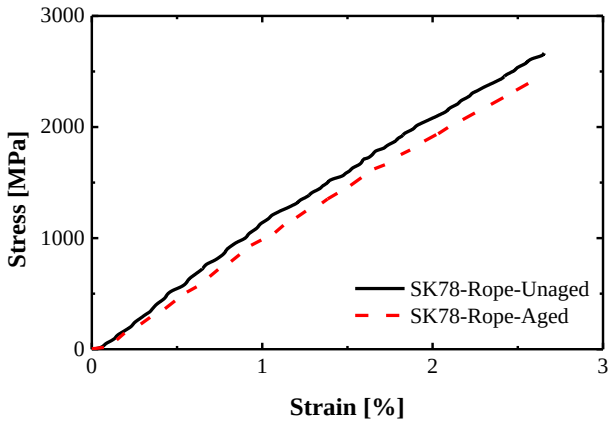

Figure 3.10. Quasi-static tensile behaviour of SK78 unaged and aged

When we focus on the rope behaviour after ageing we can notice some deviation from the

unaged case. First, the modulus value decreases significantly after ageing (from 111.2 to 93.9 GPa). Since the water does not diffuse inside the HMPE material, this change can only be induced by either the finish leaching out or water inclusion in the construction. Moreover, a decrease in the modulus can only be the result of lubrication in the structure (reduction of friction forces). This type of phenomenon is contrary to the removal of finish, suggesting it is probably induced by the water insertion in the rope structure.

Finally, after immersion the ropes' behaviour is slightly modified by lubrication effects of water inside the structure. This phenomenon allows the construction to reach higher strain levels for a given applied stress.

3.3.2. Tensile static creep behaviour

The previous section has investigated the quasi-static mechanical behaviour of fibre materials. Nevertheless, real applications necessarily induce stresses throughout the material lifetime. Therefore a quasi-static test is not sufficient to characterize the behaviour, and in order to get closer to the application we have performed creep tests on yarn and rope materials.

In this section we do not consider the monofilament level due to the slippage issue which can appear during long tests. The Nylon behaviour is studied on yarns, and we present the previous results on SK78 yarns and the results obtained during this study on SK78 ropes.

3.3.2.1. Nylon yarn behaviour

Nylon polymer appears to follow standard logarithmic viscoelastic/viscoplastic creep behaviour [112]–[114]. This type of mechanical response can be represented with a thermodynamic model based on the Schapery's theory.

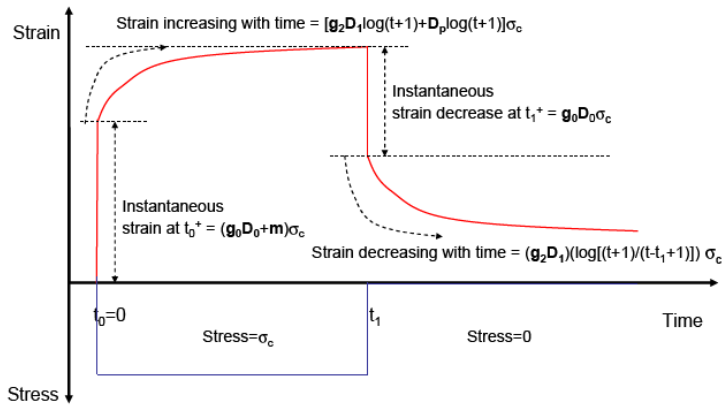

Figure 3.11. Description of the viscoelastic/viscoplastc parameters during a creep-recovery test [118].

In this study we use the model identification and prediction developed at IFREMER and detailed in [116], [117]. This technique is based on multiple creep/recovery cycles with different stress levels (Figure 3.12) for which the different viscoelastic/viscoplastic parameters (g_0D_0, g_2D_1, m, D_p) are identified by minimising the differences between the model equations Eq. 3.2 and the experimental data for each cycle.

$$\begin{cases} \varepsilon_c = g_0 D_0 \sigma_c + g_2 D_1 \sigma_c \, log_{10}(t+1) + \sigma_c \left(m + D_p \, log_{10}(t+1) \right) \\ \varepsilon_r = g_2 D_1 \sigma_c \, log_{10}\left(\frac{t}{t - t_1} \right) + \sigma_c \left(m + D_p \, log_{10}(t_1 + 1) \right) \end{cases} \quad \textbf{Eq. 3.2}$$

In this set of equations σ_c is the stress applied on the specimen from 0 to t_1 seconds and the parameters g_0D_0, g_2D_1, m, D_p are the identified viscoelastic/viscoplastic parameters. They respectively correspond to the instantaneous compliance (g_0D_0), the creep rate (g_2D_1), the instantaneous plasticity (m) and the plastic rate (D_p) as reported in Figure 3.11.

After identification (detailed in Chapter 2) of these parameters at different loading levels, interpolations were made on each parameter in order to predict their value for any applied stress (with polynomial functions).

In the study, we performed seven creep/recovery cycles from 10 to 70N, which corresponds to 58 to 409MPa (Figure 3.12). These stresses correspond to the usual range of application of nylon ropes (below 50% of their ultimate stress).

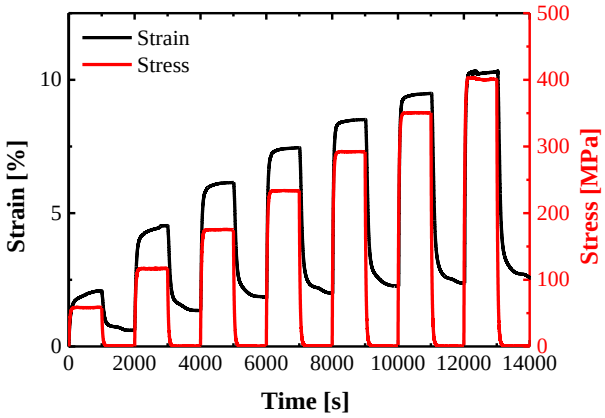

Figure 3.12. Creep/recovery behaviour of a Nylon 6 yarn at 0%RH and 25°C

The results obtained for Nylon 6 at 25°C and 0%RH are reported on Figure 3.13. This gives information on the creep/recovery behaviour of dried Nylon 6. Nevertheless, applications induce necessarily some relative humidity or immersion, therefore in the next chapter we will perform the same identifications on Nylon in both humid environment and immersed.

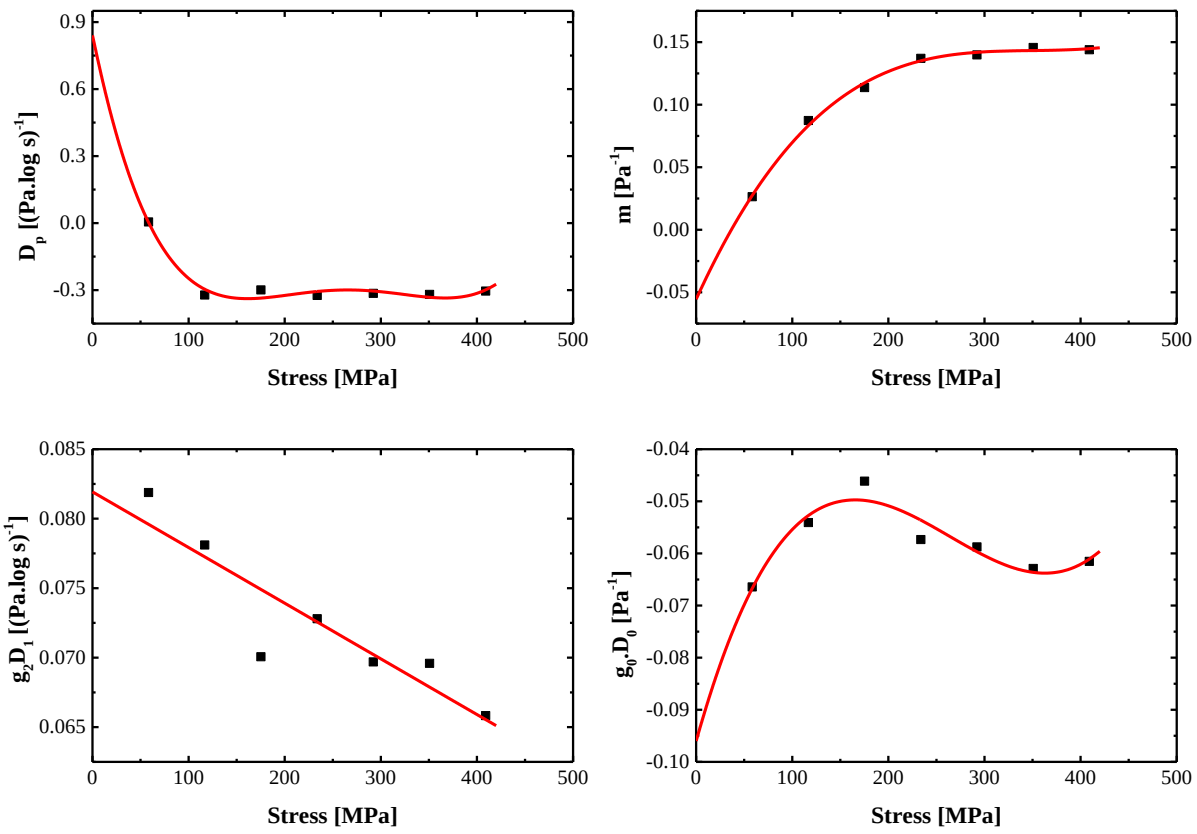

Figure 3.13. Viscoelastic/viscoplastic parameters identified with Chailleux's method [points] and their interpolations with polynomial functions [lines]

3.3.2.2. HMPE rope behaviour

In order to understand the transition from yarn to a more representative scale, we have studied the creep behaviour on SK78 ropes and tried to link it with the data and theory established on yarns

Theory and previous results on HMPE yarn

Previous studies [144], [149] have shown that creep failure occurs when plastic strain reaches a critical value: $\varepsilon_{pl-crit}$ (independent of the loading case), which can be defined as the integration of strain rate over yarn life time (see Eq. 3.3.). In this expression, $\dot{\varepsilon}_{pl-s}$ and $\dot{\varepsilon}_{pl-d}$ respectively stand for the plastic strain rates under static and dynamic loading and $tt_{fs}$and tt_{fd} respectively stand for the time to failure in static and dynamic loading.

Studies [110], [111], [150] on HMPE established expressions for the creep strain rate as a function of temperature and stress. In this study we use the expression from [150] which considers the creep strain rate as a power function of the stress and follows an Arrhenius law of the temperature. The plastic strain rate under cyclic loading can be expressed as in the

static case by replacing the constant stress by a dynamic one (see Eq. 3.4.), where K is a constant, and A_T is a parameter following an Arrhenius law of the temperature: $A_T = e^{\frac{\Delta U}{R_g}\left(\frac{1}{T_0}-\frac{1}{T}\right)}$.

$$\varepsilon_{pl-crit} = \int_0^{tt_{fd}} \dot{\varepsilon}_{pl-d}\, dt = \int_0^{tt_{fs}} \dot{\varepsilon}_{pl-s}\, dt \qquad \textbf{Eq. 3.3.}$$

The parameters (C, ΔU, T_0, m and $\varepsilon_{pl-crit}$) can be identified with the data base for static creep life time at different temperatures and stress levels.

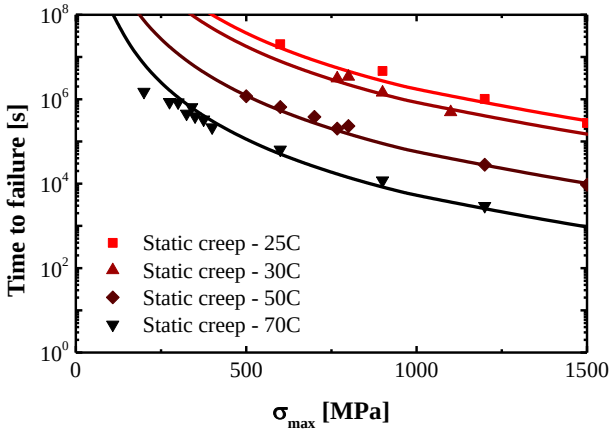

Figure 3.14. Creep time to failure identified [lines] from experimental data [points] on SK78 yarns.

$$\dot{\varepsilon}_{pl-d}(t) = K.A_T.\sigma(t)^m \qquad \textbf{Eq. 3.4.}$$

Finally, this theory leads to the prediction shown in Figure 3.14 for different temperature, showing a good correlation with the experimental results obtained by testing SK78 yarns under tensile creep.

Experimental results on ropes

$$F_{yarn}(t) = \frac{F_{rope}(t)}{cos\,(\alpha)} \qquad \textbf{Eq. 3.5.}$$

The prediction model has been established on yarn experiments, for which the constants have been determined. Here we investigate the rope time to failure and compare it to the prediction based on yarn results, but to do so we have to know the stress applied on the individual yarns during a creep test on the rope. This stress has been determined considering the braided angle as constant and using a simple projection on the yarn axis; we obtain an evaluation of its value from Eq. 3.5.

This leads to the results and prediction shown in Figure 3.15.

The figure below shows a good correlation between prediction of the time to failure under static creep (based on the yarn results) and experimental data on ropes.

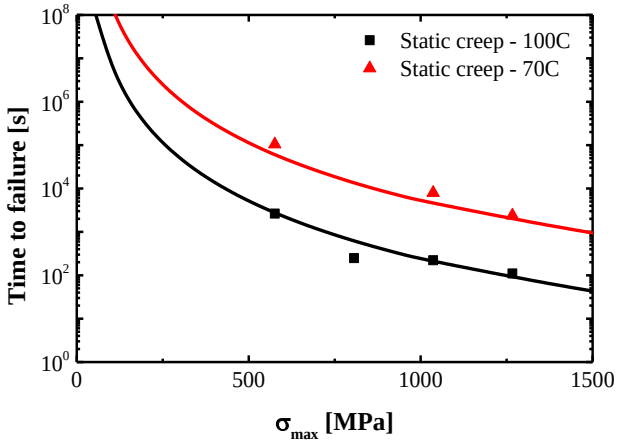

Figure 3.15: Creep time to failure prediction compared to experimental data on ropes (at 70 and 100°C)

3.3.3. Tensile dynamic behaviour of HMPE

Static creep behaviour gives important information on the rope life time for some applications; nevertheless most of the real case stresses are dynamic. For example when we look at marine applications, the wave loading induces a non negligible dynamic cyclic component in the stress.

This section is dedicated to the study of SK78, in order to investigate the possibilities to transfer a life time prediction model established for static creep (in previous work) to the dynamic case.

3.3.3.1. Theory and previous results on yarn

The first stage of the study was to verify if this transition from static to dynamic can be made at the yarn scale.

General case

As suggested in Chapter 2, the HMPE yarn life time under dynamic loading is controlled by the creep mechanism. This hypothesis implies the assumption that time to failure is quite long compared to the period of the dynamic loading t_{cycle}, and that we can consider the strain as the integration of the stress function over one cycle multiplied by the number of cycles. Appling this transformation to Eq. 3.3., we obtain a relationship between tt_{fd} and tt_{fs} , linked with an acceleration factor a_{cycle} as written in

Eq. 3.6. The theory behind the acceleration factor is developed in [149].

$$tt_{fd} = tt_{fs}\frac{\int_0^{t_{cycle}} {\sigma_{max}}^m \, dt}{\int_0^{t_{cycle}} \sigma(t)^m \, dt} = \frac{tt_{fs}}{a_{cycle}} \qquad \text{Eq. 3.6.}$$

With $tt_{fs} = \frac{\varepsilon_{pl-crit}}{K.A_T.{\sigma_{max}}^m}$ *and* $a_{cycle} = \frac{\int_0^{t_{cycle}} \sigma(t)^m \, dt}{t_{cycle} \cdot {\sigma_{max}}^m}$

To go further in the acceleration factor calculation, we have to apply a specific function for dynamic stress.

Sinusoidal case

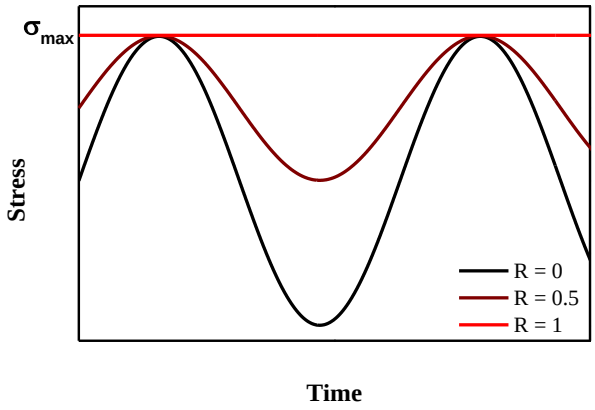

Figure 3.16: Sinusoidal stress versus time for different R ratios

The dynamic load is chosen as a sinusoidal function of time. There are three main ways to express sinusoidal stress, either with the maximal and minimal stresses, with mean and amplitude, or with maximal stress and the stress ratio ($R = \sigma_{min}/\sigma_{max}$). In our case we want to compare the creep test with the fatigue response, so the use of the R ratio allows us to represent the case of a creep test for R=1 (see Figure 3.16). Then, the sinusoidal stress expression can be introduced in the previous equation Eq. 3.4. to get the dynamic creep strain rate, as shown in Eq. 3.7.

The acceleration factor expression can then be simplified, using the variable $t' = {}^{t}/_{t_{cycle}}$ and the integration of the parameter $\varepsilon_{pl-crit}$ gives Eq. 3.8., presented hereafter.

$$\varepsilon_{pl-crit}(t) = K.A_T.\left[\left(\sigma_{max}\frac{1+R}{2}\right) + \left(\sigma_{max}\frac{1-R}{2}\right)\sin(t\omega)\right]^m \qquad \text{Eq. 3.7.}$$

With $\omega = {}^{2\pi}/_{t_{cycle}}$ *the pulsation*

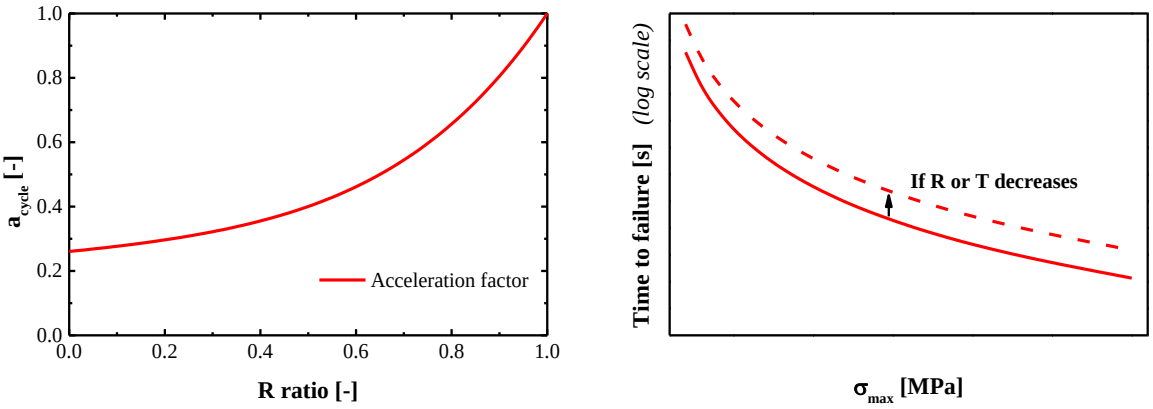

Figure 3.17: Influence of R on acceleration factor for m=4.43 [left] and influence of stress level, R and temperature on dynamic time to failure prediction [right]

The expression in Eq. 3.8. for the acceleration factor from static to dynamic loading shows a time to failure which is independent of frequency. For a given material, a_{cycle} is only dependent on the R ratio and temperature T, which induces variations of time to failure inversely proportional to variations of the R ratio and temperature (see Figure 3.17). To conclude, the prediction curve from static to dynamic tests is only shifted along the time to failure axis.

$$a_{cycle} = \frac{\int_0^{t_{cycle}} \left(\frac{1+R}{2} + \frac{1-R}{2}\sin(t.\omega)\right)^m dt}{{\sigma_{max}}^m} = t_{cycle}\int_0^1 \left(\frac{1+R}{2} + \frac{1-R}{2}\sin(2\pi.t')\right)^m dt' \qquad \textbf{Eq. 3.8.}$$

Time-Temperature superposition

To avoid end termination effects and to reach failure in the central part of the rope sample which is only loaded in tension, the tests can be performed at high temperature, to accelerate this phenomenon. The problem is that at high temperature the time to failure for high stress will be too short and at lower temperature and stress it could be too long. This issue can be avoided by using the time-temperature equivalence method to create a master curve.

$$tt_{fd}(T_1) = tt_{fd}(T_2)e^{\frac{\Delta U}{R_g}\left(\frac{1}{T_1}-\frac{1}{T_2}\right)} = tt_{fd}(T_2).A_{T_{1-2}} \qquad \textbf{Eq. 3.9.}$$

As noted above, the creep strain rate is temperature dependent as shown in Eq. 3.4. So if we compare times to failure at different temperatures under the same loading condition, we

can get a relationship between times to failure involving only a shift factor ($A_{T_{1-2}}$) as shown in Figure 3.17 and Eq. 3.9.

For one couple of temperatures this shift factor is constant, which means that the master curve can be created by a simple translation of the results along the time axis for each temperature as shown in Figure 3.17 [right].

Previous works on yarns

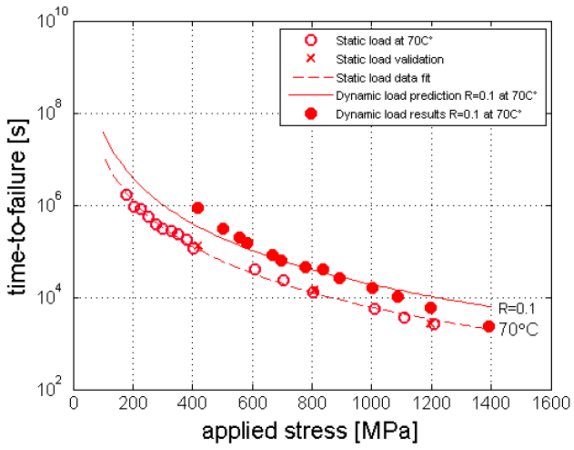

Figure 3.18. Time-to-failure at 70°C for SK75 yarns under static and dynamic loading obtained by model prediction [lines] and by experimental testing [points] [141]

First this model has been verified on HMPE SK75 yarn samples in the study [151]. These results show a good correlation between the model prediction and experimental data. There is only a slight deviation which can be highlighted at high stress, most probably induced by viscous heating in the material.

Given this good agreement between prediction and experiment at the yarn level the same tests were then performed at the rope scale.

3.3.3.2. Rope behaviour

The previous section showed a good prediction of the model in the case of yarns stressed under dynamic tension. Nevertheless, this model cannot be transferred immediately from yarns to ropes. First, we have to consider some possible limitations and modifications induced by the rope construction. Therefore, the next two sub-sections focus on these issues, and the last one is dedicated to the comparison between experimental data and the model, by taking into account these considerations.

Theory for rope

In order to get closer to the final application it is important to consider the rope scale. The construction chosen is a braided rope made of 12 twisted strands each of 3 yarns of 1760 dtex Dyneema SK78 HMPE fibres.

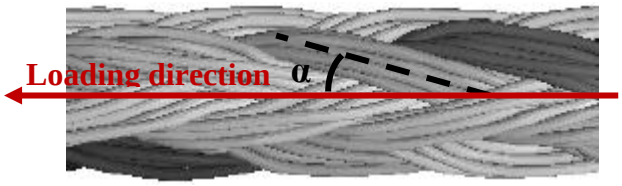

Figure 3.19: Representation of the average angle of filaments (α) to the loading direction, defined to be equal to the braided angle.

For ropes subjected to cyclic loading we can apply the same theory by taking into account the angle of filaments in the ropes to calculate the stress in the yarns. Various studies have established simple analytical relationships between load applied to twisted ropes and stress in the filament (as [105], [152]–[155]), but in our case the construction is a braid, for which there is no simple theory (see [102]). Another way to estimate the stress in yarns is simply to take the average braided angle (α=24°) and consider that all the filaments have this same angle with respect to the loading direction (see Figure 3.19). From this assumption we can find the stress applied on the yarns considering that the load on the rope is the projection of the load on yarns over the loading direction (see Eq. 3.5.)

The rope construction also induces higher friction effects between the yarns and the terminations; these can generate premature failure in some cases such as at high frequencies, amplitudes or loads. Finally, increased diameter ropes lead to higher temperatures than within a single yarn, since the heat created by plastic deformation diffuses more slowly than in yarns. The friction phenomena can also increase the heating process. These issues must be studied before testing ropes, in order to define the range of validity of the study and to avoid unrealistic heating or abrasion effects.

Scope of the study

In order to develop a valid procedure for testing ropes in fatigue we have to eliminate the failures induced by external abrasion on the clamps. Once this phenomenon is understood and controlled, we can define the relevant parameters for the study (frequency, temperature, maximum stress).

To investigate this aspect, cyclic tests were first performed at room temperature (23^{o}C) to increase the contribution of creep to time to failure without affecting abrasion. The testing

device used consisted of a special oven to heat the rope and clamps to avoid slippage, this equipment is detailed in Chapter 2. Moreover, to check that this is a real cycle dependent phenomenon these tests were performed at two different frequencies.

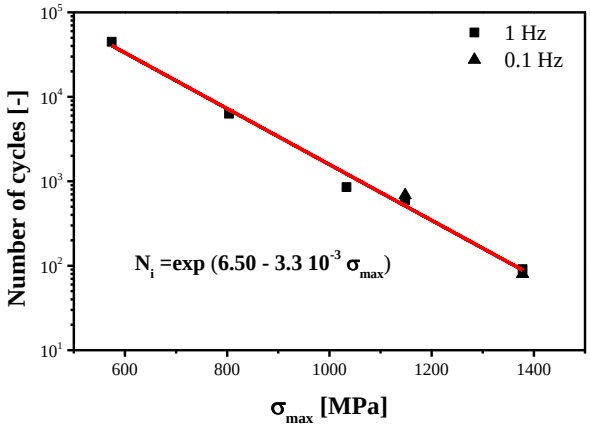

Figure 3.20: S-N curve corresponding to failure in clamps (external abrasion) for different frequencies at 23°C

During these tests it was also verified that failures were indeed the result of an external abrasion (failures near clamps).

Results are summarized in Figure 3.20 and show two main characteristics of external abrasion failures:

- The failure induced by abrasion is entirely dictated by the number of cycles (no influence of the frequency)
- The number of cycles to failure is an exponential function of the maximum stress applied.

In this work we want to characterize the creep failure mode in fatigue. To do so we have to avoid any abrasion failures. The approach adopted is to reduce cyclic damage (by applying low frequency fatigue) and increase creep rates (using high temperature testing). From the experimental results of abrasion failure (shown in Figure 3.20) we established a lifetime prediction model for any frequency, so that creep dominant failure on SK78 ropes can be predicted from the yarn creep behaviour (see part 3.3.3.2 – Theory on ropes) at different temperatures. This failure model allows us to determine the temperature and frequency of the fatigue tests required to obtain a creep failure mode (T=100°C and f=0.1 Hz see Figure 3.21). A frequency of 0.1 Hz was adopted as it represents a wave period of 10s, and the temperature of 100°C allows us to perform tests in an experimentally feasible timescale but avoids going too close to the melting range of the material (T_m=144-152°C). Moreover, we should be able to perform tests at stresses up to 1500 MPa (75% of ultimate stress). Higher loads would not be interesting since ropes in practical applications are usually stressed in the range below 400

to 600 MPa.

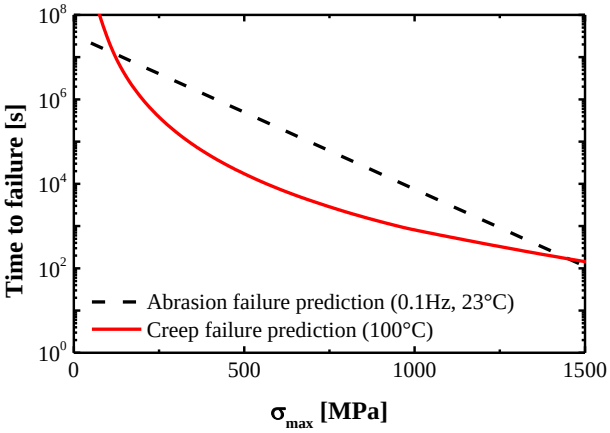

Figure 3.21: Prediction of external abrasion failure compared to prediction of time to failure in creep mode at 100°C.

The second issue is the hysteretic loops created by the viscoelastic behaviour of HMPE. These loops translate energy dissipation during each loading cycle of tension-tension fatigue, and for a stressed material the main way to lose energy is by heat generation (see Figure 3.22). Heating can have two negative effects on experimental results: if the temperature rise stabilises, it will induce a behaviour modification as Eq. 3.9. indicates; if viscous heating rises without finding an equilibrium, it will result in melting inside the sample.

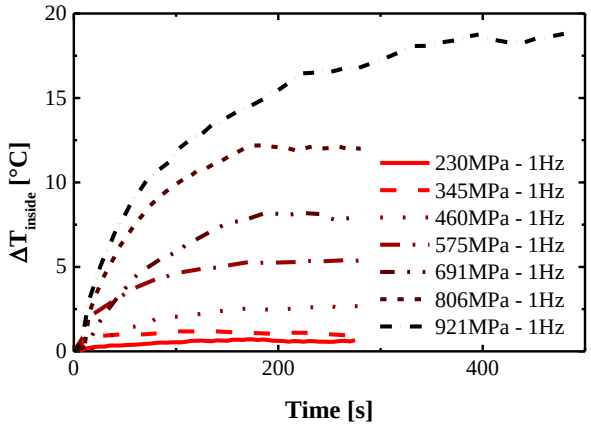

Figure 3.22: Temperature rise inside the rope vs. time for different applied maximum stresses at 23°C

In order to examine this point cyclic experiments have been performed on the rope samples and the internal temperature has been recorded using an inserted thermocouple (type K). A recording period equal to at least three fatigue cycles was used, to reduce the noise induced by cycles. Figure 3.20 shows examples of results for different test conditions.

Based on these observations we developed an empirical model, which can predict the

heating process inside the rope using simple mathematical laws. For this study we do not consider the transient state, only the maximum temperature value inside the rope (Figure 3.22).

The heating process inside the rope is dependent on the maximal applied stress σ, the surrounding temperature T, the frequency f and also the R value. To identify the influence of these parameters on heating, each of them was successively considered as a variable while the others were fixed (e.g. 3.23 [a.] shows the influence of maximum stress), which provides an expression of the heating dependency on the variable parameter. In this case we assume that the influence of each parameter on heating is independent of the others.

The observation of temperature variations allowed an exponential dependence on maximum applied stress to be identified (3.23 [a.]). Moreover we know that when the stress is equal to zero, no heating will take place, so we obtain the following expression:

$$\Delta T_{max} = \left(e^{\sigma_{max}/\sigma_0} - 1\right).g(T,f,R) \qquad \textbf{Eq. 3.10.}$$

With g a function of temperature (T), frequency (f) and R ratio; σ_{max} the maximal stress applied; σ_0 a constant proportional to a stress and equal to 357 MPa for this case.

The frequency effects have been studied for four different stresses, represented in 3.23 [upper right], and in each case there is a linear dependence of temperature rise on frequency. Moreover, the heating process will disappear for a frequency equal to zero (case of static creep loading). These two observations led to the development of a heating process expression, from Eq. 3.10. to Eq. 3.11.

$$\Delta T_{inside} = \left(e^{\sigma_{max}/\sigma_0} - 1\right).f.h(T,R) \qquad \textbf{Eq. 3.11.}$$

With h a function of T and R. For a frequency of 0.1 Hz, the heating process can therefore be neglected for the stress range here (up to 1500 MPa).

Finally the heating process is dependent on the surrounding temperature. To identify its influence on the temperature rise within the rope we conducted tests under different conditions in an oven. Results summarised in 3.23 [bottom] show a linear dependence of the heating process on the surrounding temperature, and for temperatures below 0^oC there is no heating phenomenon, which modifies Eq. 3.11. to Eq. 3.12., considering $k(R)$ as a function of R ratio, equal to 7.10^{-2} s.^oC for R=0.1.

$$\Delta T_{max} = \left(e^{\sigma_{max}/\sigma_0} - 1\right).T.f.k(R) \qquad \textbf{Eq. 3.12.}$$

This empirical law (Eq. 3.12.) provides a tool to determine if the heating process will be

significant based on the testing conditions. Nevertheless the equation has been established for a specific HMPE grade and rope construction (braid angle, linear weight, diameter, coating) it should not be applied directly to a rope with different parameter(s).

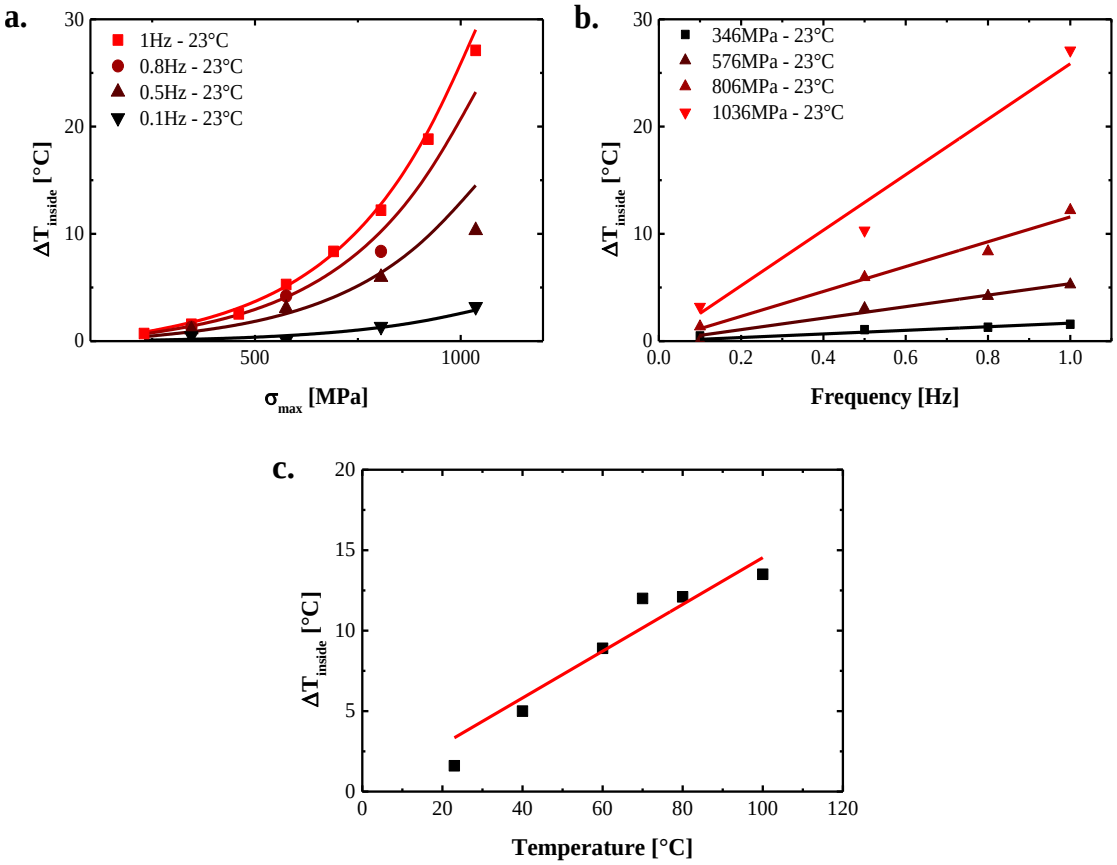

Figure 3.23: Maximum rise of temperature vs. stress applied for different frequencies (R=0.1, T=296K) [a.]. Maximum temperature rise as a function of frequency for diffrent stresses (R=0.1, T=296K) [b.]. Maximum temperature rise as a function of the surrounding temperature (R=0.1, f=1Hz, σ=345MPa) [c.]

Experimental results

At 100°C, 0.1Hz and R=0.1:

It is now possible to define the dynamic test conditions. In order to perform the dynamic experiments the frequency was chosen to be 0.1 Hz frequency, and to avoid external abrasion failure it was necessary to test at 100°C. The stress ratio has been chosen to be equal to 0.1 to simulate a worst case scenario in terms of loading. The experimental set-up details, the clamps and oven, are described in Chapter 2.

Figure 3.24 shows the test results and the dynamic creep prediction (from Eq. 3.6). The prediction is quite accurate up to 900 MPa under these conditions (black dots, Figure 3.24). Above this value the experimental data deviate from the prediction (red triangles, Figure 3.24). Boleij already noticed this deviation for the case of yarns in [141]; it could be

explained by hysteretic heating. In the previous sub-section we established the dependence of temperature rise on temperature, frequency and stress variation (Eq. 3.12.). Therefore if we want to take into account this heating process in the life time calculation we have to substitute the constant temperature in Eq. 3.9. by the relation Eq. 3.12. Finally, the prediction model is changed and controlled by Eq. 3.13., and can then predict the deviation time to failure change (Figure 3.24 –right–).

$$A_T = e^{\frac{\Delta U}{R_g}\left(\frac{1}{T_0}-\frac{1}{T+\Delta T}\right)} = e^{\frac{\Delta U}{R_g}\left(\frac{1}{T_0}-\frac{1}{T+\left(e^{\sigma max/\sigma_0}-1\right).T.f.k(R)}\right)} \qquad \textbf{Eq. 3.13.}$$

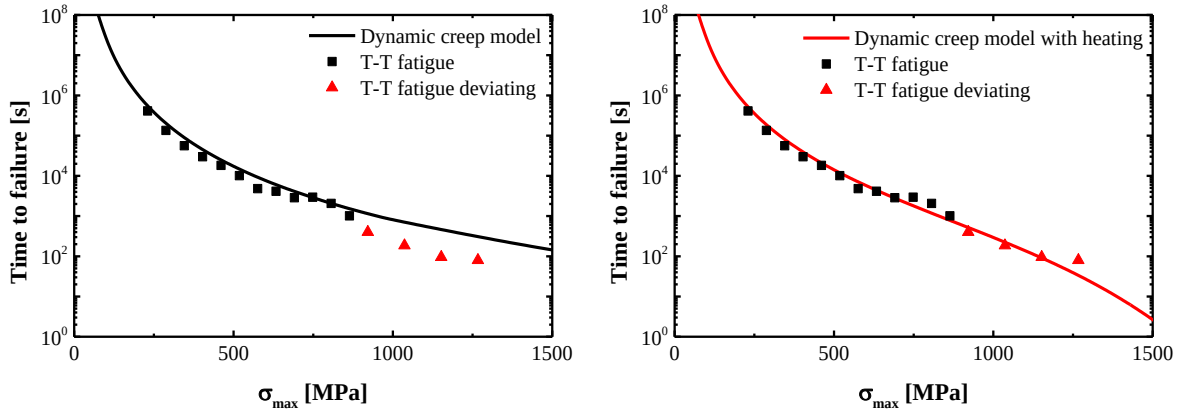

Figure 3.24: Dynamic time to failure prediction compared to experimental data (at 100°C, R=0.1 and 0.1Hz) without (left) and with (right) heating taken into account

At 100°C, 0.1Hz and R=0.5:

The choice to take an R value of 0.1 was made in order to investigate the reliability of the model for extreme dynamic loading. Nevertheless in marine applications the amplitude rarely reaches such high values; R values are usually in the range between 0.3 and 0.6. To test the robustness of the model for R variation we performed two verification tests at R=0.5 (within the application range) in order to verify the model consistency.

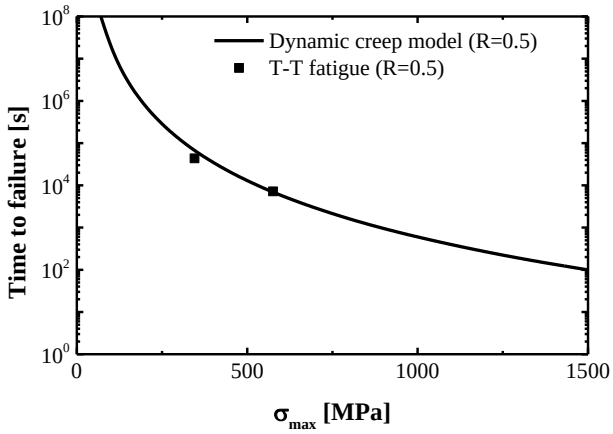

Figure 3.25: Time to failure vs. maximum applied stress for an R value of 0.5 (100°C and 0.1Hz)

Increasing R ratio induces a change in the acceleration factor as shown in Eq. 3.8 which will induce a shift of the failure curve parallel to the time to failure axis. In this case, for an R value of 0.5 the shift factor is equal to 0.4 which reduces significantly the rope's life time compare to the case of R=0.1. Experimental results and model predictions in this case are summarised in Figure 3.25. Moreover, in this case the relative displacement between fibres will be reduced compared to tests with an R ratio of 0.1, and hence induce lower abrasion so that we can neglect the influence of heating on the time to failure.

Results are quite conclusive; the experimental data agree well with the model prediction in this case which shows the reliability of the model for different stress ratios. The model was also verified for the static creep case, which can be compared to the dynamic case with a frequency equal to zero.

3.4. Conclusion

The aim of this chapter was to understand the water diffusion and mechanical behaviour as both uncoupled and semi-coupled phenomenon at the yarn and rope scale.

Water diffusion in yarns is a complex quantity to identify: first because of the rapid diffusion kinetics which limit the acceptable testing time, second due to the number of filaments which can trap water molecules between fibres and affect the results. Once these two issues had been addressed it was possible to identify the water uptake in Nylon 6 yarns. These results indicate behaviour comparable to that of bulk polyamide 6, therefore the transition between bulk and fibre material can be made in terms of maximal moisture content. The pre-loading appears to have no impact on this quantity (up to 80% of ultimate stress). There is still one aspect which should be verified in the future, modelling of the diffusion kinetics in such materials. Some models already exist to model the diffusion in cylinders (fibres) therefore a diffusion coefficient could be identified by optimisation of the model on experimental DVS results.

The study also examined water uptake within ropes. For this investigation an experimental technique was developed to avoid measurement problems (e.g. variable water content on the outside of the specimen when weighed) and uncoupled diffusion phenomena caused by the finish leaching out. The results obtained with this technique show significant amounts of water within the structure (more than 10%) and a significant effect of the finish removal on the rope weight. For further studies FTIR analysis would be useful to provide information on the exact impact of water immersion on the finish.

The study on the mechanical behaviour has focused on three different tests: quasi-

static, static creep and dynamic tensile loadings. The aim was to understand the rope life time for a real application.

Quasi-static response has been studied at the filament, yarn and rope levels on both materials. These tests highlight the difference between both type of fibres and give information on their mechanical limits. The construction appears to have an influence on the failure which occurs prematurely for larger scale construction. Moreover, a loading history effect is noted in the HMPE rope, due to molecular reorientation, which results in a rope modulus which can exceed that of the new yarn. This has been noted previously and requires further study. Finally, HMPE yarns tested after immersion show no significant modifications in contrast to the case of Nylon yarns and HMPE ropes. Nylon 6 yarns have mechanical properties degraded by water ageing, and HMPE ropes appear to be impacted by lubrication effects of water inside the structure which lower their initial modulus. Again, further work is needed to examine how these effects change with time.

The static creep behaviours identified on each material are quite different. The creep strain in Nylon 6 yarns follows a logarithmic function of the time which has been identified using a Schapery based non-linear viscoelastic-viscoplastic model. On the contrary SK78, as most other HMPE fibres, has a constant creep strain rate which follows an Arrhenius law of the temperature and a power law of the stress.

This latter model has also been used for life time prediction in the case of HMPE ropes with some slight modifications. First, the stress applied has been estimated by considering the average angles of filaments in the rope (braided angle). Second, the rope scale induces important viscous heating phenomena. Therefore an empirical heating model has been established in order to predict the premature failure in the case of significant temperature rise. Once these modifications have been added to the model we obtain a good correlation between times-to-failure from experiments and model predictions.

Chapter 4.

Coupled behaviour

4.1. Introduction

The previous chapter highlights the influence of water on the behaviour of the fibre material and on the rope structure as semi coupled responses. Therefore, in order to understand the phenomena involved in real life applications, the last step of the study is focused on fully coupled behaviour. This chapter is organised in two parts: the first is devoted to the coupled effect on the fibre material (Nylon 6) and the second focused on this effect on the rope construction (SK78).

The first section on coupled behaviour of Nylon 6 fibre aims to understand the effect of water uptake on the mechanical state of the material. To do so, the glass transition temperature (Tg) and the hygroscopic elongation are studied in different humid environments. In the case of the Tg analysis, we also use a T-Tg transposition technique to compare the different relative humidities. Finally, by using previous results (Chapter 3) which link the relative humidity with the water content, we aim to predict both Tg and elongation variation with the water uptake.

Second, we focus on coupled behaviour of Nylon 6 subjected to creep in different humid environments. The results from these tests are identified in the same way as in the case of uncoupled creep behaviour and compared.

In the last section, we discuss the effect of water (relative humidity or immersion) on the fibre material's creep behaviour.

The study of coupled behaviour effects on the rope structure is divided into two sections. First, their quasi-static response in tension was studied dried in ambient air (50%RH) and immersed in tap water, both tests were performed at 21°C. For each case, tensile parameters were identified and compared, to quantify the impact of immersion on the rope behaviour.

Second, we perform the same tensile fatigue tests as those presented in chapter 3 on ropes, but for samples immersed in tap water at 35°C. This last section aims to understand the effect of water inside the rope during long term loading. Therefore, these results are compared to the predictions of the model established in chapter 3 and the deviations are discussed in order to understand the phenomena involved.

The chapter will end with a general conclusion on the benefits and limits of coupled tests. Moreover, first conclusions on the effect of coupling are summarised and some prospects for future work are proposed.

4.2. Coupled behaviour at the yarn level

The first step is to consider the effect of coupled phenomena at the scale of fibres. As shown in chapter 3, yarn sample behaviour does not diverge significantly from the filament response. Therefore, the tests presented in the following section were made on yarn specimens.

Two main subjects are investigated here, first, the passive coupled phenomena: changes in Tg, determined by DMA, and hygroscopic elongation. Both properties are identified with existing models, the Sihma-Boyer equation [128] for Tg and a constant law for hygroscopic elongation at low water content [135].

Second, modifications to the mechanical response due to water uptake are examined. For Nylon 6, we focus exclusively on static creep response, since dynamic stresses could introduce additional coupling effects. This static issue is studied in two steps. The first aims to identify the full creep and recovery behaviour of Nylon 6 and its variation with the relative humidity. The second examines the effect of immersion on the creep response.

4.2.1. Relative humidity effects on yarn

Water uptake induces two passive coupled phenomena: plasticization of the material (Tg decrease) and hygroscopic elongation. The first one was determined by DMA testing in relative humidity environments from 0%RH to 80%RH (Figure 4.1 and Figure 4.3). The second coupled response was obtained by performing tests in the DMA under different humidity conditions, on samples stressed at 0.5MPa.

4.2.1.1. Glass transition temperature

The glass transition temperature was first studied in 0%RH environment in order to obtain a reference value, Figure 4.1.

. These tests were performed in a standard oven device filled with silica gel dehydrate. The results obtained show a typical polyamide response. The glass transition temperature was determined by considering the drop in storage modulus E’ which corresponds to 55°C on average.

In a second step, we performed DMA tests at a fixed temperature while the relative humidity was increasing in steps, as shown in Figure 4.2. Then, the average E’ value was recorded at each step and corresponds to the quantity for a particular temperature and relative humidity. The range of temperatures which can be studied is much smaller than in the 0%RH case. For this type of test, we perform analysis from 25 to 50 °C; for the highest temperature

we cannot reach the highest relative humidity values (Figure 4.3), but this is not important since the increase in relative humidity reduces the glass transition temperature. Therefore, we can use a T-Tg translation of each curve (Figure 4.3) in order to create a master curve and deduce the new Tg of Nylon 6.

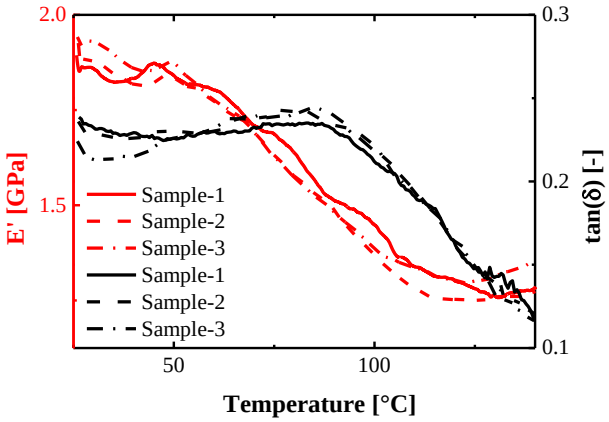

Figure 4.1 E' and tan(δ) thermal response of nylon6 yarn while stressed at 1Hz under 0%RH atmosphere.

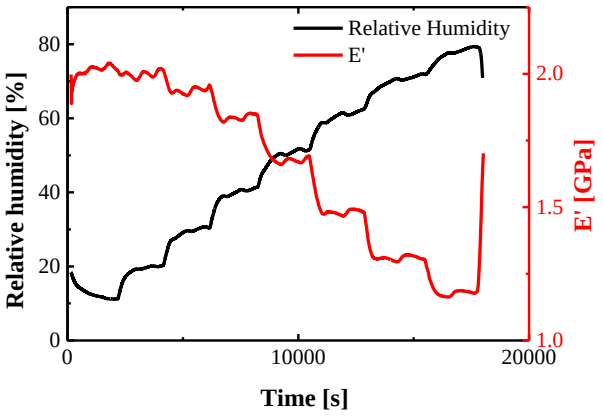

Figure 4.2. Example of a DMA test at 25°C under different humidity conditions.

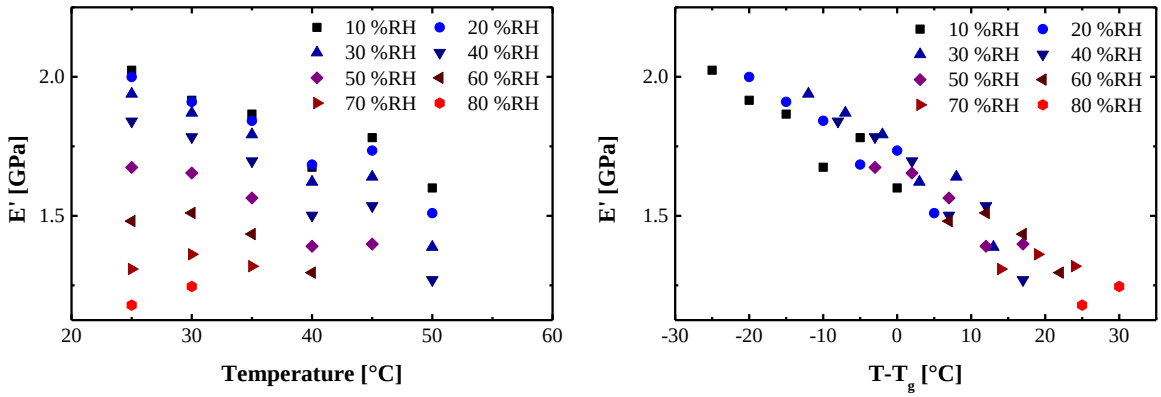

Figure 4.3. E' thermal response of nylon6 yarns under different temperatures and humidity conditions.

This study provides the results for Tg variation with the relative humidity reported in Figure

4.4 (black points).

$$T_g = \frac{T_{gp}.T_{gs}}{T_{gs} + v_{w,a}.\left(T_{gp} - T_{gs}\right)} \qquad \textbf{Eq. 4.1}$$

Some previous studies have established models which predict the Tg variation of a material with the water takes up [78], [156]. Among them the Sihma-Boyer expression [78] appears to be in good agreement with experimental results in the case of polyamide material [128]. This approach predicts the variation in T_g as a function of glass transition temperature of the polymer in the dry state: T_{gp}, of the solvent (water) T_{gs} and the relative volume of water in the amorphous phase of the polymer $v_{w,a}$ (Eq. 5.1). In this case, T_{gp} and T_{gs} are respectively taken equal to 328K (Figure 4.1) and 110K [157], $v_{w,a}$ is defined by the equations Eq. 4.2 and Eq. 4.3 detailed in Chapter 2.

$$C_a(t) = \frac{C(t)}{C(t) + (1 - X_c)} \qquad \textbf{Eq. 4.2}$$

$$v_{w,a} = \frac{C_a \rho_a}{C_a \rho_a + (1 - C_a)\rho_w} \qquad \textbf{Eq. 4.3}$$

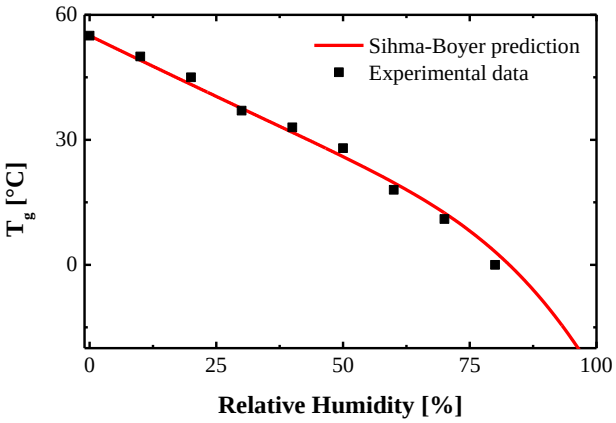

Figure 4.4. Glass transition temperature variation as a function of the relative humidity.

To summarise, the equations Eq. 5.1, Eq. 4.2 and Eq. 4.3 combined provide the relationship between the glass transition temperature of the polymer (T_g) and water uptake in the polymer ($C(t)$). Moreover, in Chapter 3 we related the moisture water uptake in the polymer to the water activity (a) (Eq. 4.4). Therefore, by replacing $C(t)$ in Eq. 4.2 by $C_\infty(a)$ for each temperature and relative humidity, we can predict the variation of T_g with relative humidity according to Sihma-Boyer theory (Figure 4.4, red line).

To conclude, the prediction used (red line) and experimental data (black points) in Figure 4.4 show a good correlation. This observation is true even for the highest relative humidity values

(80%RH), this result was not obvious in a first assumption.

$$C_\infty(a) = H_0.\exp\left(-\frac{E_a}{R.T}\right).a + b.a^m \qquad \textbf{Eq. 4.4}$$

To go further in this investigation, it would be interesting to test samples on the DMA under immersion conditions, in order to compare the experimental results with the Sihma-Boyer predictions.

4.2.1.2. Hygroscopic elongation

The other mechanical change induced by water in the polymer is the hygroscopic elongation. This phenomenon is created by the insertion of the water molecules in the material which generates swelling.

For this study, the hygroscopic elongation was recorded on Nylon 6 yarn samples stressed at a negligible load (0.5MPa) in a relative humidity regulated from 20 to 80%RH at 25°C. These tests were performed in the DMA device with the same clamps as before (presented in Chapter 2). The results obtained are reported in Figure 4.5.

Some previous work is available on this subject for bulk [158] and fibre [135] polymers. A linear dependence of hygroscopic elongation on the water uptake was indicated, with a threshold value. For the water content close to the saturation value, this relation does not appear to be verified, probably due to clustering effects in the polyamide [135]. Indeed, for high water content the molecules start to gather in clusters and therefore the increase in water uptake will generate lower hygroscopic elongation than in the case of isolated molecules.

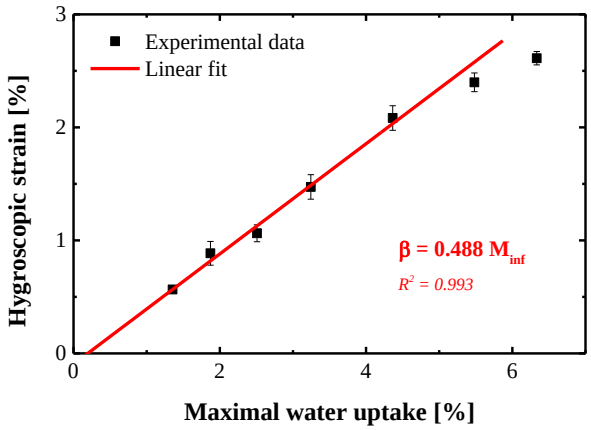

Figure 4.5. Hygroscopic elongation as a function of the water content in the Nylon 6 yarn.

The results of the present study highlight the same trend, with a hygroscopic coefficient (β) equal to 0.488. This linear law is verified up to a 5% water uptake in the fibres, nevertheless

we do not have the threshold value since it appears to be reached for relative humidity lower than 20%RH. Further studies should aim to get the threshold value in the case of polyamide 6 values. Nevertheless, this type of test will require the development of a special test device which can maintain low relative humidities in the range from 0 to 20%RH.

4.2.2. Creep in humid environment

To go further in the investigation of coupled behaviour, we study the simultaneous effect of water exposure and mechanical stress on the yarn material. Water effects are necessarily time dependent, and among time dependent mechanical responses, a study of creep behaviour allows the influence of coupling to be examined while limiting the number of other coupled phenomena such as heat generation.

In the following section, results from a creep study in humid environment on yarns are presented as follows: first, we report and comment on the experimental results. Second, an identification is performed on the different creep results and we show the general trend of water influence on the creep behaviour.

4.2.2.1. Experimental results

The experiment was performed in the same relative humidity device, clamps and DMA equipment as the previous study. The tests were carried out at 25°C and with the same protocol as creep tests at 0%RH (Chapter 3) in order to compare both cases. Three different humidity conditions were studied (20, 40 and 60%RH) and in each case samples were loaded at seven different load levels from 10 to 70 N.

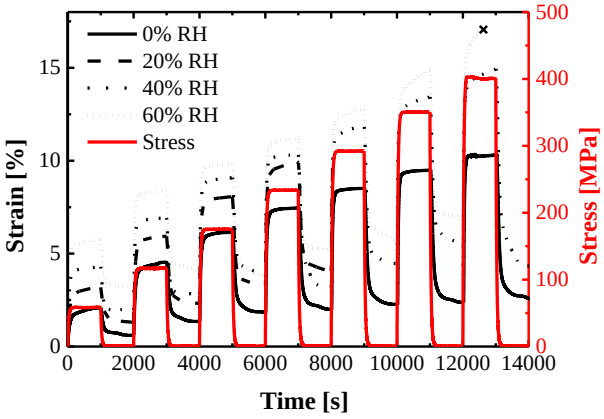

Figure 4.6. Creep tests performed under different humid conditions from 0 to 60%RH.

The creep strain results (Figure 4.6) obtained before identification show the large increase in the initial value and creep rate induced by water uptake. The recovery data show a permanent

elongation increasing with the relative humidity.

These results are as expected: as we observed in section 4.2.1.1, water uptake induces significant plasticization (Tg decrease) and therefore makes the material more ductile.

4.2.2.2. Model identification

In the same way as in Chapter 3, we identified the different visco-plastic and visco-elastic parameters (m, D_p, g_0D_0 and g_2D_1) following Schapery's theory [117]. These quantities are identified for each stress and relative humidity condition (Figure 4.7). Finally, for each environmental condition, we optimize a polynomial law on these parameters in order to be able to predict the strain induced by any loading/unloading sequence and relative humidity exposures.

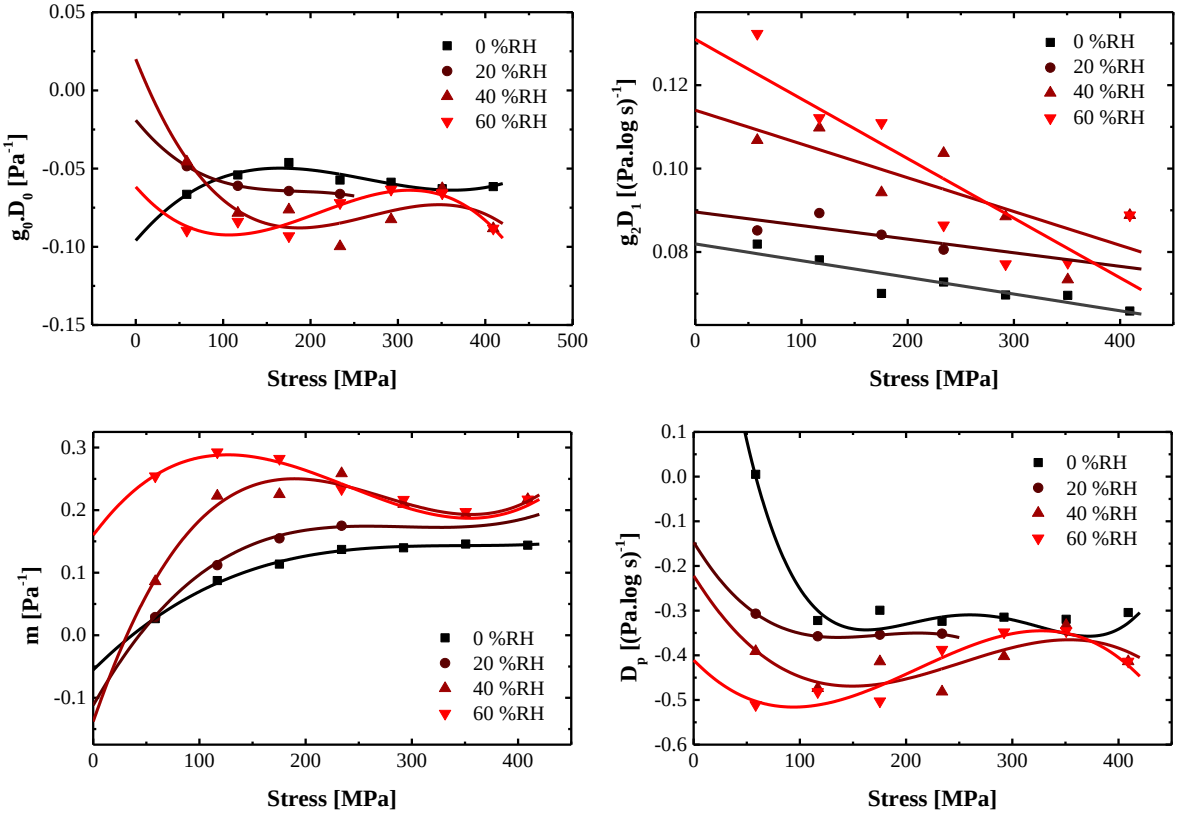

Figure 4.7. Example of identified parameters under different relative humidities.

For each parameter, we identify a law with an optimised polynomial degree which gives a reasonable fit. We obtain a polynomial equation of the first degree for g_2D_1 parameter, the third degree for g_0D_0 and fourth degree for m and D_p. The polynomial laws identified show a clear effect of water uptake on the viscous parameter variation with stress.

In order to better understand the effect of relative humidity on the polynomial coefficients, we report in Figure 4.8 their variations, normalised with respect to their initial value, for each

viscous parameter as a function of the relative humidity. We observe an influence of water diffusion which is quite different for each parameter.

First, the instantaneous compliance (g_0D_0) only shows no significant evolution with stress variation, for any humidity condition (from 0 to 60%RH).

Second, for all humidity conditions the creep rate (g_2D_1) decreases with creep stress increase. Nevertheless, water uptake has a significant influence on the creep rate. First, its initial value increases with the relative humidity. Second, the absolute value of creep strain rate vs. stress slope increases with relative humidity.

Third, the instantaneous plasticity (m) does not highlight a general trend which is easy to identify. If we look to the overall trend, we can only conclude that instantaneous plasticity increases with relative humidity rise.

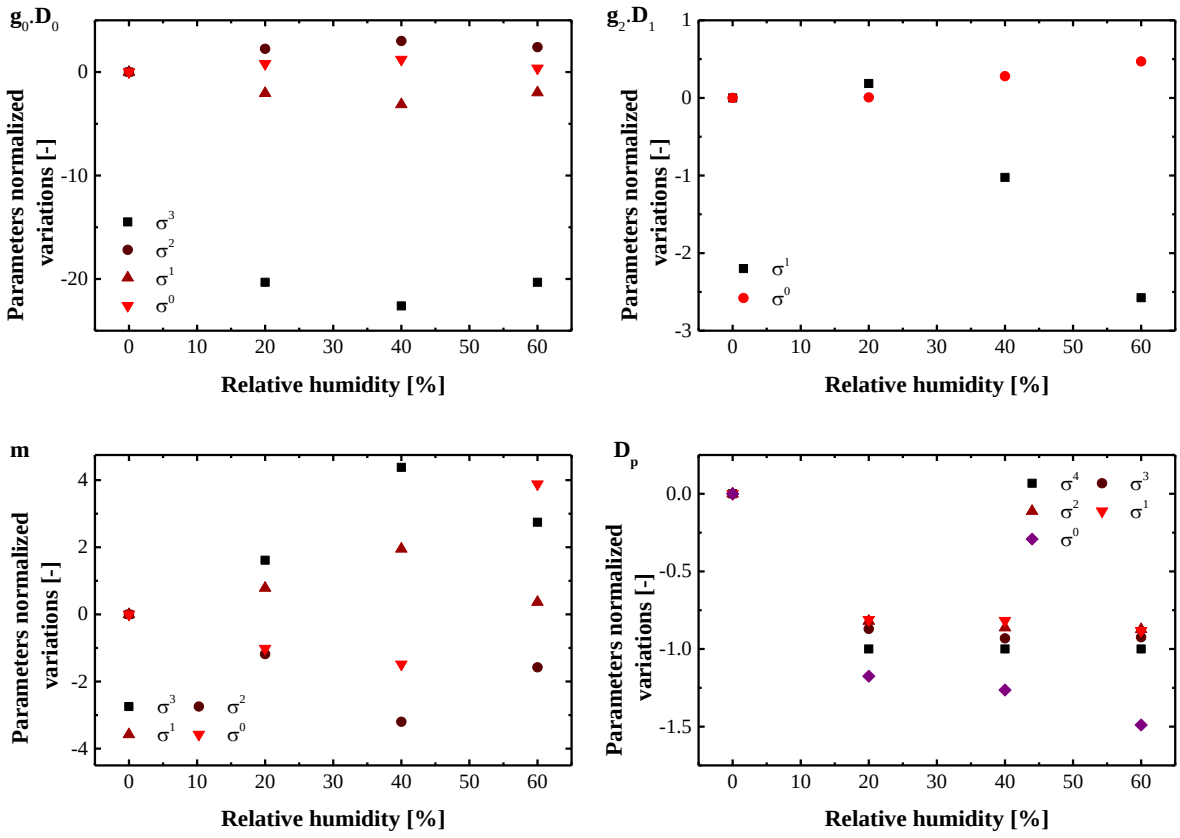

Figure 4.8. Normalised variations of the polynomial coefficients identified on visco-elastic visco-plastic parameters with the relative humidity.

Finally, the plasticity rate (D_p) has polynomial coefficients which tend to decrease with water uptake and stabilise for higher values.

To conclude, a modified version of Schapery's model has been identified on creep/recovery tests performed under different humidity environments. Moreover, by a purely empirical identification of polynomial laws on the viscous parameters, the first elements of a

tool have been developed which should allow the prediction of the strain response induced by any sequence of loading/unloading.

Nevertheless, it is necessary to perform more tests on samples with different loading sequences and humidity conditions in order to validate this approach.

4.2.3. Creep during immersion and discussion

In the previous section the coupled behaviour of yarn stressed in creep under humid conditions was examined. Nevertheless, in real marine applications such as mooring lines the material is fully immersed. Therefore, the next section is devoted to the study of creep behaviour of immersed Nylon 6 yarns .

First the experimental results will be presented, then a simple creep model will be described and the immersion effects will be discussed.

4.2.3.1. Experimental results

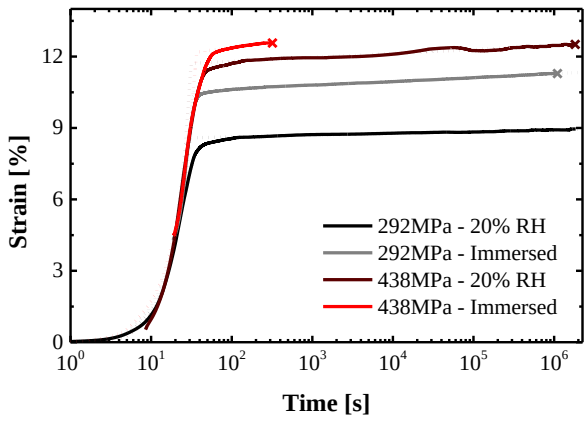

Figure 4.9. Creep strains for Nylon 6 yarns stressed under two different load levels, tested immersed or in a humid environment (crosses represent the failure of specimens).

In the case of immersed tests, we use a different testing device compared to the humid environment tests. Here, the testing devices are horizontal benches. Two versions have been developed; one allows a total immersion of the yarn in tap water at 25°C and another can be introduced in a humid chamber to test samples under 20%RH at 25°C. These devices are fully detailed in Chapter 2.

The results reported in Figure 4.9 show the same kind of creep behaviour in both cases (immersed and humid environment), but with significant variations. Indeed, we can observe an initial strain increased for immersed samples compared to the ones tested in relative humidity. Moreover, we can observe in the second part of the curve (for $t > 10^2$s) a slight

increase of the strain rate value between immersed samples and specimens in humid environment.

These first observations are in agreement with the results from the study of the impact of moisture content increase on the creep strain behaviour in humid environment (4.2.2).

4.2.3.2. Model identification

The testing devices used for these tests do not allow simple unloading of the yarns, as it is necessary to maintain the sample under load to be able to measure strains, therefore the strain was only recorded during creep. For this reason, the full creep-recovery curves, used in section 4.2.2, cannot be identified here. , Therefore here a simple empirical creep model has been identified, Equation 4.5, based on the observation of the results obtained.

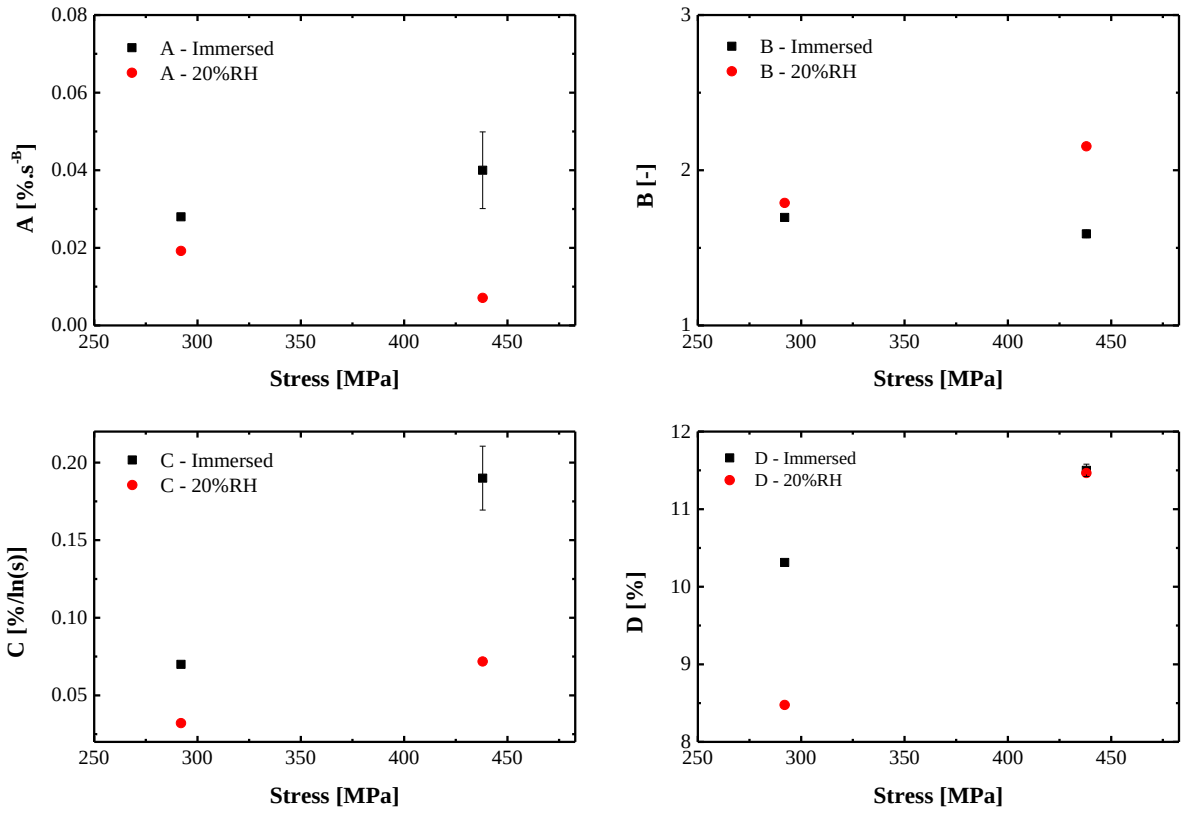

Figure 4.10. Identified parameters of the empirical creep model for polyamide 6 yarns, as a function of stress in immersed and humid environments (20%RH).

Creep tests on polyamide 6 show two regimes: a first one which is quite short (up to t_c seconds) which follows a power law behaviour, and a second which represents the main part of the creep time and which can be modelled by a logarithmic law. The time of the transition between both stages (t_c) is defined as the time when both laws coincide. This latter observation is comparable to the creep strain behaviour observed in section 4.2.2. Therefore,

the creep behaviour is considered to be governed by the set of equations Eq. 4.5. The parameters (A,B,C and D) are then identified on both parts of the curves by a least squares method and the results are reported in Figure 4.10.

$$\begin{cases} \varepsilon(t) = C.\ln(t) + D & for\ 0 < t < t_c \\ \varepsilon(t) = A.t^B & for\ t > t_c \end{cases} \quad \textbf{Eq. 4.5}$$

The parameters identified in Figure 4.10 show good agreement between experimental data and the model in Figure 4.9. Moreover, the parameters identified (Table 4.1) on the first stage of the creep strain curve indicate no significant evolution with stress or environmental conditions variations. Nevertheless the value t_c varies significantly with stress and for immersed samples due to the variation of the second stage of the behaviour. Indeed, we observe two changes in the last part of the creep strain curve. First, the initial strain (*D*) is more important for immersed specimens but increases less with stress rise than in the case of samples exposed to 20% of relative humidity. Second, the strain rate (*C*) is also higher in the immersed case and it increases more with stress when exposed to tap water.

To conclude, immersion has a major impact on the creep strain in the second stage of the behaviour (increase of the rates and initial values). Nevertheless, this study does not give us information on the impact of immersion compared to the exposure to 100% relative humidity. The DMA and humidity chamber could not reach this relative humidity value, so to obtain these data a new device should be designed, in order to install a saturated saline solution in a confined environment.

		292 MPa		**438 MPa**	
		Immersed	20%RH	Immersed	20%RH
Phase I	A [%.s^{-B}]	*0.03*	*0.02*	*0.04*	*0.01*
$\varepsilon = A.t^B$	B [-]	*1.7*	*1.8*	*1.6*	*2.2*
Phase II	C [%/ln(s)]	*0.07*	*0.03*	*0.19*	*0.07*
$\varepsilon = C.\ln(t)+D$	D [%]	*10.3*	*8.5*	*11.5*	*11.5*
Phase III	Time to failure [s]			*6.17E+02*	*1.86E+06*

Table 4.1. Parameters identified using the empirical model for nylon 6 tested immersed and at 20%RH

4.3. Coupled behaviour at the rope level

The previous part of the chapter was focused on the effect of coupling on the fibre material. Now, we investigate water and stress coupled behaviour at the rope level. Therefore, the study considers HMPE (SK78) ropes, in order to understand the impact of water inclusion within the rope structure. First, we focus on the coupled response of ropes tested under quasi-

static loading. Then, we investigate the coupled fatigue behaviour of the same ropes and compare results to the prediction previously introduced in Chapter 3.

4.3.1. Quasi-static behaviour immersed

The study of coupled effects on the rope structure starts with immersed quasi static tensile tests. This section aims to understand the possible impact of water insertion in the structure on short term mechanical tests.

First, we present the experimental results obtained with this type of tests. Second, we discuss the possible phenomena involved during these mechanical experiments.

4.3.1.1. Experimental results

The quasi-static tests on rope samples while immersed were performed on the testing device used for immersed tension fatigue presented in Chapter 2. All the samples tested were immersed 24 hours before the experiment. This exposure time induces a water uptake in the structure around 10% in weight, which corresponds to the beginning of the second stage of water diffusion in the rope (Chapter 3). In order to avoid any side effects due to the modification of the quasi-static testing method, we performed tests on dry samples at the same time to have a reference curve.

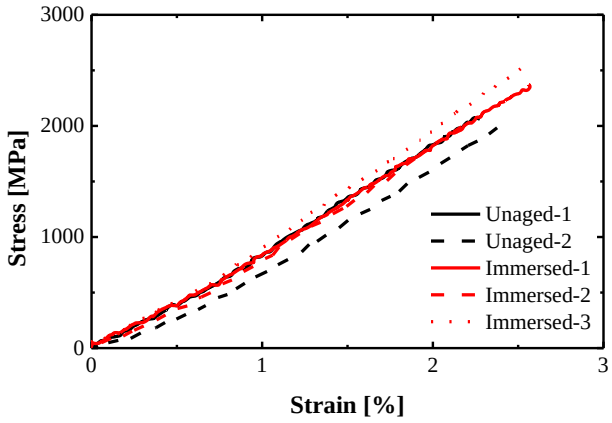

Figure 4.11. Stress/strain curve for quasi-static tensile tests on unaged and immersed SK78 ropes.

The results obtained from these tests are reported in Figure 4.11 and the mechanical constants identified are given in Table 4.2. From these we observe two trends, first initial modulus and breaking strain remain unchanged by immersion (the variations are within the standard deviation). Second, the break stress increases slightly when samples are tested while immersed.

4.3.1.2. Discussion

If we compare the results obtained here with those in Chapter 3, we can note some divergences. The previous study showed a decrease in the initial modulus and an increase of the strain at failure after immersion, while the results of this section show only a slight increase in failure stress when samples are tested immersed.

After immersion, the change in mechanical behaviour was explained by lubrication effects in the structure. In the case of the quasi-static tests immersed here, friction will be reduced in the same way as for the semi-coupled tests (Chapter 3). Nevertheless, in the fully coupled immersion test, we can postulate that the water in the surrounding environment will constrain the water inside the structure (unlike in air). Therefore when a stress is applied, some water remains inside the rope and allows the fibres to reorient less than in the previous cases. This mechanism would result in a modulus and a break strain rise.

		Modulus [GPa]	Break Stress [GPa]	Break Strain [%]
Unaged	Average	90.0	2.1	2.4
	Standard deviation	*5.3*	*0.0*	*0.1*
Immersed	Average	94.8	2.3	2.4
	Standard deviation	*5.6*	*0.1*	*0.2*

Table 4.2. Tensile mechanical constants for SK78 ropes tested unaged and immersed at 25°C.

For further study, it would be interesting to examine the friction in more detail, and especially the influence of water on this parameter. Nevertheless, it is hard to perform representative tests of this phenomenon inside the rope (short relative displacement and high compaction forces). One option might be to study alternative fibre grades with low friction coatings, such as the XBO coating from DSM.

4.3.2. Dynamic fatigue behaviour immersed

As previously mentioned in Chapter 3, the creep behaviour of SK78 yarn has been well studied, moreover the section 4.3.1 showed no significant changes in the static mechanical response of ropes tested immersed. Therefore, the final step of this coupled study is focused on the effects of dynamic tensile stress combined with immersion.

As in the previous section, first we present the experimental results obtained and then discuss the phenomena which could explain them.

4.3.2.1. Experimental results

For this investigation, another special testing device has been developed (detailed in

Chapter 2) in order to load immersed ropes in fatigue at 35°C in tap water. All the samples were immersed in water 24 hours before testing, in order to reach 10% of water content by weight. They were tested at a loading frequency of 0.1 Hz, with an R-ratio of 0.1. We compare the results obtained to the predictions presented in Chapter 3, considering or not the heating process inside the rope.

The times-to failure obtained under such conditions are reported on Figure 4.12. The first point to notice is that specimens tested while immersed (red points) last much longer than the predicted failure made from the model established in air (black solid line: prediction with heating). Moreover, we can still see a deviation from the curve at very high maximum stresses (over 1200MPa), which represents an extreme case not encountered in practice.

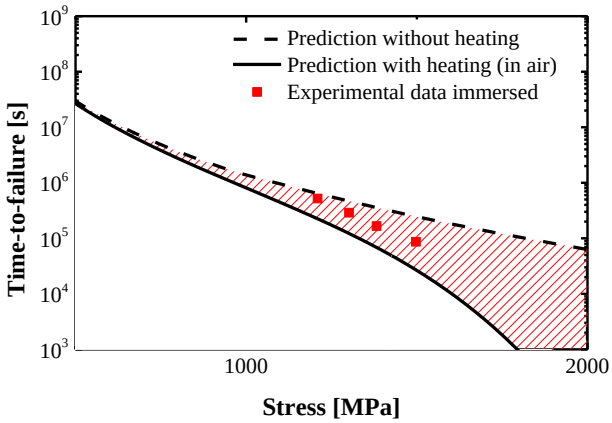

Figure 4.12. Time-to failure vs. stress for immersed ropes stressed in tension fatigue, compared to both prediction laws presented in Chapter 3.

4.3.2.2. Discussion

Deviation from the curve for high stresses seems to follow the same trend as the prediction with heating translated along the stress axis. Therefore, there could still be some heating phenomena which create a deviation from the prediction without considering heating.

In order to estimate the theoretical temperature rise in the rope from the time-to-failure results, we use the prediction equation from Chapter 3 reported as Eq. 3.9. here.

Then, we associate the first temperature (T_1) to the water temperature (T_w = 35°C) and the second one to the temperature inside the rope (T_r). Finally the equation Eq. 3.9. is transformed in order to express T_r as a function of time-to failure from prediction without heating ($tt_{fd}(T_w)$), time to failure measured experimentally ($tt_{fd}(T_r)$) and T_w (Eq. 4.7). The maximum temperature reached inside the rope determined by theory is reported in Figure 4.13 [right] (black points).

$$tt_{fd}(T_1) = tt_{fd}(T_2)e^{\frac{\Delta U}{R_g}\left(\frac{1}{T_1}-\frac{1}{T_2}\right)} \quad \text{Eq. 4.6}$$

$$T_r = \frac{T_w.\Delta U}{\Delta U + T_w.R_g.\ln\left(\frac{tt_{fd}(T_r)}{tt_{fd}(T_w)}\right)} \quad \text{Eq. 4.7}$$

In addition, we have performed measurements with a thermocouple (in the same way as in Chapter 3) to determine the temperature rise inside the structure. The results reported in Figure 4.13 show a good correlation between experimental measurements and the prediction method used.

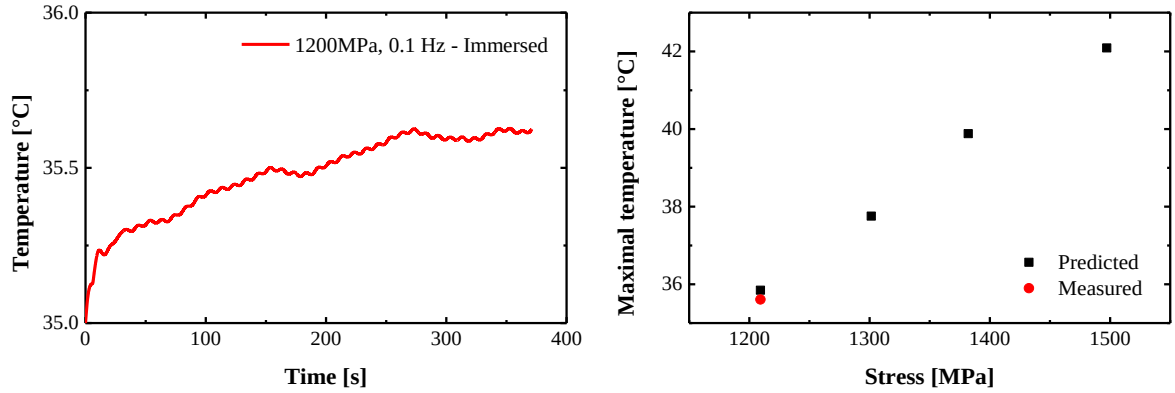

Figure 4.13. Temperature rise measurements during a fatigue test while immersed (1200MPa, R=0.1 and 0.1Hz) [left] and comparison between measured and predicted maximal temperature inside the rope [right].

The results obtained indicate times-to-failure which are increased by immersion. This phenomenon is the result of a reduced temperature rise, which is much lower in the case of immersion due to better heat dissipation. Moreover, additional measurements should be performed in order to verify the prediction of heating inside the rope for high stresses. This will be of particular importance when we consider the large diameter ropes used offshore.

4.4. Conclusion

The aim of this chapter was to understand if coupled behaviours need to be studied to understand the phenomena involved during real life applications of fibres and ropes. To achieve this goal, we developed specific testing devices to perform experiments on yarns and ropes in coupled configurations. The results obtained from these tests were compared to uncoupled and semi-coupled behaviours, to highlight the necessity or not to perform such experiments

For Nylon 6, we focused on two aspects of the coupling: one can be called “passive” and the other “standard”. For the passive coupling, we investigated the influence of water

uptake in polyamide fibre on its internal mechanical state. Two quantities can be used to evaluate this type of phenomenon: the glass transition temperature and the hygroscopic elongation. Both parameters show an important impact of water uptake (in relative humidity environments) on their values. Moreover in both cases, we were able to establish laws to predict their variations with the humidity conditions: Using the Sihma-Boyer theory for Tg, and through a linear dependence for the hygroscopic expansion β with humid conditions (up to 5% of water uptake).

The second section, focused on the fibre scale level, investigated the coupled effect of tensile creep stress combined with water diffusion. This part of the study also revealed an important modification of the creep strain response due to water uptake in the material both in humid environments and immersed. In this case, we identified a creep model based on Schapery's theory and by interpolating the variations in the parameters with stress we established an empirical prediction law for each humidity condition.

Moreover, at the fibre level, water diffusion appeared to be almost instantaneous compared to handling and testing times (Chapter 3). Therefore, all the previous variations could only be observed during fully coupled testing, otherwise the material will be desorbed instantaneously.

To go further in the investigation of coupled effects on the fibre material, tests should be performed in immersed conditions, with the same protocol as for humid environment tests.

The study at the rope level was organised around two aspects: first, the impact of water immersion on tensile quasi-static behaviour and second, its effects on the dynamic tension response. Quasi-static tests were performed in tap water and no significant variations were noted compared with the results in 50%RH air. The quasi-static coupled tests show differences compared with the semi-coupled case (Chapter 3) which indicated a slight decrease in modulus and an increase in failure strain.

Moreover, the investigation of coupled effects in the case of dynamic loading showed significant divergences compared with the uncoupled results. These deviations can be explained by the heat dissipation, which is reduced by water immersion. For this reason the times-to-failure observed during coupled cases are longer than when ropes are tested in ambient air. Additional experiments could be performed at higher loads in order to verify the hypothesis of lower heating inside the rope when immersed.

In this part, the semi-coupled effects were not studied due to the long testing times (more than 24h) compared to the diffusion characteristic time in ropes (see Chapter 3).

Finally, coupled studies at both scales, fibre and rope, highlight differences between

uncoupled, semi-coupled and coupled behaviour. Therefore, further investigations for marine ropes applications should be performed as coupled tests whenever possible, in order to avoid unexpected behaviour in service.

General conclusion

The aim of the study was to understand the impact of coupling on water diffusion and mechanical behaviour on marine structures. Moreover, we intended to identify the key phenomena involved during this type of application. We can distinguish two types of materials used: one for the structure, floating or underwater and another for mooring systems. The highest performance materials for marine structures appear to be composites, while the most effective anchor lines are made with synthetic fibre ropes. Therefore, we decided to investigate both materials with the same approach: first examining the properties when uncoupled, second, as semi-coupled behaviours and finally as one coupled phenomenon.

The first part of the document is focused on the study of composite materials, and investigates two types of coupling: tension loading and hydrostatic pressure loading of immersed materials. For both loading types there is a significant influence of coupling on the water diffusion behaviour.

First, gravimetric measurements of composite samples immersed and stressed under tension highlight an acceleration of the water diffusion's kinetic. This water diffusion increase is more important and appears sooner when the composite matrix is highly stressed (e.g. in a ±45° configuration).

Second, for specimens stressed under hydrostatic pressure the water diffusion behaviour reveals differences compared with the reference (diffusion under atmospheric pressure) only for composites produced with a hand-lay up process. For these materials there is a large acceleration of the weight gain kinetics for high pressure and a saturation plateau for samples loaded at pressures below 5 bar.

This modification of moisture uptake under stress appears to be induced by the inclusion of water inside either existing defects or damage. In the case of tension stress, it is the damage which increases with the applied stress, and therefore the water diffusion increases at the same time. For hydrostatic pressure loading, the presence of defects (voids) in the composites can modify the water diffusion when the pressure rises: water will be constrained to fill the porosity. Tests on samples without porosity confirmed this hypothesis. Therefore in both cases the inclusion of free space within the composite (defects or cracks) induces modification of the moisture diffusion.

In order to better understand this phenomenon a model has been developed, based on representing the moisture diffusion with a Fickian law combined with a sink term representing the defects. This type of model appears to show good correlation with the experimental data.

In all these cases, water included inside voids will not directly impact the mechanical

behaviour of the materials. However, the weight increase it generates can be critical in some applications where the buoyancy of the structure is crucial. Moreover in the case of fatigue loading, the water included inside voids during the unloading can accelerate the crack propagation inside the material [26]. Therefore, further work on these subjects should be oriented to explore these two aspects.

The second part of the work was dedicated to coupling effects in synthetic fibres. The hierarchical construction of ropes led us to consider the two scales: yarn and rope, in separated sections. In order to better understand the effect of water on each scale we focused the study on a hydrophilic fibre for yarns to examine the moisture impact on the material, and on a hydrophobic fibre for ropes to highlight the effects of water in the rope structure.

At the yarn scale the mechanical behaviour only showed differences when the hydrophilic specimens were tested coupled, while results for semi-coupled and uncoupled tests remained identical. This phenomenon is the result of very fast diffusion kinetics in these fibres, indeed, when the samples are tested semi-coupled de-sorption is almost completed at the end of the test. Therefore the results obtained will be comparable to the uncoupled case. On the other hand in the case of coupled tests performed on yarn samples we observed modification of the behaviour only for hydrophilic material (Nylon 6). Therefore, the exposure of yarns to humidity only impacts the properties of the polymer fibres.

By identification of the experimental data with an empirical model we quantified the impact of water uptake on the yarns' creep response. This analysis allowed an increase of the initial (instantaneous deformation) and of the creep rate to be identified when the water content increases. In order to pursue this investigation, the variation of both parameters with water uptake should be studied in order to quantify the impact of moisture on the yarn behaviour.

At the rope scale, the study was exclusively focused on hydrophobic materials (HMPE) in order to understand the effect of water within the rope construction. In this case the differences between results from semi-coupled and uncoupled mechanical tests are not significant. However, the results obtained in coupled tests show a significant divergence from the previous tests. Indeed, when the ropes were tested under cyclic tension in water, their life time increased for high loads compared to the uncoupled case. The temperature inside the rope during cycling is significantly lower in the case of immersed samples. These heating and lifetime differences can be explained by the lubrication and heat dissipation effects of water included in the structure.

A viscoplastic model was developed to predict the fatigue life time of these ropes. This is

based on parameters identified at the yarn level and original fatigue tests were developed to validate it. This theory appears to be well adapted to the material and rope construction studied provided we take into account the heating process inside the material. Further study should be devoted to establishing a proper link between both: heating process and time to failure in the case of immersed ropes in order to verify the hypotheses made.

Both parts of this work highlight important modifications to the behaviour when the samples are stressed in a coupled configuration. The study on composite materials reveals a clear modification of their diffusive behaviour, while the investigation on ropes shows modification of the mechanical behaviour when they are subjected to coupled stresses. In the case of composite materials, the presence of free space, whether due to manufacturing defects or damage, appears to be the most significant parameter affecting the moisture uptake behaviour under load. For the fibre materials there is a strong influence of internal heating on their mechanical behaviour.

It is clear from the results of this study that while knowledge of uncoupled and semi-coupled behaviours is important to define the reference of material responses, nevertheless this is insufficient to dimension offshore structures, vessels or moorings with confidence. In all the cases some coupled tests should be performed in order to quantify the transposition from semi-coupled or uncoupled behaviour to the coupled case.

Finally this study has established and verified some hypotheses about the origin of the differences between uncoupled, semi-coupled and coupled behaviours. And for the case of hydrostatic pressure a model was developed which can predict the diffusive behaviour of composites as a function of the defects present.

Nevertheless, the study only establishes the bases of coupled behaviour, and highlights the lack of knowledge on this subject. We are now in a position to propose ideas for further studies which could provide a better understanding of this phenomenon.

First, we should perform further tests, in order to get additional experimental data following the method developed in this study. For example some additional creep tests on composites under static tension in both air and water could provide the full evolution of the water diffusion with stress variation, and allow creep effects to be separated from those introduced by water. We should increase the number of creep tests on immersed yarns, in order to relate the yarn’s creep to the water content in the material. And finally, some additional tests to

record temperature rise inside immersed ropes during fatigue loading could validate or not the assumption of reduced heating mechanisms when the fibres are surrounded by water. The application of efficient numerical tools to simulate braided ropes (e.g. [102]) would be very beneficial in improving our understanding of these mechanisms.

Second, it would be interesting in a future study to continue to develop the generic nature of these phenomena by transposing methods for one material (rope or composite) to the other, in order to clarify the resemblances and differences between them. As an example the diffusion model with a sink term can be applied to water diffusion in ropes and compared with the experimental data obtained in the present study. In this case the sink term could be associated to the gaps between yarns in the construction, gaps which vary with the stress or pre-stress applied on the rope. In the same way this type of model can be used for water diffusion inside composites stressed under static tension. For this application the model should be modified in order to introduce a damage ratio, which can vary with the time.

And finally, it would be interesting to get more information on the impact of coupling effects on the materials' behaviour. For example, some accurate strain measurements could be performed on immersed composites under tensile stress in order to understand the mechanical behaviour during the coupling. In a similar way, the hydrostatic pressure tests could be made in a transparent pressure vessel (e.g. [159]) to get quantify strain variation induced by pressure using image analysis. Both types of information could be useful to improve the model developed for coupling, by adding a mechanical component. For fibre rope materials some more precise gravimetric measurements could be performed on samples after different loading cycles in order to understand their effects on the water diffusion in the rope structure. Ultimately, uncoupled, semi-coupled and coupled tests could be performed on more complex nylon ropes in order to include water diffusion both in their construction and in the fibres.

In summary, the present work has highlighted the divergences between uncoupled, semi-coupled and coupled behaviours for two of the main types of materials used for marine and offshore structures: The need to perform coupled tests to dimension such systems has been fully justified.

Moreover, this study proposes an important number of hypotheses to explain these differences when we test such materials under coupled conditions. Additional studies should be performed on other type or composites and fibre materials in order to extend the data base on coupled behaviour.

References

[1] T. M. Bourgeois, D. G. Godfrey, and M. J. Bailey, “Race on for deepwater acreage, 3500-meter depth capability,” *Offshore*, vol. 58, no. 10, pp. 40–41, 1998.

[2] B. B. Bernstein, “Decision framework for platform decommissioning in California,” *Integr. Environ. Assess. Manag.*, vol. 11, no. 4, pp. 542–553, 2015.

[3] J. Chianis and P. Poll, “Studies clear TLP cost, depth limit misconceptions,” *Offshore*, pp. 42–44, 1997.

[4] J. W. Chianis and P. B. Poll, “New concepts extend dry-tree production into deeper water,” *Oil Gas J.*, vol. 97, no. 18, 1999.

[5] N. Le Bozec, “Réaction de réduction de l’oxygène sur les aciers inoxydables en eau de mer naturelle. Influence du biofilm sur les processus de corrosion,” PhD thesis, Université de Bretagne Occidentale, 2000.

[6] D. Féron, “Comportement des aciers en environnement naturel : cas des aciers inoxydables en eau de mer,” *Matér. Tech.*, vol. 93, p. s.43-s.58, 2005.

[7] J.-L. Crolet and G. Beranger, “Corrosion en milieu aqueux des métaux et alliages,” *Tech. Ing. Matér. Métalliques*, vol. MB3, no. M150, p. M150.1-M150.21, 1998.

[8] D. Melot, “Present and Future Composites Requirements for the Offshore Oil and Gas Industry,” in *Durability of Composites in a Marine Environment 2*, Springer, Cham, 2018, pp. 151–172.

[9] R. Thomas *et al.*, “Miscibility, morphology, thermal, and mechanical properties of a DGEBA based epoxy resin toughened with a liquid rubber,” *Polymer*, vol. 49, no. 1, pp. 278–294, Jan. 2008.

[10] Grafil Inc., “Property of TR50S-12K Carbon fiber.pdf,” 2008. [Online]. Available: https://www.rockwestcomposites.com/downloads/TR50S-12K-14002-Fiber_(07-2008).pdf. [Accessed: 18-Sep-2017].

[11] D. Roylance, “Laminated composite plates,” *Mass. Inst. Technol. Camb.*, 2000.

[12] S. Barré and M. L. Benzeggagh, “On the use of acoustic emission to investigate damage mechanisms in glass-fibre-reinforced polypropylene,” *Compos. Sci. Technol.*, vol. 52, no. 3, pp. 369–376, Jan. 1994.

[13] S. Huguet, N. Godin, R. Gaertner, L. Salmon, and D. Villard, “Use of acoustic emission to identify damage modes in glass fibre reinforced polyester,” *Compos. Sci. Technol.*, vol. 62, no. 10–11, pp. 1433–1444, Aug. 2002.

[14] P. J. Schilling, B. R. Karedla, A. K. Tatiparthi, M. A. Verges, and P. D. Herrington, “X-ray computed microtomography of internal damage in fiber reinforced polymer matrix composites,” *Compos. Sci. Technol.*, vol. 65, no. 14, pp. 2071–2078, Nov. 2005.

[15] F. Awaja, M.-T. Nguyen, S. Zhang, and B. Arhatari, “The investigation of inner structural damage of UV and heat degraded polymer composites using X-ray micro CT,” *Compos. Part Appl. Sci. Manuf.*, vol. 42, no. 4, pp. 408–418, Apr. 2011.

[16] P. Wright, X. Fu, I. Sinclair, and S. M. Spearing, “Ultra High Resolution Computed Tomography of Damage in Notched Carbon Fiber—Epoxy Composites,” *J. Compos. Mater.*, vol. 42, no. 19, pp. 1993–2002, Oct. 2008.

[17] N. Tual, N. Carrere, P. Davies, T. Bonnemains, and E. Lolive, “Characterization of sea water ageing effects on mechanical properties of carbon/epoxy composites for tidal turbine blades,” *Compos. Part Appl. Sci. Manuf.*, vol. 78, pp. 380–389, Nov. 2015.

[18] A. Parvizi and J. E. Bailey, “On multiple transverse cracking in glass fibre epoxy cross-ply laminates,” *J. Mater. Sci.*, vol. 13, no. 10, pp. 2131–2136, Oct. 1978.
[19] B. Dewimille and A. R. Bunsell, “Vieillissement hygrothermique d’un matériau composite fibres de verre–résine époxyde,” *Thesis Ecole Mines Paris*, 1981.
[20] I. Ghorbel, *Mécanismes d’endommagement des tubes verre-resine pour le transport d’eau chaude : influence de la ductilité de la matrice*. Paris, Ecole nationale supèrieure des mines, 1990.
[21] E. Morel, V. Bellenger, and J. Verdu, “Relations Structure-Hydrophilie des Réticulats Epoxyde-Amine,” presented at the JNC, Paris, 1984, pp. 598–614.
[22] J. Zhou and J. P. Lucas, “Hygrothermal effects of epoxy resin. Part I: the nature of water in epoxy,” *Polymer*, vol. 40, no. 20, pp. 5505–5512, Sep. 1999.
[23] J. B. J. baron Fourier, *Théorie analytique de la chaleur*. Chez Firmin Didot, père et fils, 1822.
[24] D. A. Fick, “V. On liquid diffusion,” *Philos. Mag. Ser. 4*, vol. 10, no. 63, pp. 30–39, juillet 1855.
[25] J. Crank, *The mathematics of diffusion*, 2d ed. Oxford, [Eng]: Clarendon Press, 1975.
[26] Y. Weitsman, *Moisture in composites: sorption and damage*. Elsevier Science Publishers BV, 1991.
[27] F. Pierron, Y. Poirette, and A. Vautrin, “A Novel Procedure for Identification of 3D Moisture Diffusion Parameters on Thick Composites: Theory, Validation and Experimental Results,” *J. Compos. Mater.*, vol. 36, no. 19, pp. 2219–2243, Oct. 2002.
[28] A. C. Loos and G. S. Springer, “Moisture Absorption of Graphite-Epoxy Composites Immersed in Liquids and in Humid Air,” *J. Compos. Mater.*, vol. 13, no. 2, pp. 131–147, Apr. 1979.
[29] G. Copin-Montégut, *Chimie de l’eau de mer*. Institut océanographique, 1996.
[30] H. R. Dana, A. Perronnet, S. Fréour, P. Casari, and F. Jacquemin, “Identification of moisture diffusion parameters in organic matrix composites,” *J. Compos. Mater.*, vol. 47, no. 9, pp. 1081–1092, Apr. 2013.
[31] H. T. Hahn and S. W. Tsai, *Introduction to composite materials*. CRC Press, 1980.
[32] D. Gueribiz, M. Rahmani, F. Jacquemin, S. Fréour, R. Guillen, and K. Loucif, “Homogenization of Moisture Diffusing Behavior of Composite Materials with Impermeable or Permeable Fibers — Application to Porous Composite Materials,” *J. Compos. Mater.*, vol. 43, no. 12, pp. 1391–1408, Jun. 2009.
[33] C.-H. Shen and G. S. Springer, “Moisture Absorption and Desorption of Composite Materials,” *J. Compos. Mater.*, vol. 10, no. 1, pp. 2–20, Jan. 1976.
[34] G. S. Springer and S. W. Tsai, “Thermal Conductivities of Unidirectional Materials,” *J. Compos. Mater.*, vol. 1, no. 2, pp. 166–173, Apr. 1967.
[35] C. D. Shirrell and J. Halpin, “Moisture absorption and desorption in epoxy composite laminates,” *ASTM Spec. Tech. Publ.*, no. 617, pp. 514–528, 1977.
[36] L. R. S. R.S, “XIX. On the instability of cylindrical fluid surfaces,” *Philos. Mag. Ser. 5*, vol. 34, no. 207, pp. 177–180, Aug. 1892.
[37] J. Verdu, *Action de L’eau Sur les Plastiques*. Ed. Techniques Ingénieur, 2000.
[38] B. De’Nève and M. E. R. Shanahan, “Water absorption by an epoxy resin and its effect on the mechanical properties and infra-red spectra,” *Polymer*, vol. 34, no. 24, pp. 5099–5105, Dec. 1993.
[39] Y. Weitsman, “Coupled damage and moisture-transport in fiber-reinforced, polymeric composites,” *Int. J. Solids Struct.*, vol. 23, no. 7, pp. 1003–1025, 1987.
[40] K. Derrien and P. Gilormini, “The effect of moisture-induced swelling on the absorption capacity of transversely isotropic elastic polymer–matrix composites,” *Int. J. Solids Struct.*, vol. 46, no. 6, pp. 1547–1553, Mar. 2009.

[41] A.-L. Durier, “Contribution à l’étude de l’interaction contraintes-diffusion dans les polymères,” PhD thesis, Arts et Métiers ParisTech, 2008.
[42] G. Youssef, “Couplage diffusion d’humidité / contraintes internes dans les matériaux composites,” PhD thesis, Université de Nantes, 2009.
[43] G. Youssef, S. Freour, and F. Jacquemin, “Stress-Dependent Moisture Diffusion in Composite Materials,” *J. Compos. Mater.*, Jun. 2009.
[44] A. A. Fahmy and J. C. Hurt, “Stress dependence of water diffusion in epoxy resin,” *Polym. Compos.*, vol. 1, no. 2, pp. 77–80, décembre 1980.
[45] S. Neumann and G. Marom, “Free-volume dependent moisture diffusion under stress in composite materials,” *J. Mater. Sci.*, vol. 21, no. 1, pp. 26–30, Jan. 1986.
[46] S. Roy, W. Xu, S. Patel, and S. Case, “Modeling of moisture diffusion in the presence of bi-axial damage in polymer matrix composite laminates,” *Int. J. Solids Struct.*, vol. 38, no. 42–43, pp. 7627–7641, Oct. 2001.
[47] S. Roy and W. Xu, “Modeling of diffusion in the presence of damage in polymer matrix composites,” *Int. J. Solids Struct.*, vol. 38, no. 1, pp. 115–126, Jan. 2001.
[48] C. Suri and D. Perreux, “The effects of mechanical damage in a glass fibre/epoxy composite on the absorption rate,” *Compos. Eng.*, vol. 5, no. 4, pp. 415–424, Jan. 1995.
[49] D. Perreux and F. Thiebaud, “Damaged elasto-plastic behaviour of [+ϑ,-ϑ] n fibre-reinforced composite laminates in biaxial loading,” *Compos. Sci. Technol.*, vol. 54, no. 3, pp. 275–285, 1995.
[50] D. Perreux and C. Suri, “A study of the coupling between the phenomena of water absorption and damage in glass/epoxy composite pipes,” *Compos. Sci. Technol.*, vol. 57, no. 9, pp. 1403–1413, Jan. 1997.
[51] D. Perreux and C. Oytana, “Continuum damage mechanics for microcracked composites,” *Compos. Eng.*, vol. 3, no. 2, pp. 115–122, 1993.
[52] J.-E. Lundgren and P. Gudmundson, “A Model for Moisture Absorption in Cross-Ply Composite Laminates with Matrix Cracks,” *J. Compos. Mater.*, vol. 32, no. 24, pp. 2226–2253, Dec. 1998.
[53] J.-E. Lundgren and P. Gudmundson, “Moisture absorption in glass-fibre/epoxy laminates with transverse matrix cracks,” *Compos. Sci. Technol.*, vol. 59, no. 13, pp. 1983–1991, Oct. 1999.
[54] Y. J. Weitsman, *Fluid Effects in Polymers and Polymeric Composites*. Springer Science & Business Media, 2011.
[55] Y. Weitsman and M. Henson, “Stress Effects on Moisture Transport in an Epoxy Resin and Its Composite.,” DTIC Document, 1986.
[56] A. Siriruk and D. Penumadu, “Degradation in fatigue behavior of carbon fiber–vinyl ester based composites due to sea environment,” *Compos. Part B Eng.*, vol. 61, pp. 94–98, May 2014.
[57] F. R. Jones, “Durability of reinforced plastics in liquid environments,” in *Reinforced Plastics Durability*, G. Pritchard, Ed. CRC Press, 1999, pp. 70–110.
[58] T. J. Searle and J. Summerscales, “Review of the durability of marine laminates,” in *Reinforced Plastics Durability*, G. Pritchard, Ed. CRC Press, 1999, pp. 219–266.
[59] J. D. Garcia-Espinel, D. Castro-Fresno, P. Parbole Gayo, and F. Ballester-Muñoz, “Effects of sea water environment on glass fiber reinforced plastic materials used for marine civil engineering constructions,” *Mater. Des.*, vol. 66, Part A, pp. 46–50, Feb. 2015.
[60] A. Hawa *et al.*, “Burst strength and impact behaviour of hydrothermally aged glass fibre/epoxy composite pipes,” *Mater. Des.*, vol. 89, pp. 455–464, Jan. 2016.
[61] Y. Zhong and S. C. Joshi, “Impact behavior and damage characteristics of hygrothermally conditioned carbon epoxy composite laminates,” *Mater. Des.*, vol. 65,

pp. 254–264, Jan. 2015.
[62] M. Assarar, D. Scida, A. El Mahi, C. Poilâne, and R. Ayad, “Influence of water ageing on mechanical properties and damage events of two reinforced composite materials: Flax–fibres and glass–fibres,” *Mater. Des.*, vol. 32, no. 2, pp. 788–795, Feb. 2011.
[63] K. Berketis, D. Tzetzis, and P. J. Hogg, “The influence of long term water immersion ageing on impact damage behaviour and residual compression strength of glass fibre reinforced polymer (GFRP),” *Mater. Des.*, vol. 29, no. 7, pp. 1300–1310, 2008.
[64] P. Davies, D. Choqueuse, and F. Mazéas, “Composites Underwater,” presented at the DURACOSYS conference, Progress in Durability Analysis of Composites Systems, Rotterdam, 1997, pp. 19–24.
[65] A. Avena and A. R. Bunsell, “Effect of hydrostatic pressure on the water absorption of glass fibre-reinforced epoxy resin,” *Composites*, vol. 19, no. 5, pp. 355–357, Sep. 1988.
[66] B. E. Sar, S. Fréour, P. Davies, and F. Jacquemin, “Coupling moisture diffusion and internal mechanical states in polymers – A thermodynamical approach,” *Eur. J. Mech. - ASolids*, vol. 36, pp. 38–43, Nov. 2012.
[67] A. Pollard, R. Baggott, G. H. Wostenholm, B. Yates, and A. P. George, “Influence of hydrostatic pressure on the moisture absorption of glass fibre-reinforced polyester,” *J. Mater. Sci.*, vol. 24, no. 5, pp. 1665–1669, May 1989.
[68] G. Whitaker *et al.*, “Influence of temperature and hydrostatic pressure on moisture absorption in polymer resins,” *J. Mater. Sci.*, vol. 26, no. 1, pp. 49–55, Jan. 1991.
[69] D. O. Adams and D. F. Adams, “Tabbing Guide for Composite Test Specimens,” Oct. 2002.
[70] D. ASTM, “D638-14, Standard Test Method for Tensile Properties of Plastics,” *Annu. Book ASTM Stand.*, vol. 08.01, p. 01, 2014.
[71] A. Standard and others, “Standard test method for tensile properties of polymer matrix composite materials,” *ASTM D3039D 3039M*, 2008.
[72] D20 Committee, “Test Methods for Flexural Properties of Unreinforced and Reinforced Plastics and Electrical Insulating Materials,” ASTM International, 2010.
[73] D30 Committee, “D2344: Test Method for Short-Beam Strength of Polymer Matrix Composite Materials and Their Laminates,” ASTM International, 2013.
[74] *Norme NF EN ISO 7822: Septembre 1999 T57-109, Plastiques renforcés de verre textile : Détermination de la teneur en vide : Méthodes par perte au feu, par désintégration mécanique et par comptage statistique*. Saint-Denis La Plaine, France: AFNOR, 1999.
[75] N. Tual, “Durabilité des composites carbone/époxy pour applications pales d’hydroliennes,” 2015. .
[76] M. Fichera and L. A. Carlsson, “Moisture transport in unidirectional carbon/vinylester panels with imperfect fiber/matrix interface,” *J. Compos. Mater.*, vol. 50, no. 6, pp. 751–760, Mar. 2016.
[77] C. C. López *et al.*, “Effect of porosity and hydrostatic pressure on water absorption in a semicrystalline fluoropolymer,” *J. Mater. Sci.*, vol. 51, no. 8, pp. 3750–3761, Apr. 2016.
[78] H. K. Reimschuessel, “Relationships on the effect of water on glass transition temperature and young’s modulus of nylon 6,” *J. Polym. Sci. Polym. Chem. Ed.*, vol. 16, no. 6, pp. 1229–1236, Jun. 1978.
[79] S. L. Phoenix, P. Schwartz, and H. H. Robinson, “Statistics for the strength and lifetime in creep-rupture of model carbon/epoxy composites,” *Compos. Sci. Technol.*, vol. 32, no. 2, pp. 81–120, Jan. 1988.
[80] E. M. Filyanov, O. G. Tarakanov, and I. V. Shamov, “Effect of hydrostatic pressure on the water absorption of epoxy polymers,” *Polym. Mech.*, vol. 10, no. 1, pp. 136–138, Jan. 1974.

[81] H. S. da Costa Mattos and F. E. G. Chimisso, “Modelling creep tests in HMPE fibres used in ultra-deep-sea mooring ropes,” *Int. J. Solids Struct.*, vol. 48, no. 1, pp. 144–152, Jan. 2011.
[82] P. Smeets, M. Jacobs, and M. Mertens, “Creep as a design tool for HMPE Ropes in Long Term Marine and Offshore Applications,” in *OCEANS, 2001. MTS/IEEE Conference and Exhibition*, 2001, vol. 2, pp. 685–690.
[83] M. Vlasblom, J. Boesten, S. Leite, P. Davies, and others, “Development of HMPE fiber for permanent deepwater offshore mooring,” in *Offshore Technology Conference*, 2012.
[84] K. H. Lo, H. Xü, and L. A. Skogsberg, “Polyester Rope Mooring Design Considerations,” presented at the The Ninth International Offshore and Polar Engineering Conference, 1999.
[85] P. Davies, M. François, F. Grosjean, P. Baron, K. Salomon, and D. Trassoudaine, “Synthetic Mooring Lines for Depths to 3000 Meters,” presented at the Offshore Technology Conference, 2002.
[86] J. F. Flory, S. J. Banfield, C. Berryman, and others, “Polyester mooring lines on platforms and MODUs in deep water,” in *Offshore Technology Conference*, 2007.
[87] S. Banfield, T. Versavel, R. O. Snell, R. V. Ahilan, and others, “Fatigue curves for polyester moorings-a state-of-the-art review,” in *Offshore Technology Conference*, 2000.
[88] M. Vlasblom, J. Boesten, S. Leite, and P. Davies, “Creep and stiffness of HMPE fiber for permanent deepwater offshore mooring,” in *2012 Oceans-Yeosu*, 2012, pp. 1–7.
[89] M. Zehnder, Ed., *Atomistic simulation of the elasticity of polymers*. Zürich, 1997.
[90] D. N. Theodorou and U. W. Suter, “Detailed molecular structure of a vinyl polymer glass,” *Macromolecules*, vol. 18, no. 7, pp. 1467–1478, Jul. 1985.
[91] S. Dasgupta, W. B. Hammond, and W. A. Goddard, “Crystal structures and properties of nylon polymers from theory,” *J. Am. Chem. Soc.*, vol. 118, no. 49, pp. 12291–12301, 1996.
[92] K. Tashiro and H. Tadokoro, “Calculation of three-dimensional elastic constants of polymer crystals. 3. α and γ Forms of nylon 6,” *Macromolecules*, vol. 14, no. 3, pp. 781–785, mai 1981.
[93] K. Tashiro, M. Kobayashi, and H. Tadokoro, “Calculation of Three-Dimensional Elastic Constants of Polymer Crystals. 2. Application to Orthorhombic Polyethylene and Poly(vinyl alcohol),” *Macromolecules*, vol. 11, no. 5, pp. 914–918, Sep. 1978.
[94] K. Miyasaka, T. Isomoto, H. Koganeya, K. Uehara, K. Ishikawa, and N. Ogata, “Nylon-6 α-phase crystal: Chain repeat distance and modulus in the chain direction at low temperature,” *J. Polym. Sci. Polym. Phys. Ed.*, vol. 18, no. 5, pp. 1047–1052, mai 1980.
[95] K. Kaji, “Relation between the polymer conformation and the elastic modulus of the crystalline region of polymer,” PhD thesis, Kyoto University, Kyoto, Japan, 1970.
[96] L. Holliday and J. W. White, “The stiffness of polymers in relation to their structure,” *Pure Appl. Chem.*, vol. 26, no. 3–4, pp. 545–582, 1971.
[97] A. Marcellan, A. R. Bunsell, L. Laiarinandrasana, and R. Piques, “A multi-scale analysis of the microstructure and the tensile mechanical behaviour of polyamide 66 fibre,” *Polymer*, vol. 47, no. 1, pp. 367–378, Jan. 2006.
[98] S. K. Mukhopadhyay, “Chapter 8: Manufacturing, properties and tensile failure of nylon fibres,” in *Handbook of Tensile Properties of Textile and Technical Fibres*, A. R. Bunsell, Ed. Woodhead Publishing, 2009, pp. 197–222.
[99] B. Le Bourdiec, “Etude multi-échelle de cordages synthétiques,” Rapport interne Ifremer, 2011.
[100] C. Lechat, “Comportement mécanique de fibres et d’assemblages de fibres en polyester pour câbles d’amarrage de plates-formes offshore,” PhD thesis, Ecole Nationale Supérieure des Mines de Paris, 2007.

[101] T. D. Vu, D. Durville, and P. Davies, “Finite element simulation of the mechanical behavior of synthetic braided ropes and validation on a tensile test,” *Int. J. Solids Struct.*, vol. 58, pp. 106–116, Apr. 2015.
[102] T. D. Vu, “Lifetime of fibre ropes for deep sea handling,” PhD thesis, UBO, LCSM (Ifremer, Brest) and LMSSMat (Ecole Centrale Paris), 2014.
[103] J. W. S. Hearle, P. Grosberg, and S. Backer, “Structural Mechanics of Yarns and Fabrics (Vol. 1, Chapter 6),” *Theory Mech. Staple Yarns*, p. 255.
[104] G. Amaniampong, “Variability and viscoelasticity of parallel-lay ropes.,” PhD thesis, University of Cambridge, 1992.
[105] S. R. Ghoreishi, P. Davies, P. Cartraud, and T. Messager, “Analytical modeling of synthetic fiber ropes. Part II: A linear elastic model for 1 + 6 fibrous structures,” *Int. J. Solids Struct.*, vol. 44, no. 9, pp. 2943–2960, May 2007.
[106] N. Tolosana, M. Carrera, R. G. de Villoria, L. Castejon, and A. Miravete, “Numerical Analysis of Three-Dimensional Braided Composite by Means of Geometrical Modeling Based on Machine Emulation,” *Mech. Adv. Mater. Struct.*, vol. 19, no. 1–3, pp. 207–215, Jan. 2012.
[107] A. K. Pickett, J. Sirtautas, and A. Erber, “Braiding Simulation and Prediction of Mechanical Properties,” *Appl. Compos. Mater.*, vol. 16, no. 6, pp. 345–364, Sep. 2009.
[108] M. P. Vlasblom and J. L. J. Van Dingenen, “Chapter 13: The manufacture, properties and applications of high strength, high modulus polyethylene fibers,” in *Handbook of Tensile Properties of Textile and Technical Fibres*, A. R. Bunsell, Ed. Woodhead Publishing, 2009, pp. 437–485.
[109] L. E. Govaert and P. J. Lemstra, “Deformation behavior of oriented UHMW-PE fibers,” *Colloid Polym. Sci.*, vol. 270, no. 5, pp. 455–464, May 1992.
[110] M. J. N. Jacobs, “Creep of gel-spun polyethylene fibres: Improvements by impregnation and crosslinking,” PhD thesis, Eindhoven University, 1999.
[111] M. P. Vlasblom and R. L. M. Bosman, “Predicting the Creep Lifetime of HMPE Mooring Rope Applications,” in *OCEANS 2006*, 2006, pp. 1–10.
[112] D. G. Hunt and M. W. Darlington, “Accurate measurement of creep of nylon-6,6 at constant temperature and humidity,” *Polymer*, vol. 19, no. 8, pp. 977–983, août 1978.
[113] D. G. Hunt and M. W. Darlington, “Prediction of creep of nylon-6,6 at constant stress, temperature and moisture content,” *Polymer*, vol. 20, no. 2, pp. 241–246, février 1979.
[114] D. G. Hunt and M. W. Darlington, “Creep of nylon-6,6 during concurrent moisture changes,” *Polymer*, vol. 21, no. 5, pp. 502–508, mai 1980.
[115] K. S. Fancey, “A mechanical model for creep, recovery and stress relaxation in polymeric materials,” *J. Mater. Sci.*, vol. 40, no. 18, pp. 4827–4831, Sep. 2005.
[116] E. Chailleux and P. Davies, “A Non-Linear Viscoelastic Viscoplastic Model for the Behaviour of Polyester Fibres,” *Mech. Time-Depend. Mater.*, vol. 9, no. 2–3, pp. 147–160.
[117] E. Chailleux and P. Davies, “Modelling the Non-Linear Viscoelastic and Viscoplastic Behaviour of Aramid Fibre Yarns,” *Mech. Time-Depend. Mater.*, vol. 7, no. 3–4, pp. 291–303, Sep. 2003.
[118] G. Derombise *et al.*, “Long-term mechanical behavior of aramid fibers in seawater,” *Polym. Eng. Sci.*, vol. 51, no. 7, pp. 1366–1375, Jul. 2011.
[119] R. A. Schapery, “On the characterization of nonlinear viscoelastic materials,” *Polym. Eng. Sci.*, vol. 9, no. 4, pp. 295–310, juillet 1969.
[120] R. A. Schapery, “Nonlinear Viscoelastic and Viscoplastic Constitutive Equations Based on Thermodynamics,” *Mech. Time-Depend. Mater.*, vol. 1, no. 2, pp. 209–240.
[121] R. A. Schapery, “Nonlinear viscoelastic and viscoplastic constitutive equations with growing damage,” *Int. J. Fract.*, vol. 97, no. 1–4, pp. 33–66.

[122] J. Lai and A. Bakker, “An integral constitutive equation for nonlinear plasto-viscoelastic behavior of high-density polyethylene,” *Polym. Eng. Sci.*, vol. 35, no. 17, pp. 1339–1347, 1995.
[123] J.-M. Herrera-Ramirez, “Les mécanismes de fatigue dans les fibres thermoplastiques,” PhD thesis, École Nationale Supérieure des Mines de Paris, 2004.
[124] J. W. S. Hearle, “Fatigue in fibres and plastics (a review),” *J. Mater. Sci.*, vol. 2, no. 5, pp. 474–488, Sep. 1967.
[125] P. V. K. Pant and R. H. Boyd, “Molecular-dynamics simulation of diffusion of small penetrants in polymers,” *Macromolecules*, vol. 26, no. 4, pp. 679–686, 1993.
[126] A. Börjesson, E. Erdtman, P. Ahlström, M. Berlin, T. Andersson, and K. Bolton, “Molecular modelling of oxygen and water permeation in polyethylene,” *Polymer*, vol. 54, no. 12, pp. 2988–2998, May 2013.
[127] L. Silva, S. Tognana, and W. Salgueiro, “Study of the water absorption and its influence on the Young’s modulus in a commercial polyamide,” *Polym. Test.*, vol. 32, no. 1, pp. 158–164, Feb. 2013.
[128] M. Arhant, P.-Y. Le Gac, M. Le Gall, C. Burtin, C. Briançon, and P. Davies, “Modelling the non Fickian water absorption in polyamide 6,” *Polym. Degrad. Stab.*, vol. 133, pp. 404–412, Nov. 2016.
[129] M. Broudin *et al.*, “Moisture sorption in polyamide 6.6: Experimental investigation and comparison to four physical-based models,” *Polym. Test.*, vol. 43, pp. 10–20, mai 2015.
[130] G. S. Park, “Transport Principles—Solution, Diffusion and Permeation in Polymer Membranes,” in *Synthetic Membranes: Science, Engineering and Applications*, P. M. Bungay, H. K. Lonsdale, and M. N. de Pinho, Eds. Springer Netherlands, 1986, pp. 57–107.
[131] E. A. Guggenheim, *Applications of statistical mechanics*. Clarendon press Oxford, 1966.
[132] C. H. Klute, “Diffusion of small molecules in semicrystalline polymers: Water in polyethylene,” *J. Appl. Polym. Sci.*, vol. 1, no. 3, pp. 340–350, 1959.
[133] I. Pires, “Vieillissement dans l’antigel de matériaux composites polyamide-6,6 renforcé par des fibres de verre courtes,” PhD thesis, Université des sciences et techniques de Montpellier 2, France, 2000.
[134] V. M. Litvinov and J. P. Penning, “Phase Composition and Molecular Mobility in Nylon 6 Fibers as Studied by Proton NMR Transverse Magnetization Relaxation,” *Macromol. Chem. Phys.*, vol. 205, no. 13, pp. 1721–1734, août 2004.
[135] K. Kawasaki, Y. Sekita, and K. Kanou, “The extension of nylon 6 as a function of the extent and nature of sorbed water,” *J. Colloid Sci.*, vol. 17, no. 9, pp. 865–871, Dec. 1962.
[136] T. Peret, “Durabilité des matériaux composites soumis à des chargements statiques ou cycliques en milieu humide ou immergé.,” *http://www.theses.fr*. [Online]. Available: http://www.theses.fr/s112502. [Accessed: 16-Nov-2015].
[137] C. L. Clerc, A. R. Bunsell, A. Piant, and B. Monasse, “Role of skin/core structure and inclusions in the fatigue crack initiation and propagation in organic fibres,” *J. Mater. Sci.*, vol. 41, no. 20, pp. 6830–6842, Oct. 2006.
[138] A. R. Bunsell, *Handbook of Tensile Properties of Textile and Technical Fibres*. Elsevier, 2009.
[139] D. ASTM, “D885 / D885M-10A(2014)e1, Standard Test Methods for Tire Cords, Tire Cord Fabrics, and Industrial Filament Yarns Made from Manufactured Organic-Base Fibers,” *Annu. Book ASTM Stand.*, vol. 07.01, p. 01, 2014.
[140] P. Y. Le Gac, G. Roux, P. Davies, B. Fayolle, and J. Verdu, “Water clustering in

polychloroprene," *Polymer*, vol. 55, no. 12, pp. 2861–2866, juin 2014.
[141] W. X. Boleij, T. Engels, and L. Govaert, "Dynamic load performance of Dyneema," DSM, Geleen, Internal at DSM, 2015.
[142] J. W. S. Hearle, B. Lomas, and W. D. Cooke, *Atlas of Fibre Fracture and Damage to Textiles*. Elsevier, 1998.
[143] A. Launay, Y. Marco, M. H. Maitournam, and I. Raoult, "Modelling the influence of temperature and relative humidity on the time-dependent mechanical behaviour of a short glass fibre reinforced polyamide," *Mech. Mater.*, vol. 56, pp. 1–10, Jan. 2013.
[144] V. Miri, O. Persyn, J.-M. Lefebvre, and R. Seguela, "Effect of water absorption on the plastic deformation behavior of nylon 6," *Eur. Polym. J.*, vol. 45, no. 3, pp. 757–762, Mar. 2009.
[145] I. Boukal, "Effect of water on the mechanism of deformation of nylon 6," *J. Appl. Polym. Sci.*, vol. 11, no. 8, pp. 1483–1494, Aug. 1967.
[146] P. Davies, Y. Reaud, L. Dussud, and P. Woerther, "Mechanical behaviour of HMPE and aramid fibre ropes for deep sea handling operations," *Ocean Eng.*, vol. 38, no. 17–18, pp. 2208–2214, Dec. 2011.
[147] S. Banfield and N. Casey, "Evaluation of fibre rope properties for offshore mooring," *Ocean Eng.*, vol. 25, no. 10, pp. 861–879, Nov. 1998.
[148] M. G. Northolt, J. J. M. Baltussen, and B. Schaffers-Korff, "Yielding and hysteresis of polymer fibres," *Polymer*, vol. 36, no. 18, pp. 3485–3492, Jan. 1995.
[149] R. P. M. Janssen, "Quantitative prediction of polymer failure," PhD thesis, Eindhoven University, 2007.
[150] L. E. Govaert, C. W. M. Bastiaansen, and P. J. R. Leblans, "Stress-strain analysis of oriented polyethylene," *Polymer*, vol. 34, no. 3, pp. 534–540, Jan. 1993.
[151] M. Vlasblom, T. Engels, and C. Humeau, "Tension endurance of HMPE fiber ropes," presented at the OTC, Offshore Technology Conference, Aberdeen, Scotland, 2017.
[152] S. R. Ghoreishi, P. Cartraud, P. Davies, and T. Messager, "Analytical modeling of synthetic fiber ropes subjected to axial loads. Part I: A new continuum model for multilayered fibrous structures," *Int. J. Solids Struct.*, vol. 44, no. 9, pp. 2924–2942, May 2007.
[153] R. Chudoba, M. Vořechovský, V. Eckers, and T. Gries, "Effect of Twist, Fineness, Loading Rate and Length on Tensile Behavior of Multifilament Yarns (A Multivariate Study)," *Text. Res. J.*, vol. 77, no. 11, pp. 880–891, Nov. 2007.
[154] R. Chudoba, M. Vořechovský, and M. Konrad, "Stochastic modeling of multi-filament yarns. I. Random properties within the cross-section and size effect," *Int. J. Solids Struct.*, vol. 43, no. 3, pp. 413–434, Feb. 2006.
[155] M. Vořechovský and R. Chudoba, "Stochastic modeling of multi-filament yarns: II. Random properties over the length and size effect," *Int. J. Solids Struct.*, vol. 43, no. 3, pp. 435–458, Feb. 2006.
[156] F. N. Kelley and F. Bueche, "Viscosity and glass temperature relations for polymer-diluent systems," *J. Polym. Sci.*, vol. 50, no. 154, pp. 549–556, Apr. 1961.
[157] M. Broudin *et al.*, "Water diffusivity in PA66: Experimental characterization and modeling based on free volume theory," *Eur. Polym. J.*, vol. 67, pp. 326–334, Jun. 2015.
[158] M. J. Adamson, "Thermal expansion and swelling of cured epoxy resin used in graphite/epoxy composite materials," *J. Mater. Sci.*, vol. 15, no. 7, pp. 1736–1745, Jul. 1980.
[159] J.-Y. Cognard, R. Créac'Hcadec, J. Maurice, P. Davies, M. Peleau, and L. F. M. Da Silva, "Analysis of the Influence of Hydrostatic Stress on the Behaviour of an Adhesive in a Bonded Assembly," *J. Adhes. Sci. Technol.*, vol. 24, no. 11–12, pp. 1977–1994, 2010.

Appendixes

Appendix 1. Experimental tests details

The present appendix summarizes all the experimental tests used in the previous study which were performed on composites and fibre materials.

I. Composite materials

Composite materials

	Type of test	Type of material	Temperature [°C]	Humid condition [%RH]	Number of sample tested	Comments
Uncoupled tests	Water diffusion	Neat LY556 epoxy	60	Immersed	5	
		LY556 epoxy reinforced with ±45° carbon fibres	25	Immersed	3	
			40		3	
			60		3	
			80		3	
		LY556 epoxy reinforced with 0/90° carbon fibres	25	Immersed	3	
			40		3	
			60		3	
			80		3	
		LY556 epoxy reinforced with Quasi-isotropic carbon fibres	25	Immersed	3	
			40		3	
			60		3	
			80		3	
	Tensile tests	Neat LY556 epoxy (ASTM D638)	21	50	3	With crack investigation
		LY556 epoxy reinforced with ±45° carbon fibres (ASTM D3039)	21	50	3	With crack density study
		LY556 epoxy reinforced with 0/90° carbon fibres (ASTM D3039)	21	50	3	With crack density study
		LY556 epoxy reinforced with Quasi-isotropic carbon fibres (ASTM D3039)	21	50	3	With crack density study
	Damage characterisation by X-ray tomography	LY556 epoxy reinforced with ±45° carbon fibres (ASTM D3039)			3	Samples from tensile tests
		LY556 epoxy reinforced with Quasi-isotropic carbon fibres (ASTM D3039)			2	Samples from tensile tests
	Cyclic tensile tests	Neat LY556 epoxy LY556 epoxy reinforced with ±45° carbon fibres	21	50	3	
	Inter-laminar shear stress tests	LY556 epoxy reinforced with Quasi-isotropic carbon fibres (ASTM D2344)	21	50	4	
	Four points bending tests	LY556 epoxy reinforced with 0/90° carbon fibres (ASTM D6272)	21	50	3	

Figure I. Uncoupled tests performed on composite materials

Composite materials

	Type of test	Type of material	Temperature [°C]	Humid condition [%RH]	Number of sample tested	Comments
Semi-coupled tests	Water diffusion on pre-stressed samples	Neat LY556 epoxy	60	Immersed	5	
		LY556 epoxy reinforced with ±45° carbon fibres	25	Immersed	3	
			40		3	
			60		3	
			80		3	
		LY556 epoxy reinforced with 0/90° carbon fibres	25	Immersed	3	
			40		3	
			60		3	
			80		3	
		LY556 epoxy reinforced with Quasi-isotropic carbon fibres	25	Immersed	3	
			40		3	
			60		3	
			80		3	
	Tensile tests and DMA analysis during ageing	Neat LY556 epoxy (ASTM D638)	21	50	3x2	After 218 h of ageing
		Neat LY556 epoxy (ASTM D638)	21	50	3x2	After 1008 h of ageing
	Tensile tests at saturation	Neat LY556 epoxy (ASTM D638)	21	50	3	
		LY556 epoxy reinforced with ±45° carbon fibres (ASTM D3039)	21	50	3	With crack density study
		LY556 epoxy reinforced with 0/90° carbon fibres (ASTM D3039)	21	50	2	With crack density study
		LY556 epoxy reinforced with Quasi-isotropic carbon fibres (ASTM D3039)	21	50	3	With crack density study
	Inter-laminar shear stress tests at saturation	LY556 epoxy reinforced with Quasi-isotropic carbon fibres (ASTM D2344)	21	50	3	
	Four points bending tests at saturation	LY556 epoxy reinforced with 0/90° carbon fibres (ASTM D6272)	21	50	2	
Coupled tests	Water diffusion in stressed samples (+ permanent strain measurement)	LY556 epoxy reinforced with ±45° carbon fibres	60	Immersed	3	With σ = 30MPa
					3	With σ = 60MPa
					3	With σ = 110MPa
					3	With σ = 130MPa
		LY556 epoxy reinforced with ±45° carbon fibres (Thin samples)	60	Immersed	3	With σ = 60MPa
		LY556 epoxy reinforced with Quasi-isotropic carbon fibres	60	Immersed	3	With σ = 300MPa
					3	With σ = 430MPa
	Water diffusion under hydrostatic pressure	Neat SR1500 epoxy (square plates)	60	Immersed	5	With P = 1bar
					5	With P = 50bar
					5	With P = 500bar
		Neat SR1500 epoxy (longitudinal plates)	60	Immersed	5	With P = 500bar
		Neat SR1500 epoxy (transversal plates)	60	Immersed	5	With P = 500bar
		SR1500 epoxy reinforced with Uni-directional glass fibres	60	Immersed	5	With P = 1bar
					5	With P = 5bar
					5	With P = 50bar
					5	With P = 500bar
	Porosity characterisation by X-ray tomography	SR1500 epoxy reinforced with Uni-directional glass fibres			3	
	Determination of porosity ratio	SR1500 epoxy reinforced with Uni-directional glass fibres			15	For samples at 1, 50 and 500 bar
	Void filling investigation by Ultra-sonic analysis	SR1500 epoxy reinforced with Uni-directional glass fibres			12	For samples dried and at saturation under 1 and 500 bar

Figure II. Semi-coupled and coupled tests performed on composite materials

II. Synthetic fibres and ropes

Synthetic fibres

	Type of test	Type of material	Temperature [°C]	Humid condition [%RH]	Number of sample tested	Comments
Uncoupled and semi-coupled tests	Water diffusion	Nylon 6 yarns	25	At: 10, 20, 30, 40, 50, 60, 70, 80	3	
			40		3	
			60		3	
			80		3	
			25	Immersed	3	
		SK78 yarns	25	At: 10, 20, 30, 40, 50, 60, 70, 80	3	
			80		3	
		SK78 ropes	25	Immersed	3	For each sample the following cycle is applied: Sorption/De-sorption/Sorption
	Classical DMA analysis	Nylon 6 yarns	From 25 to 150	0	3	
	Tensile quasi-static tests	Nylon 6 mono-filaments	21	50 previously dried	5	
		Nylon 6 yarns	21	50 previously dried	5	
				50 after ageing	5	
		SK78 mono-filaments	21	50 previously dried	5	
		SK78 yarns	21	50 previously dried	5	
				50 after ageing	5	
		SK78 ropes	21	50 previously dried	5	
				50 after ageing	5	
	Tensile creep tests	Nylon 6 yarns	25	0	7 stress levels	
		SK78 yarns	25	50	3 stress levels	
			30		4 stress levels	
			50		6 stress levels	
			70		11 stress levels	
		SK78 ropes	70	50	3 stress levels	
			100		4 stress levels	
	Tensile dynamic tests, time to failure investigation	SK78 ropes	21	50	2 stress levels	f = 0.1 Hz, R = 0.1
					5 stress levels	f = 1 Hz, R = 0.1
			100	50	16 stress levels	f = 0.1 Hz, R = 0.1
					2 stress levels	f = 0.1 Hz, R = 0.5
	Tensile dynamic tests, heating process investigation	SK78 ropes	23	50	5 stress levels	f = 0.1 Hz, R = 0.1
					5 stress levels	f = 0.5 Hz, R = 0.1
					4 stress levels	f = 0.8 Hz, R = 0.1
					8 stress levels	f = 1 Hz, R = 0.1
			40		1 stress level	f = 1 Hz, R = 0.1
			60			
			70		2 stress levels	f = 0.5 Hz, R = 0.1
						f = 1 Hz, R = 0.1
			80		1 stress level	f = 0.5 Hz, R = 0.1
						f = 0.8 Hz, R = 0.1
						f = 1 Hz, R = 0.1
			100		1 stress level	f = 0.5 Hz, R = 0.1
						f = 1 Hz, R = 0.1

Figure III. Uncoupled tests performed on synthetic fibres

Synthetic fibres

	Type of test	Type of material	Temperature [°C]	Humid condition [%RH]	Number of sample tested	Comments
Coupled tests	**Classical DMA analysis in humid environment**	Nylon 6 yarns	25	10, 20, 30, 40, 50, 60, 70 and 80	1 sample for each condition (8 in total)	
			30	10, 20, 30, 40, 50, 60, 70 and 80	2 samples for each condition (16 in total)	
			35	10, 20, 30, 40, 50, 60 and 70	1 sample for each condition (8 in total)	
			40	10, 20, 30, 40, 50 and 60	2 samples for each condition (16 in total)	
			45	10, 20, 30, 40 and 50	2 samples for each condition (16 in total)	
			50	10, 20, 30 and 40	2 samples for each condition (16 in total)	
	Hygroscopic elongation determined with DMA device	Nylon 6 yarns	25	20, 30, 40, 50, 60, 70 and 80	2 samples for each condition (14 in total)	
	Tensile quasi static tests in humid environment	SK78 ropes	21	Immersed	3	
	Tensile creep tests in humid environment	Nylon 6 yarns	25	0	5 stress levels	
				20	5 stress levels	
				40	5 stress levels	
				60	5 stress levels	
				Immersed	2 stress levels	
	Tensile dynamictests, time to failure investigation	SK78 ropes	35	Immersed	4 stress levels	
	Tensile dynamictests, heating process investigation	SK78 ropes	35	Immersed	2	

Figure IV. Semi-coupled and coupled tests performed on synthetic fibres

Appendix 2. Parametric study of sink diffusion model (on COMSOL)

This parametric study is based on the sink diffusion theory developed in Part A, Chapter 5. This model is based on two "diffusions": one inside the composite's polymer matrix and a fill rate in the voids. To implement this type of two phase diffusion in COMSOL we can make different hypotheses. In this appendix we treat the case of a concentric diffusion with a centered porosity and a 2D diffusion in a rectangular plate with a porosity movable in space. In these models the diffusion coefficient impact on the results is not studied.

I. Numerical study of a concentric diffusion

The first section is dedicated to the simplest representation (concentric) since it involves few parameters (void ratio, sample dimension and fill rate).

a. Definition of the concentric model

In this case, the geometric properties of the concentric representation of the samples allows the calculation to be performed with a 2D axi-symmetric model (as shown in Figure V).

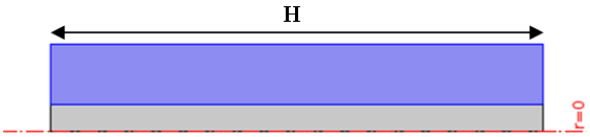

Figure V. Geometric representation of the concentric model.

In this representation we made some assumptions in order to simplify the model and its resolution, we consider:

- Two domains: One with an homogeneous material corresponding to the composite (fibre and matrix), managed by Fick's diffusion –in blue– and another representing the voids, characterized by a fill rate (τ) and a homogeneous water content –in grey–.
- Symmetry conditions: on the center axis and at the cylinder extreme edges (right and left) to avoid edge effects.
- Imposed concentration: on the external face of the cylinder (upper one): concentration fixed equal to the concentration at saturation (Cm=Cm_sat).
- Imposed flux: at the interface of the two phases using the relationship between water concentration in voids and material established in Part A, Chapter 5.

b. Parametric study of the concentric model

- Influence of the voids' fill rate on the total water uptake :

In this case we fixed the two other parameters to realistic values: the diameter to 2.7 mm (equivalent to the samples thickness), the height (defined in Figure V) toH=25mm, and void ratio to Xv_c=0.08. Then, we make the fill rate vary and we obtain the results in Figure VI.

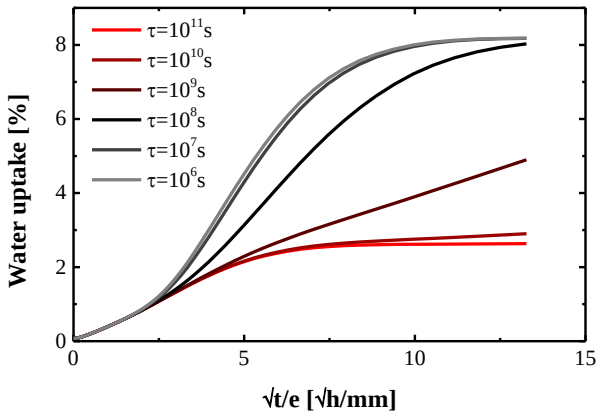

Figure VI. Water diffusion results obtained with a concentric model for different fill rates.

The Figure VI shows on important acceleration of the second phase of the diffusion curve when the fill rate decreases. Moreover, for high fill rate (τ above 10^{10}s) the water uptake seems to saturate at a lower value. Nevertheless, the saturation levels should be the same for all the cases, for high fill rate the second step of the diffusion will be extremely slow.

- Influence of the sample length on the total water uptake :

In this case we fixed the two other parameters to realistic values: the fill rate to $\tau = 10^6$s, and voids ratio to Xv_c=0.08. Then, we make the length of the specimen vary and we obtain the results in Figure VII.

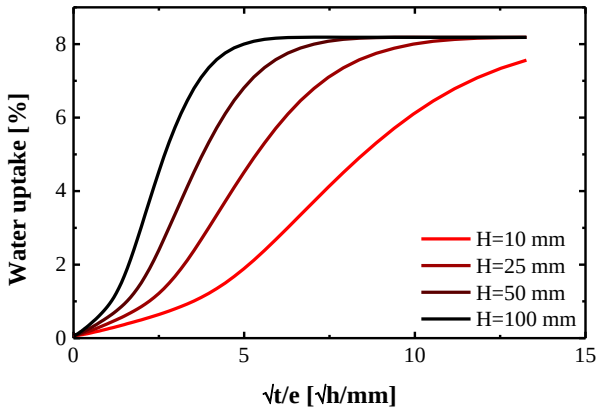

Figure VII. Water diffusion results obtained with a concentric model for different sample dimensions.

The Figure VI shows an acceleration of global diffusion kinetics when the sample takes a more elongated shape.

- Influence of the porosity ratio.

In this case we fixed the two other parameters to realistic values: the fill rate to $\tau = 10^6$s, and the height to H=25mm. Then, we make the porosity ratio in the specimen vary and we obtain the results in Figure VIII.

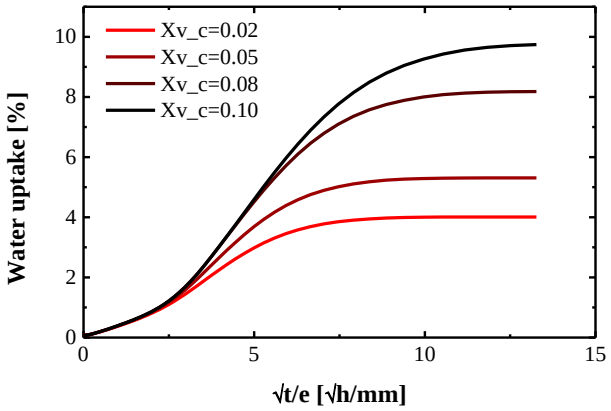

Figure VIII. Water diffusion results obtained with a concentric model for different sample dimensions.

The porosity ratio appears to have a major impact on the second stage of the diffusion, the maximal water uptake and the diffusion kinetic increases with the porosity ratio rise (see Figure VIII).

Finally, the best parameters to represent the water diffusion behaviour in the composites are: H = 50 mm and Xv_c = 0.08, and the best fill rates for 1, 5, 50 and 500 bar are respectively: 10^{10}, 4.10^9, 10^6 and 10^6s.

These parameters remains realistic, nevertheless for high diffusion, the model cannot match the initial experimental data.

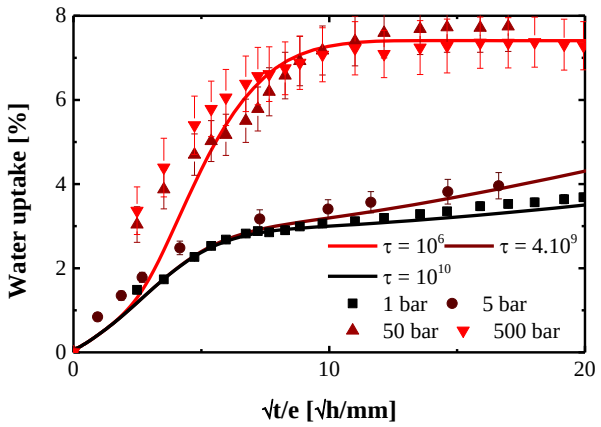

Figure IX. Water diffusion for experiment and from the concentric model after optimisation.

II. Numerical study of a pure 2D diffusion

This section is focused on another representation of the diffusion (planar) which involves more parameters than the previous one (void ratio, porosity shape factor, void distance to the edge and the fill rate).

a. Definition of the concentric model

In this case, the geometric properties of the concentric representation of the samples allow the calculation to be performed on a 2D model (as shown in Figure X). This representation permit to model a un-centered void.

Figure X. Geometric representation of the pure 2D model.

In this representation we made some assumptions in order to simplify the model and its resolution, we consider:

- Two domains: One with an homogeneous material corresponding to the composite (fibre and matrix), managed by Fick's diffusion –in blue– and another representing the voids, characterized by a fill rate (τ) and a homogeneous water content –in grey–.
- Symmetry conditions: On the middle edge (at the right on Figure X) in order to perform the calculation on one half of the sample.
- Imposed concentration: On the external faces of the sample (upper, lower and left edges): fixed concentration equal to the concentration at saturation (Cm=Cm_sat).
- Imposed flux: at the interface of the two phases using the relationship between water concentration in the void and in polymer at the frontier (established in Part A, section 5.3.3.1).

b. Parametric study

In this case we do not perform the study on the porosity ratio, since it has been shown that it influences the maximal water uptake. Moreover, this parameter has shown good correlation with experimental data for a value of 0.08, which corresponds to the porosity ratio observed experimentally in Part A, Chapter 5.

- Influence of the porosity shape factor (f) on the total water uptake:

In this case we fixed the two other parameters to realistic values: the fill rate to $\tau = 10^6$s, the distance between the porosity centre and the material edge to 0.2e (with e the sample's depth) and void ratio to Xv_c=0.08. Then, we make the shape factor of the void vary and we obtain the results in Figure XI.

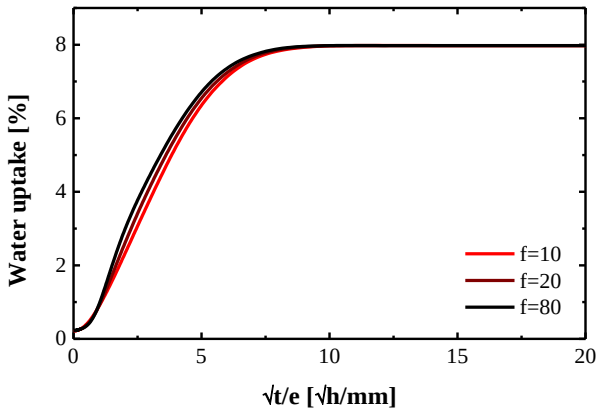

Figure XI. Water diffusion results obtained with a pure 2D model for different porosity shape factor.

The shape factor of the porosity does not appear to have an important impact on the water diffusion in the sample (Figure XI). Therefore, for further consideration, f is considered equal to 20, which corresponds to the realistic value (observed in Part A, Chapter 5)

- Influence of the distance (d) between the porosity centre and the material edge and the fill rate (τ) on the water uptake:

In this case we fixed the two other parameters to realistic values: the shape factor to f = 20 and void ratio to Xv_c = 0.08. Then, we varied d and τ and we obtain the results in Figure XII.

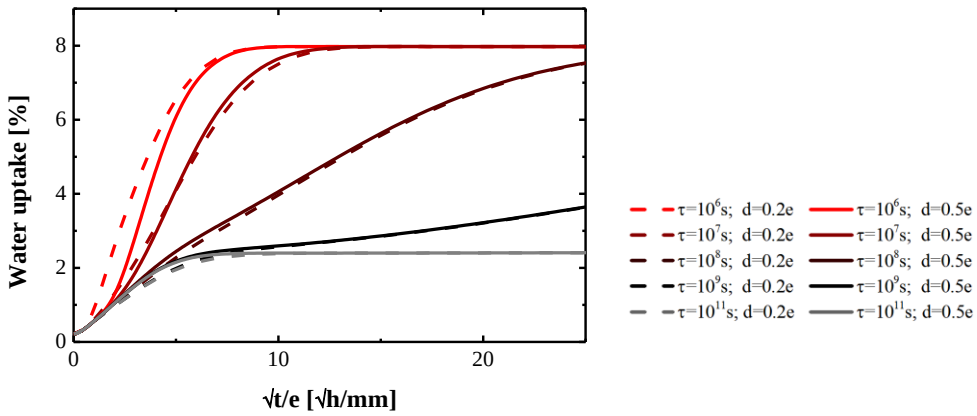

Figure XII. Water diffusion results obtained with a pure 2D model for different porosity shape factor.

The fill rate has the same influence on the water uptake as in the previous model. Moreover, the distance between the porosity centre and the material edge does not have a significant

influence for low pressure. Nevertheless, at 500 bar when *d* decreases the diffusion kinetics of the first diffusive behaviour stage increase.

This last phenomenon finally provides a better representation of the diffusive behaviour than the concentric model (Figure XIII).

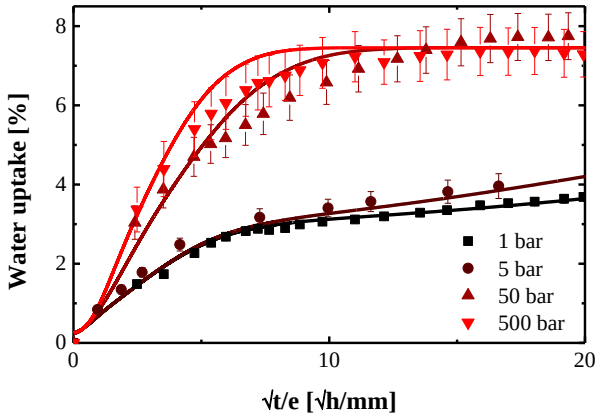

Figure XIII. Water diffusion for experiment and from the pure 2D model after optimisation.

Appendix 3. Discretisation of the sink diffusion model for Matlab™ application

I. Set of equations to solve:

The initial set of equations to solve is the same as for the finite element model:

$$\begin{cases} \dfrac{\partial c_m(r,t)}{\partial t} = D\ div\ \vec{\nabla} c_m(r,t) - \dfrac{\partial c_c(r,t)}{\partial t} \\ \dfrac{\partial c_c(r,t)}{\partial t} = \dfrac{1}{\tau}\left(c_m(r,t)\dfrac{c_c(r,t_\infty)}{c_m(r,t_\infty)} - c_c(r,t) \right) \end{cases}$$

In this case we will use finite differences in order to solve the problem with Matlab™ software. Moreover, we consider this set of equations for any point of the space which corresponds to the homogenised case.

II. Discrete expressions

The discretisation is performed on the space and time variables. Here we present the case of a concentric model, therefore the concentration is considered as a constant of the high and the angle. Then, we perform the discretisation on *r* (the radius) and *t* (time) variables:

$r_i = r_0 + i.\Delta r$
$t_j = t_0 + j.\Delta t$

The concentration in the homogeneous material (c_m) and in voids (c_c) will be expressed as:

$$\begin{cases} c_m(r_i, t_j) = c_{m_{i,j}} \\ c_c(r_i, t_j) = c_{c_{i,j}} \end{cases}$$

The discrete derivative expressions can be summarised as:

$$\boldsymbol{\frac{\partial c_m(r_i, t_j)}{\partial t}} = \frac{c_{m_{i,j+1}} - c_{m_{i,j}}}{\Delta t}$$

$$\boldsymbol{D\ div\ \vec{\nabla} c_m(r,t)} = \frac{\partial^2 c_m(r_i,t_j)}{\partial r^2} + \frac{1}{r_i}\frac{\partial c_m(r_i,t_j)}{\partial r}$$

$$\frac{\partial c_m(r_i,t_j)}{\partial r} = \frac{c_{m_{i+1,j}} - c_{m_{i,j}}}{\Delta r}$$

$$\frac{\partial^2 c_m(r_i,t_j)}{\partial r^2} = \frac{c_{m_{i+1,j}} + c_{m_{i-1,j}} - 2c_{m_{i,j}}}{\Delta r^2}$$

$$\boldsymbol{\frac{\partial c_c(r_i, t_j)}{\partial t}} = \frac{c_{c_{i,j+1}} - c_{c_{i,j}}}{\Delta t}$$

III. Discrete system

Finally, we obtain the following set of discrete equation.

$$\begin{cases} \dfrac{c_{m_{i,j+1}} - c_{m_{i,j}}}{\Delta t} = \dfrac{D}{\Delta r}\left(\dfrac{c_{m_{i+1,j}} + c_{m_{i-1,j}} - 2c_{m_{i,j}}}{\Delta r} + \dfrac{c_{m_{i+1,j}} - c_{m_{i,j}}}{r_i}\right) - \dfrac{c_{c_{i,j+1}} - c_{c_{i,j}}}{\Delta t} \\ \dfrac{c_{c_{i,j+1}} - c_{c_{i,j}}}{\Delta t} = \dfrac{1}{\tau}\left(c_{m_{i,j}}.\alpha - c_{c_{i,j}}\right) \end{cases}$$

With

$$\alpha = \frac{c_{c_{i,j_\infty}}}{c_{m_{i,j_\infty}}}$$

In order to solve this problem we have to establish a modelling strategy and define the limit conditions.

a. The two steps of the modelling:

The set of equations is solved in two steps for each point of the space and time:

1. Calculation of c_c

$$c_{c_{i,j+1}} = \frac{\Delta t}{\tau}\left(c_{m_{i,j}}.\alpha - c_{c_j}\right) + c_{c_{i,j}}$$

$$\boxed{c_{c_{i,j+1}} = \alpha\frac{\Delta t}{\tau}c_{m_{i,j}} + \left(1 - \frac{\Delta t}{\tau}\right)c_{c_{i,j}}}$$

2. Calculation of c_m in each point (i)

$$c_{m_{i,j+1}} = \frac{D.\Delta t}{\Delta r}\left(\frac{c_{m_{i+1,j}} + c_{m_{i-1,j}} - 2c_{m_{i,j}}}{\Delta r} + \frac{c_{m_{i+1,j}} - c_{m_{i,j}}}{r_i}\right) - c_{c_{j+1}} + c_{c_j} + c_{m_{i,j}}$$

$$\boxed{c_{m_{i,j+1}} = \frac{D.\Delta t}{\Delta r}\left[\left(\frac{1}{\Delta r} + \frac{1}{r_i}\right)c_{m_{i+1,j}} + \frac{1}{\Delta r}c_{m_{i-1,j}}\right] + \left[1 - \frac{D.\Delta t}{\Delta r}\left(\frac{2}{\Delta r} + \frac{1}{r_i}\right)\right]c_{m_{i,j}} - c_{c_{i,j+1}} + c_{c_{i,j}}}$$

b. Limits conditions:

As for the previous model, we establish limit conditions in order to initiate the model resolution; the conditions are fixed on the external surface of the sample.

$$c_{m_{i_{max},j+1}} = \frac{D.\Delta t}{\Delta r}\left[\left(\frac{1}{\Delta r} + \frac{1}{r_{i_{max}}}\right)c_{m_\infty} + \frac{1}{\Delta r}c_{m_{i_{max}-1,j}}\right] + \left[1 - \frac{D.\Delta t}{\Delta r}\left(\frac{2}{\Delta r} + \frac{1}{r_{i_{max}}}\right)\right]c_{m_{i_{max},j}} - c_{c_{i,j+1}} + c_{c_{i,j}}$$

IV. Stability conditions

In order to get a stable solution, the coefficients of $c_{m_{i+1,j}}$, $c_{m_{i-1,j}}$, $c_{m_{i,j}}$, $c_{c_{i,j+1}}$ and $c_{c_{i,j}}$ in the set of equations have to be positive. This results in two conditions, one from the cc equation and the other from the cm expression.

a. On c_c

$$\Delta t < \frac{\tau}{1+\alpha}$$

b. On c_m

$$\Delta t < \frac{\Delta r^2 . r_0}{D.(\Delta r + 2.r_0)}$$

If one of these conditions is not verified Δt is modified. For the second condition we could also change Δt and Δr simultaneously in order to verify the stability conditions.

Appendix 4. French summary

Au cours des dernières décennies, les nombreuses crises économiques et environnementales ont initié une réflexion sur de nouvelles façons de produire l'énergie.

D'une part, les sources d'énergie fossile ont commencé à se raréfier, ce qui a induit le développement de nouvelles techniques d'exploitation (tel que l'exploitation de gisement en grande profondeur).

D'autre part, les récents problèmes environnementaux ont entraîné l'exploitation de nouvelles sources d'énergie renouvelable.

Par ailleurs, les océans représentent plus de 70% de la surface de la Terre et renferment de nombreuses sources d'énergie aussi bien renouvelables (courant, marée, vent) que fossiles (pétrole, gaz, minerai). Ces observations ont ainsi orienté les recherches autour de deux grands axes : d'abord, l'exploration de nouvelles sources d'énergie fossile et ensuite, l'exploitation des sources d'énergies renouvelables marines.

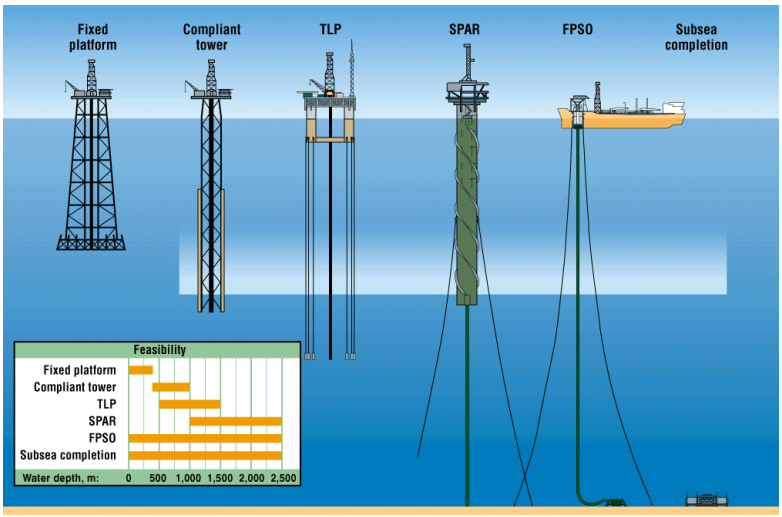

Figure A. Les différents types d'ancrage et leurs profondeurs d'utilisation [1].

Avant le développement des technologies marines, toutes les installations navales et offshores étaient limitées en raison du manque de techniques d'amarrage en eaux profondes. En effet, comme le résume la Figure A, les structures rigides ne peuvent être utilisées que pour des eaux peu profondes (jusqu'à 1 000 mètres de profondeur) [2]. Le développement de ces types d'installations métalliques en grande profondeur est limité par leur rigidité et leur poids. Dans le but d'accroître la profondeur de l'implantation des systèmes offshores, de nouvelles techniques d'amarrage ont été développées depuis le début des années 80 à l'exemple des TLP [3] et FPSO. Tous ces types d'amarrage sont basés sur l'utilisation de cordage permettant de relier la plate-forme au fond marin tout en résistant aux contraintes environnementales liées au vent, au courant et à la houle [4]. Les premières installations offshores de ce type ont été construites en utilisant des câbles métalliques (principalement en acier).

Ce type de liaison induit deux problèmes majeurs : premièrement, le milieu marin provoque une très forte corrosion de l'acier, deuxièmement, pour les applications en eau profonde, le poids de la liaison en acier peut devenir critique et provoquer la rupture du câble. Bien que le problème de corrosion puisse être évité en utilisant un revêtement polymère, le problème du poids de l'acier est une propriété intrinsèque au matériau qui ne peut être évité. Aujourd'hui, des projets visent à remplacer l'acier par des matériaux polymères dans les lignes d'amarrage. Certains de ces matériaux peuvent, en effet, combiner une bonne tenue au vieillissement en milieu marin et un ratio poids/ténacité supérieure à celui de l'acier.

Un autre problème clé, rencontré lors d'applications marines, réside dans l'utilisation de matériaux performants et fiables dans la construction des structures offshores. Initialement, les matériaux métalliques étaient utilisés dans tous les types d'applications marines, depuis la construction des bateaux à la réalisation de plates-formes pétrolières.

Cependant, pour les mêmes raisons que pour les câbles acier, les structures métalliques possèdent des propriétés assez limitées pour les applications offshores : la plupart d'entre elles sont fortement soumises à la corrosion et induisent des structures lourdes. Or la corrosion est un élément essentiel dans le cadre des applications offshores car elle peut générer la ruine de la structure [5]–[7], en particulier, en réduisant les performances mécaniques du matériau ou en créant des voies d'eau (critiques dans les applications navales et les sous-marines).

D'autre part, le rapport poids/ténacité n'est pas optimal dans le cas des métaux. Ainsi les structures métalliques soumises à des contraintes mécaniques élevées sont nécessairement lourdes et donc difficiles à manipuler.

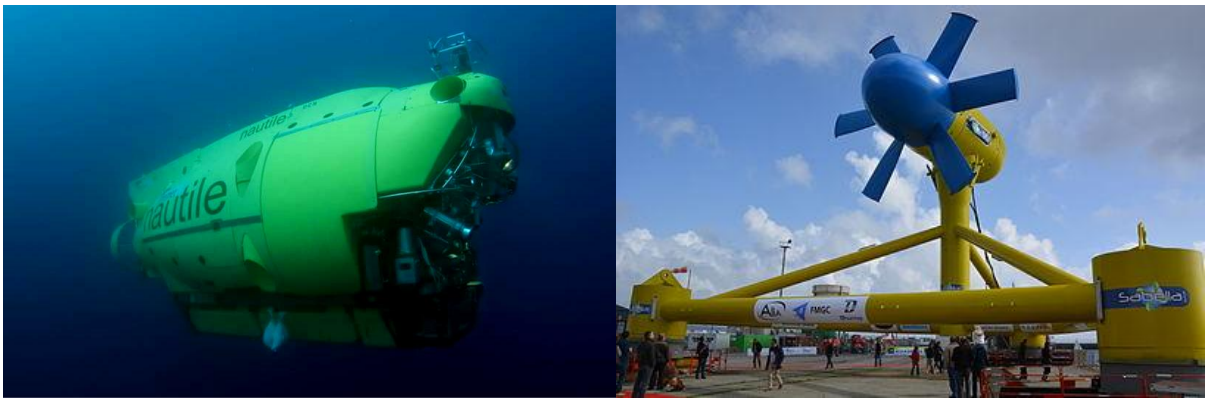

Figure B. Exemples d'applications marines utilisant les matériaux composites : sous-marin Nautile [gauche] et hydrolienne Sabella [droite]

Au vu des inconvénients présentés par l'utilisation des matériaux métalliques une modification progressive du type de matériau utilisé dans les structures offshores est apparue. En effet, les matériaux de structures à base de polymères présentent de meilleures propriétés en immersion en eau de mer et un rapport poids/ténacité plus intéressant, en particulier, lorsqu'ils sont combinés à des renforts (fibres de verre, carbon, etc) permettant d'accroître leurs propriétés mécaniques et de créer des

matériaux composites. De plus, ce type de matériaux présente de bonnes propriétés mécaniques statiques et en fatigue. C'est pour ces raisons que les métaux sont régulièrement supplantés par les composites dans des applications offshores telles que celles présentées en Figure B.

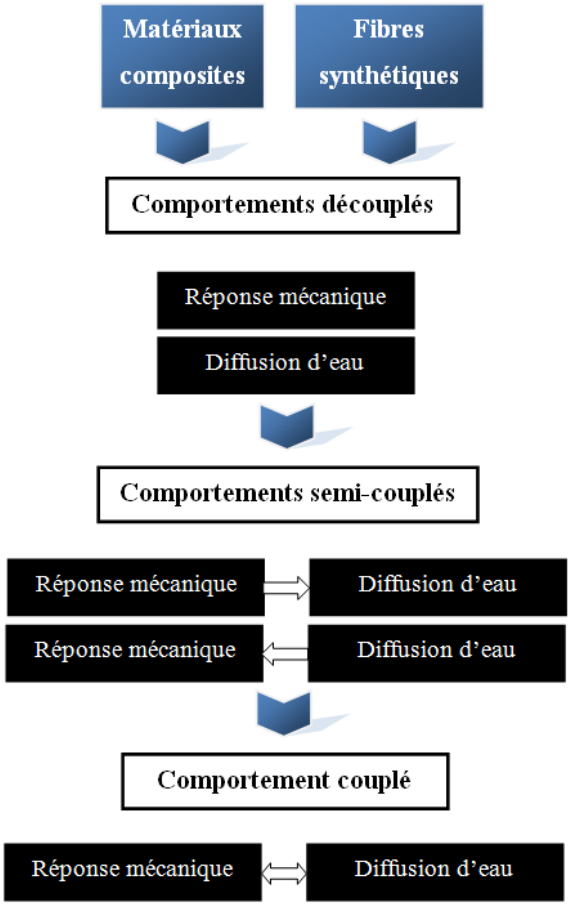

Figure C. Plan de l'étude

Dans cette première partie, nous avons vu que les matériaux marins hautes-performances peuvent être séparés en deux grandes catégories : d'un coté, les cordages synthétiques et de l'autre, les matériaux composites. De même, les contraintes induites par le milieu marin peuvent se distinguer en deux catégories : d'une part, les contraintes mécaniques et d'autre part, l'impact de l'eau sur les matériaux. De plus dans leurs conditions réelles d'utilisation, les matériaux sont soumis à ces deux phénomènes de façon simultanée. Néanmoins, les études traitant de l'effet de ces sollicitations de façon couplée sont rares, car il est difficile de réaliser les essais dans de telles conditions.

L'objectif de cette recherche est donc de réaliser des essais dans différentes configurations : non couplées, semi-couplées et couplées (Figure C) ; de façon à mettre en évidence les informations supplémentaires apportées par les tests couplés et à conclure quant à leur nécessité ou non.

Pour ce faire, l'étude est divisée en deux parties distinctes dédiées chacune à un type de matériau haute-performance. Pour chaque cas, les comportements découplés, semi-couplés et couplés sont successivement étudiés.

La première partie, consacrée à l'étude des matériaux composites, aborde deux types de couplage: traction immergée et pression hydrostatique. Ces deux expériences mettent en évidence une influence importante du couplage sur le comportement diffusif dans les matériaux.

Tout d'abord, dans le cas des échantillons immergés sous contrainte de traction, les mesures gravimétriques mettent en évidence une accélération de la cinétique de diffusion d'eau lorsque le niveau de contrainte augmente (Figure D). De plus, plus la contrainte est importante, plus cette accélération de diffusion intervient rapidement. Enfin, cette augmentation semble d'autant plus importante lorsque la matrice du composite est fortement sollicitée (comme dans le cas du ± 45°).

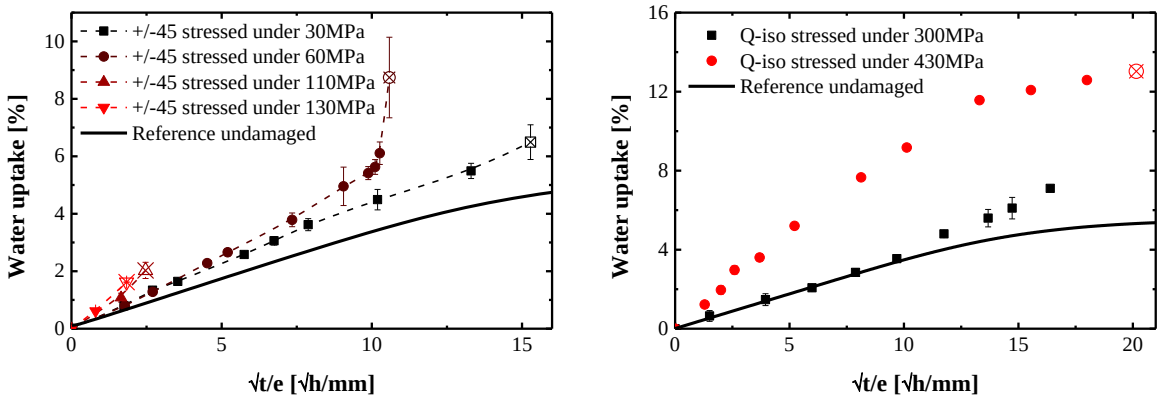

Figure D. Comportements diffusifs des composites ±45° [gauche] et quasi-isotrope [droite] contraint en traction et immergée en eau douce à 60°C.

Dans le cas des échantillons testés sous pression hydrostatique, l'étude met en évidence des diffusions d'eau divergentes uniquement pour les composites réalisés par procédé de fabrication contact (Figure E). Ceci se traduit par une augmentation de quantité d'eau maximale dans les matériaux soumis aux pressions les plus élevées et une non-saturation des échantillons contraints à des pressions inférieures à 5 bars.

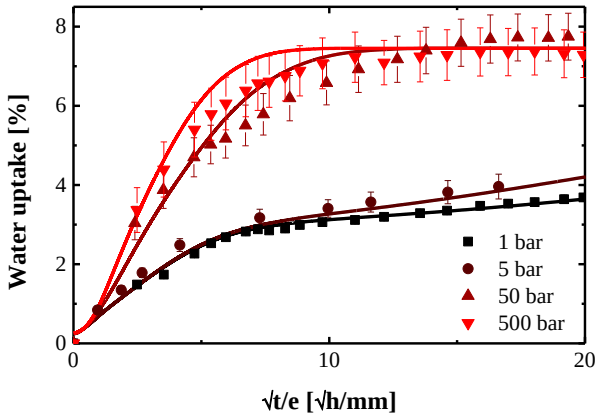

Figure E. Comportements diffusifs des composites à renforts unidirectionnelle sous pression hydrostatique en eau douce à 60°C.

Cette modification de l'absorption d'humidité semble être induite par l'inclusion d'eau dans des défauts ou des dégâts internes. Dans le cas des contraintes de traction, l'endommagement augmente avec la contrainte, ce qui induit une augmentation de la diffusion d'eau dans le même temps. Pour la pression hydrostatique, l'inclusion de défauts (porosités) dans les composites peut modifier la diffusion d'eau lorsque la pression augmente : l'eau semble contrainte de remplir la porosité. En résumé, dans les deux cas, l'inclusion de vides (défauts ou fissures) induit une modification de la diffusion d'eau.
Dans le cas de la pression hydrostatique, l'étude va plus loin et modélise la diffusion de l'humidité à partir de la loi de Fick combinée à un terme puits représentant les défauts. Ce type de modèle semble avoir une très bonne corrélation avec les données expérimentales (Figure E).

Dans tous ces cas étudiés, l'action de l'eau incluse dans les porosités sur le comportement mécanique des matériaux n'a pas directement été analysée. Néanmoins, l'augmentation de poids qu'elle génère peut être critique dans certaines applications où la légèreté de la structure est primordiale. De plus, dans le cas d'une sollicitation en fatigue, l'eau incluse dans les vides pendant le déchargement mécanique peut accélérer la propagation des fissures à l'intérieur du matériau. Dans l'avenir, pour approfondir ces sujets, les études devront s'orienter suivant ces deux axes.

La deuxième partie du travail a été consacrée aux effets de couplage dans les fibres synthétiques. La structure des cordages oblige à considérer les deux échelles suivantes : celle du filament et celle du cordage, dans des parties séparées. Afin de mieux comprendre l'effet de l'eau sur chacune d'elle, nous avons étudié deux types de fibre : un premier hydrophile (Nylon 6) afin comprendre l'influence de l'eau sur le filament et un second hydrophobe (Dyneemas SK78) pour mettre en avant les effets de l'eau sur la structure du cordage.

A l'échelle du brin, le comportement mécanique des échantillons hydrophiles est identique lorsqu'ils sont testés de façon découplée et semi-couplée. A l'inverse, lors d'essais couplés, on observe une perte de propriétés mécaniques dépendante de la teneur en eau dans le matériau (Figure F). Ce phénomène est dû au caractère hydrophile du matériau et à une cinétique de diffusion très rapide. En effet, lorsque les échantillons sont testés de façon semi-couplée, la désorption est totale dès la fin de la mise en place de l'échantillon sur la machine de traction. Par conséquent, les résultats obtenus sont comparables à ceux du cas découplé. De plus, les essais effectués sur le matériau hydrophobe n'ont mis en évidence aucune influence de l'eau sur son comportement mécanique. Par conséquent, le milieu humide environnant affecte uniquement les propriétés du matériau fibreux hydrophile.

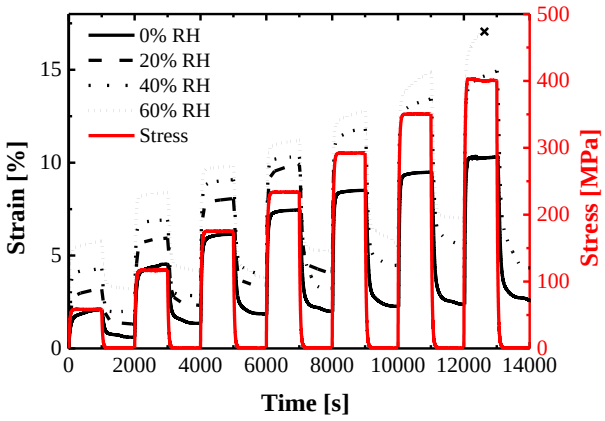

Figure F. Comportement en fluage des brins de Nylon 6 sous différentes conditions hygrothermique.

En identifiant un modèle empirique viscoélastique viscoplastique sur les données expérimentales, nous avons pu quantifier l'impact de l'absorption d'eau sur la réponse en fluage des brins hydrophiles. Cette analyse permet d'identifier une augmentation de la déformation initiale (déformation instantanée) et du taux de fluage lorsque la teneur en eau augmente. Pour une analyse plus approfondie, la variation des deux paramètres avec l'absorption d'eau doit être étudiée, afin de quantifier l'effet de l'humidité sur le comportement du brin.

A l'échelle du cordage, l'étude est exclusivement axée sur les matériaux hydrophobes afin de comprendre l'effet de l'eau sur la structure du cordage. Dans ce cas, les différences entre les essais mécaniques semi-couplés et découplés ne sont pas significatives. Néanmoins, les résultats obtenus par les tests couplés montrent une divergence importante par rapport aux tests précédents. En effet, lorsque les cordages sont testés en fatigue immergée, leur durée de vie augmente pour les chargements élevés. De plus, l'étude du suivi de la température interne du cordage souligne un échauffement moindre dans le cas d'échantillons immergés. Ces deux phénomènes s'expliquent par l'effet lubrifiant et dissipateur de chaleur de l'eau incluse dans la structure. Ainsi, ces deux phénomènes améliorent les propriétés en fatigue immergée des cordages synthétiques.

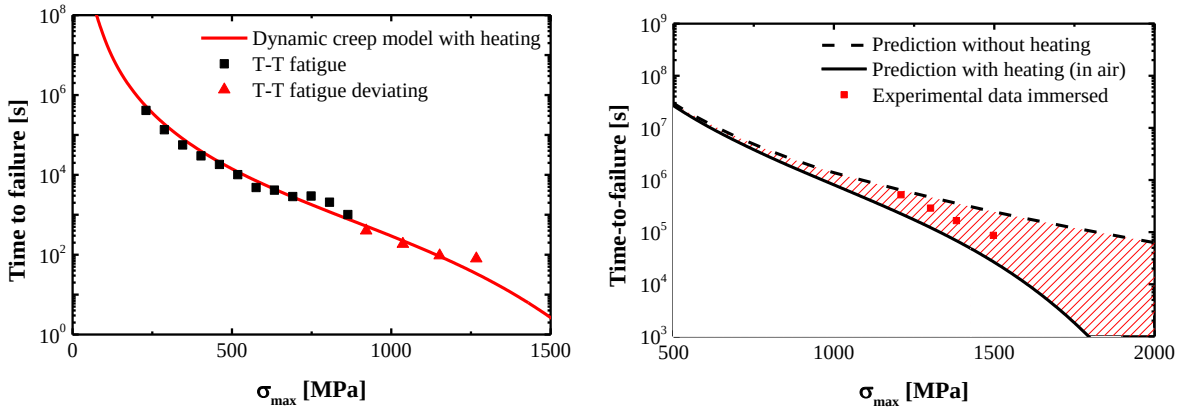

Figure G. Durée de vie des cordages SK78 en fonction de la contrainte maximale appliquée, à 50%RH [gauche] et immergés [droite]. Conditions des essais dynamiques : f=0.1Hz, R=0.1.

Dans un deuxième temps, un modèle viscoplastique a été utilisé pour prédire la durée de vie des cordages sollicités en fatigue. Cette approche théorique, associée à la prise en compte de l'auto-échauffement interne, semble bien adaptée au matériau et à la structure du cordage étudié. Une étude plus approfondie devrait être menée pour établir le lien entre les deux phénomènes (auto-échauffement et temps à la rupture) dans le cas de cordages immergés afin de vérifier l'hypothèse proposée.

Les deux parties de ce travail mettent en évidence une modification importante du comportement lorsque les échantillons sont sollicités de manière couplée. L'étude des matériaux composites met en évidence une modification claire de leurs comportements diffusifs tandis que l'étude des cordages montre une modification du comportement mécanique lorsqu'il est soumis à des contraintes couplées. Dans le cas d'un matériau massique, la présence de vides semble être le paramètre le plus important sur le comportement d'absorption d'humidité. Pour les matériaux fibreux, leur comportement mécanique est très dépendant de la température externe et interne de la structure.
Par conséquent, les études précédentes sur les comportements non couplés et semi-couplés sont importantes pour définir la référence des réponses matérielles, mais elles ne peuvent pas être utilisées directement pour dimensionner des structures, des navires ou des amarrages offshores. Dans tous les cas, des tests couplés doivent être effectués afin de dimensionner les systèmes offshores ou de quantifier les facteurs permettant la transposition du comportement semi-couplé ou non couplé au cas couplé.

Enfin, cette étude permet d'affirmer le besoin d'effectuer des tests couplés en raison de la différence de comportement du matériau à partir de cas semi-couplés et découplés. De plus, nous avons réussi à établir et à vérifier une hypothèse sur l'origine des différences entre les comportements non couplés, semi-couplés et couplés. Et, pour le cas de la pression hydrostatique, nous avons également développé un modèle qui peut prédire le comportement diffusif des composites avec des défauts. Néanmoins, l'étude ne définit que les bases du comportement couplé et souligne le manque de connaissances sur ce sujet. De plus, nous avons proposé des axes d'expériences pour de futures études qui permettraient de mieux comprendre ces phénomènes couplés. Suite aux résultats obtenus dans cette étude, nous pouvons proposer différents axes d'expérimentations pour compléter et développer la connaissance des comportements couplés.

Premièrement, il serait important d'augmenter le nombre de tests de fluage sur brin immergé afin de décrire son comportement en fluage en fonction de la teneur en eau dans le matériau.
De plus, des tests complémentaires à ceux réalisés dans l'étude sur le composite immergé sous traction statique, permettraient une meilleure compréhension du comportement diffusif dans le matériau en fonction de la contrainte appliquée sur celui-ci.

Enfin, il serait judicieux de réaliser des essais supplémentaires d'acquisition de la température intérieure des cordages soumis aux contraintes de fatigue en immersion. Ceci, permettrait de valider ou non l'hypothèse émise, selon laquelle l'échauffement du cordage est moindre dans le cas immergé.

Deuxièmement, une étude plus approfondie permettrait de transposer d'avantage les méthodes utilisées d'un matériau à l'autre (du cordage au composite ou inversement). Ainsi, il serait possible de mettre d'avantage en évidence les ressemblances et les différences de comportement entre ces deux types de matériau.

À titre d'exemple, le modèle de diffusion « puits » pourrait être appliqué à la diffusion d'eau dans les cordages et comparé aux données expérimentales obtenues dans cette étude. Dans ce cas, le terme puits pourrait être associé aux vides inter-brins et/ou inter-fibres dans la construction. Ces vides pourraient être pilotés par la contrainte ou précontrainte appliquée au cordage.

De la même manière, ce modèle peut être utilisé pour la diffusion d'eau dans les composites soumis à une contrainte de traction statique. Pour cette application, le modèle devrait être modifié afin d'obtenir un taux d'endommagement pouvant varier en fonction du temps.

Troisièmement, des études pourraient être développées afin d'obtenir d'autres informations sur l'impact du couplage sur le comportement des matériaux.

Dans cette perspective, des mesures de contraintes précises pourraient être effectuées sur un composite immergé sollicité en traction afin de comprendre le comportement mécanique pendant un essai de couplage.

De la même manière, les essais hydrostatiques pourraient être effectués dans un caisson haute pression, transparent, permettant de mesurer la déformation du matériau induite par la pression. Ces deux types d'informations pourraient servir à améliorer le modèle développé dans le cadre de la diffusion d'eau couplée, en y ajoutant une composante mécanique.

Dans le cas des matériaux fibreux, certaines mesures gravimétriques pourraient être effectuées sur des échantillons après un cycle de chargement afin de comprendre ses effets sur la diffusion d'eau dans la structure du cordage.

Finalement, des tests couplés, semi-couplés et couplés, pourraient être effectués sur des cordages plus complexes impliquant une diffusion d'eau dans leur structure et dans les fibres (à l'exemple des cordages en Nylon 6).

En résumé, ce travail souligne les divergences entre les comportements non couplés, semi-couplés et couplés pour les deux principaux types de matériaux utilisés pour les applications marines et offshores. Par conséquent, la nécessité d'effectuer des tests couplés pour dimensionner les systèmes offshore est entièrement justifiée.

En outre, cette étude propose un important nombre d'hypothèses permettant d'expliquer le comportement des matériaux couplés. Pour ces raisons, il serait intéressant d'effectuer de nouvelles

études sur ce sujet pour d'autres types de matériaux composites ou fibreux dans le but d'augmenter la base de données sur les comportements couplés des matériaux.

UNIVERSITE BRETAGNE LOIRE

UNIVERSITÉ DE NANTES

Thèse de Doctorat

Corentin HUMEAU

Contribution to the study of coupling between moisture diffusion and mechanical stress in high performance marine material

Contribution à l'étude du couplage entre diffusion d'eau et contraintes mécaniques dans les matériaux marins hautes performances

Résumé

Les cordages en fibres synthétiques et les matériaux composites trouvent de nombreuses applications marines (respectivement : amarrage de bateaux, de plateformes pétrolières flottantes, manutention en mer… et bateaux de compétition, enceinte sous-marine, sous-marins,...).
Malgré l'étendue des applications de ces deux matériaux, on ne connait que très peu leur comportement à long terme, en particulier les interactions entre l'eau de mer et les chargements en service.
Cette étude aborde cette problématique d'un point de vue fondamental et par la suite les modèles numériques, développés dans le projet, permettront de considérer les différentes échelles du problème : fibres unitaires, brins, cordages ; résine, matériau composite. L'étude est articulée suivant deux parties : d'une part l'étude des matériaux composites et d'autre part celle des cordages synthétique. Ce travail vise à mettre en avant l'influence du couplage entre contrainte mécanique et diffusion d'eau dans ces deux types de matériaux, en ces phénomènes découples, semi-couplés puis couplés.
La corrélation entre essais et simulations numériques contribuera à la mise au point d'un modèle prédictif qui devrait intéresser tous les utilisateurs de ces matériaux.

Mots clés
Couplage ; Diffusion d'eau ; Contrainte mécanique ; Vieillissement ; Polymères ; Cordages synthétiques ; Composites

Abstract

The aim of the study was to understand the impact of coupling on water diffusion and mechanical stress on marine installations.
Moreover, we identified the key phenomena involved during this type of exposure. When we look to these type of applications we can distinguish two type of materials used: one for the structure and another for mooring facilities. The best performing structural materials appear to be composites, while the most effective mooring devices are made with synthetic ropes.
Therefore, we decided to investigate both materials with the same method: first the properties uncoupled, second, as semi-coupled behaviours and finally as one coupled phenomenon. The present work highlights the divergences between uncoupled, semi-coupled and coupled behaviours for the two main types of material used for marine and offshore applications. The need to perform coupled tests to dimension the offshore systems is fully justified.
Moreover, this study proposes an important number of hypotheses to explain these differences when we test the materials coupled. For these reasons, additional work should be performed on the subject for other types or composites and fibre materials in order to increase the data base on coupled behaviour.

Key Words
Coupling; Water diffusion; Mechanical stress; Ageing; Polymers; Synthetic ropes; Composites